The Interplay of Multiple ADME Mechanisms: Prediction of Hepatic Drug-Drug Interactions from In Vitro.

2014

'A thesis submitted to the University of Strathclyde, Strathclyde Institute of Pharmacy and Biomedical Sciences for the degree of Master of Philosophy'

Michael Hobbs
GlaxoSmithKline
Park Road
Ware
Hertfordshire
SG12 0DP
Michael.J.Hobbs@GSK.com

Declaration

‘This thesis is the result of the author’s original research. It has been composed by the author and has not been previously submitted for examination which has led to the award of a degree.’

Copyright Statement

Signed: Date:

Table of Contents

List of Tables .....

List of Figures

Abbreviations

ADME	Absorption, Distribution, Metabolism and Excretion
BCRP	Breast Cancer Resistance Protein
CAR	Constitutive androstane receptor
CL	Clearance
CHO	Chinese Hamster Ovary
CsA	Cyclosporin A
AM1	Cyclosporin AM1
Cytochrome	CYP
CV	Coefficient of variation
DDI	Drug-drug Interaction
EG	Estradiol-17β-D-Glucuronide
ES	Estrone-3-Sulphate
Fu_{cell}	Fraction unbound in the cell
HEK293	Human Embryonic Kidney 293 Cells
IC_{50}	Half maximum inhibitory concentration
IPRL	Isolated Perfused Rat Liver
KO	Knock out
K_m	Michaelis-Menten constant
MDCK	Madine Darby Canine Kidney Cells
MRP	Multi Drug Resistance Protein
NTCP	Sodium Taurocholate Co-transporting Polypeptide
OATP	Organic Anion Transporting Polypeptide
PBPK	Physiologically Based Pharmacokinetic
P_{diff}	Passive diffusion clearance
P-gp	P-Glycoprotein
PXR	Pregnane X receptor
RSV	Rosuvastatin
S_{med}	Nominal substrate concentration in the media
SLCO	Solute carrier
V_{max}	Michaelis-Menten maximum uptake rate
WME	Williams' medium E
WT	Wild type

Abstract

Rosuvastatin has poor passive membrane permeability and its uptake into the liver is mediated predominately by the transporter, Organic Anion Transporting Polypeptide 1B1 (OATP1B1). Cyclosporin A (CsA) is a potent inhibitor of a range of transporters, including OATP1B1 and clinical drug-drug interactions (DDI) have been reported with rosuvastatin. The aim of this study was to determine the uptake kinetics of rosuvastatin in human hepatocytes using a mechanistic model and to determine the inhibitory effect of CsA upon those kinetics. These data may then allow the extrapolation of *in vitro* to *in vivo* kinetics and provide an understanding of the interplay between different disposition mechanisms, with particular regard to the potential to predict DDI.

This study was divided into method development and experimental phases. In the development phase, paediatric hepatocytes from a single donor were used to develop the methods. The uptake parameters (V_{max}, $K_{m,u}$, $P_{diff,u}$, Fu_{cell} and CL_{uptake}) using estradiol-17β-D-glucuronide (EG) and rosuvastatin were determined using a mechanistic two-compartment model developed by Menochet et al (2012a). The uptake of rosuvastatin was also determined using sodium free media, which prevents the efficient functioning of the uptake transporter Sodium Taurocholate Dependent Transporter (NTCP), another transporter thought to contribute to the uptake of rosuvastatin. Inhibition parameters (IC_{50}) of the uptake of EG and rosuvastatin by CsA and rosuvastatin and rifampicin were determined.

The uptake kinetic parameters of EG and rosuvastatin in the paediatric human hepatocytes were in agreement with the quoted literature values for adult human hepatocytes. The hepatocytes were robust enough to be used for method development and to plan for the future studies. The IC_{50} values for EG and rosuvastatin as the probe substrates using CsA and rifampicin as inhibitors were in agreement with quoted literature values and suggested a predominate role for OATP1B1 in EG and rosuvastatin uptake. In these paediatric human hepatocytes NTCP did not appear to play a role in the uptake of rosuvastatin.

The paediatric human hepatocyte data were used to help define and refine the studies conducted in the experimental phase of the study. The same uptake parameters for rosuvastatin were determined in human hepatocytes from three adult donors using the mechanistic two-compartment model. The time of the incubation was extended to 60 minutes to ensure that steady state kinetics were reached.

Inhibition of the uptake of rosuvastatin was determined with co- and pre-incubation of CsA and its main metabolite, AM1. The time-dependent nature of the inhibitors have been studied by ourselves, but not in human hepatocytes [Gertz et al 2012]. There did not appear to be an effect of co- versus pre-incubation of the inhibitors.

The mechanistic two-compartment model was also used to determine the uptake parameters for a GSK compound, namely GSK2879552, using the same adult human hepatocytes from three adult donors. However, the hepatic uptake clearance (CL_{uptake}) values suggested that active saturable uptake of GSK2879552 was not evident. This may explain the high variability observed between the three donors for the uptake parameters (V_{max}, $K_{m,u}$, $P_{diff,u}$ and Fu_{cell}) and the high coefficient of variation observed about each parameter. These data provided a useful learning with regards to understanding the limitations of the model.

CHAPTER 1. INTRODUCTION.

1.1. Introduction

The overall aim of this study is to contribute to the understanding of the interplay of hepatic transporters in the disposition of drug substrates and the impact of inhibitors on these processes. In this chapter several topics are discussed with relation to the overall aim. These include, drug-drug interactions (DDI), with a focus on statins and cyclosporin A, the 'pros and cons' of the *in vitro* models available to determine hepatic uptake and the reasons for choosing the model for this study, Organic Anion Transporting Polypeptides (OATP) and their clinically important inhibitors and finally a review of mass spectrometry and the reasons for choosing this technique as the analytical methodology.

1.2. Drug-drug interactions

1.2.1 Introduction

Predicting and understanding the mechanism of DDI are of great importance for the pharmaceutical industry. DDI may occur when one drug, the 'perpetrator', inhibits (or induces) a metabolic and/or transporter process which is key to the disposition of another drug, the 'victim', leading to increased (or decreased) exposure to the victim drug. Predicting the magnitude of the interactions and understanding the mechanisms involved is critical to drug development within the pharmaceutical industry [Ayrton & Morgan 2001; Ayrton & Morgan 2008] . The prediction of a DDI may be justification to conduct a clinical study, to determine the impact on the safety or efficacy of a new drug. The implications of a DDI may impact patient recruitment, inclusion of co-medication, exclusions on the drug label, or even termination of development.

DDI are often associated with the Cytochrome P450 enzymes (CYP450) and the prediction of clinically relevant CYP450 mediated DDI is relatively well understood [Zhang & Wong 2005]. However, the role of membrane transporters in the ADME process is still emerging and therefore prediction of DDI with transporters in isolation or in combination with CYP450 enzymes remains only partially understood [Lu et al 2010]. Many clinically relevant DDI that have been attributed to changes in metabolic clearance, have been documented to be the result of changes in transporter function [Giacomini et al 2010].

The Federal Drug Administration (FDA) and the European Medicines Evaluation Agency (EMEA) have both recently published guidance on the most important membrane

transporters and suggest the use of static models for the prediction of transporter mediated DDI. However, these models cannot account for the involvement of multiple transporters, transporter-enzyme interplay and passive membrane permeability in the disposition of xenobiotics [Hinton et al 2008]. Where multiple processes are compromised, the magnitude of the change in exposure is not always predictable. For example, in knockout (KO) mice, where P-glycoprotein/CYP3A4 and P-glycoprotein/Breast cancer resistance protein had been genetically silenced, the increased magnitude in the respective substrate exposures was much greater than expected when compared to the single KO strains [Polli et al 2009; Van Waterschoot & Schinkel 2011].

Static extrapolation models are also unable to take into account the dynamics of the disposition of a xenobiotic. Physiologically-based pharmacokinetic (PBPK) models provide a means to understand the dynamic mechanism of the disposition of a compound and to predict the clinical pharmacokinetics [Zhao et al 2011]. The models require numerous parameters and some of these such as, organ size, blood flow and predictions for partition coefficients are available already [Davies & Morris 1993; Poulin et al 2000; Rodgers et al 2005, Rodgers et al 2006]. However, parameters such as active uptake or efflux clearance need to be determined experimentally. Application of 'simple' *in vitro*/*in situ* models allows the mechanistic processes to be determined and therefore allow us to understand the interplay between individual transporters and/or metabolic processes [Bi et al 2012; Jones et al 2012; Menochet et al 2012a; Poirier et al 2008; Poirier et al 2009]. These can then be interrogated quantitatively and integrated into more complex *in vivo* models which can simulate drug disposition under varying conditions, including inhibition of key processes and prediction of changes in disposition [Aoyama et al 2010; Hall et al 2012; Watanbe et al 2009].

Membrane transporters are expressed in many cell types. In hepatocytes, which are polarised, they are typically expressed on one side only [Giacomini et al 2010; Li et al 2009; Figure 1.1]. Organic Anion Transporting Polypeptides (OATP) and Sodium Taurocholate Co-transporting Polypeptide (NTCP) are solute carrier transporters expressed on the sinusoidal surface, where their function is to import substrates into the tissue [Hagenbuch & Meier 2004; Tirano & Kim 2007]. P-glycoprotein (P-gp), Breast Cancer Resistance Protein (BCRP) and Multi-Drug Resistance Protein 2 (MRP2) are examples of ATP-binding cassette (ABC) transporters, which are primarily expressed on the canalicular membrane, where in the liver they efflux substrates into the bile [Tirano & Kim 2007].

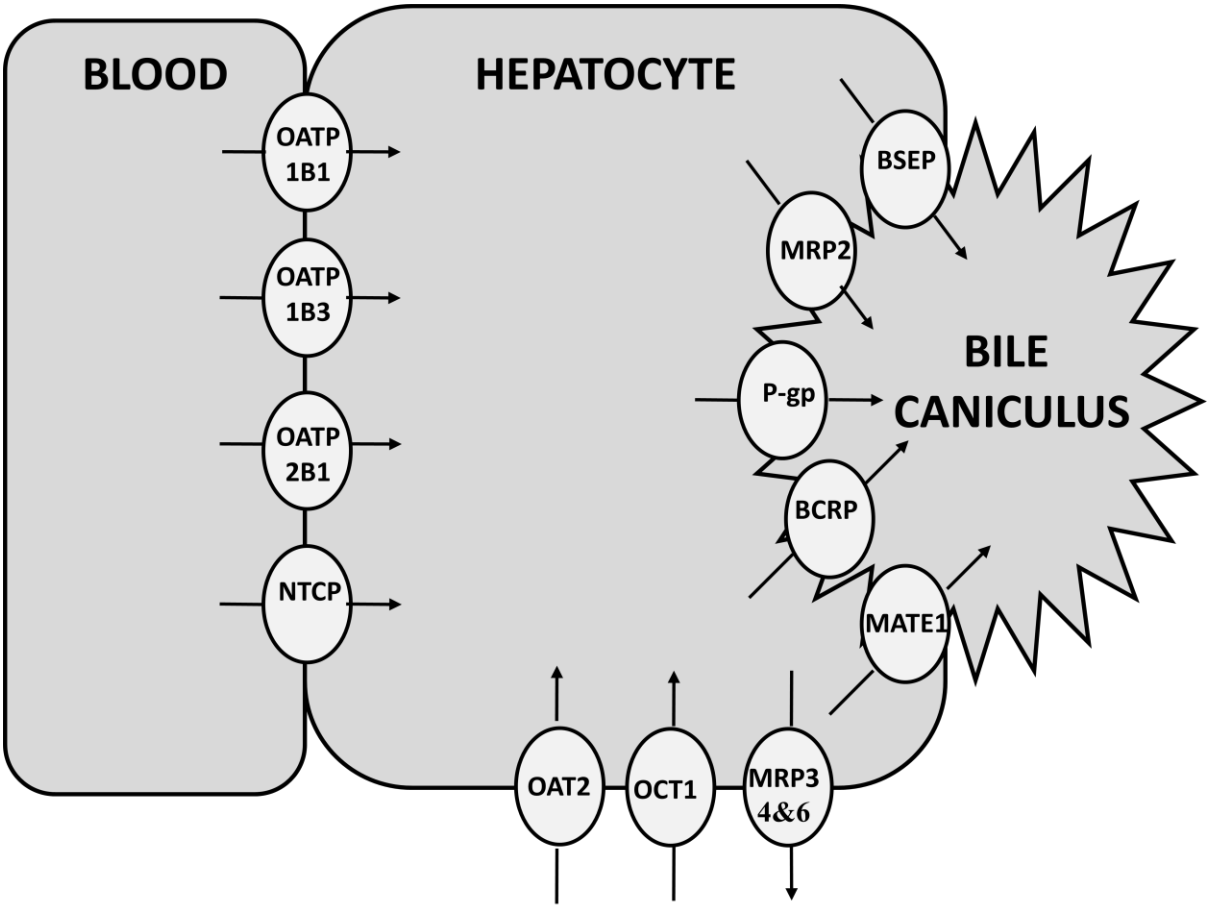

Figure 1.1. A diagrammatic summary of the major hepatic uptake and efflux transporters. OATP = Organic Anion Transporting Polypeptide, OAT = Organic Anion Transporter, OCT = Organic Cation Transporter, NTCP = Sodium Taurocholate Co-transporting Polypeptide, MRP = Multi Drug Associated Resistance Protein, P-gp = P-Glycoprotein, BCRP = Breast Cancer Resistance Protein, BSEP = Bile Salt Export Pump and MATE = Multidrug and Toxin Extrusion Protein.

Various *in vitro*, *in situ* and *in vivo* tools are available to study membrane transporters and each has its advantages and limitations. Membrane‐based ATPase assay systems and inverted plasma membrane vesicles are a relatively simple way to evaluate the interactions of substrates and inhibitors with certain transporters [Huang et al 2006]. However, cell‐based assay systems are more robust and may allow the identification of substrates and inhibitors for individual transporters, as well as providing a mechanistic understanding of the disposition of a compound. The Caco-2 cell line, derived from a human colorectal carcinoma and Madin Darby Canine Kidney (MDCK) cell lines are polarised cells. Movement from the

apical (A) side to the baso-lateral (B) side is a measure of the apparent permeability coefficient (P_{app}). In the A:B direction, P_{app} is the combination of passive permeability and active transport, whereas in the B:A ratio, P_{app}, is passive permeability only. If the ratio of P_{app} in the A:B direction is >2-fold than the B:A movement than this is indicative of carrier-mediated transport [Lu et al 2010].

Cultured cell lines, such as MDCK, Human Embryonic Kidney (HEK293) or Chinese hamster ovary (CHO), can be stably or transiently transfected (single or multiple) with recombinant transporters [Hirouchi et al 2009; Sasaki et al 2002]. In these cell lines the transporters are over-expressed, so there is less chance of native transporters contributing significantly to the disposition of the compound. Also, the requirement for chemical inhibitors that are specific for a transporter are less important.

Primary cells, derived from intact tissue, whether fresh or cryopreserved, express the full complement of drug transporters that are present. Hepatocytes, suspended or plated, have uptake transporters that appear to retain their full function [Maeda & Sugiyama 2010]. They allow the uptake of substrates to be determined, but neither method can replicate canalicular efflux. Sandwich-cultured hepatocytes, grown between two layers of gelled collagen, allow the bile caniculi to form and therefore determine the biliary efflux of a compound [Abe et al 2009]. However, cells that have been cryopreserved or cultured over several days may have reduced expression of the uptake transporters.

Genetically altered mouse and rat models (e.g. knockouts or natural mutants) of specific transport processes have been utilised to demonstrate the role of individual processes in drug disposition [Iusuf et al 2012; Iusuf et al 2013]. Although studies with animals allow the whole process of disposition to be studied, certain rodent transporters have limited homology to human ones, in particular OATP/oatp [Hagenbuch & Meier 2004]. This can make absolute comparison to human difficult, but nevertheless allows complex interplay of the disposition mechanisms to be studied. Newer models are becoming available that have human genes knocked in and mouse genes knocked out [Van de Steeg et al 2009].

KO models allow the role of an individual transporter or the interplay of multiple transporters/enzymes upon the disposition mechanism to be studied. However, they can represent a worst case scenario because the entire transporter expression has been silenced,

which is unlikely to occur in a DDI . Chemical inhibitors may represent a more realistic DDI scenario, but they may not be specific in their inhibition. Consideration of the target tissue is important, because although similar transporters are expressed in different tissue types, the relative amounts may differ. DDI at the blood brain barrier is often difficult to achieve, even with potent inhibitors such as cyclosporin A (CsA) [Hsaio et al 2006].

Isolated tissues, such as the isolated perfused rat liver (IPRL), have increased complexity over isolated cells, but also simplify the *in vivo* situation [Lau et al 2006]. It is a useful technique to understand the interplay between disposition mechanisms in the whole organ [Hobbs et al 2011].

1.2.2. Focus on cyclosporin A and statins

Cyclosporin A (CsA) is a neutral and highly lipophilic cyclic peptide that has been accepted for some years as a first-line immunosuppressive therapy for patients undergoing solid organ transplantation [Figure 1.2; Akhlaghi and Trull 2002; Dunn et al 2001; Fahr 1993; Faulds et al 1993]. It is a potent inhibitor of several uptake and efflux transporters *in vitro*, including OATP1B1, OATP2B1, OATP1B3, NTCP, BCRP, P-gp and MRP2 as well as CYP3A4 [Ho 2006 and Xia 2007]. DDI with CsA are well documented, in particular with statins, where systemic exposures were increased from 2- to 20-fold [Table 1.1; Åsberg 2003]. Statins are a family of drugs that are widely prescribed for the treatment of elevated cholesterol and their different physicochemical properties, metabolism and their affinity for different transporters contribute to their disposition [Table 1.2; Neuvonen et al 2006; Neuvonen 2010; Shitara et al 2006;].

Clinical studies with individuals who are polymorphic for key transporters have helped to understand the relative contributions of different transporters on statin disposition. Of particular importance are individuals with polymorphic genes for the solute carriers (SLCO1B1, OATP1B1) and the ATP-cassette transporters ABCG2 (BCRP) and ABCB1 (P-gp), where these transporters are under-expressed [Neimi et al 2011]. All of the statins, with the exception of fluvastatin, are substrates of OATP1B1. Rosuvastatin, atorvastatin, simvastatin acid and pravastatin systemic exposures were increased in SLOC1B1 polymorphic individuals, indicating OATP1B1 is important for hepatic uptake [Akao et al 2012; Keskitalo et al 2008; Keskitalo et al 2009c; Neimi et al 2006; Pasanen et al 2006; Pasanen et al 2007]. However, inhibition of hepatic uptake is only one of the mechanisms

that leads to increased systemic exposure and cannot always explain the magnitude of some of the DDI observed with CsA.

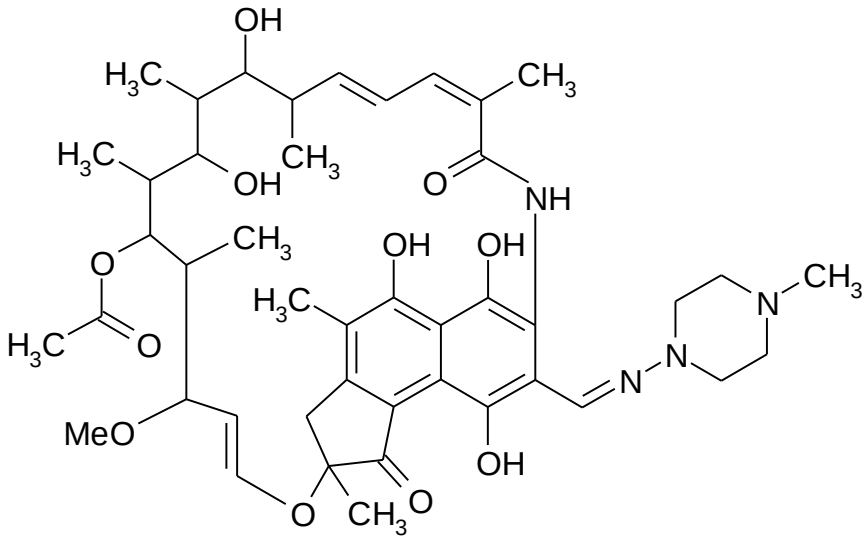

Figure 1.2. The chemical structure of cyclosporin A (Molecular Formula: $C_{62}H_{111}N_{11}O_{12}$, molecular weight: 1202.61 g/mol).

1.2.3. Rosuvastatin and pravastatin

Rosuvastatin and pravastatin both have poor passive membrane permeability and their uptake into the liver is mediated predominately by OATP1B1, but in addition hepatic uptake of rosuvastatin also involves OATP1B3 and NTCP [Figure 1.3., Crouse 2008; Ho et al 2006; Watanabe et al 2009]. With limited metabolism, their disposition from the liver is mediated predominately by transporters. Rosuvastatin is a substrate for BCRP *in vitro* and in ABCG2 polymorphic individuals the systemic exposure was increased compared to normal individuals [Table 1.1; Huang et al 2006; Keskitalo et al 2009a; Tomlinson et al 2010]. It is not a substrate for either P-gp or MRP2 *in vitro* and in ABCB1 polymorphic individuals the pharmacokinetics were unaffected [Table 1.1; Huang et al 2006; Keskitalo et al 2009b]. Pravastatin efflux is thought to be mediated *via* MRP2 and systemic exposure was unaffected in individuals with ABCB1 and ABCG2 polymorphisms [Table 1.1; Keskitalo et al 2009a; Keskitalo et al 2009c; Watanabe et al 2009]. In a double transfected cell line, *in vitro*, pravastatin was a substrate for OATP1B1 and MRP2 [Sasaki et al 2002].

Table 1.1. Summary of the fold changes in the systemic exposures of different statins in different polymorphic individuals and also in patients co-administered statins and cyclosporin A, or ritonavir (and combinations) or rifampicin.

Statin	Polymorphism			Cyclosporin A	Ritonavir / Combination	Rifampicin	Reference
	SLCO1B1	ABCG2	ABCB1				
Rosuvastatin	2-fold[a]	2-2.4-fold[b]	No Change[c]	7-fold[d]	2.1-fold[e] (Lopinavir) 2-fold[f] (Atazanavir) 1.3-fold[g] (Tipranavir) No change[f] (Fosamprenavir)	No change[h]	a = Pasanen 2007 b = Keskitalo 2009b c = Keskitalo 2009a d = Simonson 2004 e = Kiser 2008 f = Busti 2008 g = Pham 2009 h = Zhang 2008 i = Keskitalo 2008 j = Åsberg 2001 k = Hermann 2004 l = Lau 2007 m = Keskitalo 2009c n = Pasanen 2006 o = Arnadottir 1993 p = Campana 1995 q = Olbricht 1997 r = Gullestad 1999 s = Neimi 2006 t = Hedman 2004 u = Regazzi 1994 v = Park 2002 w = Aquilante 2011 x = Deng 2009
Atorvastatin	0.4-fold[a]	1.7-fold[b]	1.5-fold[i] (acid)	6-fold[j] 10-fold[k]	9.4-fold[g] (Tipranavir)	7-fold (acid)[l] 2.5-fold lactone[l]	
Simvastatin Acid	1.6- and 3.2-fold[m,n]	No Change[o]	1.6-fold[i,p]	3-fold[q] 6-fold[r]			
Simvastatin Lactone	No Change[i]	2.2-fold[j]	No Change[k]				
Lovastatin	-	-	-	20-fold[q] 5-fold[r]			
Pravastatin	2-3.7-fold[s]	-	-	10-fold[t] 23-fold[u] 5-fold[q] 12-fold[v]	No Change[w] (Darunavir)	2.8-fold[x]	

Table 1.2. Physiochemical properties, pharmacokinetics, metabolism and disposition of statins in human.

	Simvastatin	Lovastatin	Atorvastatin	Pravastatin	Rosuvastatin
Lactone Prodrug	Yes	Yes	No*	No	No
Absorption	60-85%	30%	30%	35%	50%
Lipophilicity	++++	++++	+++	+	++
Bioavailability	<5%	5%	12%	18%	20%
Hepatic Extraction	>80%	>70%	70%	45%	63%
Metabolism	Extensive	Extensive	Extensive	Mainly Unchanged	Mainly Unchanged
Enzymes	CYP3A4 & CYP2C8	CYP3A4 & CYP2C8	CYP3A4, CYP2C8 & UGT	CYP3A4**	CYP2C9 & CYP2C19
Substrate of					
OATP1B1	Yes	Yes	Yes	Yes	Yes
OATP1B3	-	-	-	Yes	Yes
OATP2B1	-	-	Yes	Yes	Yes
NTCP	-	-	-	-	Yes
BCRP	Yes (lactone)		Yes	Yes**	Yes
MDR1	Yes (acid)	Yes	Yes	Yes	No
MRP2	-	-	Yes (?)	Yes	Yes

Adapted from Neuvonen 2006 and 2010.
* dosed as the acid (can convert to the lactone)
** of minor importance

Ritonavir is used to treat HIV-1 infections and its potent inhibition of CYP3A4, CYP2D6 and OATP1B1 is utilised to enhance the systemic exposures of other co-administered antiretrovirals [Eron et al 2006]. Rifampicin is an antibiotic and can induce many CYP enzymes, but is also a potent inhibitor of OATP1B1 (and OATP1B3) [Figure 1.4., Chen and Raymond 2006; Smith et al 2005].

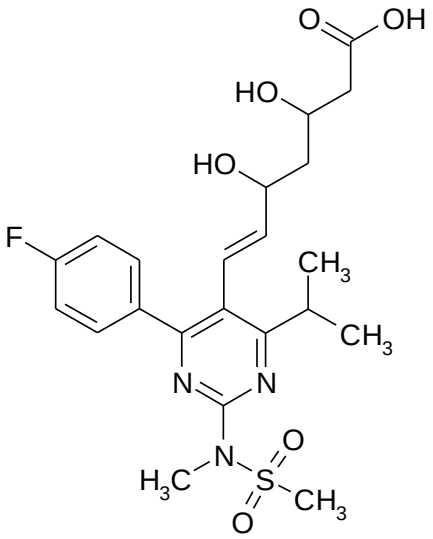

Figure 1.3. The chemical structure of rosuvastatin (Molecular Formula: $C_{22}H_{28}FN_3O_6S$, Molecular Weight: 481.54 g/mol).

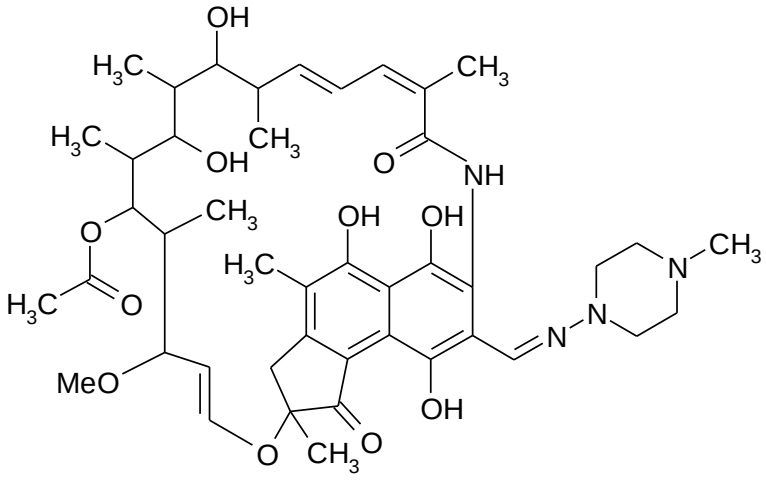

Figure 1.4. The chemical structure of rifampicin (Molecular Formula: $C_{43}H_{58}N_4O_{12}$, Molecular Weight: 822.94 g/mol).

The magnitude of the interaction observed with CsA and rosuvastatin was much greater than that observed with either rifampicin or ritonavir combinations, which would suggest

simultaneous inhibition of both OATP1B1 and BCRP [Busti et al 2008; Kiser et al 2008; Pham et al 2009; Simonson et al 2004]. It has been suggested that BCRP would have a low potential to cause DDI because the inhibitory effect at normal therapeutic blood concentrations would be weak [Xia et al 2007]. However, it is important to consider the role of BCRP in the lumen of the gut, where local concentrations of CsA would be very much higher.

Rifampicin and the combination of ritonavir/fosamprenavir had no effect upon the pharmacokinetics of rosuvastatin, which would appear to conflict with the polymorphic studies [Table 1.1; Zhang et al 2008]. The lack of an interaction may be related to the time of administration and the resulting pharmacokinetic profiles of rosuvastatin relative to the inhibitors. Alternatively, the expression of OATP1B1 (and NTCP and OATP1B3) may be different, such that rosuvastatin may utilise another transporter(s) [Neimi et al 2011].

As with rosuvastatin, the systemic exposure of pravastatin increased greatly in recipients receiving CsA compared to rifampicin or the combination of ritonavir/darunavir suggesting inhibition of the efflux transporter, MRP2, is crucial to the DDI [Table 1.1; Hedman et al 2004; Olbricht et al 1997; Park et al 2002; Regazzi et al 1994]. In contrast to rosuvastatin, the systemic exposure of pravastatin increased with co-administration of a single dose of rifampicin, but not with the combination of ritonavir/darunavir [Table 1.1; Aquilante et al 2011; Deng et al 2009]. This may be due to the reduced ability of pravastatin to be accepted by alternative uptake transporters or the reduced exposure of ritonavir in this particular combination.

1.2.4. Atorvastatin

Atorvastatin is administered as the hydroxyl acid form, which is then converted to the lactone, where both species circulate systemically in approximately equal concentrations [Lennernas 2003]. In SLOC1B1 polymorphic individuals the increase in atorvastatin exposure was modest and another transporter, the H^+-mono-carboxylic transporter, may also be involved in the hepatic uptake of atorvastatin [Table 1.1; Pasanen et al 2007; Lennernas 2003]. The lactone is more lipophilic and although the passive membrane permeability of the hydroxyl acid is still thought to be good, different opinions concerning the actual role of passive uptake are quoted. Both species are substrates for CYP3A4, but the lactone is

metabolised more rapidly than the acid, mainly in the liver, but also in the GI tract [Lennernas 2003].

Atorvastatin acid is a P-gp and BCRP substrate *in vitro* and the systemic exposures were increased in ABCB1 and ABCG2 polymorphic individuals, but the pharmacokinetics of the lactone were unaltered [Table 1.1; Campana et al 1995; Hochman et al 2004; Keskitalo et al 2008; Keskitalo et al 2009b].

Atorvastatin systemic exposure increased in recipients that received daily treatment of CsA [Table 1.1; Åsberg et al 2001; Herman et al 2004]. The disposition of atorvastatin involves multiple transporters, metabolic clearance as well as the inter-conversion of the acid to the lactone, which makes it difficult to pin point the role of any one process.

Rifampicin and the combination of ritonavir/tipranavir increased the systemic exposure of atorvastatin acid and lactone in healthy volunteers and in individuals with different SLCO1B1 genotypes [Table 1.1; He et al 2009; Lau et al 2007; Pham et al 2009]. The magnitude of the interactions might suggest that in addition to inhibition of OATP1B1, inhibition of CYP3A4 is also important. However, this does not rule out inhibition of one or more of the other processes as concomitant administration of CsA affected the acid forms of atorvastatin more than the lactones, which may also be the result of inhibition of the efflux transporters P-gp and BCRP.

1.2.5. Simvastatin and lovastatin

Simvastatin is administered as the lactone pro-drug, which can then be converted to the acid [Neuvonen et al 2006; Neuvonen et al 2010]. The lactone has high passive membrane permeability and its disposition is unaffected by OATP1B1, unlike the acid which is affected by SLOC1B1 polymorphisms [Table 1.1; Keskitalo et al 2008; Keskitalo et al 2009c; Pasanen et al 2006]. Bio-availability is limited because first pass metabolism by CYP3A4 is high both in the GI tract and liver.

Simvastatin acid is also a P-gp and BCRP substrate *in vitro* and the systemic exposures were increased in ABCB1 and ABCG2 polymorphic individuals, although only simvastatin lactone appeared to be affected by the ABCG2 variant allele [Table 1.1; Keskitalo et al 2008; Campana et al 1995; Åsberg et al 2001; Herman et al 2004].

Simvastatin exposure increased in recipients treated with CsA [Table 1.1; Arnadottir et al 1993; Campana et al 1995]. Again with multiple disposition pathways it is difficult to predict the relative contributions of each pathway *in vivo*. Although, the similarity in the magnitude of the increased systemic exposures between the polymorphic and CsA dosed individuals might suggest that OATP1B1 is more relevant in the disposition of simvastatin (acid).

Lovastatin is also administered as the lactone pro-drug, has good passive membrane permeability and is metabolised extensively in the GI tract and liver by CYP3A4 [Table 1.1; García et al 2003]. It is also a substrate for OATP1B1, although its relevance in the disposition of lovastatin *in vivo* has not been demonstrated [Ieiri et al 2009]. Lovastatin acid is a substrate of P-gp, but there were no observed change in systemic exposures in individuals with an ABCB1 polymorphism [Table 1.1; Keskitalo et al 2009a].

The systemic exposure of lovastatin increased in recipients receiving CsA when compared with healthy controls [Table 1.1; Gullestad et al 1999; Olbricht et al 1997]. The magnitudes of the interactions of CsA with lovastatin are interesting when compared to those of simvastatin. Both of these statins have good passive permeability, but only simvastatin appears to be affected by OATP1B1 *in vivo*. CsA administration with simvastatin inhibits OATP1B1 and may reduce uptake into the liver and therefore reduce the importance of CYP3A4 to the DDI. Lovastatin enters the liver by physicochemical means and inhibition of CYP3A4 may be more important in its DDI.

1.2.6. Summary

CsA is a potent inhibitor of multiple transporters and represents a useful academic tool to understand the interplay between different transporters with regards to the disposition of key prescribed medicines. Further, GSK has been asked by regulatory authorities to consider conducting clinical DDI studies using CsA to provide 'worst case' scenarios to mitigate risk. Understanding the relative inhibition of CsA upon the different transporters may allow more detailed clinical studies to be designed or even remove the need to do the study altogether. In addition, GSK has used rosuvastatin as a probe substrate to understand DDI with OATP1B1, but it is possible that the disposition of this drug is more complex and involves contribution from other transporters.

1.3. Review of in vitro systems to determine hepatic uptake

1.3.1. Introduction

Hepatocytes are parenchymal cells that make up the majority of the cells in the liver. They perform a variety of roles, including bile salt production, storage of glycogen and buffering blood glucose, urea, plasma proteins and cholesterol synthesis and processing steroid hormones and vitamin D. However, of importance to drug discovery and development, is their role in the detoxification, modification and excretion of exogenous, as well as endogenous, chemicals.

The liver is the largest internal organ in the body and is divided into four lobes in human. In addition to hepatocytes, it also contains non-parenchymal cells such as, sinusoidal endothelial cells, kupffer cells and hepatic stellate cells. It receives deoxygenated venous blood from the small intestine *via* the hepatic portal vein and oxygenated arterial blood from the general circulation *via* the hepatic artery, in an approximate ratio of 3:1. The blood mixes as it enters the sinusoids in the liver, which are vascular channels lined with highly fenestrated endothelial cells and bounded in circumference by the hepatocytes. The "space of Disse" is the region between the endothelium and hepatocytes. The blood flows through the sinusoids and exits the liver *via* the hepatic vein.

Hepatocytes contain cellular organelles associated with metabolic and secretary functions, including endoplasmic reticulum (smooth and rough), Golgi apparatus and mitochondria. They are cuboidal in shape and are polarised such that the apical surface faces the sinusoids (blood) and the basal surface faces the bile canaliculi. The biliary system is a series of channels and ducts that convey bile from the hepatocytes into the lumen of the small intestine. The common bile-duct runs parallel to the sinusoids, but the bile flow is in the opposite direction to that of the blood. The gall bladder is situated on the posterior surface of the liver and stores bile synthesised by the liver.

A variety of *in vitro* systems such as, recombinant enzymes, liver microsomes, post-mitochondrial fraction (S9), immortalized and expressed cell lines are available to study xenobiotic metabolism and toxicity. However, intact primary human hepatocytes are considered the 'gold standard' *in vitro* model because they retain their ability to support mature hepatic phenotypes, such as metabolism, transport and induction. They can have a

limited and unpredictable availability, variability between lots, lot sizes, as well as cost considerations [Mudra 2001].

1.3.2. Preparation of hepatocytes

One of the first consistent methods of isolating rat hepatocytes was described by Howard using a combined mechanical/enzymatic digestion technique and was subsequently modified by Berry and Friend [Berry and Friend 1969; Howard et al 1967]. The tissue is perfused directly with a calcium free buffer, also containing a crude collagenase and hyaluronidase mix, that digests the hepatic tissue. An important modification was introduced by Seglen, who showed that calcium must be removed first from the liver before perfusion with the collagenase solution, which is the technique widely used today [Seglan 1976]. Firstly, the liver tissue is perfused with a calcium-free buffer containing a calcium chelating agent (e.g. EGTA) to deplete the calcium and weaken the cell-cell adhesion. Secondly, the tissue is perfused with a buffer solution containing calcium and purified collagenase to digest the cell-cell adhesion to create a suspension of hepatocytes. The hepatocytes are separated by low speed centrifugation and the hepatocyte pellet obtained is washed with ice-cold buffer solution to purify the cells [Mudra 2001]. However, extensive comparisons of the methods described here have not demonstrated any significant differences in terms of cell yield, viability and isolated hepatocyte function [Puviani et al 1998].

With small non-clinical species perfusion of the liver *in situ via* the hepatic portal vein provides superior yield and viability, but with larger non-clinical species and human, only excised liver tissue is available. Here, the larger blood vessels are cannulated and blood is removed with a physiological salt solution and the liver tissue then digested. The hepatocytes are centrifuged, washed and re-suspended in an incubation medium. The cells can be used immediately or cryopreserved, providing a means of long term storage [Mudra 2001; Terry & Hughes 2009].

Improvements to increase yield and quality of the hepatocytes have been described. Collagenase is prepared from bacteria and may contain a blend of poorly purified enzymes, leading to inconsistent batch performance. Liberase® is a new preparation of a highly purified blend of collagenase isoforms which have been used for the preparation of hepatocytes with higher cell viability [Mitry et al 2002]. Other methods have been

described and the addition of elastase, with the purified collagenase, has been claimed to give superior yields of undamaged hepatocytes [Berry and Philips 2000].

A number of different media formulations have been used for the cultivation of human hepatocytes. Some of the more common ones include Dulbecco's modified Eagle's medium (DMEM), Leibovitz's L-15, modified Chee's medium (MCM) and Williams' E medium (WEM). However, when MCM, WEM and hepatocyte medium (HM) were compared, there was little or no difference in the induction of CYP3A4 activity by rifampicin [Puviani et al 1998].

1.3.3. Hepatocyte culture methodology

Hepatic clearance (CL_H) is often determined using hepatic microsomes rather than hepatocytes as they are more flexible, easier to prepare, can be stored long term and are widely available. However, isolated hepatocytes suspended in a suitable medium can provide an alternative to microsomes to determine CL_H. They not only contain phase I enzymes, but also phase II enzymes and membrane transporters in the correct spatial arrangement and represent a more physiologically relevant model [Soars et al 2007]. These criteria make them useful to understand the interplay of all of the processes of the hepatic disposition of drug. However, care should still be taken when extrapolating hepatocyte data to the *in vivo* scenario. Using cryopreserved hepatocytes, the *in vivo* CL_H was under predicted for certain drugs and differences were observed between the inhibitory potency of microsomes and hepatocytes [Brown et al 2007; Brown et al 2010].

Suspended hepatocytes have also been used to determine the role of uptake transporters in the disposition of a drug or the potential of a drug to inhibit the uptake of a probe substrate of a specific transporter. Two methodologies have been developed. In the traditional 'oil spin' method, hepatocytes are separated from the media by rapid centrifugation through a silicone/mineral oil layer and the drug (or probe substrate) concentrations associated with the hepatocytes analysed [Petzinger & Fuckel 1992; Yabe et al 2011]. Alternatively, the hepatocytes can be centrifuged into a pellet and the supernatant analysed for loss of drug [Soars et al 2007]. Uptake is usually measured over a short time (less than two minutes) and because of the concentration gradient between the cell and medium, passive diffusion is assumed to be unidirectional from media to cell. In addition, following isolation the efflux transporters on the canalicular membrane are thought to be internalised and would therefore not contribute to the kinetics. It takes at least three days for P-gp and MRP2 to be expressed

correctly on the canalicular membrane of sandwich-cultured hepatocytes [Bow et al 2008; Hoffmaster et al 2004].

Without suitable attachment matrices, such as collagen type I or Matrigel®, plated hepatocytes de-differentiate to fibroblasts after a few days of culture. These different matrix configurations may influence the morphology of the cells. Hepatocytes cultured on a rigid collagen substratum, without an overlay of extracellular matrix, spread and flatten until confluence is attained [LeCluyse 2001]. A layer of Matrigel® or collagen on top of these hepatocytes does not appear to affect the hepatocytes spreading and forming confluent monolayers, however, they do maintain a more three-dimensional cuboidal shape. Very little or no differences are observed in the morphology of cultured hepatocytes overlaid with collagen versus Matrigel® [Mitry et al 2002; Puviani 1998].

Mature hepatocytes usually do not survive for more than fourteen days and do not proliferate. For longer term culture, the culture media used must be supplemented and Hino describes a method that allows human hepatocytes to be cultured for over two months without the need to co-culture with epithelial cells [Hino et al 1999].

Hepatocytes cultured between two layers in a sandwich configuration are able to re-polarise and re-establish bile canaliculi, along with active efflux transporters [Abe et al 2009, Kotani et al 2011, Jones et al 2012]. The morphology of the hepatocytes is different depending upon the matrix used. With collagen the cells remain in cord-like arrays throughout the culture period, but with cells coated with a layer of Matrigel® form distinct clusters or aggregates of cells within two days [Mitry et al 2002; Puviani 1998].

Sandwich culture has been used to study active uptake and biliary excretion in rat and human [Abe et al 2008; Abe et al 2009; Bi et al 2006; Bi et al 2012]. However, the complexity of the processes occurring in this model means that estimation of the kinetic parameters from a single set of incubations is not possible. Three different incubation conditions have to be studied simultaneously to determine the active and passive uptake clearance and the biliary excretion rate. Therefore, this experimental setting is not appropriate to study uptake kinetics in isolation [Li et al 2010].

Hepatocytes in a monolayer cultured over a short term are suitable to study uptake and/or metabolism simultaneously or in isolation. They maintain cellular integrity and retain the majority of their CYP and OATP activity for up to 6 hours [LeCluyse 2001; Ulvestad et al 2011]. Similar to the suspended hepatocytes, their efflux transporters are not expressed on the cellular membrane [Bow et al 2008; Hoffmaster et al 2004].

1.3.4. Primary and cryopreserved hepatocytes

Although cryopreservation usually results in low cell recovery and early alterations of functional activities, drug metabolism can be comparable with fresh cells [Guillouzo et al 1999]. Cryopreserved human hepatocytes retained similar functional activities of CYP and UGT enzymes compared to fresh hepatocytes in terms of determining intrinsic clearance [Li et al 1999; McGinnity et al 2004]. In addition, there was no evidence that fresh hepatocytes provided quantitatively improved estimates of intrinsic clearance over cryopreserved hepatocytes [Halifax et al 2008]. After five days in culture human hepatocytes expressed the same level of CYP450 activity as they did immediately after isolation [LeCluyse 2001; Kimoto et al 2012].

Glutathione (GSH) is a tri-peptide (cysteine, glycine and glutamate) and functions as an antioxidant, preventing damage to important cellular components caused by reactive oxygen species such as free radicals and peroxides [Moldeus & Jernstrom 1983]. Cryopreservation of mono-layers of hepatocytes can result in a loss of intracellular reduced glutathione of up to 50%, but levels are only slightly reduced when compared with non-cryopreserved monolayer cultures. However, of importance is the total loss of expression of glutathione synthetase, which means that cryopreserved hepatocytes cannot replenish GSH and if GSH levels are depleted then toxicity may result [Stevenson et al 2007]. However, in primary cultures of chick embryo hepatocytes cellular GSH concentrations remained stable for up to three days in culture. Buthionine sulphoximine reduced glutathione concentrations rapidly (15-30% of control levels), but toxicity was not observed [Shedlofsky et al 1984].

The variability in the expression of transporters may depend upon several individual factors and even combinations of these factors. The type of transporter (uptake or efflux), the species, whether the cells are plated or suspended and the length of time in culture can all influence transporter expression. As discussed, freshly suspended hepatocytes have their efflux transporters internalised following isolation [Bow et al 2008; Hoffmaster et al 2004].

However, cryopreserved human hepatocytes in suspension were shown to have adequate NTCP, OATP and OCT uptake transporter activity [DeBruyn et al 2011].

There are different reports of the activity of uptake transporters in plated hepatocytes. In plated primary human hepatocytes, the activity of OATP1B1 and OATP1B3 decreased with time, such that activity had been abolished from 6-24 hours [Ulverstad et al 2011]. Although the uptake transporters NTCP and OATP1B1 were shown to be functional in cryopreserved hepatocytes, there was considerable variability in comparison to fresh cells [Bi et al 2006; Shitara et al 2003]. In contrast, in sandwich cultured human hepatocytes following five days of incubation OATP1B1, OATP1B3 and OATP2B1 activity was maintained, compared with sandwich-cultured rat hepatocytes which was reduced considerably [Bi et al 2012; Kotani et al 2011; Schaefer et al 2012].

Efflux transporters such as P-gp, BCRP, BSEP and MRP2, internalised after isolation, are also expressed on the canalicular membranes from three to six days in rat and human sandwich cultured hepatocytes, respectively [Fukada et al 2008; Fenner et al 2012; Hoffmaster et al 2004; Nakakariya et al 2012; Zhang et al 2005]. However, the level of expression of Mrp2, Bcrp and Bsep may be altered in sandwich cultured rat hepatocyte [Li et al 2010].

1.3.5. Primary and hepatoma hepatocytes

Alternatives to hepatocytes derived from fresh healthy livers include hepatocyte cell lines obtained by oncogenic immortalisation or derived from tumours. The two most used human hepatoma cell lines are the HepG2™ and Fa2N-4. Both have been considered for certain screening applications, such as the nuclear receptors androstane receptor (CAR) and pregnane X receptor (PXR) mediated induction, but have failed to match the functionality of primary human hepatocytes. They are able to carry out biotransformation of xenobiotic compounds, but their basal gene expression levels of phase I and II biotransformation enzymes are generally lower compared to fresh hepatocytes. Some of the major CYPs and transporters may be 50-fold lower than in primary human hepatocytes and CYP2B6 and CYP3A4 may have no response at all [Guguen-Guillouzo & Guillouzo et al 2010; Jennon et al 2010].

The more recent HepaRG™ Cells were derived from a female with hepato-cellular carcinoma by the Institute National de la Santé et de la Recherche Médicale in France. When plated at

low density they demonstrated a similar morphology to typical hepatocytes and were shown to support mature hepatic phenotypes. Expression of CYP1A2, 2B6, 2C9, 2E1 and 3A4 as well as CAR and PXR are higher than HepG2™ and comparable to primary human hepatocytes. They also express Phase II enzymes and numerous membrane transporters [Guillouzo et al 2007].

1.4. Determination of uptake kinetics

Drugs may be taken up into the hepatocyte by passive diffusion through the cell membrane or actively *via* a transporter protein. The rate of uptake can be determined at different substrate concentrations and the kinetic parameters V_{max}, K_m and P_{diff} can be estimated from equation 1-1.

Equation 1-1. $$v = \frac{V_{max} \times S_{med}}{K_m + S_{med}} + P_{diff} \times S_{med}$$

where v is the uptake rate, V_{max} is the maximum uptake rate, K_m is the Michaelis-Menten constant, P_{diff} is the passive diffusion clearance and S_{med} is the substrate concentration in the media.

Passive diffusion has proved difficult to measure and various techniques have been used. Enzyme and transporter activity is reduced greatly at 4°C, but the fluidity of the membrane is altered at this temperature [Frezard & Garnier-Suillerot 1998]. The use of chemicals that inhibit OATP activity has been used and often involves a cocktail of potent inhibitors such as rifampicin and cyclosporin A, although rifamycin has been suggested as a pan inhibitor of OATP [Treiber et al 2004; Bi et al 2012]. Nevertheless, the impact of high concentrations of these inhibitors on the viability of the cell needs to be considered. An alternative has been to compute the three kinetic parameters from the uptake rates and although negating the need to determine passive diffusion experimentally, the technique may lack accuracy due to the limited number of data points, with one uptake rate per substrate concentration [Hirano et al 2004; Parker & Houston 2008; Yabe et al 2011].

Active uptake may also be estimated from the cell-to-media ratios, either total (K_p) or unbound (K_{pu}) [Halifax & Houston 2006]. Both parameters are dependent upon the media concentrations, but where K_p can be determined directly from the hepatocyte incubations,

K_{pu} has to be estimated indirectly from the uptake kinetic parameters [Parker & Houston 2008; Yabe et al 2011]. At media concentrations much lower than the K_m, K_{pu} can be expressed as the ratio of total over passive uptake [Parker and Houston 2008; Yabe et al 2011]. The intracellular unbound fraction (fu_{cell}) can also be derived as the ratio of the K_{pu} over K_p. A K_p value of greater than 3,000 has been reported for nelfinavir in rat hepatocytes after only two minutes incubations. Intracellular unbound concentrations were 5-7-fold greater than unbound concentrations in the media, suggesting that drugs might permeate back from the cells into the media [Parker and Houston 2008]. Also, this conventional approach does not account for binding in the cell, which may act as a sink and influence active uptake [Baker & Parton 2007: Halifax & Houston 2006]. Mechanistic modelling has allowed the fraction unbound in the cell to be estimated.

A two-compartment model that determined both the active uptake and the bidirectional passive diffusion using the oil spin method has been developed [Paine et al 2008]. However, uptake kinetics were not defined as the experiments were carried out at a single concentration and in addition, intracellular binding was not calculated. Using this model, *in vivo* pharmacokinetics were predicted in conjunction with a seven-compartment physiologically based pharmacokinetic (PBPK) model, but investigation of the active uptake kinetics was not possible because of the use of single concentrations [Gardiner and Paine 2011].

A more detailed two compartmental mechanistic model was developed to determine nonspecific binding, bidirectional passive diffusion and active uptake kinetics [Figure 1.6, Poirier et al 2008]. This model allows the simultaneous fitting of all time and substrate concentration points, resulting in a significant improvement in the precision of the estimation of P_{diff}, K_m and V_{max} compared to the conventional two-step approach. The model was also used to supply kinetic parameters to input into a fully mechanistic PBPK model where the scaled kinetic parameters of hepatic uptake and transport enabled the prediction of *in vivo* PK profiles and plasma clearances [Poirier et al 2009].

However, the model does not calculate intracellular binding, although it has a binding constant to correct for the concentrations at time = 0. A mechanistic two-compartment model was developed that determined the kinetic parameters of bidirectional passive diffusion, intracellular binding and metabolism in freshly isolated plated rat hepatocytes and plated cryopreserved human hepatocytes [Figure 1.7; Menochet et al 2012a; Menochet et al 2012b].

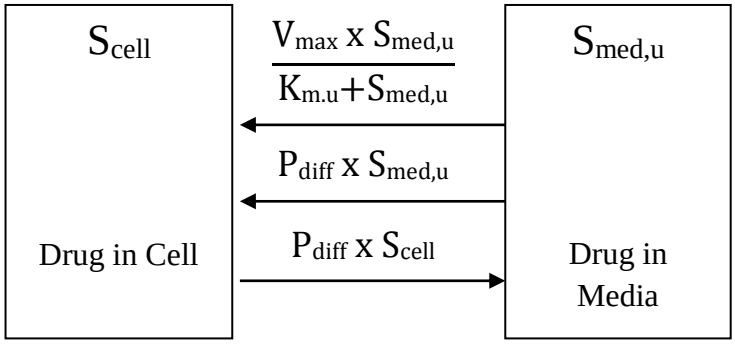

Figure 1.5. An in vitro two compartmental model developed by Poirier et al (2008) to determine the uptake parameters of different substrates.

All concentration-time points were analyzed simultaneously by using a mechanistic two-compartment model describing the unbound affinity constant ($K_{m,u}$), the maximum uptake rate (V_{max}), unbound passive diffusion clearance ($P_{diff,u}$) and intracellular unbound fraction (fu_{cell}). When metabolism is important, the model can be extended by addition of extra compartments with the inclusion of an unbound metabolic clearance ($CL_{met,u}$). Extended incubation times (up to 45 min) allowed steady state to be reached between media and intracellular compartment concentrations and reduced the error in certain parameter estimates observed with shorter incubation times.

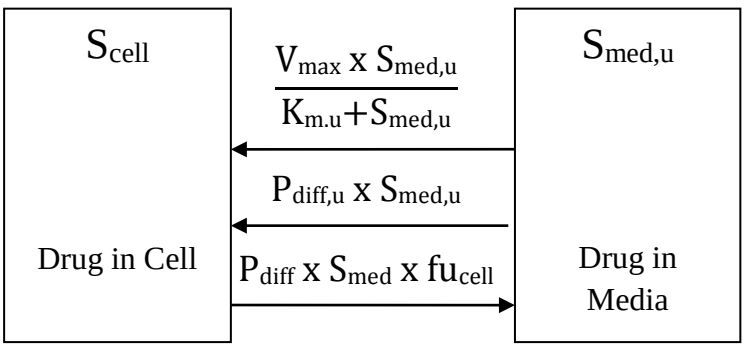

Figure 1.6. An in vitro two compartmental model developed by Menochet et al (2012a) to determine the uptake parameters of different substrates.

As discussed fresh hepatocytes provide the closest 'functionality' to the intact liver and so should provide data that equates more readily to the in vivo situation, or can be more easily extrapolated. However, the reduction in functionality of cryopreserved hepatocytes is modest when compared to fresh cells. It should also be remembered that fresh hepatocytes have a

greater reduction in functionality compared to cells in the liver, than cryopreserved have in comparison to fresh cells. The downside to all cells is the variability between different donors, such that enough cells are required to complete all the incubations required. With fresh cells they have to be used as soon as possible and there may not be enough time or cells available to complete the incubations required. With cryopreserved cells it is possible to make sure there are enough cells available before starting the experiments.

Plating offers the ability to incubate for a longer time period, allowing the kinetics to saturate, versus the more traditional suspension methods. This allows mechanistic models such as the one described by Menochet to fit the data simultaneously and provide more robust determinations of the parameters. These can then be incorporated into more detailed PBPK models such as the one described by Gertz et al 2012.

As discussed previously, the sandwiched culture technique is not really applicable to understand uptake kinetics. Its main utility is to determine biliary efflux and this may be something worth considering in the future. However, despite the many claims on the utility of the methodology, there are some considerations. The biliary efflux values quoted actually include the uptake clearance. With the potentially reduced expression of the uptake transporters, care should be taken in the interpretation of the data observed, as it may really be a measure of the reduced uptake clearance. To really determine the biliary efflux, then the intracellular concentrations need to be determined, which may also require modelling.

Although non-clinical species can provide hepatocytes to determine the mechanistic understanding of the disposition of rosuvastatin and cyclosporin A, the difference between the transporters, particularly the OATP/Oatp, prevents extrapolation to human. In addition, the hepatoma cell lines do not approximate to the *in vivo* situation sufficiently.

Therefore, for the reasons outlined, cryopreserved plated human hepatocytes are the preferred choice for this study.

1.5. Review of the inhibitors of organic anion transporting polypeptides

1.5.1. Introduction

In this study, the uptake of rosuvastatin into human hepatocytes and the mechanism of its inhibition by CsA are being investigated. Rosuvastatin is a substrate for the uptake

transporters, OATP1B1 and 1B3 and NTCP. CsA is a known inhibitor of these transporters, among many others.

OATP1B1 and OATP1B3 share a high level of amino acid sequence and often have similar substrate specificity. However, they also have differences, such as paclitaxel and docetaxel, which are substrates of OATP1B3 only. Substrates are often anionic amphipathic molecules, with a relatively high molecular weight (>350 g/mol) and a high degree of albumin binding under physiological conditions [Neimi et al 2011].

Endogenous substrates of OATP1B1 include bile acids such as cholic acid, as well as secondary bile acids, such as glycocholic acid, glycoursodeoxycholic acid, taurocholic acid and tauroursodeoxycholic acid. Estradiol-17β-D-glucuronide (EG) and estrone-3-sulphate (ES) are also substrates and are regularly used as probe tool compounds to study OATP1B1 and OATP1B3 function.

Numerous drugs have been identified as substrates of the OATPs, with the most clinically relevant listed in Table 1.3 [Bloomer et al 2013; Kalliokoski and Neimi 2009; Neimi et al 2011]. Numerous (over 200) drugs have been identified as inhibitors of the OATPs and a list of the ones likely to cause a greater than 5-fold increase in the systemic exposure of the victim drug are listed in Table 1.4 [Bloomer et al 2013; Karlgren et al 2012a & 2012b; Kalliokoski and Neimi 2009; Neimi et al 2011]. Many of the inhibitors are not OATP substrates, even though substrates can competitively inhibit other substrates that interact at the same site of OATP [DeBruyn et al 2013].

This review focuses on the inhibition parameters determined in vitro for CsA that have been quoted in the literature. Rifampicin, an antibiotic macrolide, is also highlighted because it is intended to be used to investigate the mechanism of CsA inhibition of rosuvastatin uptake into human hepatocytes. In addition, focus is given to in vitro studies that have used clinically relevant OATP substrates and inhibitors.

In these studies we plan to utilise chemical inhibitors to determine the interplay between the transporters. However, other groups have used alternative approaches. Naturally occurring polymorphisms exist of OATP and human hepatocytes with these polymorphisms have been used to study the relative contribution of theses transporters [Ho et al 2006]. Novel RNA

interference knockdown technology has been used to reduce the expression and transport activity of OATPs in human hepatocytes. In human sandwich-cultured hepatocytes, the total uptake of cerivastatin was reduced by 50% [Liao et al 2010]. In another study, the relative contribution of each transporter was determined by comparison with reference compounds and not inhibitors.

Pitavastatin uptake kinetics were determined in human cryopreserved hepatocytes and OATP1B1 and OATP1B3 over-expressed HEK293 cells. The method is similar to the relative activity factor method used to estimate the contribution of each cytochrome P450 isoform to the overall metabolism. The observed uptake clearance of pitavastatin in human hepatocytes was almost completely accounted for by OATP1B1 and OATP1B3, with approximately 90% of the total hepatic clearance accounted for by OATP1B1 [Hirano et al 2004].

Finally, the choice of in vitro system can be very important to the overall conclusions. As discussed previously, primary hepatocytes are considered the 'gold standard' with regards in vitro models. To highlight this, the uptake of fluvastatin was determined in primary human hepatocytes as well as OATP1B1 and OATP1B3 CHO or HEK293 over-expressing cells. Fluvastatin was taken up into the hepatocytes and was also shown to be a substrate for OATP1B1 and OATP1B3 in the over-expressed cells. In the over-expressed OATP1B1and OATP1B3 cells fluvastatin transport was inhibited by gemfibrozil by 97 and 62%, respectively, whereas only a small inhibitory effect by gemfibrozil on fluvastatin uptake into primary human hepatocytes was observed (27%). Therefore, the choice of in vitro model and the interpretation of the data need to be put into context and considered fully when extrapolating to the clinical scenario [Noe´ J et al 2007].

1.5.2. Cyclosporin A

CsA is being used in this study, but has been used previously by other groups and a listing of the *in vitro* systems, the substrates and the IC_{50} (or Ki) values are detailed in Table 1.5. The cell lines used included human hepatocytes, as well as Chinese hamster ovary (CHO), human embryonic kidney (HEK293), Madin-Darby canine kidney (MDCKII), recombinant vaccinia HeLa and oocyte (*Xenopus laevis*) cell lines, all over-expressing the relevant OATP transporter.

Table 1.3. A summary of the clinically relevant substrates (and estradiol glucuronide, EG) of organic anion transporting polypeptides (OATP) 1B1 and 1B3*.

Substrate	In Vitro System	OATP1B1 Km (μM)	OATP1B3 Km (μM)	Reference
Atorvastatin	HEK293	12.4	NI	Kameyama 2005
Bosentan	CHO	44	141	Treiber 2007
Fexofenadine	MDCKII	+	108	Matsushima 2008
EG	HEK293	8.2		Cui 2001
	HEK293	2.5		Yamazaki 2005
	HEK293	5.4		Gui 2008
	HEK293	5.9		Gui 2009
	HEK293	8.29		Hirano 2004
	HEK293	5.6		Ulvestad 2007
	XL Oocyte	5.9		Ulvestad 2007
	HepRG	22.3		Ulvestad 2007
Glyburide	NI	NI	NI	
Pitavastatin	HEK293	3.0	3.3	Hirano 2004
	XL Oocyte	6.7		Deng 2008
Repaglinide	NI	NI	NI	
Rosuvastatin	HeLa**	4.0	9.8	Ho 2006
	XL Oocyte	7.3		Brown 2001
	XL Oocyte	+		Simonson 2004
	XL Oocyte	8.5		Schneck 2004
	HEK293	0.802		Kitamura 2008
Simvastatin	NI	NI	NI	

*List of substrates taken from Bloomer et al 2013
**recombinant vaccinia
+ = substrate, but no value calculated
NI = no information
XL = Xenopus laevis

Table 1.4. A summary of the clinically relevant inhibitors of organic anion transporting polypeptides (OATP) 1B1 and 1B3*.

Compound	Cell Type	Substrate	OATP1B1 IC_{50} (μM)	OATP1B3 IC_{50} (μM)	Reference
Clarithromycin	HEK293 HEK293	BSP Pitavastatin	96 8.26	32 NI	Seithal 2007 Hirano 2006
Eryththromycin	HEK293 HEK293	BSP Pitavastatin	217 11.4	34 NI	Seithal 2007 Hirano 2006
Fruit Juices			NI	NI	
Gemfibrozil	HEK293 XL Ooctyes MDCKII HeLa	Pitavastatin Rosuvastatin Cerivastatin Rosuvastatin Fluvastatin	25.2 4.0 72 25 63	NI NI NI ND* >100 NI	Hirano 2006 Schneck 2004 Shitara 2004 Ho 2006 Noe´ 2007
Itraconazole	HEK293	Pitavastatin	>100	NI	Hirano 2006
Lopinavir	CHO	CGamF	0.5	2.0	Annaert 2010
Nelfinavir	HeLa CHO	EG CGamF	0.93 ND**	NI ND**	Tirona 2003 Annaert 2010
Ritonavir	HEK293 HeLa CHO	Pitavastatin EG CGamF	0.78 0.71 1.6	NI NI 3.6	Hirano 2006 Tirona 2003 Annaert 2010

*List of inhibitors taken from Bloomer et al 2013
NI = No information
ND* = Not determined, but greater than 100 μM
ND** = Not determined, solubility limited top concentration to 20 μM
CGamF = cholyl-glycylamido-fluorescein
BSP = sulphobromophthalein
EG = estradiol-17β-D-glucuronide

Of particular relevance was the study that used human hepatocytes to determine the mechanism of the clinically relevant drug-drug interaction (DDI) between cerivastatin and CsA and the potential role of the transporter(s) involved [Shitara et al 2003b]. Cerivastatin uptake into hepatocytes was inhibited by CsA, with quoted Ki values ranging between 0.3-0.7 μM. The authors also determined the Ki in MDCKII cells over-expressing OATP1B1 and quoted a Ki of 0.2 μM. The conclusion from these data is that the DDI *in vivo*, is likely to be mediated at least in part by OATP1B1.

Two studies used rosuvastatin as the substrate, in HeLa recombinant vaccinia and oocyte over-expressed cell lines [Ho et al 2006; Simonson 2004]. In the HeLa cell lines the IC_{50} values quoted for OATP1B1 and OATP1B3 were 0.31 and 0.06 µM, respectively, in good agreement with our data. With the oocytes, the IC_{50} value was higher at 2.2 µM, which may reflect the cell line used.

We have also used the OATP1B1 and OATP1B3 probe substrate EG in the paediatric human hepatocytes and OATP1B1 and OATP1B3 over-expressed MDCKII cells [Gertz et al 2012]. In the hepatocytes, the IC_{50} value was 0.055 µM and in the over-expressed OATP1B1 and OATP1B3 cells the IC_{50} values were 0.019 and 0.032 µM, respectively. In a study with HEK293 cell lines, Campbell et al 2004 obtained an IC_{50} value of 0.2 µM. However, here the authors added the CsA at the same time as EG and did not pre-incubate, which we have found lead to a less potent inhibition.

Other statins, atorvastatin and pitavastatin, have been used as substrates in HEK293 cells over-expressing OATP1B1 and had IC_{50} values of 0.021 and 0.24 µM, respectively [Amundsen et al 2010; Hirano et al 2006]. Other substrates included, phallodin, bosentan and 8-fluoroscein-cAMP [Fehrenbach et al 2003; Treiber et al 2007; Bednarczyk D 2010]. The overall IC_{50} values for over-expressed OATP1B1 and OATP1B3 cell lines ranged from 0.021 – 0.7 µM, a 30-fold difference. However, comparison of like substrates with different cell lines is interesting. With cerivastatin, the IC_{50} values for human hepatocytes and MDCKII-OATP1B1 cells were very similar (within 2-3-fold), but in contrast, with rosuvastatin in HeLa and oocyte cell lines there was a difference (7-fold). Within the same cell line, but with different substrates, a similar trend is observed. The IC_{50} values for pitavastatin and EG transport are similar, but against atorvastatin, CsA was 10-fold more potent.

Although CsA has clearly demonstrated inhibition of substrate transport in OATP1B1 and OATP1B3 over-expressed cell lines, there are differences in the IC_{50} values obtained, which might be due to the different types of cell lines, the choice of substrates and the pre-incubation time.

1.5.3. Rifampicin

An alternative inhibitor of OATP1B1 and OATP1B3 is the macrolide rifampicin, which has also been used previously by other groups and a listing of the *in vitro* systems, the substrates and the IC_{50} (or Ki) values are detailed in Table 1.6. The cell lines used included, Chinese hamster ovary (CHO), human embryonic kidney (HEK293) and oocyte (*Xenopus laevis*) cell lines, all over-expressing the relevant OATP transporter.

Rifampicin appears not to be as potent an inhibitor of OATP1B1 and OATP1B3 in over-expressed cell lines, with IC_{50} values ranging from 0.99 – 11.9 µM, compared to 0.021 – 0.8 µM for CsA. With similar substrates, atorvastatin, bosentan and 8-fluoroscein-cAMP, CsA potency was 2 - 155-fold greater than rifampicin [Lau et al 2007; Trieber 2007; Bednarczyk D 2010]. This also seems to be the case with cryopreserved human hepatocyte suspensions, where uptake of EG and ES were inhibited to 48% and 70% of the control value, respectively, by rifampicin at 25 µM [De Bruyn et al 2011].

It is interesting that rifampicin is quoted as a potent inhibitor of OATP1B1 and OATP1B3 and clinical interactions with rosuvastatin have been reported, but there appears to be no data using rosuvastatin as the substrate and rifampicin as the inhibitor *in vitro*.

1.5.4. Human immunodeficiency virus protease inhibitors

Lopinavir and ritonavir both inhibited transport of cholyl-glycylamido-fluorescein (CGamF) in OATP1B1 and OATP1B3 over-expressed Chinese hamster ovary (CHO) cell lines, with IC_{50} values ranging from 0.5 – 3.6 µM [Annaert et al 2010]. An IC_{50} could not be calculated for nelvinavir due to solubility issues, but atazanavir, darunavir and saquinavir had IC_{50} values ranging from 1.7 – 4.8 µM. Similar IC_{50} values were obtained with HEK293 and HeLa cell lines using pitavastatin and EG as substrates [Hirano 2006; Tirona 2007].

1.5.5. Macrolide antibiotics

Clarithromycin and erythromycin inhibited the uptake of pitavastatin in transfected OATP1B1 HEK293 cells, with IC_{50} values of 8.3 and 11.4 µM, respectively [Hirano et al 2006].

Table 1.5. A summary of the inhibition of organic anion transporting polypeptides (OATP) 1B1 and 1B3 in vitro, by cyclosporin A.

Transporter	Cell Type	Substrate	IC_{50} (μM)	Reference
All	Human hepatocytes	Cerivastatin	0.3- 0.7**	Shitara 2003
OATP1B1	MDCKII	Cerivastatin	0.2**	Shitara 2003
	HEK293	Atorvastatin	0.021	Amundsen 2010
	HEK293	Phalloidin	0.051**	Fehrenbach 2003
	HEK293	Estradiol-17β-D-glucuronide	0.2**	Campbell 2004
	HEK293	Pitavastatin	0.24**	Hirano 2006
	HEK293	Estradiol-17β-D-glucuronide	0.02 (0.25)	Gertz 2012
	HeLa*	Rosuvastatin	0.31	Ho 2006
	HeLa*	Estradiol-17β-D-glucuronide	0.37	Tirona 2003
	XL Oocytes	Rosuvastatin	2.2	Simonson 2004
	CHO	Bosentan	0.3	Trieber 2007
	CHO	8-fluorescein-cAMP	0.25	Bednarczyk 2010
OATP1B3	HeLa*	Rosuvastatin	0.06	Ho 2006
	CHO	Bosentan	0.8	Trieber 2007
	CHO	8-fluorescein-cAMP	0.2	Bednarczyk 2010
	HEK293	Estradiol-17β-D-glucuronide	0.03 (0.21)	Gertz 2012

*recombinant vaccinia
** Ki (μM) quoted and not IC_{50}
XL = Xenopus Laevis

In HEK293 with over-expressed OATP1B1 and OATP1B3 the uptake of sulphobromophthalein (BSP) was inhibited by clarithromycin and erythromycin, with IC_{50} values for OATP1B1 and OATP1B3 of 96 and 217 μM, respectively and 32 and 34 μM, respectively [Seithel et al 2007]. Pravastatin uptake was also inhibited by clarithromycin and erythromycin, but IC_{50} values were not calculated. Instead, the inhibited uptake was determined at two concentrations (10 and 100 μM). Clarithromycin and erythromycin

inhibited the uptake of pravastatin by 60 and 30% and 0 and 50% for 10 and 100 µM, respectively. This would suggest that the IC_{50} values would be between 10 and 100 µM for clarithromycin and approximately 100 µM for erythromycin.

1.5.6. Gemfibrozil

The IC_{50} values quoted for the inhibition of OATP1B1 by gemfibrozil of a variety of statins in different cell lines varied from 4 – 72 µM [Hirano et al 2006; Schneck et al 2004; Shitara et al 2004; Ho et al 2006; Noe´ et al 2007]. In addition, the major metabolite of gemfibrozil, namely gemfibrozil-1-O-glucuronide, also inhibited OATP1B1 [Shitara et al 2004; Hirano et al 2006]. Despite the varied and quite high IC_{50} values quoted for genfibrozil, DDIs are still thought possible with OATP1B1 substrates because plasma concentration can reach 250 µM [Ho et al 2006].

Clinically, gemfibrozil increased rosuvastatin plasma concentrations approximately 2-fold, similar to its interaction with pravastatin, simvastatin acid and lovastatin acid, but substantially less than the effect observed for cerivastatin [Schneck et al 2004]. The authors concluded that gemfibrozil inhibited OATP1B1 and reduced rosuvastatin hepatic uptake. Further, gemfibrozil-1-O-glucuronide was shown to have a greater unbound concentration in the liver and plasma than parent gemfibrozil and its inhibition of the CYP2C8-mediated metabolism of cerivastatin appears to be the main mechanism for the clinically relevant DDI observed [Shitara et al 2004].

In double transfected MDCKII cell lines, OATP1B1/BCRP, OATP1B1/MDR1 and OATP1B1/MRP2, CsA decreased the trans-cellular transport of pitavastatin and its efflux clearance. However, gemfibrozil and gemfibrozil-1-O-glucuronide did not alter either [Hirano et al 2006].

1.5.7. Fruit juice

Limited data are available for the inhibition of OATP1B1 and OATP1B3 by fruit juices, but other data for different OATPs are reported. Grapefruit juice reduced the exposure of fexofenidine probably by the inhibition of the intestinal OATP transporter 1A2 [Dresser et al 2005; Bailey D 2010]. In HEK293 cells over-expressing OATP2B1 the transport of ES was inhibited by grapefruit juice and orange juice [Satoh et al 2005].

Table 1.6. A summary of the inhibition of organic anion transporting polypeptides (OATP) 1B1 and 1B3 in vitro, by rifampicin.

Transporter	Cell Type	Substrate	IC_{50} (μM)	Reference
OATP1B1	HEK293	Atorvastatin	3.25	Lau 2007
	HEK293	Gd-EOB-DTPA*	11.9	Leonhardt 2010
	HEK293	Pitavastatin	0.17 – 0.48	Hirano 2006
	HeLa	Estradiol glucuronide	0.94	Tirano 2003
	CHO	Estradiol glucuronide	1.5	Gui 2008
	CHO	Bosentan	3.2	Trieber 2007
	CHO	8-fluorescein-cAMP	0.99	Bednarczyk 2010
OATP1B3	CHO	Bosentan	1.6	Trieber 2007
	CHO	8-fluorescein-cAMP	0.65	Bednarczyk 2010
	XL Oocytes	BSP	5	Vavricka 2002
	HEK293	Gd-EOB-DTPA	1.4	Leonhardt 2010

*gadolinium-ethoxybenzyl-diethylenetriamine pentaacetic acid (Gd-EOB-DTPA)
XL = Xenopus Laevis
BSP = Sulphobromophthalein

1.5.8. Summary

The *in vitro* and clinical DDI observations, in particular with gemfibrozil, show that understanding the complete mechanism of a DDI can be very complex. The interaction not only involves the disposition of the victim substrate to be fully understood, but also the disposition of the inhibitor as well. With gemfibrozil, its main metabolite the glucuronide, also demonstrates the potential to inhibit metabolism as well as transporters. Cerivastatin has metabolic clearance by CYP2C8, in addition to OATP1B1. Any *in vitro* system hoping to provide meaningful data has to replicate these processes otherwise a false conclusion may be drawn [Noe´ et al 2007].

1.6. Mass spectrometry

1.6.1. Introduction

Mass spectrometry (MS) is based upon the movement of a charged particle (ion) in an electric or magnetic field. The mass to charge ratio, *m*/*z*, where *m* is the mass and *z* is the charge, is a measure of the ions mass. The mass spectrometer consists of an inlet region, a

source, a mass analyser and a detector. From the inlet region, the sample is introduced into the source, where it is ionised and accelerated into the mass analyser. Both of these regions are under high vacuum, to prevent ion-molecule interactions. The mass analyser separates ions, either in space or in time, according to their *m*/*z* ratio. After the ions are separated, they are detected and the signal is transferred to a data system for analysis.

1.6.2. Experimental design

Mass spectrometry is used in all phases of drug discovery and development including structural characterization of new compounds, high throughput screening assays, *in vitro* and *in vivo* absorption, distribution, metabolism and excretion (ADME) assays, quantification of parent (key metabolites) in non-clinical and clinical pharmacokinetic studies, detection and identification of drug metabolites and biomarker quantification.

Isolated hepatocytes allow the interplay between phase I and phase II metabolism as well as uptake and/or efflux drug transporters [Soars et al 2007]. Numerous studies to determine the uptake of substrates into hepatocytes have been published, using different methods of bio-analysis. Radio-labelled substrates, such as taurocholate and estradiol glucuronide, with limited metabolism and very low permeability can be analysed accurately and quickly by liquid scintillation counting [Shitara et al 2003a]. The uptake of radio-labelled marketed drugs with similar chemical properties, such as pravastatin, rosuvastatin, cervivastatin, fexofenidine, cimetidine and nizatidine have also been determined [Watanabe et al 2009; Nezasa et al 2003; Shitara et al 2004; Poirier et al 2008; Nakamura et al 1994].
However, the choice of radio-labelled compounds is limited and LC/MS-MS can be used to quantify the substrate concentration and/or key metabolites that may be produced. In several studies that compared metabolic clearance values derived in hepatocytes, with those from liver microsomes, numerous and diverse probe substrates, including tolbutamide, diclofenac, S-warfarin, S-mephenytoin, dextromethorphan, bufuralol, quinidine, nifedipine, testosterone, terfenadine, theophylline, midazolam, triazolam, diazepam, flunitrazepam and alprazolam were analysed using LC/MS-MS methods [Brown et al 2007 & 2010; Hallifax et al 2008].

In other studies using plated hepatocytes, the role of uptake and efflux transporters were determined using various probe substrates, including atorvastatin, cerivastatin, indomethacin, pravastatin, cerivastatin, bosentan, fluvastatin, rosuvastatin, valsartan, repaglinide, saquinavir, ritonavir, erythromycin, clarithromycin, nateglinide, repaglinide, fexofenadine,

bosentan, olmesartan and valsartan [Paine et al 2008; Jones et al 2012; Gardiner and Paine 2011; Li A et al 2010; Yabe 2011; Abe et al 2009].

Rosuvastatin has limited metabolism and poor permeability and is therefore a good choice for *in vitro* and *in vivo* radio-labelled studies [Nezasa 2002a, 2002b, 2003]. It is hydrophilic, with a log $D_{7.4}$ of −0.33 and an estimated pKa of 4.2-4.6 [Chapman and McTaggart 2002; Varma et al 2011]. Therefore it would exist primarily in the anionic form at physiological pH and the pH-partition driven permeability would be predicted to be very low. The calculated passive membrane permeability values were, 0.25 and 0.28 $x10^{-6}$ cm/sec in Caco-2 and MDCK cells, respectively [Li et al 2012].

In clinical studies using [^{14}C]-rosuvastatin, the majority of the dose was recovered in the faeces (90%), with the remainder in the urine (10%) [Chapman and McTaggart 2002]. The majority of the radioactivity in the faeces (92%) was unchanged parent, with less recovered in the urine (50%). This would suggest limited metabolism of rosuvastatin *in vivo*. *In vitro* studies with human liver microsomes, heterologously expressed CYP enzymes and cultured human hepatocytes suggested a limited role for CYP2C9 and CYP2C19 in the metabolism of rosuvastatin.

However, despite the advantages of radio-labelled analysis, in this study the choice to use LC/MS-MS to analyse rosuvastatin stemmed from several observations. Firstly, the radio-chemical stability of tritiated rosuvastatin in our experience was very poor, with degradation observed even with new batches [Figure 1.8; Appendix 1]. Radio-labelled carbon (^{14}C) would probably be more stable and these have been used previously, however, the cost of producing ^{14}C rosuvastatin is prohibitive (~£40,000). Secondly, within the bio-analytical department at GSK Ware, there already existed a robust LC/MS-MS methodology to quantify rosuvastatin in biological matrices. Although cell lysates had not been used before this study, numerous and diverse *in vivo* and *in situ* samples had been previously processed effectively [Hobbs et al 2012 and Iusuf et al 2013]. In addition, several studies have been published that have used LC/MS-MS to determine the uptake of rosuvastatin into plated hepatocytes [Abe et al 2008 & 2009; Bi et al 2006; Fukuda et al 2008; Ménochet et al 2012a and 2012b; Nakakariya et al 2012].

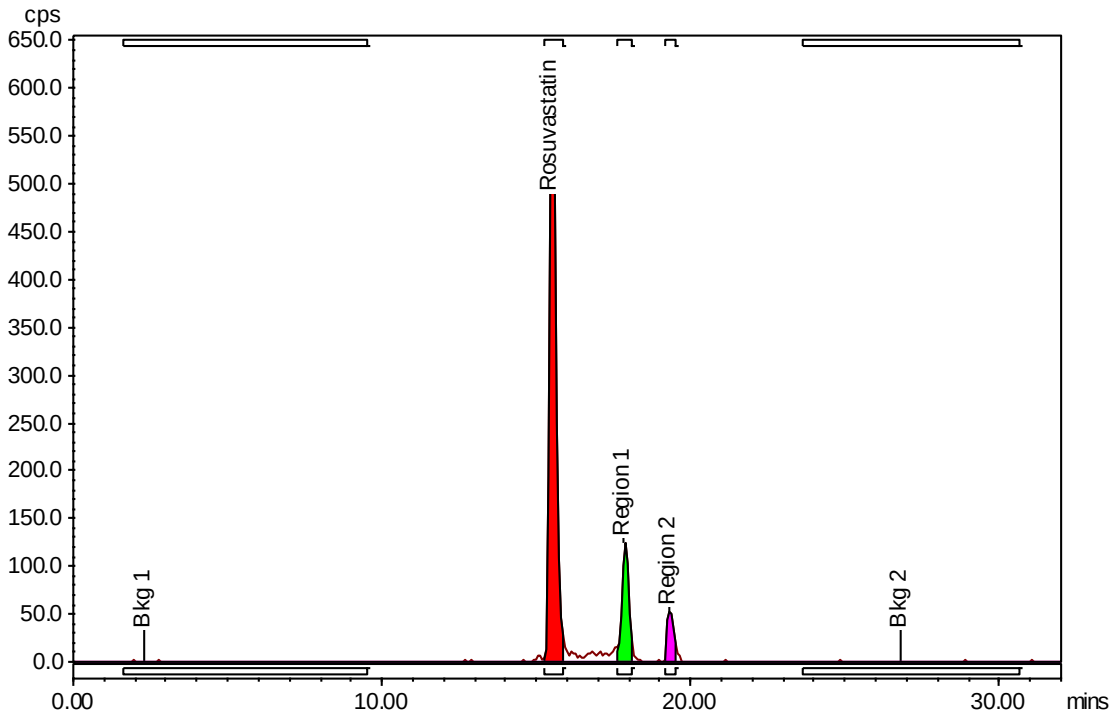

Figure 1.7. Representative radio-chromatogram for the purity check [^{3}H]-rosuvastatin

Other forms of liquid chromatography using alternative detectors such as UV, were dismissed as they do not have the sensitivity required and also require complex chromatography conditions to separate the analyte from endogenous chemicals that have similar UV spectra.

For these studies we have used UPLC by Waters Aquity System and a Sciex API-4000 mass spectrometer from Applied Biosystems/MDS. The chromatography conditions are isocratic and used a Synergi Fusion column (50 x 3 mm, 4µ) (Phenomenex, Torrance, CA.). The internal standard is a stable isotope label of rosuvastatin.

The chromatography systems of the other authors varied, but only Fukada et al used UPLC (Waters Aquity System), the others used the more traditional reversed phase HPLC [Abe et al 2008 & 2009; Bi et al 2006; Fukuda et al 2008; Ménochet et al 2012a and 2012b; Nakakariya et al 2012]. The types of columns varied and included Luna C18 column (3 µ 50 x 4.6 mm) (Phenomenex, Torrance, CA), Aquasil C18, 50 x 2.1-mm column, with a 5-µ particle size (Thermo Electron Corporation, Waltham, MA), Acquity UPLC BEH C18 column (50 mm x 2.1 mm, 1.7µ particle size; Waters) and Shim-pack XR-ODS C18 column (20 x 2.0 mm, 5 µ; Shimadzu).

With the exception of Ménochet et al and Fukuda et al the authors also used Sciex API-4000 mass spectrometers from Applied Biosystems/MDS. Ménochet and Fukuda used a Micromass Quattro Ultima mass spectrometer (Waters, Milford, MA) and a Quattro Premier XE tandem quadrupole mass spectrometer (Waters), respectively.

1.6.3. History of the mass spectrometer

MS has developed into a very important research tool and has enabled scientific breakthroughs, such as the discovery of isotopes, the exact determination of atomic weights, the characterisation of new elements, quantitative gas analysis, stable isotope labelling, fast identification of trace pollutants and drugs and the characterisation of molecular structure.

Sir J.J. Thompson laid the foundations of mass spectrometry with his discovery of the electron, using an electric field inside a cathode ray tube. The first mass spectrometer (parabola spectrograph) generated ions in a discharge tube, which were passed into electric and magnetic fields and the rays detected on a fluorescent screen or photographic plate.

Aston and Dempster, both students of Thompson, developed the mass spectrometer further. Aston's design dispersed and focused ions by mass and velocity, which improved the resolution and Dempster developed a magnetic deflection instrument with direction focusing, a format later adopted commercially and still in use today. Dempster also developed the first electron impact source, which ionises volatile molecules with a beam of electrons from a hot wire filament. Electron impact ion sources are still very widely used in modern mass spectrometers.

In the 1940's mass spectrometry developed into areas such as nuclear isotope enrichment and the analysis of the components of petroleum. Alfred Nier separated uranium-235 from uranium-238 and the Consolidated Engineering Corporation produced an analytical mass spectrometer, based upon Dempster's single-focusing design, which was used in the petroleum industry. The World's first commercial instrument became available in 1948, the MS-2 marketed by Metropolitan Vickers in Manchester, England. Other manufacturers included Westinghouse and General Electric in the U.S. and Atlas-Werke in Germany.

In the early 1950's, the fragmentation of small organic molecules was beginning to be understood and magnetic deflection instruments (Dempster, Mattauch-Herzog and Nier-

Johnson) were used for the identification of organic compounds. These instruments were used into the 1990's before the cheaper time-of-flight (TOF), quadrupole and ion trap mass spectrometers became more widely available.

The TOF-MS instrument was proposed by William Stephens in 1946 and further developed by the Bendix Corporation (Wiley and Maclaren) in the 1950's. However, it wasn't until 1974 that the mass resolution was greatly improved by Boris Mamyrin. In the 1950's the Dow Chemical Company (Gohlke and McLafferty) in collaboration with the Bendix Corporation (Wiley and Maclaren) coupled TOF-MS and gas chromatography (GC). In the 1960's GC-MS developed with the advent of carrier gas separators that removed the GC carrier gas prior to sample introduction into the high-vacuum mass spectrometer.

In the 1950's Wolfgang Paul designed the quadrupole mass filter which was also compatible with GC. Although not as accurate and precise as double-focusing instruments, they are fast, which is important for GC detection. Paul also designed the quadrupole ion trap and in 1983 Finnigan (Stafford and co-workers) produced a GC-ion trap system instrument. Today, ion trap instruments are coupled with Liquid Chromatography (LC), as well as being used as standalone instruments.

In 1968 Jennings and McLafferty introduced the collision-induced dissociation procedure (tandem MS). In 1980, one of the most popular types of tandem MS instrument, the triple quadrupole mass spectrometer, was introduced first by Finnigan and Sciex.

Other MS detection instruments include the ion cyclotron resonance MS (ICR MS) which developed further into Fourier transform ICR mass spectrometry (FT-ICR MS). The major advantage of FT-ICR MS is that it allows many different ions to be determined at once, instead of one at a time. The technique is also known for its mass resolution, which is higher than that of any other type of mass spectrometer.

Novel ionisation techniques have extended the capabilities of MS beyond those available with the electron impact source. Field ionisation allows the determination of non-volatile or thermally unstable molecules, such as biologicals. Chemical ionisation MS ionises volatile molecules and is referred to as 'soft' ionisation technique because the process is less energetic than electron impact ionisation and generates fewer fragment ions.

A variety of desorption MS techniques have been developed recently and include electrospray ionisation MS (ESI MS) and matrix-assisted laser desorption/ionisation MS (MALDI MS), which allows the study of large bio-molecules.

1.6.4. Sample introduction

Sample introduction depends upon the sample type, but as most ionisation techniques are designed for molecules in the gas phase, the inlet must transfer the sample in this state. Gases and high vapour pressure samples can be introduced directly, but liquids and solids may require heating.

The Direct Vapour Inlet (DVI) is the simplest method where the sample is introduced directly into the source region of the mass spectrometer through a needle valve. This technique is limited to stable compounds with high vapour pressures. The Direct Insertion Probe (DIP) can be used to introduce low vapour pressure liquids and solids, where the sample is loaded into a short capillary tube at the end of a heated sleeve, inserted through a vacuum lock into the source region and the temperature increased to vaporise the sample. This method is more complex than DVI, but can be used for a wider range of samples.

Chromatography techniques separate complex samples on a column, with GC separating gases and Liquid Chromatography (LC) liquids, with detection using a MS. With GC, capillary columns have a low carrier gas flow rate such that the sample is introduced directly into the source region, whereas wide bore capillaries and packed GC columns have higher flow rates and therefore the gas flow must be reduced. LC allows thermally labile compounds not easily separated by GC to be quantified and identified. However, the use of temperature sensitive compounds means the sample is ionised directly from the condensed phase. Direct Ionisation (DI) is used where samples either decompose when heated or have no significant vapour pressure. These samples are introduced into the mass spectrometer by direct ionisation from the condensed phase and are used for LC/MS-MS, glow discharge mass spectrometry, fast atom bombardment and laser ablation.

1.6.5. Ionisation techniques

Ionisation techniques can form radical cations (M^+) by removing an electron from the neutral analyte or produce adduct ions by a chemical reaction between an ion and a neutral molecule (MH^+). Electron and chemical ionisation are used when the sample is in the gas phase, but to

ionise condensed phase samples, fast atom bombardment, secondary ion mass spectrometry, electrospray and matrix assisted laser desorption are required. The ionisation energy determines the amount of fragmentation, which can complicate the mass spectrum, but can also provide structural information for the identification of unknown compounds. Soft techniques produce only the ionised analyte and others can produce multiple fragments.

Electron Ionisation (EI) is used with many gas phase molecules, where electrons are produced and accelerated by an electric field to produce a high energy beam which can remove an electron from the analyte and form a radical cation (M+). Although the mass spectra are very reproducible, it can cause extensive fragmentation so that the molecular ion is not observed for many compounds.

Chemical Ionisation (CI) produces ions with little excess energy and less fragmentation. In CI the electron beam, the reagent gas and the sample are enclosed in a small cell. A cloud of ions are produced when the reagent gas is ionised with an electron beam. The reagent gas ions are proton donors and convert the analyte molecules (M) to produce MH+ ions. The most common reagent gases are methane, isobutane and ammonia.

Fast Atom Bombardment (FAB) and Secondary Ion Mass Spectrometry (SIMS) focus a beam of rare gas neutrals (FAB) or ions (SIMS) onto the liquid or solid sample. These high energy beams cause the analyte molecules to 'sputter' into the gas phase and ionise in a single step. Neither technique requires heating and both are useful for studying thermally labile compounds that decompose in conventional inlets. In FAB the analyte is dissolved in a liquid matrix, a droplet of which is placed at in an insertion probe and introduced to the source region. The fast atom beam is focused on this droplet to produce analyte ions. With SIMS, the technique studies surface species and solid samples. The ionising beam is focused directly on the sample to study surface chemistry.

Atmospheric Pressure Ionization (API) sources ionise thermally labile samples directly from the condensed phase at atmospheric pressure and then transfer the ions into the mass spectrometer. Electro Spray Ionisation (ESI) is the most common API application and can be used for LC/MS-MS of thermally labile and high molecular weight compounds. An electro-spray is created by applying a large potential between the inlet needle and the first API source to produce multiply charged ions, where high molecular weight compounds are

observed at lower *m*/*z* ratios. This increases the mass range of the analyzer so that higher molecular weight compounds may be analyzed with a less expensive mass spectrometer e.g. quadrupole analyzer.

API Sources can also be used for Inductively Coupled Plasma Mass Spectrometry (ICP/MS) and glow discharge experiments. With ICP/MS nebulised liquid samples are ionised by a high temperature plasma. These ions are introduced to the mass spectrometer using a series of differentially pumped regions similar to the electro-spray technique. Glow discharge experiments are similar, but are used for solid samples. The high sensitivity and selectivity of the mass spectrometer provides rapid multi-element detection at very low levels.

Matrix Assisted Laser Desorption/Ionisation (MALDI) can be used to analyse extremely large molecules and works by a single laser pulse causing both desorption and ionisation. The analyte and a matrix compound, which can absorb the laser wavelength, are mixed and placed upon a probe tip and dried. A vacuum lock is used to insert the probe into the source region of the mass spectrometer and a laser beam is then focused on this dried mixture and the energy from a laser pulse is absorbed by the matrix. This energy ejects analyte ions from the surface so that a mass spectrum is acquired for each laser pulse. The mechanism for this process is not well understood and is the subject of much controversy in the literature. This technique is more universal (works with more compounds) than other laser ionisation techniques because the matrix absorbs the laser pulse. With other laser ionisation techniques, the analyte must absorb at the laser wavelength. Typical MALDI spectra include the molecular ion, some multiply charged ions and very few fragments.

There are other ionisation methods used for mass spectrometry which include Field Desorption, typically used for non-polar polymers and petroleum samples, Plasma Desorption (PD) used to analyse high molecular weight compounds (before MALDI) and Resonance Ionisation Mass Spectrometry (RIMS) used for selective atomic and molecular ionisation. Photoionisation with lasers, lamps, and synchrotron sources are used to study the photochemistry and energetics of many compounds.

1.6.6. Mass analysers

Ions formed in the source region are accelerated into the mass analyser by an electric field and separated by their *m*/*z* ratio. Each type of analyser has its own advantages and choice

will depend upon the resolution, mass range, scan rate and detection limits required. They can be continuous (quadrupole filters and magnetic sectors) or pulsed (time-of-flight, ion cyclotron resonance and quadrupole ion trap).

1.6.7. Quadrupole

Ions accelerated out of the source into the quadrupole are filtered according to their *m*/*z* ratio so that only a single *m*/*z* ratio ion is detected. Radio frequencies (RF) and direct current voltages applied to the electrodes produce an oscillating electric field that can select the required *m*/*z* ratio. The quadrupole analyser consists of four electrodes connected in pairs and the radio frequency potential applied causes the top and bottom electrodes to be positive and the right and left negative. In the second cycle, these polarities are reversed and this causes the ions to undergo a complex set of motions that produces a three-dimensional wave.

The compact size, fast scan rate, high transmission efficiency and modest vacuum requirements make the quadrupole the most common and inexpensive mass analyser instrument. Many are limited to unit *m*/*z* resolution and have a mass range from *m*/*z* 500 - 4000.

1.6.8. Magnetic sector

J.J. Thompson's first mass spectrometer used a magnet to measure the *m*/*z* of an electron. In a magnetic sector instrument ions are accelerated (faster than quadrupole) from the source region into the magnetic sector and the charged ions are deflected by the magnetic field. The radius of this arc depends upon the magnetic field strength, the momentum and the charge of the ion. Only one *m*/*z* value will be detected for a given radius, magnetic field and acceleration voltage. Older magnetic instruments used a photographic plate to simultaneously detect ions at different radii, but modern instruments have a set of slits at a fixed radius to transmit a single *m*/*z* to the detector and some new instruments use multichannel diode array detectors to simultaneously detect ions over a range of *m*/*z* values. They have higher resolution and greater mass range than quadrupole instruments, typically with mass ranges from *m*/*z* 5,000 - 30,000. They are often used in series with an electric sector for high resolution and tandem mass spectrometry experiments.

1.6.9. Electric sector/double focusing mass spectrometers

An electric sector consists of two concentric curved plates where a voltage is applied across the plates to bend the ion beam as it travels through the analyser. The radius of the ion trajectory depends upon the kinetic energy of the ion and the potential field applied across the plates. However, an electric sector will not separate ions accelerated to a uniform kinetic energy, so the electric sector is not useful as a standalone mass analyzer, but is used in series with a magnetic sector. An electric sector improves significantly the resolution of the magnetic sector by reducing the kinetic energy distribution of the ions.

1.6.10. Time-of-Flight

This is a very simple mass spectrometer that does not require a magnetic field and separates ions in time as they travel down a flight tube. Ions are formed in the source by a very fast ionisation pulse and accelerated into the flight tube by an electric field where low *m*/*z* ions are detected first. Their downside is that they have poor mass resolution, but they do have high transmission efficiency, no upper *m/z* limit, very low detection limits and fast scan rates, which may outweigh the low resolution.

1.6.11. Quadrupole ion trap

The Quadrupole ion storage trap mass spectrometer (QUISTOR) consists of a doughnut shaped ring electrodes and two end-cap electrodes and when a combination of RF and DC voltages are applied to the electrodes a quadrupole electric field is created similar to the electric field for the quadrupole mass analyzer. The electric field traps ions in a potential energy well at the centre of the analyser and the mass spectrum is acquired by scanning the RF and DC fields to destabilize low *m*/*z* ions, which are ejected through a hole in one end-cap electrode and are detected. Ions of increasing *m*/*z* value are ejected from the cell and detected and the trap is refilled. The mass resolution of the ion trap is increased by adding a small amount of Helium, which dampens the motion of the ions and increases the trapping efficiency of the analyzer.

1.6.12. Ion cyclotron resonance

The Ion Cyclotron Resonance (ICR) mass spectrometer traps ions in a magnetic field which causes them to travel in a circular path. The ion's cyclotron frequency is determined by the magnetic field strength and the *m/z* value of the ion. The ions are detected by measuring the signal at this cyclotron frequency by placing electrodes on each side of the ions circular orbit.

It has an extremely high mass resolution and is also useful for tandem mass spectrometry experiments. These instruments are very expensive and are typically used for specialized research applications.

1.6.13. Detectors

Ion detection is based upon their charge or momentum and for large signals a faraday cup is used to collect the ions and measure the current. Most detectors amplify the ion signal using a collector similar to a photomultiplier tube. These amplifying detectors include, electron multipliers, channel-trons and multichannel plates. All mass spectrometers operate at very low pressure (high vacuum;10^{-2} to 10^{-5} Pa) to reduce the chance of the ions colliding with other molecules in the mass analyzer and so reduce scattering or fragmentation.

1.6.14. Data system

The final component of a mass spectrometer is the data system, which has evolved from photographic plates and strip chart recorders to data systems that control the instrument, acquire hundreds of spectra in a minute and search tens of thousands of reference spectra to identify an unknown.

1.7. Aims

- The overall aim was to contribute to the understanding of the interplay of hepatic transporters in the disposition of drug substrates and the impact of inhibitors on these processes.
- The uptake parameters of rosuvastatin in cryopreserved plated human hepatocytes and the effect of cyclosporin A (and its main metabolite cyclosporin AM1) upon its kinetics were determined.

Experimental plan

- **Method development**
- Determine uptake kinetic parameters for rosuvastatin uptake in plated paediatric human cryopreserved hepatocytes.
- Determine uptake kinetic parameters for rosuvastatin in sodium free media, as above, to determine the role of Sodium Taurocholate Co-transporting Polypeptide (NTCP).
- Determine inhibition parameters ('IC_{50}') in paediatric human hepatocytes with the inhibitors, rifampicin and cyclosporin A.
- **Main Study Outline**
- Determine uptake kinetic parameters for rosuvastatin uptake in three plated adult human cryopreserved hepatocytes.
- Determine inhibition parameters ('IC_{50}') in three adult human hepatocytes with and without pre-incubation using the inhibitors, cyclosporin A and cyclosporin AM1.
- Determine uptake kinetic parameters for GSK2879552 uptake in the same three plated adult human cryopreserved hepatocytes.
- Evaluate new mechanistic modelling software called 'uptakeFIT'.

CHAPTER 2: METHOD DEVELOPMENT USING PAEDIATRIC HEPATOCYTES.

2.1. Materials and methods

2.1.1. Chemicals

β-Estradiol-17-(β-D-glucuronide) sodium salt (E1127), rifampicin (R3501) and cyclosporin A (30024) were purchased from Sigma-Aldrich, with stated chemical purities of 98.0, 98.0 and 99.7%, respectively. β-Estradiol-17-β-D-glucuronide, [estradiol-6-7-^{3}H(N)] the tritiated radio-labelled version (NET1106), was purchased from Perkin Elmer, with a stated radio-chemical purity of >97%. Rosuvastatin was purchased from Sequoia Research Products, UK, with a stated chemical purity of 99.3%. The stable isotope label (SIL) [$^{2}H_{7}$ $^{15}N_{2}$]-rosuvastatin was supplied by GSK Chemical Development, with a stated chemical purity of 100%. Optiphase Supermix (liquid scintillation fluid) was purchased from Perkin Elmer. All other chemicals were reagent grade or equivalent.

2.1.2. Hepatocyte media

Cell maintenance cocktail-B (A13448, lot 118751) and FBS (A13450, lot 1081541) were purchased from Gibco® Life Technologies, U.K. Williams' medium E (W1878, lot RNBC3580) was purchased from Sigma-Aldrich. Cyro-recovery medium (CHRM, cat 70001, lot PLN00374, Invitrogen CM7000) was purchased from APS Sciences.

2.1.3. Hepatocyte preparation

The human biological samples were sourced ethically and used in accordance with the terms of the informed consents and GlaxoSmithKline's policies on the use of human tissue. Cryopreserved human hepatocytes from one paediatric donor (lots HU4088) were purchased from Invitrogen (Paisley, UK). The hepatocytes were removed from the liquid nitrogen store and thawed immediately in a water bath at 37°C. The vial was completely submerged, kept horizontal and thawed for approximately 90 seconds until the ice crystals disappeared. The contents were decanted into pre-warmed Cryopreserved Hepatocyte Recovery Media (Invitrogen, U.K.) and centrifuged at 60 g for 10 minutes. The supernatant was decanted gently so that approximately 1 mL remained and the pellet re-suspended gently. The volume was made up to 5 mL with Cell maintenance media, which consisted of de-gased Williams' Medium E (500 mL) with Cell Maintenance Supplement Pack (cocktail B 50 mL, Invitrogen, U.K.). Cell viability was determined using the Trypan blue exclusion assay by counting cells on a haemocytometer using light microscopy. The cells were diluted in pre-incubation media

which consisted of the Cell maintenance media described already (100 mL) with foetal calf serum (5 mL) at a cell density of 1,000,000 cells/mL. The cells, in suspension, were added to each well of a 24 well (0.4 mL) collagen I-coated plates and agitated to spread evenly (BD Sciences, Oxford, U.K.). They were incubated at 37°C in a humidified incubator with 5% CO_2. The cells were allowed 4 hours to attach to the matrix and were checked visually for attachment using light microscopy prior to use.

2.1.4. Measurement of estradiol glucuronide uptake in paediatric human hepatocytes

Incubations were carried out in duplicate at 37°C and EG uptake was measured using 6 concentrations (0.3, 1, 3, 10, 30 and 100 µM). The medium was removed after plating and the mono-layers were rinsed three times with pre-warmed serum-free Dulbecco's phosphate-buffered saline (DPBS). EG was dissolved in dimethyl sulphoxide (DMSO) and diluted in DPBS (maximum 1% DMSO). The incubation was started by the addition of the substrate (400 µL) on top of the mono-layers. Incubation times were 0.5, 1, 1.5, 2, 5, 15 and 30 minutes. Cells were washed three times with ice-cold DPBS and triton X (1% v/v in water) was added (200 µL) and left for at least one hour to solubilise the cells. Duplicate aliquots (50 µL) were analysed using a Liquid Scintilant Analyser (Tricarb 2900TR, Perkin Elmer) after the addition of scintillation fluid (10 mL). The radio-chemical purity of EG was determined on the day of use and a representative radio-chromatogram and radio-HPLC conditions are detailed in Appendix 2 and Appendix 3, respectively.

2.1.5. Inhibition of estradiol glucuronide uptake in paediatric human hepatocytes

The uptake of a single concentration of EG (0.3 µM) over 5 minutes was determined with 10 concentrations (6, 3, 1.5, 0.6, 0.3, 0.15, 0.06, 0.03, 0.006 and 0.003 µM) of cyclosporin A (CsA). CsA was pre-incubated with the cells for 30-45 minutes prior to the addition of EG.

The modelling software Phoenix™ WinNonlin® (version 6.1) was used to derive the inhibition constant that reduced the uptake by 50%.

2.1.6. Measurement of rosuvastatin uptake in paediatric human hepatocytes

Incubations were carried out in duplicate at 37°C and rosuvastatin uptake was measured using 6 concentrations (0.3, 1, 3, 10, 30 and 100 µM). The medium was removed after plating and the mono-layers were rinsed three times with pre-warmed serum-free Dulbecco's

phosphate-buffered saline (DPBS). Rosuvastatin was dissolved in DMSO and diluted in DPBS (maximum 1% DMSO). The incubation was started by the addition of the substrate (400 µL) on top of the mono-layers. Incubation times were 0.5, 1, 1.5, 2, 5, 15, 30 and 45 minutes. Cells were washed three times with ice-cold DPBS and water was added (200 µL), left overnight (4°C) and analysed the following morning. An aliquot (25 µL) of the water lysate was prepared as described in the mass spectrometry methods (Section 2.2.3. Sample Preparation and Extraction).

In addition, the uptake of rosuvastatin was determined in sodium free media to reduce the impact of the sodium dependent transporter NTCP. The media was removed and the cells washed five times with a modified Krebs–Henseleit bicarbonate (KHB) buffer containing $MgSO_4$ 1.2 mM, KH_2PO_4 0.96 mM, KCl 4.83 mM, Choline Cl 118 mM, $CaCl_2$ 1.53 mM, Choline bicarbonate 23.8 mM, HEPES 12.5 mM, glucose 5 mM at pH 7.4. Rosuvastatin was administered and analysed as above.

2.1.7. Inhibition of rosuvastatin uptake in paediatric human hepatocytes

The uptake of a single concentration of rosuvastatin (1 µM) over 5 minutes was determined with 10 concentrations of CsA (6, 3, 1.5, 0.6, 0.3, 0.15, 0.06, 0.03, 0.006 and 0.003 µM). The CsA was pre-incubated with the cells for 30-45 minutes prior to the addition of rosuvastatin. Similarly, the uptake of rosuvastatin (1 µM) over 5 minutes was determined with 10 concentrations of rifampicin (0.025, 0.05, 0.25, 0.5, 1.25, 2.5, 5, 12.5, 25, 50µM) also pre-incubated for 30-45 minutes.

2.2 Liquid chromatography and mass spectrometry analysis of rosuvastatin

2.2.1. Preparation of the analyte solutions of rosuvastatin

Analytical stock solutions (100 µg/mL) of rosuvastatin (A/B) were prepared in dimethyl formamide (DMF). These were further diluted in DMF (10, 1 and 0.1 µg/mL) to produce working solutions as detailed in Appendix 4. The A and B stock solutions provided the calibration standards and quality control (QC) samples, respectively. The calibration and QC standards were prepared fresh in control matrix (water) as detailed in Appendices 5 and Appendix 6.

2.2.2.Preparation of analytical solutions of the internal standard.

An internal standard stock solution of [$^{2}H_{7}$ $^{15}N_{2}$]-rosuvastatin (C) was prepared in DMF (2 mg/mL). From this a working solution (500 ng/mL) was prepared in acetonitrile/methanol/formic acid (95/5/0.1 v/v/v) as detailed in Appendix 7.

2.2.3. Sample preparation and extraction

Aliquots (25 µL) of the samples, standards and QCs were mixed thoroughly with an aliquot of internal standard working solution (C1; 500 ng/mL) and centrifuged for 10 minutes at 4000 g. A total blank of water (25 µL) and acetonitrile (100 µL) was prepared in a similar way.

Aliquots (100 µL) of the supernatant were transferred to a clean tube and an aliquot of water (50 µL) added. The tubes were mixed thoroughly and an aliquot injected (10 µL) onto the HPLC MS/MS system for analysis as detailed in Appendices 8, 9 and 10.

2.3. Determination of uptake kinetic parameters using a mechanistic modelling approach.

A two-compartment model, based on the work by Ménochet et al (2012a and b), was implemented in Matlab version R2012a (The MathWorks, Inc., Natick, MA). This model allows simultaneous fitting of all concentration-time points made at 37°C during the experiment. It allows the assessment of multiple processes, namely active uptake into the hepatocytes, bidirectional passive diffusion, and intracellular binding. Later incubation times were included to allow steady state to be reached between concentrations in the media and intracellular compartment. The mechanistic model for the assessment of active uptake in hepatocytes is illustrated in Figure 1.6. Differential equations 2-1 and 2-2 show the change in cell and media concentrations over time, respectively. All parameters are expressed per well and therefore are normalized for the number of cells per well.

Equation 2-1.

$$\frac{dS_{med,u}}{dt} = \frac{\frac{V_{max} \times S_{med,u}}{K_{m,u} + S_{med,u}} + P_{diff,u} \times S_{med,u} - P_{diff,u} \times S_{cell} \times fu_{cell}}{V_{cell}}$$

Equation 2-2.

$$\frac{dS_{med,u}}{dt} = \frac{-\frac{V_{max} \times S_{med,u}}{K_{m,u}+S_{med,u}} - P_{diff,u} \times S_{med,u} + P_{diff,u} \times S_{cell} \times fu_{cell}}{V_{med}}$$

where S_{cell} is the total cell concentration, $S_{med,u}$ is the unbound media concentration (nM), fu_{cell} as a parameter reflects both nonspecific intracellular binding and active processes for transport. V_{cell} intracellular volume of 3.9 µL/10^6 cells, V_{med} media volume of 400 µL (expressed in L), V_{max} (nmoles/min), $K_{m,u}$ (nmoles) and $P_{diff,u}$ (L/min)

The nominal concentrations corrected for fu_{med} were used as initial media concentrations. Initial cell concentrations were obtained by extrapolating the first four time points for each of the concentrations to Time = 0. The rationale was that not all of the drug could be washed from the cell membranes or experimental plates with DPBS during the washing steps.

2.3.1. Statistical Analysis.

A Jacobian approach was used in Matlab to estimate the standard error (S.E.) associated with each parameter estimate generated from the mechanistic two-compartment model. Coefficient of Variations (CV) were calculated to assess the quality of each parameter estimate. Arithmetic means, S.E.s, and CVs associated with each kinetic parameter were calculated for rosuvastatin.

2.4. Determination of the uptake clearance

The uptake clearance (CL_{uptake}; µL/10^6 Cells) of rosuvastatin was determined as the amount of rosuvastatin in the cell (nmol/10^6 Cells) divided by the concentration in the media (nmol/µL) and normalised for time (µL/min/10^6 Cells), using the linear time points (0-2 minutes). The uptake rates were corrected for non-specific binding by subtracting the initial intracellular concentrations at Time = 0 minutes and were averaged to provide a mean CL_{uptake} value for each of the rosuvastatin media concentrations.

In addition, a statistical comparison of the CL_{uptake} between the lowest media (0.3 µM) and highest media concentration (100 µM) was made using a two tailed Student's T-test in Excel. The difference between the CL_{uptake} from the highest media concentration to the lowest is a measure of the contribution of the active saturable process [Shitara et al 2003a].

2.5. Results

2.5.1. Determination of the uptake kinetic parameters based upon a mechanistic modelling approach

The uptake kinetic parameters (V_{max}, $K_{m,u}$, $P_{diff,u}$ and Fu_{cell}) for rosuvastatin and estradiol glucuronide (EG) were determined in cryopreserved paediatric human hepatocytes using a mechanistic two-compartment model developed by Menochet et al (2012a). A summary of the uptake kinetic parameters for rosuvastatin and EG are detailed in Table 2.1 and the predicted and observed uptake profiles of EG, rosuvastatin and rosuvastatin in sodium free media are detailed in Appendices 11, 12 and 13, respectively.

Table 2.1. Summary of the uptake kinetic parameters of rosuvastatin (RSV) and estradiol-17β-D-glucuronide (EG) in plated cryopreserved paediatric human hepatocytes. Each parameter is the mean ± standard deviation (coefficient of variation %).

Substrate	V_{max} (pmol/min/10^6 cells)	$K_{m,u}$ (μM)	$P_{diff,u}$ (μL/min/10^6 cells)	Fu_{cell}
EG	8.82 ± 6.11 (69)	3.52 ± 2.76 (78)	2.40 ± 0.29 (12)	0.39 ± 0.04 (11)
RSV	7.98 ± 2.07 (26)	2.66 ± 0.85 (32)	0.74 ± 0.10 (13)	0.44 ± 0.06 (12)
RSV (sodium free)	24.7 ± 4.50 (18)	6.76 ± 1.33 (20)	0.26 ± 0.09 (33)	1.00 ± 0.32 (32)

The uptake kinetic parameters for EG were, V_{max} 8.82 pmol/min/10^6 cells, $K_{m,u}$ 3.52 μM, $P_{diff,u}$ 2.40 μL/min/10^6 cells and Fu_{cell} 0.39. The uptake kinetic parameter values for rosuvastatin in normal and sodium free media were, V_{max} 7.98 and 24.7 pmol/min/10^6 cells, respectively, $K_{m,u}$ 2.66 and 6.76 μM, respectively, $P_{diff,u}$ 0.74 and 0.26 μL/min/10^6 cells, respectively and Fu_{cell} 0.44 and 1.00, respectively.

2.5.2. Cyclosporin A and rifampicin inhibition of rosuvastatin and estradiol glucuronide uptake

A summary of the inhibition kinetic parameters ('IC_{50}') for the inhibition of the uptake of EG and rosuvastatin by cyclosporin A (CsA) and rifampicin into paediatric human hepatocytes are detailed in Table 2.2. Plots of the inhibition curves of the uptake EG and rosuvastatin by CsA are detailed in Appendices 14 and 15, respectively and inhibition of rosuvastatin by rifampicin is detailed in Appendix 16.

CsA inhibition of EG uptake was very potent, with an IC_{50} value of 0.06 µM. Similar potency was observed when rosuvastatin was used as the substrate, with a value of 0.12 µM, but the potency reduced with rifampicin as the inhibitor, with a value of 3.72 µM.

Table 2.2. Summary of the inhibition kinetic parameters of rosuvastatin (RSV) and estradiol-17β-D-glucuronide (EG) at 1 and 0.1 µM, respectively, incubated for 5 minutes in plated cryopreserved paediatric human hepatocytes following pre-incubation (30 minutes) with cyclosporin A (CsA) and rifampicin. An estimate of the IC_{50}, the standard error (SE) and the coefficient of variation (CV) were derived using the modelling software Phoenix™ WinNonlin® (version 6.1).

Substrate	IC_{50} (µM)	SE	CV (%)
EG + CsA	0.06	0.01	17
Rosuvastatin + CsA	0.12	0.04	61
Rosuvastatin + Rifampicin	3.72	1.01	54

2.5.3. Comparison of the uptake clearance of rosuvastatin in the presence and absence of sodium in the media

The mean data for the uptake clearance (CL_{uptake}) of EG and rosuvastatin in cryopreserved paediatric human hepatocytes is shown in Table 2.3.

Generally, the CL_{uptake} values decrease with an increase in the media concentration for rosuvastatin in normal media, rosuvastatin in sodium free media and EG. In fact there were statistical differences ($p<0.05$ rosuvastatin and EG; $p<0.01$ for rosuvastatin sodium free) between the CL_{uptake} values from the highest media (100 µM) to the lowest media (0.3 µM) for rosuvastatin in normal media, rosuvastatin in sodium free media and EG using a two-tailed Student's T-test in Excel. This would indicate that active saturable processes are involved in the uptake of both of rosuvastatin and EG in these paediatric hepatocytes.

The saturable component of the hepatic uptake process (CL_{hep}) can be determined by subtracting the hepatic uptake clearance CL_{uptake} at 0.3 µM, from the CL_{uptake} at 100 µM [Shitara 2003a]. The CL_{hep} of rosuvastatin in paediatric human hepatocytes was 2.21 and 1.82 µL/min/10^6 cells in the normal and sodium free media, respectively, which equates to 73% of the uptake for both normal and sodium free media *via* saturable processes.

Using a two-tailed Student's T-test in Excel, a comparison of rosuvastatin uptake between a normal and sodium free media at similar concentrations suggested that there were no differences in the CL_{uptake} of rosuvastatin between normal and sodium free media,

Table 2.3. Summary of the uptake clearance (CL_{uptake}) of rosuvastatin (RSV) and estradiol-17β-D-glucuronide (EG) in plated cryopreserved paediatric human hepatocytes with and without sodium in the media. CL_{uptake} was calculated over the linear range (0-2 minutes) at all of the concentrations used (0.1, 0.3, 1, 3, 10, 30 and 100 µM). Each parameter is the mean ± standard deviation (coefficient of variation %)

Concentration (µM)	Mean CL_{uptake} (µL/min/10^6 Cells) ± SD (CV)		
	RSV	RSV sodium free	EG
0.3	3.03 ± 1.94 (64)	2.48 ± 0.79 (32)	2.67 ± 1.45 (54)
1	1.25 ± 0.48 (39)	2.11 ± 0.40 (19)	2.26 ± 0.92 (41)
3	0.89 ± 0.59 (66)	2.39 ± 0.71 (30)	2.14 ± 0.60 (28)
10	1.13 ± 0.29 (26)	1.73 ± 0.35 (20)	1.86 ± 0.93 (50)
30	0.95 ± 0.30 (31)	1.24 ± 0.82 (66)	2.93 ± 1.16 (40)
100	0.82 ± 0.18 (22)	0.66 ± 0.68 (112)	1.45 ± 1.15 (79)

2.6. Discussion

As outlined previously, several different methods have been utilised to determine the uptake kinetic parameters of probe substrates of key transporters into human hepatocytes. These have included primary and cryopreserved suspended and plated cells, with the use of inhibitors and cold temperature (4°C), in combination with various *in silico* models. In this study, the mechanistic modelling method of Ménochet et al 2012 has been used to evaluate the uptake of estradiol-17β-D-glucuronide (EG) and rosuvastatin into a plated cryopreserved paediatric human hepatocyte cell line, to provide preliminary data to help refine the experimental design for the main part of the study.

The choice of paediatric human hepatocytes was based upon the availability and the transporter characterisation of the cell line. The cells were available within the department and because of their donors age were unlikely to be used for project studies. In addition, these cells were platable and had been transporter characterised by the vendor. It is possible that the paediatric cells may have different expression levels of the key transporters and this was considered, but for method development it was felt that it would not be a concern because absolute values were not critical. The method development was to introduce the mechanistic model and determine the optimum time points and concentration values to study rosuvastatin disposition.

The uptake clearance (CL_{uptake}) of EG was determined in the paediatric human hepatocyte and compared with studies published in the literature. As detailed in the methods section, the CL_{uptake} values were corrected for non-specific binding to the cells/matrix and the mean CL_{uptake} of EG at 0.3 µM was 2.67 µL/min/10^6 cells. However, when non-specific binding was not corrected for, the CL_{uptake} value was 8.37 µL/min/10^6 cells. The V_{max}, K_m and P_{diff} values were 8.82 pmol/min/10^6 cells, 3.52 µM and 2.40 µL/min/10^6 cells, respectively.

Shitara et al 2003a determined the utility of cryopreserved hepatocytes versus primary hepatocytes in suspension to study uptake transporters, using the probe substrates EG and taurocholate and a comparison of their data and that in this study is detailed in Table 2.4. They calculated a mean CL_{uptake} of EG with cryopreserved cells of 8.47 µL/min/10^6 cells.

Table 2.4. Summary of the uptake kinetic parameters of estradiol-17β-D-glucuronide (EG) in plated cryopreserved human hepatocytes from this study and that of Shitara et al 2003. Each parameter is the mean ± standard deviation.

Study	V_{max} (pmol/min/10^6 cells)	$K_{m,u}$ (µM)	$P_{diff,u}$ (µL/min/10^6 cells)	CL_{uptake}
Hobbs	8.82 ± 6.11	3.52 ± 2.76	2.40 ± 0.29	2.67 ± 1.45
Shitara	33.1 ± 7.5	8.44 ± 2.86	2.51 ± 0.60	8.47 ± 4.49

Although not detailed in the reference, it is doubtful that Shitara corrected for non-specific binding, which means that the value calculated in this study is in good agreement with their value. The P_{diff} values were very similar between the studies with values of 2.40 and 2.51 µL/min/10^6 cells. The K_m value was lower in this study when compared to Shitara, with values of 3.52 and 8.44 µM, respectively. However, K_m values for EG in alternative cell lines, such as HEK293, oocytes and HepRG, ranged from 2.5 – 22.3 µM, putting the value obtained in this study at the lower end of the range, but still acceptable [Table 1.3.]. V_{max} was lower in this study, 8.82 compared with 33.1 pmol/min/10^6 cells and the consequences of this will be discussed later.

The CL_{uptake} of rosuvastatin in the paediatric human cell line was 3.03 µL/min/10^6 cells (at 0.3 µM), compared to 9.21 µL/min/10^6 cells in the study by Ménochet et al 2012b, where similar methodology was used. The uptake kinetic parameters, V_{max}, K_m, P_{diff} and Fu_{cell} are compared in Table 2.5.

Table 2.5. Summary of the uptake kinetic parameters of rosuvastatin in plated cryopreserved human hepatocytes from this study and that of Ménochet et al 2012. Each parameter is the mean ± standard deviation .

Study	V_{max} (pmol/min/10^6 cells)	$K_{m,u}$ (µM)	$P_{diff,u}$ (µL/min/10^6 cells)	Fu_{cell}
Hobbs	7.98 ± 2.07	2.66 ± 0.85	0.74 ± 0.10	0.44 ± 0.06
Ménochet	104	11.2	0.391	0.477

P_{diff} and Fu_{cell} were similar between the two studies. However, V_{max} and K_m were lower in this study. In alternative cell lines, such as HeLa, HEK293 and oocytes, the K_m values for rosuvastatin ranged between 0.8 – 8.5 µM, spanning the value derived here of 2.7 µM [Table 1.3.]. The V_{max} values were lower in the paediatric cell line, a consequence of the uptake transporters not being as well expressed.

Although in this study the incubation times were much longer (45 minutes) in comparison with the Ménochet study, it is still apparent that steady state had not been reached. In future studies the incubation time will need to increase to help describe the parameters P_{diff} and Fu_{cell} with more accuracy.

The uptake kinetics of rosuvastatin in a media devoid of sodium, which prevents full functioning of the transporters that rely upon sodium ion exchange, in particular Sodium Taurocholate Co-transporting Polypeptide (NTCP) were determined. A comparison of the CL_{uptake} of rosuvastatin between normal and sodium free media with 'like for like' media concentrations, showed that the values were similar. In addition, the K_m and P_{diff} values were similar between the normal and sodium free media, but V_{max} was actually higher in the sodium free media [Tables 2.1. and 2.3.]. The data for the CL_{uptake} values would tend to suggest that NTCP has no role in the initial uptake of rosuvastatin and further the uptake kinetic parameters (V_{max} , K_m and P_{diff}) suggest no role for NTCP over the whole incubation.

The role of NTCP in the uptake of rosuvastatin was first reported by Ho et al 2006, where uptake was determined in fresh human hepatocytes over 1 minute at a concentration of 0.1 µM in normal and sodium free media. The total amount of rosuvastatin was then compared between the two and in the sodium free media there was a ~35% reduction in rosuvastatin. The authors concluded this was due to the inhibition of NTCP, which was therefore

responsible for ~35% of the uptake of rosuvastatin in human hepatocytes. In studies using taurocholate, uptake was reduced ~45 and ~70% in suspended fresh and cryopreserved human hepatocytes in a sodium free media, respectively [Ho et al 2006; Shitara et al 2003]. In cryopreserved hepatocytes the CL_{uptake} of rosuvastatin was reduced by ~28% in sodium free media [Bi et al 2013].

However, it should be remembered that in this study paediatric human cells were used, which may not express NTCP to the same degree as the adult cell lines. Unfortunately, it was not possible to characterise the activity of NTCP in this cell line using the probe substrate taurocholate because there were not enough cells remaining. Another consideration is that, although the media is sodium free and the cells were washed thoroughly with sodium free media, the cells themselves may still contain sodium such that the NTCP transporter can still function adequately over the time frame of the incubations.

There does appear to be a reduction in the CL_{uptake} of rosuvastatin in both media at 100 μM, which may suggest saturation of active uptake processes. This concentration is above the K_m values calculated here and is in excess of the K_m (63 μM) quoted for NTCP in an expressed system quoted by Ho et al 2006.

Inhibition parameters for the uptake of EG and rosuvastatin with cyclosporin A (CsA) and rosuvastatin with rifampicin were also calculated. They have been annotated 'IC_{50}', which is not strictly true, as each inhibitor is known to inhibit multiple transporters, all of which are active in the hepatocytes. The 'IC_{50}' quoted is really a composite of potentially several inhibition mechanisms, but for the sake of clarity the parameter will be called 'IC_{50}' for the purposes of this report.

One of the aims of this study is to determine the role of OATP1B1 in the uptake of rosuvastatin and the effect of inhibiting this transporter with a pan inhibitor, i.e. CsA and an OATP inhibitor, i.e. rifampicin. A comparison between the two inhibitors might show the interplay between the different transporters in the disposition of rosuvastatin.

In a study conducted by ourselves, different pre-incubation times of CsA can lead to different IC_{50} values making a comparison between different studies difficult. A pre-incubation time

of 30 minutes with HEK293 cell lines over-expressing OATP1B1 and OATP1B3 gave IC_{50} values of 0.02 and 0.03 μM, respectively, but without any pre-incubation the IC_{50} values for OATP1B1 and 1B3 were 0.25 and 0.21 μM, respectively [Gertz et al 2012].

To avoid time based pre-incubation issues in this study, CsA was pre-incubated for 30 minutes prior to the addition of the probe substrate. CsA was a very potent inhibitor of EG uptake, with an IC_{50} value of 0.06 μM, in agreement with data that have been published by ourselves [Gertz et al 2012]. Campbell et al 2004 used HEK293 cells and Tirona et al 2003 used HeLa cells and both obtained less potent IC_{50} values of 0.2 and 0.37 μM, respectively, without pre-incubation and in agreement with Gertz et al 2012. The similarity of the IC_{50} values obtained using EG as the probe substrate in this study using human hepatocytes and HEK293 over-expressed cells would suggest that the inhibition observed in the hepatocytes is mediated by CsA inhibition of OATP1B1.

CsA was also very potent inhibitor of rosuvastatin uptake, with an IC_{50} value of 0.12 μM. This value is in agreement with the study by Ho et al 2006, with IC_{50} values for OATP1B1 and OATP1B3 in HeLa recombinant vaccinia cells of 0.31 and 0.06 μM, respectively. In another study by Simonson et al 2004 in *Xenopus laevis* oocytes over-expressing OATP1B1, the IC_{50} value was higher at 2.2 μM, which may reflect the pre-incubation time used. Other statins had IC_{50} values for OATP1B1 of 0.021 μM (atorvastatin HEK293), 0.2 μM (cerivastatin MDCKII) and 0.24 μM (pitavastatin HEK293).

The predominate transporter for EG is OATP1B1 and the similarity of the IC_{50} values obtained with CsA using rosuvastatin and EG as the substrates in the human hepatocytes might suggest that OATP1B1 is also the predominate uptake transporter for rosuvastatin, in conjunction with apparent lack of NTCP activity in this cell line. Both substrates have similar uptake kinetic parameters, limited metabolism and low passive permeability, which may suggest that EG IC_{50} values could be used as a surrogate for substrates with similar properties.

However, with two other statins, atorvastatin and pitavastatin, in HEK293 cells over-expressing OATP1B1, the IC_{50} values ranged 10-fold with CsA inhibition (0.021 and 0.24 μM, respectively) [Amundsen et al 2010; Hirano et al 2006]. The overall IC_{50} values for

over-expressed OATP1B1 cell lines ranged from 0.021 – 0.7 µM, a 30-fold difference [Table 1.5.].

Comparison of like substrates with different cell lines is interesting. With cerivastatin, the IC_{50} values with CsA inhibition for human hepatocytes and MDCKII-OATP1B1 cells were very similar (within 2-3-fold), but in contrast, with rosuvastatin in HeLa and oocyte cell lines there was a bigger difference (7-fold). Within the same cell line, but with different substrates, the IC_{50} values for pitavastatin and EG inhibition are similar, but with atorvastatin, CsA was 10-fold more potent.

Although CsA has clearly demonstrated inhibition of substrate transport by OATP1B1 and OATP1B3 in over-expressed cell lines, there are differences in the IC_{50} values obtained, which might be due to the different types of cell lines, the choice of substrates or the pre-incubation time. The relatively small data set and the different methodologies from different laboratories makes any real comparison and conclusion very difficult. For these reasons therefore, it would be advisable to determine the kinetics and inhibition of the compound of interest and not rely upon probe substrate data sets.

CsA has a C_{max} of approximately 1 µM systemically and with a bioavailability of 30% could give portal vein concentrations of 3 µM [Fahr 1993; Faulds et al 1993]. These concentrations are much higher than the IC_{50} value and it would be expected that following a clinically relevant dose of CsA that OATP1B1 and 1B3 would be inhibited, which may explain the observed interactions with rosuvastatin (and other OATP substrates) in the clinic.

In comparison with CsA, rifampicin was not as potent an inhibitor of rosuvastatin uptake, with an IC_{50} value of 3.72 µM. There does not appear to be any data for rosuvastatin and rifampicin interactions *in vitro*, but the IC_{50} for atorvastatin in HEK293 cells was very similar at 3.25 µM. In general, regardless of the variability observed, the probe substrate used or the type of cell line, rifampicin does not appear to be as potent an inhibitor of OATP1B1 as CsA.

Rifampicin has a C_{max} of approximately 14 µM systemically and although bioavailability can be variable absorption into the portal vein is thought to be high [Pahlda et al 1999]. Therefore, even though the IC_{50} of rifampicin is lower than CsA, its pharmacokinetic profile

would suggest that at a clinically relevant dose OATP1B1 and 1B3 would be inhibited and may explain the observed interactions in the clinic.

Overall, the parameters calculated in this study were in agreement with those published in the literature and these data confirm that the paediatric cryopreserved human hepatocytes used in this study were fully functional with respect to EG and rosuvastatin uptake, which may suggest that the transporters involved (i.e. OATP1B1 and 1B3) were also expressed and functional. They also confirmed that the methodology and the model fitting were robust and also gave confidence that these hepatocytes were more than suitable to guide further method development.

2.7. Conclusions

- Uptake kinetics of estradiol-17β-D-glucuronide (EG) and rosuvastatin in a paediatric human hepatocytes were in agreement with quoted literature values.
- The paediatric human hepatocytes was robust enough to be used as a method development tool to plan for the future studies.
- The IC_{50} values for EG and rosuvastatin as the probe substrates using cyclosporin A and rifampicin were in agreement with quoted literature values and suggested a pre-dominate role for OATP1B1.
- In these paediatric human hepatocytes NTCP did not appear to play a role in the uptake of rosuvastatin. However, certain caveats need to be considered, including that the expression of NTCP in this cell line was not determined.

2.8. Future Studies

- Human hepatocytes from three adult donors have been obtained.
- Perform uptake experiments and determine kinetic parameters with all three donors.
- Use six concentrations (0.3, 1.0, 3.0, 10, 30, 100 µM).
- Use eight time points (0.5, 1.0, 1.5, 2.0, 5.0, 20, 40, 60 minutes) to define the linear and steady state kinetics.
- Determine inhibition parameters ('IC_{50}') in human hepatocytes with;
    - Cyclosporin A
    - Cyclosporin AM1

CHAPTER 3: HEPATIC UPTAKE OF ROSUVASTATIN IN ADULT HUMAN HEPATOCYTES

3.1. Materials and methods

3.1.1. Chemicals

Rifampicin (R3501) and cyclosporin A (30024) were purchased from Sigma-Aldrich, U.K., with stated chemical purities of 98.0 and 99.7%, respectively. Rosuvastatin was purchased from Sequoia Research Products, U.K., with a stated chemical purity of 99.3%. Cyclosporin AM1 (C988915) was purchased from Toronto Research Chemicals, Canada, with a stated chemical purity of 98.0%. The stable isotope label, [$^{2}H_{7}$ $^{15}N_{2}$]-rosuvastatin, was supplied by GlaxoSmithKline, Chemical Development, U.K., with a stated chemical purity of 100%. All other chemicals were reagent grade or equivalent.

3.1.2. Hepatocyte media

The details are as described previously in Chapter 2, section 2.1.2.

3.1.3. Hepatocyte preparation

The human biological samples were sourced ethically and used in accordance with the terms of the informed consents and GlaxoSmithKline's policies on the use of human tissue. Cryopreserved human hepatocytes from three adult donors (lots HU1411, HU8116 and HU8119) were purchased from Invitrogen (Paisley, UK).

Further details are as described previously in Chapter 2, section 2.1.3.

3.1.4. Measurement of rosuvastatin uptake in adult human hepatocytes

The details are as described previously in Chapter 2, section 2.1.6. with the exception of the incubation times, which were extended (0.5, 1, 1.5, 2, 5, 20, 40 and 60 minutes) so that steady state kinetics would be described.

3.1.5. Inhibition of rosuvastatin uptake in adult human hepatocytes

The uptake of a single concentration of rosuvastatin (1 µM) over 3 minutes was determined in the presence of 10 concentrations (6, 3, 1.5, 0.6, 0.3, 0.15, 0.06, 0.03, 0.006 and 0.003 µM) of cyclosporin A (CsA) and cyclosporin AM1 (AM1). CsA and AM1 were co-incubated (i.e. added at exactly the same time as rosuvastatin) and also pre-incubated with the cells for 30-45 minutes prior to the addition of rosuvastatin.

3.2 Liquid chromatography and mass spectrometry analysis of rosuvastatin

The details are as described previously in Chapter 2, sections 2.2, 2.2.1, 2.2.2 and 2.2.3.

3.3. Determination of the uptake kinetic parameters using a mechanistic modelling approach.

The details are as described previously in Chapter 2, sections 2.3. and 2.3.1.

3.4. Determination of the uptake clearance

The details are as described previously in Chapter 2, sections 2.4.

3.5. Prediction of hepatic clearance in human from active uptake clearance measured in human hepatocytes.

The unbound *in vitro* intrinsic clearance ($CL_{int,u}$) for each donor was determined using the parameters V_{max} divided by $K_{m,u}$, as detailed in Table 3.1. These were scaled to *in vivo* intrinsic clearances (CL_u, mL/min/kg) using Equation 3-1 using the physiological scaling factors of hepato-cellularity (120 million cells per gram of liver) and liver weight (21.4 gram of liver per kg of body weight), respectively [Brown et al 2007; Houston and Galetin 2008].

Equation 3-1.

CL_u (*in vivo*) = $CL_{active,u}$ (*in vitro*) x Hepato-cellularity x Liver weight

The unbound *in vivo* intrinsic clearance ($CL_{int,u}$, mL/min/kg) was calculated from the scaled *in vitro* clearances as detailed in Equation 3-2 [Shitara et al 2006].

Equation 3-2.

$$CL_{int,u} = (CL_{active,u} + P_{diff,u}) \times \frac{CL_{met,u} + CL_{bile,u}}{CL_{met,u} + CL_{bile,u} + P_{diff,u}}$$

where $CL_{active,u}$ and $P_{diff,u}$ are the unbound active uptake clearance and the passive diffusion clearance scaled to a whole liver, respectively. $CL_{met,u}$ and $CL_{bile,u}$ are the metabolic clearance and the unbound biliary clearance for rosuvastatin, respectively, derived from a clinical study following an intravenous administration of rosuvastatin [Martin et al 2003]. Biliary clearances were obtained by multiplying the proportion of the dose recovered unchanged in the faeces after IV administration by the unbound total plasma clearance. $CL_{met,u}$ was

considered to be zero because metabolism of rosuvastatin in humans, both *in vivo* and *in vitro* is considered negligible (Table 3.1).

Values obtained from the *in vitro* results derived in Equation 3-2 were compared to the *in vivo* intrinsic clearances ($CL_{int,h}$) derived from data from the literature and expressed as described in Equation 3-3 [Table 3.2; Pang and Rowland 1977; Martin et al 2003].

Equation 3-3.

$$CL_{int,u} = \frac{CL_h}{Fu_b \times \left[1 - \frac{CL_h}{Q_h}\right]}$$

where CL_h is the hepatic blood clearance, obtained from a clinical study using intravenous administration [Martin et al 2003]. CL_h was determined by multiplying the non-renal plasma clearance (CL_{nr}) by the ratio of plasma to blood concentrations (C_p/C_b). CL_{nr} was calculated as the total plasma clearance (CL_{total}) minus the renal clearance (CL_r). The C_p/C_b ratio was taken as 1.45 [Martin et al 2003]. Q_h is liver blood flow (20.7 mL/min/kg) [Houston and Galetin 2008].

To account for the under prediction of the in vitro-in vivo extrapolation an empirical scaling factor was determined for $CL_{active,\ u}$ for the three individual donors.

3.6. Determination of the uptake kinetic parameters using a mechanistic model (UptakeFIT) developed by the Centre for Applied Pharmacokinetic Research.

The Centre for Applied Pharmacokinetic Research, Manchester School of Pharmacy, The University of Manchester, Manchester, U.K., have developed a free software (UptakeFIT v 1.0, 2013) for parameter estimation and design evaluation in hepatocyte uptake experiments using a two-compartment mechanistic modelling approach. The software is run in Matlab (version R2012a) with a graphic user interface (GUI) and is based upon the two-compartment model described already by Ménochet et al 2012a. The authors are allowing anyone to use the software in good faith, but also ask for constructive comments.

The UptakeFIT interface is divided into three 3 main sections ("User input", "Parameter estimation" and "Plots") and operates under three different modes ("Estimation", "Simulation" and "Design evaluation" mode) as detailed in Appendix 17. Here, only the estimation mode has been evaluated and the outputs compared and discussed with those derived using the mechanistic model developed in Matlab code.

Table 3.1. Summary of the clearance parameters for rosuvastatin in human following an intravenous dose, where CL_{total} is the total clearance, CL_r is the renal clearance, CL_{bile} is the biliary clearance, CL_{met} is the metabolic clearance, CL_h is the hepatic blood clearance and Fu_p is the fraction unbound in the plasma [Martin et al 2003].

Rosuvastatin PK Parameters	**Total**
CL_{total} (mL/min/kg)	11.6
CL_r (mL/min/kg)	3.24
CL_{bile} (mL/min/kg)	3.12
CL_{met} (mL/min/kg)	0.0
CL_h (mL/min/kg)	12.1
Fu_p	0.12

3.7. Results

3.7.1. Determination of the uptake kinetic parameters based upon a mechanistic modelling approach

The uptake kinetic parameters (V_{max}, $K_{m,u}$, $P_{diff,u}$ and Fu_{cell}) for rosuvastatin were determined in cryopreserved adult human hepatocytes from three donors (HU8116, HU8119 and HU1411) using a mechanistic two-compartment model developed by Menochet et al (2012a). A summary of the uptake kinetic parameters for rosuvastatin are detailed in Table 3.3. The predicted cell concentration – time profiles with the observed cell concentrations and the predicted versus the observed data for the three donors are detailed in Appendices 18, 19 and 20 and Appendices 21, 22 and 23, respectively. Profiles of the mean (± standard error of the mean, SEM) intracellular rosuvastatin concentrations for each individual media concentration are detailed in Appendices 24, 25, 26, 27, 28 and 29.

The individual uptake kinetic parameter values for rosuvastatin in donors HU8116, HU8119 and HU1411 were, V_{max} 8.35, 18.3, 50.7 pmol/min/10^6 cells, respectively, $K_{m,u}$ 0.63, 3.42, 6.92 µM, respectively, $P_{diff,u}$ 1.49, 0.80, 0.41 µL/min/10^6 cells, respectively and Fu_{cell} 0.12, 0.13, 0.27, respectively. The mean (± standard error of the mean) uptake kinetic parameter

values for rosuvastatin were, V_{max} 25.8 ± 12.8 pmol/min/10^6 cells, $K_{m,u}$ 3.66 ± 1.82 µM, $P_{diff,u}$ 0.90 ± 0.32 µL/min/10^6 cells and Fu_{cell} 0.17 ± 0.05.

The active clearance ($CL_{active,\ u}$) were also calculated (V_{max} / K_m) in donors HU8116, HU8119 and HU1411 and were 13.1, 5.36 and 7.33 µL/min/10^6 cells, respectively. The mean (± standard error of the mean) value was 8.58 ± 2.31.

3.7.2. Determination of the uptake kinetic parameters using the UptakeFIT modelling software.

The uptake kinetic parameters (V_{max}, $K_{m,u}$, $P_{diff,u}$ and Fu_{cell}) for rosuvastatin were also determined using the UptakeFIT modelling software developed by Capkr. A summary of the uptake kinetic parameters for rosuvastatin are detailed in Table 3.3. The predicted cell concentration – time profiles with the observed cell concentrations (Appendices 30, 31 and 32), the predicted versus the observed data (Appendices 33, 34 and 35), the weighted residuals versus predicted cell concentrations (Appendices 36, 37 and 38), the weighted residuals versus time (Appendices 39, 40 and 41) and the kinetic plots where the rates of active, passive and total uptake processes are plotted against the initial media concentrations (Appendices 42, 43 and 44) for the three donors (HU8116, HU8119 and HU1411) are detailed.

The individual uptake kinetic parameter values for rosuvastatin in donors HU8116, HU8119 and HU1411 were, V_{max} 9.08, 21.3, 44.2 pmol/min/10^6 cells, respectively, $K_{m,u}$ 2.00, 3.76, 5.70 µM, respectively, $P_{diff,u}$ 1.19, 0.67, 0.46 µL/min/10^6 cells, respectively and Fu_{cell} 0.10, 0.18, 0.26, respectively. The mean (± standard error of the mean) uptake kinetic parameter values for rosuvastatin were, V_{max} 24.8 ± 10.3 pmol/min/10^6 cells, $K_{m,u}$ 3.81 ± 1.07 µM, $P_{diff,u}$ 0.77 ± 0.22 µL/min/10^6 cells and Fu_{cell} 0.18 ± 0.05. The correlation matrix is detailed in Appendix 45. The only parameters that showed a possible correlation were V_{max} and $K_{m,u}$, with values of 0.92-0.95.

The $CL_{active,\ u}$ were also calculated (V_{max} / K_m) in donors HU8116, HU8119 and HU1411 and were 4.57, 5.66 and 7.75 µL/min/10^6 cells, respectively. The mean (± standard error of the mean) value was 5.99 ± 0.93.

3.7.3. Uptake clearance of rosuvastatin

The uptake clearance (CL_{uptake}) of rosuvastatin in cryopreserved adult human hepatocytes from three donors is shown in Table 3.4. The CL_{uptake} from each individual (HU8116, HU8119 and HU1411) at each media concentration (0.1, 0.3, 1, 3, 10, 30 and 100 µM) was calculated over the linear range (0-2 minutes). These CL_{uptake} values have been corrected for non-specific binding of rosuvastatin as described in the methods section 2.3. Further, a combined mean (± standard error of the mean) was also calculated from the three donors.

The CL_{uptake} of rosuvastatin at the same media concentrations for the three donors are generally similar. There does appear to be a trend for the CL_{uptake} to decrease with increasing media concentrations, with statistical differences ($p<0.01$) observed between the CL_{uptake} values from the highest media (100 µM) to the lowest media (0.3 µM) for all three donors using a two-tailed Student's T-test in Excel. The saturable component of the hepatic uptake process (CL_{hep}) can be determined by subtracting the hepatic uptake clearance CL_{uptake} at 0.3 µM from the CL_{uptake} at 100 µM [Shitara et al 2003a]. The CL_{hep} of rosuvastatin in cryopreserved adult human hepatocytes donors HU8116, HU8119 and HU1411 represented 61.4, 82.0 and 86.6% of the CL_{uptake}, with a mean (and standard deviation) of 76.7 ± 13.4%.

The in vitro-in vivo extrapolation and the empirical scaling factors are detailed for the three individual donors are detailed in Table 3.2. The scaling factors needed to predict the in vivo clearance from the in vitro clearance values ranged from 18-28-fold with a mean of 23.7-fold.

3.7.4. Inhibition of the uptake of rosuvastatin by cyclosporin A and cyclosporin AM1

A summary of the inhibition kinetic parameters (IC_{50}) for the inhibition of the uptake of rosuvastatin by cyclosporin A (CsA) and cyclosporin AM1 (AM1), with and without pre-incubation of inhibitor, into three adult human hepatocytes are detailed in Table 3.5. All of the data were fitted simultaneously (n=3 for inhibitor concentrations and n=6 for 0 µM controls) for each donor and an estimate of the IC_{50} and a standard error were derived. The inhibition curves of the uptake of rosuvastatin by CsA and AM1 are detailed in Appendices 46,47, 48 and in Appendices 49,50, 51, respectively. The correlation matrix for CsA and AM1 are detailed in Appendices 52 and 53, respectively. The four parameters did not appear to be correlated for either CsA or AM1.

Table 3.2. Observed and predicted intrinsic hepatic clearances of rosuvastatin from three adult plated cryopreserved human hepatocyte donors, HU8116, HU8119 and HU1411 using one scaling factor per donor. The empirical scaling factors that need to be applied to the active uptake clearances of rosuvastatin to recover the intrinsic uptake clearance in human livers from the three adult plated cryopreserved human hepatocyte donors are also detailed. The individual predicted data and the mean ± standard error of the mean (SEM) obtained from three adult plated cryopreserved human hepatocyte donors, HU8116, HU8119 and HU1411 are detailed. Also included are the data for the paediatric plated cryopreserved human hepatocyte donor, HU4088.

Donor	Observed $CL_{int,h}$ (mL/min/kg)	In vitro CL_{int} with no scaling (mL/min/kg)	Predicted $CL_{int,u}$ (mL/min/kg)	Scaling Factor
HU8116	267	10.3	103	25.9
HU8119	267	9.7	172	27.5
HU1411	267	15.1	195	17.7
Mean ± SEM		11.7 ± 1.7	156 ± 28	23.7 ± 5.3
HU4088		6.1	192	43.8

In all of the incubations the intracellular concentrations of rosuvastatin did not fall to zero with maximal concentrations (i.e. 1.5-6 µM) of the inhibitors, CsA and AM1. As described previously, it is not possible to wash away all of the rosuvastatin associated with non-specific binding to the plate. However, the intracellular concentrations of rosuvastatin did plateau at the highest inhibitor concentrations, suggesting that maximal inhibition had been achieved. Therefore, the model used in Phoenix™ was one that accounted for this.

Both CsA and AM1 inhibited rosuvastatin uptake into human hepatocytes, with mean IC_{50} values of 0.40 and 0.70 µM, respectively, for the co-incubation. Using a two-tailed Student's T-test in Excel, there did not appear to be any difference in the IC_{50} values from the pre-incubation cells when compared with co-incubation cells, with mean IC_{50} values of 0.84 and 0.40 µM for CsA and AM1, respectively. This may suggest that in hepatocytes the duration of exposure to the inhibitors (CsA and AM1) prior to the addition of the substrate (rosuvastatin), is not as critical as it is in other cell lines.

3.8. Discussion

3.8.1. Introduction

In this part of the study, the uptake kinetic parameters (V_{max}, $K_{m,u}$, $P_{diff,u}$ and Fu_{cell}) of rosuvastatin into three cryopreserved adult human hepatocyte cell lines have been determined

using a mechanistic model described previously by Ménochet et al 2012a, in order to help understand the interplay of the hepatic transporters in the disposition of rosuvastatin. As outlined previously, several different methods have been utilised to determine the uptake kinetic parameters of probe substrates of key transporters into human hepatocytes. These have included primary and cryopreserved suspended and plated cells, with the use of inhibitors and cold temperature (4°C), in combination with various *in silico* models. One of the aims of this study was to implement and update these methodologies with the mechanistic model in GSK. In addition, a new modelling software (UptakeFIT) became available during this study and is compared with the Ménochet model.

3.8.2. Donor choice and functionality

The choice of donors was based upon the relative transporter activity in each donor and the availability of the cells, so that enough cells could be procured to complete the study. From the literature supplied by the vendor, the cells showed a 4-fold difference between the lowest and highest uptake rates (expressed as pmol/min/mg protein) of estradiol glucuronide (EG) [Table 3.6]. EG is used as a probe substrate of OATP1B1, thought to be the main transporter involved in the uptake of rosuvastatin and so gives an indication of the activity of this transporter.

Data for taurocholate, a substrate for NTCP, another transporter thought to be involved in the uptake of rosuvastatin, were also provided. Differences in uptake rates were observed between the donors (2-fold). However, a comparison of the uptake rates of taurocholate with EG would suggest there are relative differences in the expression of the two transporters in each donor. For example, in donor HU8119, EG uptake is the greatest, but taurocholate uptake is actually the least of the three donors [Table 3.6]. Whether these apparent differences in the expression of OATP1B1 and NTCP (based upon substrate uptake) in the donors actually reflect the original *in vivo* expressions or are an idiosyncrasy of the cryopreservation process is not known. However, the vendors data would suggest that OATP1B1 and NTCP are functional in all three donors and as such the cells were used to study the kinetics of rosuvastatin, a substrate of the transporters OATP1B1 and NTCP.

Table 3.3. Summary of the uptake kinetic parameters of rosuvastatin in plated cryopreserved adult human hepatocytes from three donors, HU8116, HU8119 and HU1411 using a mechanistic two-compartment model developed by Menochet et al (2012a) and the UptakeFIT model. Each of the four individual parameters is the mean ± standard deviation (coefficient of variation %) derived from the simultaneous fitting of all of the incubations. Also detailed are the mean and standard error of the mean (SEM) for each of these parameters for the three donors.

.

Mechanistic Model Developed by Menochet et al 2012a					
Donor	V_{max} (pmol/min/10^6 cells)	$K_{m,u}$ (µM)	$CL_{active,u}$ (µL/min/10^6 cells)	$P_{diff,u}$ (µL/min/10^6 cells)	Fu_{cell}
HU8116	8.35 ± 1.76 (21.1)	0.63 ± 0.23 (36.4)	13.1	1.49 ± 0.15 (10.4)	0.12 ± 0.02 (12.5)
HU8119	18.3 ± 2.7 (14.8)	3.42 ± 0.6 (17.5)	5.36	0.80 ± 0.08 (10.6)	0.13 ± 0.02 (13.1)
HU1411	50.7 ± 12.3 (24.3)	6.92 ± 1.82 (26.3)	7.33	0.41 ± 0.21 (51.1)	0.27 ± 0.14 (51.4)
Mean ± SEM	25.8 ± 12.8	3.66 ± 1.82	8.58 ± 2.31	0.90 ± 0.32	0.17 ± 0.05
UptakeFIT Model					
Donor					
HU8116	9.08 ± 2.26 (24.9)	2.00 ± 0.63 (31.7)	4.57	1.19 ± 0.12 (9.7)	0.10 ± 0.01 (13.2)
HU8119	21.3 ± 2.91 (13.7)	3.76 ± 0.60 (16.0)	5.66	0.67 ± 0.08 (12.0)	0.18 ± 0.02 (13.3)
HU1411	44.2 ± 10.1 (22.9)	5.70 ± 1.45 (25.5)	7.75	0.46 ± 0.19 (41.5)	0.26 ± 0.11 (41.8)
Mean ± SEM	24.8 ± 10.3	3.81 ± 1.07	5.99 ± 0.93	0.77 ± 0.22	0.18 ± 0.05

Table 3.4. Summary of the uptake clearance (CL_{uptake}) of rosuvastatin in plated cryopreserved adult human hepatocytes. The CL_{uptake} for each individual was calculated by taking the mean of the first four time points (0.5, 1, 1.5 and 2 minutes) at all of the concentrations used (0.1, 0.3, 1, 3, 10, 30 and 100 µM) as these were considered linear (n=3). Further the mean (± standard error of the mean) was calculated from the three donors.

Concentration (µM)	CL_{uptake} (µL/min/10^6 Cells)			
	HU8116	HU8119	HU1411	Mean ± SEM
0.3	3.58 ± 1.84	3.67 ± 0.20	4.55 ± 1.69	3.22 ± 0.71
1	3.33 ± 1.25	2.82 ± 0.15	3.34 ± 0.94	2.41 ± 0.48
3	1.37 ± 0.30	3.20 ± 1.63	3.34 ± 0.94	1.75 ± 0.40
10	1.57 ± 0.18	1.50 ± 0.19	2.32 ± 1.09	1.35 ± 0.35
30	1.50 ± 0.20	0.88 ± 0.26	1.24 ± 0.54	0.97 ± 0.21
100	1.38 ± 0.74	0.66 ± 0.16	0.61 ± 0.21	0.83 ± 0.22

Table 3.5. Summary of the inhibition kinetic parameters of the inhibition of the uptake of rosuvastatin (1 µM) incubated for 3 minutes in three adult human hepatocytes in the presence of the inhibitors cyclosporin A and cyclosporin AM1, both with and without pre-incubation. An estimate of the IC_{50} (± SE) were derived using Phoenix™ 6.1.

Inhibitor	Cyclosporin A		Cyclosporin AM1	
Pre-incubation	No	Yes	No	Yes
Donor				
HU8116	0.40 ± 0.22	1.40 ± 4.77	1.08 ± 0.40	0.68 ± 1.03
HU8119	0.43 ± 0.11	0.85 ± 1.32	0.73 ± 0.41	0.31 ± 0.15
HU1411	0.36 ± 0.10	0.27 ± 0.10	0.31 ± 0.12	0.22 ± 0.12
Mean	0.40 ± 0.04	0.84 ± 0.56	0.70 ± 0.39	0.40 ± 0.24

3.8.3. Mechanistic Modelling Data

The uptake of rosuvastatin was determined in three cryopreserved adult human hepatocytes (HU1411, HU8116 and HU8119) over 60 minutes and six different concentrations. The uptake profiles for each of the three donors showed that steady state kinetics were achieved from 40-60 minutes at media concentrations of rosuvastatin at and above 3.3 µM. This is important, because it is believed that this phase of the uptake process helps describe the P_{diff} and Fu_{cell} parameters and the initial linear phase (0-2 minutes) describes the K_m and V_{max} values [Appendices 24-29].

Table 3.6. Vendor supplied literature for the uptake rates of estradiol glucuronide and taurocholate in the three adult cryopreserved human hepatocytes, HU8116, HU8119 and HU1411. Estradiol glucuronide and taurocholate uptake would suggest OATP1B1 and NTCP functionality.

Donor	Uptake rate (pmol/min/mg protein)	
	Estradiol glucuronide	Taurocholate
HU8116	1.59	12.6
HU8119	8.05	9.7
HU1411	4.7	20.3

The uptake kinetic parameter with the greatest variability was K_m, with a 10-fold difference between the lowest and highest value. However, it should be remembered that rosuvastatin uptake into hepatocytes is mediated by up to three transporters, namely OATP1B1, OATP1B3 and NTCP. Therefore the K_m value calculated cannot be attributed to one individual transporter and is an 'apparent value'. Also, consider that the relative expressions

of these transporters appear to vary between the three donors, which may lead to variability in the apparent K_m value calculated. In other studies, using cryopreserved human hepatocytes from different donors, the K_m values calculated for taurocholate, EG and cerivastatin, had similar fold differences between the lowest and highest values and ranged from 5-7-fold [Shitara et al 2003b; Shitara et al 2004]. Even with the probe substrates (taurocholate and EG), variability was observed in the apparent K_m between different donors. Interestingly, the K_m data from Ménochet et al 2012 would suggest higher and less variable K_m values in cryopreserved human hepatocytes (9.8 – 12 µM). However, here the incubation times were limited to two minutes and so the kinetics had not reached steady state.

However, even in cell lines over-expressing OATP1B1, where the K_m value should reflect the affinity for the transporter, the values for rosuvastatin varied by up to 10-fold and were actually very similar to the values calculated in the hepatocytes in this study, with values that ranged from, 0.8 – 8 µM, [Table 1.3.].

V_{max} was also variable, with up to a 6-fold difference between the highest and lowest value observed in this study, which is not dissimilar to the vendors data for EG uptake. A 7-fold difference was observed previously for rosuvastatin in human hepatocytes and fold differences of 3.8-, 3.2- and 14-fold were observed for EG, taurocholate and cerivastatin, respectively [Shitara et al 2003a; Shitara et al 2004; Ménochet et al 2012].

V_{max} and K_m data demonstrated the greatest variability, but interestingly, the active clearance (i.e. V_{max} / K_m) values showed much less variability, with an approximate 2-fold difference observed in this study. This would suggest that it is possible that these two parameters are correlated to some extent. In donors with a low V_{max} there is a low K_m and conversely in donors with a high V_{max} there is a high K_m. Considering the relationship between V_{max} and K_m a correlation is not surprising.

P_{diff} was less variable with an approximate 5-fold difference compared with fold differences of 5-, 1.3-, 1.7- and 2.6-fold reported for EG, taurocholate, cerivastatin and rosuvastatin, respectively. With the exception of donor HU8116, the individual donor P_{diff} values between this study and Ménochet were very similar. The P_{diff} value of donor HU8116 was higher than the other donors, which may be related to the fact that it had the lowest V_{max} (and K_m) values.

However, as observed with the data from Shitara, this fold difference is possible even with a probe substrate, EG, that has very low passive permeability [Shitara et al 2003a].

The final parameter, namely Fu_{cell}, had the least variability between donors, with an approximate 2-fold difference in this study. The fraction unbound of rosuvastatin in the plasma (Fu_p) is quoted as 0.12 and in this study the Fu_{cell} was 0.17. The variability in the individual values of Fucell overlap with the Fu_p. The calculation of this parameter is fairly new and so comparison with other studies is limited. However, in the study by Ménochet, the Fucell of rosuvastatin was much higher and ranged from 0.8 – 1.0, but here the incubations were over just two minutes compared to this study where the time points chosen allowed steady state levels to be achieved.

3.8.4. UptakeFIT Mechanistic Modelling Data

The UptakeFIT model supplied by Capkr is based heavily upon the mechanistic model described by Ménochet. However, there are differences between the two models. The UptakeFIT model uses Matlab software, but has an interface which makes it easier to populate the model with the required data. In the Matlab model, data are entered by populating different notepad files with, cell concentration, incubation times, intracellular concentration, media concentration (corrected for fraction unbound), index number, extrapolated intracellular concentrations at Time = 0 minutes, estimates of the four parameters and finally the cell volume and media volume. In the UptakeFIT model, an excel sheet with media concentration (not corrected for fraction unbound), incubation times and intracellular concentration is all that is required. The other parameters are entered on the interface tab as detailed in Appendix 17. One major difference between the two models appears to be in the extrapolation of the intracellular concentrations at Time = 0 minutes, which will be discussed later.

In addition to the ease of data entry, another refinement is in the diagnostics that are generated. UptakeFIT generates coefficient of variation (CV), the predicted cell concentration – time profiles with the observed cell concentrations and the predicted versus the observed data, as does the Matlab code, but in addition outputs a correlation matrix of the four parameters, the weighted residuals versus predicted cell concentrations, the weighted residuals versus time and the kinetic plots where the rates of active, passive and total uptake processes are plotted against the initial media concentrations.

A comparison of the estimates of the four parameters between the Matlab model and the UptakeFIT model shows that by and large the two models predict similar values. The small differences may be due to the way that the initial intracellular concentration (T=0) was calculated. In the Matlab model, a straight line is interpolated back through the linear time points (i.e. 0.5, 1, 1.5 and 2 minutes) and the intercept of the Y-axis determined, using Excel. In the UptakeFIT model the initial intracellular concentration value is determined using an empirical equation (Equation 3.4.) derived from the regression of cell initial concentrations to media initial concentrations using data from three different sets of uptake experiments with rosuvastatin generated at Capkr.

Equation 3.4.

$$Cell_{init} = \frac{C_{media} * 1000}{0.197 * C_{media} + 9.282} * 100$$

$Cell_{init}$ represents the cell initial concentration conditions (nM) and C_{media} represents the initial concentration in the media (μM). This equation obviously allows the calculation of the initial cell concentration to be quicker and easier, but raises the question of a blanket approach for all compounds. Here, the equation maybe justified as it was determined using rosuvastatin data, but with other compounds that may have different binding properties then it may not be as appropriate. It also highlights the problems of using a locked-in software where the user is not entirely sure of what is going on underneath the interface. Having said that, this is the first draft version and feedback was asked from potential users.

It is worth making a comment on the extra diagnostic outputs produced by the UptakeFIT model. Currently, in Matlab the main diagnostic is the CV value calculated for each of the four parameters. The observed versus the predicted data, with the line of unity and 2-fold higher and lower are also plotted. In addition to these, UptakeFIT also produces a correlation matrix. With these data the only parameters that showed a possible correlation were V_{max} and K_m [Appendix 45]. This may also explain the low variability observed for $CL_{active,\ u}$, if the parameters V_{max} and K_m, are correlated.

3.8.5. In vitro to in vivo clearance predictions

The *in vitro* clearance values for rosuvastatin without using scaling factors were under predictive of the observed *in vivo* intravenous clearance value. With a scaling factor applied,

the predicted mean *in vitro* clearance value was still under predictive, but within two-fold of the observed *in vivo* clearance value. The mean scaling factor required to correct the in vitro clearance to match the in vivo clearance was 23.7-fold, which compared to the value quoted by Ménochet et al 2012 of 17-fold when using all the data sets from seven different drugs including rosuvastatin. The variability in the individual scaling factors for rosuvastatin overlap with the value quoted by Ménochet et al 2012. However, in this current study, the empirical scaling factors for rosuvastatin were lower and less variable based upon three donors than the study by Ménochet.

The under predictive nature of both *in vitro* active uptake and metabolism has been observed previously [Riley et al. 2005; Soars et al 2007b; Poirier et al 2009; Watanabe et al 2009; Gardiner and Paine 2011]. The under prediction may be a result of the isolation, cryopreservation and culture procedures [Badolo et al 2011; Ulvestad et al 2011]. Currently empirical scaling factors to predict active uptake in human from non-clinical data are being sought [Poirier et al 2009; Watanabe et al 2009; Gardiner and Paine 2011]. Using a whole-body PK model, with novel physiological scaling laws, the disposition of CsA in rats was sufficient to predict the disposition in human (as well as pig and monkey) [Hall et al 2012]. Perhaps a physiological modelling approach will be more successful in scaling non-clinical *in vivo* data to human.

3.8.6. Inhibition of the uptake of rosuvastatin by cyclosporin A and AM1

Both cyclosporin A and its major metabolite, cyclosporin AM1, inhibited the uptake of rosuvastatin into the adult cryopreserved human hepatocytes. The IC_{50} values derived using co-incubation conditions (i.e. substrate and inhibitor administered together) demonstrated that inhibition of rosuvastatin uptake was potent for both inhibitors. In terms of the actual IC_{50} values calculated in the hepatocytes, these were within two-fold of the values derived by ourselves in HEK293 cells over-expressing OATP1B1, also with co-incubation [Gertz et al 2012]. However, with both inhibitors the IC_{50} values in the hepatocytes were higher (i.e. less potent) than the expressed cells, with mean values of 0.4 and 0.7 µM for CsA and AM1 in hepatocytes and 0.2 and 0.4 µM for expressed cells, respectively. However, a comparison of pre- and co-incubation conditions in the hepatocytes did not seem to show an increase in potency with increased incubation time, whereas in the HEK293 cells this was observed.

Clinically, CsA has a C_{max} of approximately 1 µM systemically and with a bioavailability of approximately 30% could therefore have portal vein concentrations of 3 µM [Fahr 1993; Faulds et al 1993]. However, the plasma free fraction of CsA was 1.5% and so the free fraction in the portal vein might be 0.045 µM [Yang and Elmquist WF 1996]. Even this concentration is higher than the CsA IC_{50} values calculated in the hepatocytes and it would be expected that following a clinically relevant dose of CsA that OATP1B1 and 1B3 would be inhibited, which may explain the observed interactions with rosuvastatin (and other OATP substrates) in the clinic. Also consider that in the inhibition studies, the total concentrations of CsA (and AM1) were used to calculate the IC_{50} values and any potential binding was not accounted for, which may mean the IC_{50} values are in fact lower (i.e. more potent). It is likely that binding may be high, as CsA has shown to bind to many different chemicals as detailed in the next examples.

In isolated rat hepatocytes, the effect of lipids (oleic acid, low density lipoproteins and high density lipoproteins, but not cholesterol) reduced CsA cell uptake as well as its metabolism in a concentration-dependent manner. This may be due to binding to the lipid and therefore leading to a reduction in the unbound free concentration [Prueksaritanont et al 1992].
In the isolated perfused rat liver, CsA had a large volume of distribution and slow release from binding sites within the liver, in contrast to its rapid uptake after a single pass. Again, this would indicate that CsA binds intracellularly [Mehvar and Chimalakonda 2004]. CsA inhibited the uptake of radio-labelled cerivastatin into isolated rat hepatocytes in a concentration-dependent manner. However, the IC_{50} increased (i.e. less potent) when the incubations had rat plasma present. The apparent IC_{50} values were based upon the total CsA, but the presence of rat plasma might suggest the free fraction has been reduced [Shitara et al 2003b].

A 20-fold lower IC_{50} was observed with pre-incubation of CsA in HEK293 cells over-expressing OATP1B1, when compared to co-incubation, using atorvastatin acid as the substrate [Amundsen et al 2010]. In our studies, again using HEK293 cells over-expressing OATP1B1 and also HEK293 cells over-expressing OATP1B3, we demonstrated a 10- and 4-fold reduction in the IC_{50} with CsA and AM1, respectively, with estradiol glucuronide (EG) as the substrate [Gertz et al 2012]. However, in this study there does not appear to be a real difference between co- and pre-incubation conditions and there are several potential reasons as to why this might be, including differences in the cell types, uptake of rosuvastatin by

multiple transporters, the probe substrates and their media concentrations and the type of binding of the inhibitor to the active site (or alternative binding site).
One suggestion for the difference between co- and pre-incubation IC_{50} values is the possibility of time-dependent inhibition (TDI), analogous to that observed with CYP enzymes. As the topic of possible TDI with transporters is very new and really not well defined or understood, it is worth considering this phenomena with the CYP enzymes. The classification of enzyme inhibitors can be categorised as competitive, non-competitive, uncompetitive, product inhibition, transition-state analogs, slow, tight binding inhibitors and irreversible inhibitors. CYP inhibition can be more simplistically classified into reversible (mostly competitive), quasi-irreversible and irreversible binding. TDI is a general term that describes the mode of action of quasi-irreversible and irreversible inhibitors, which often leads to an increase in potency (i.e. decrease IC_{50}). Possible mechanisms include the formation of more inhibitory metabolites, mechanism-based inhibition (MBI) and the inactivation of CYPs by metabolic products that form haem or protein adducts or a metabolic inhibitory complex [Hollenberg 2002; Riley et al 2007].

All of these types of CYP inhibition can lead to significant drug interactions. With reversible inhibition, the effect is transient and the normal metabolic functions of the enzymes will continue following elimination of the inhibitor from the body. Reversible inhibition of CYP is often classified as competitive, where binding of the inhibitor to the enzyme prevents the binding of the substrate to the active site of the enzyme. Mechanism-based inhibitors are compounds that bind irreversibly to the prosthetic haem or to the protein, or that cause covalent binding of the haem prosthetic group, or its degradation product to the apoprotein. The net result is that the inhibitor titrates out the enzyme such that even when the inhibitor is eliminated the inhibition continues until new enzyme can be synthesised. The amount of inhibitor required to fully inactivate an enzyme depends upon its partition ratio, which is defined as the number of moles of end product formed per mole of enzyme inactivated. The lower the partition ratio the less inhibitor required for full inactivation. The end result is that TDI inhibitors can often perpetrate larger DDI, especially following repeat dosing.

Understanding whether inhibitors interact with transporters in a similar time-dependent way as they can with enzymes is important and may explain the magnitude of DDI seen with certain inhibitors, such as CsA. In rat primary hepatocytes, pre-exposure to CsA inhibited taurocholate uptake and the longer the pre-incubation the greater the inhibition. However,

the inhibition could be completely reversed (within 3 hours) by the addition of fresh media. The short time to recovery would suggest that the mechanism of binding is not covalent [Kukongviriyapan and Stacey1988]. When considering the experimental design of the inhibition *in vitro* assays with transporters, pre-incubation of the inhibitor should really be used to define the more potent IC_{50} and if required include a comparison with co-incubation.

The question comes as to why the time-dependent increase is observed in certain assays, but not in this study. Rosuvastatin was chosen as the probe substrate in this study because its disposition in the hepatocyte is quite complex and can be made more complex by using inhibitors (CsA and AM1) that can interact with multiple transporters. In addition, it is one of the marketed drugs suggested as a probe substrate to understand DDI clinically with OATP1B1.

The probe substrates that did demonstrate an apparent time-dependent increase in potency with CsA used different probe substrates, namely atorvastatin acid and EG [Amundsen et al 2010; Gertz et al 2012]. Clearly, these are different chemical entities and may therefore not interact with the transporters in the same way chemically or even at the same binding sites. In membranes expressing BCRP, rosuvastatin appeared to have two separate transport sites, with apparent K_m values for high and low affinity binding [Huang et al 2006]. The potential for inhibitors to have different interactions with different substrate binding sites was demonstrated with the uptake of estrone-3-sulphate in HEK293 cells over-expressing OATP1B1 (but not by 2B1). Here estrone-3-sulphate displayed biphasic saturation kinetics, with two distinct affinity components, but only the high-affinity component was inhibited by Gemfibrozil [Noe´ J et al 2007]. With the possibility of multiple (high and low affinity) binding sites for the substrate and the possible differential interaction of the inhibitors with these sites, clearly choice of substrate may be very important even with the same inhibitor (e.g. CsA).

In this study and the Amundsen study, the probe substrates used were statins at media concentrations at or just below the K_m for the representative matrix, which should allow for optimum kinetics. However, in our study with EG, the use of radio-labelled EG allowed the concentration used to be very low (>0.1 µM), much lower than the K_m. The studies with EG were conducted in a similar cell line (HEK293) to atorvastatin acid and both substrates showed fold differences in potency between pre- and co-incubation. This would suggest that

the concentration of rosuvastatin used in this study was justified and a lower concentration may not have shown a difference with co- and pre-incubation.

The choice of *in vitro* system may be important. The uptake of fluvastatin was inhibited by gemfibrozil in over-expressed OATP1B1and OATP1B3 cells, but in primary human hepatocytes, only a small inhibitory effect by gemfibrozil on fluvastatin uptake was observed [Noe´ J et al 2007]. This may be the result of redundancy in the uptake transporters in the hepatocytes with respect to fluvastatin uptake. Rosuvastatin is known to be a substrate for many uptake transporters and may utilise alternatives when the preferred uptake transporters are inhibited [Ho et al 200.

It is also possible that the inhibitors bind to the transporter protein on the inside of the cell, therefore leading to a time delay as the inhibitor has to be taken up into the cell before it can have an effect, but the substrate can interact with the transporter in the media. The HEK293 cells are straightforward to culture and transfect, but as a cell line they are not particularly representative of other cell types and are effectively a membrane to house the expressed protein. In the HEK cells there are limited transporters expressed in the membrane (except OATP1B1), but in the hepatocyte all of the relevant uptake transporter proteins found *in vivo* will be expressed in the membranes. Although there is limited information available on CsA as a substrate for transporters, it is possible that is a substrate for a transporter and can therefore enter the hepatocyte faster than in the HEK cells.

In some of the inhibition studies variability was observed with the data, in particular donors HU8116 and HU8119 with pre-incubation with CsA. One observation is that the rosuvastatin intracellular concentrations do not reach absolute zero. However, the intracellular concentrations of rosuvastatin at the highest media concentrations of CsA (and AM1) appeared to have levelled off, indicating complete inhibition. The intracellular concentrations of rosuvastatin at these highest concentrations of CsA are probably the result of the non-specific binding.

Several reasons have been put forward here, but of course the apparent lack of difference between co- and pre-incubation of the inhibitors may be a subtle combination of all the above.

3.8.7. Comparison of the adult and paediatric hepatocytes with regards the uptake of rosuvastatin

In this study a paediatric cell line (donor HU4048) was used primarily to develop the model (and allow the author to gain competency in the techniques). However, useful data were generated and although there is only one donor, a comparison of paediatric and adult transporters (*via* rosuvastatin uptake) is made here. Although the composition of the CYP enzymes is known to change with age, data about transporters in paediatrics is limited.

In this paediatric cell line, the uptake parameters for rosuvastatin uptake (V_{max}, $K_{m,u}$, $P_{diff,u}$ and Fu_{cell}) were in good agreement with the adult cell lines. So too were the uptake clearance (CL_{uptake}) values generated at each media concentration of rosuvastatin. Although the expression of the uptake transporters has not been determined, the uptake of rosuvastatin might suggest that their expression is similar between this paediatric donor and the three adult donors used in this study.

3.9. Conclusions

- Uptake kinetic parameters of rosuvastatin in three adult human hepatocytes were calculated in this study. In addition, steady state kinetics were achieved, thus allowing more accurate determinations of Fu_{cell} and P_{diff}.
- Cyclosporin A and cyclosporin AM1 were both potent inhibitors of rosuvastatin uptake in the three adult human hepatocyte cells, which suggested a pre-dominate role for OATP1B1.
- There did not appear to be a time-dependent shift in the IC_{50} values with either cyclosporin A and cyclosporin AM1 in the hepatocytes.

CHAPTER 4: HEPATIC UPTAKE OF GSK2879552 USING ADULT HUMAN HEPATOCYTES

4.1. Introduction

GSK2879552 is a Lysine-specific demethylase 1 (LSD1) inhibitor currently undergoing investigation by GlaxoSmithKline. The dihydrochloride salt was used in this study and the structure is detailed in Table 6.1.

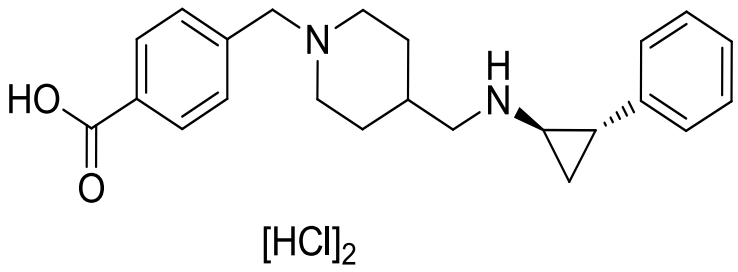

Figure 4.1. The chemical structure of GSK2879552 (the dihydrochloride salt) is detailed. (Parent molecular formula: $C_{23}H_{25}[2H]_3N_2O_2$ and parent molecular weight: 364.48 g/mol).

Studies with GSK2879552 in the rat suggested that bioavailability was complete and that renal clearance accounted for approximately 30% of the elimination. In human hepatocytes metabolism of GSK2879552 was not observed over the incubation time. These data would suggest that up to 70% of the dose of GSK2879552 could be eliminated *via* the liver unchanged, making GSK2879552 a prime candidate as a substrate for hepatic transporters. In addition, passive permeability was approximately 75 nm/sec in Caco2 cells, which is considered moderate. One of the limitations of uptake studies using a cocktail of inhibitors and/or 4ºC is that it is sometimes difficult to separate the active from the passive uptake. Therefore, the mechanistic model already described was used to determine the uptake parameters for GSK2879552.

4.2. Materials and methods

4.2.1. Chemicals

GSK2879552A (the dihydrochloride salt) with a stated chemical purity of 97.4% was supplied by Chemical Development, GlaxoSmithKline, Stevenage, UK. [$^2H_3$]-GSK2879552B (the stable isotope label dihydrochloride salt), with a stated chemical purity

of 99.3%, was supplied by Isotope Chemistry, Chemical Development, GlaxoSmithKline, Stevenage, UK.

4.2.2. Hepatocyte media

The details are as described previously in Chapter 2, section 2.1.2.

4.2.3. Hepatocyte preparation

The details are as described previously in Chapter 2, section 2.1.3.

4.2.4. Measurement of GSK2879552 uptake in adult human hepatocytes

The details are as described previously in Chapter 2, section 2.1.4. with the exception of the incubation times which were extended (0.5, 1, 1.5, 2, 5, 20, 40 and 60 minutes) so that steady state kinetics would be described.

4.2.4. Measurement of fraction unbound of GSK2879552 the incubation media

The fraction unbound of GSK2879552 was determined in the incubation media by analysing the concentrations of GSK2879552 in the media over the linear range (0-2 minutes) at all of the media concentrations. The calculated media concentrations over the linear range were plotted and the intercept at the Y-axis gives the media concentration for T = 0. By plotting the nominal concentrations against their respective analysed values, the gradient of the resulting straight line is the fraction unbound in the media.

4.3 Liquid chromatography and mass spectrometry analysis of GSK2879552

4.3.1. Preparation of the analyte solutions of GSK2879552

Analytical stock solutions (A and B) of GSK2879552 (0.1 mg/mL) were prepared in dimethyl formamide (DMF). These were further diluted in DMF (10, 1 and 0.1 µg/mL) to produce working solutions as detailed in Appendix 4. The A and B stock solutions provided the calibration standards and quality control (QC) samples, respectively. The calibration and QC standards were prepared fresh in control matrix as detailed in Appendices 5 and 6.

4.3.2.Preparation of analytical solutions of the internal standard.

An internal standard stock solution of [$^{2}H_{7}$ $^{15}N_{2}$]-GSK2879552 (C) was prepared in DMF (2 mg/mL). From this a working solution (C1; 500 ng/mL) was prepared in acetonitrile/methanol/formic acid (95/5/0.1 v/v/v) as detailed in Appendix 7.

4.3.3. Sample preparation and extraction

Aliquots (25 µL) of the samples, standards and QCs were mixed thoroughly with an aliquot (100 µL) of internal standard working solution (C1; 500 ng/mL). The tubes were mixed thoroughly and the samples were evaporated to dryness under a stream of nitrogen at approximately 35ºC and reconstituted in water:acetonitrile (90:10, v/v). The tubes were mixed thoroughly and then centrifuged for 10 minutes at 180 g. A total blank of control matrix (25 µL) and acetonitrile (100 µL) was prepared in a similar way. An aliquot (10 µL) was injected onto the HPLC MS/MS system for analysis as detailed in Appendices 8, 9 and 10.

4.3.4. Determination of the uptake kinetic parameters using a mechanistic modelling approach.

The details are as described previously in Chapter 2, sections 2.3. and 2.3.1.

The nominal concentrations of GSK2879552 in the media were corrected for the fraction unbound in the media, fu_{med}, which was 0.226 and was calculated in this study. This rationale accounted for non-specific binding, such as drug that could not be washed from the cell membranes or experimental plates during the washing steps.

In addition, the UptakeFIT v 1.0, 2013 software developed by The Centre for Applied Pharmacokinetic Research, Manchester School of Pharmacy, The University of Manchester, Manchester, U.K., was also used to evaluate the data from the hepatocyte uptake experiments using GSK2879552 and detailed in Chapter 3, section 3.5.

4.3.5. Determination of the uptake clearance

The details are as described previously in Chapter 2, sections 2.4.

4.4. Results

4.4.1. Uptake clearance of GSK2879552

The uptake clearance (CL_{uptake}) of GSK2879552 in cryopreserved adult human hepatocytes from three donors is shown in Table 4.2. The CL_{uptake} from each individual (HU8116, HU8119 and HU1411) at each media concentration (0.1, 0.3, 1, 3, 10, 30 and 100 µM) was calculated by taking the mean over the linear range (0-2 minutes). These CL_{uptake} values have been corrected for non-specific binding of GSK2879552 as described in the methods section 6.3.5. Further, a combined mean (± standard error of the mean) was also calculated from the three donors.

The CL_{uptake} of GSK2879552 at the same media concentrations for the three donors are generally similar and there does not appear to be a trend for the CL_{uptake} to decrease with increasing media concentrations. There was no significant difference between the CL_{uptake} at the highest and lowest media concentrations using a two-tailed Student's T-test in Excel for all three donors. This shows that there does not appear to be any active saturable processes involved in the uptake of GSK2879552. However, the CL_{uptake} data were generated after the data set had been analysed with the mechanistic model.

4.4.2. Determination of the uptake kinetic parameters based upon a mechanistic modelling approach

The uptake kinetic parameters (V_{max}, $K_{m,u}$, $P_{diff,u}$ and Fu_{cell}) for GSK2879552 were determined in cryopreserved adult human hepatocytes from three donors (HU8116, HU8119 and HU1411) using a mechanistic two-compartment model developed by Menochet et al (2012a). A summary of the uptake kinetic parameters for GSK2879552 are detailed in Table 4.1. The predicted cell concentration – time profiles with the observed cell concentrations and the predicted versus the observed data for the three donors are detailed in Appendices 18, 19 and 20 and Appendices 21, 22 and 23, respectively. Profiles of the mean (± standard error of the mean, SEM) intracellular GSK2879552 concentrations for each individual media concentration are detailed in Appendices 24, 25, 26, 27, 28 and 29.

The individual uptake kinetic parameter values for GSK2879552 in donors HU8116, HU8119 and HU1411 were, V_{max} 0.31, 169, 25.6 pmol/min/10^6 cells, respectively, $K_{m,u}$ 0.54, 23.0, 6.43 µM, respectively, $P_{diff,u}$ 0.85, 0.50, 4.05 µL/min/10^6 cells, respectively and Fu_{cell} 0.19,

0.56, 0.0.8, respectively. The mean (± standard error of the mean) uptake kinetic parameter values for GSK2879552 were, V_{max} 65.1 ± 53.6 pmol/min/10^6 cells, $K_{m,u}$ 10.0 ± 6.86 µM, $P_{diff,u}$ 1.80 ± 1.45 µL/min/10^6 cells and Fu_{cell} 0.29 ± 0.15.

The $CL_{active,\ u}$ were also calculated (V_{max} / K_m) in donors HU8116, HU8119 and HU1411 and were 0.5, 2.41 and 7.34 µL/min/10^6 cells, respectively. The mean (± standard error of the mean) value was 3.97 ± 1.96.

4.4.3. Determination of the uptake kinetic parameters using the UptakeFIT modelling software.

The uptake kinetic parameters (V_{max}, $K_{m,u}$, $P_{diff,u}$ and Fu_{cell}) for GSK2879552 were also determined using the UptakeFIT modelling software developed by Capkr. A summary of the uptake kinetic parameters for GSK2879552 are detailed in Table 4.1. The predicted cell concentration – time profiles with the observed cell concentrations (Appendices 30, 31 and 32), the predicted versus the observed data (Appendices 33, 34 and 35), the weighted residuals versus predicted cell concentrations (Appendices 36, 37 and 38), the weighted residuals versus time (Appendices 39, 40 and 41) and the kinetic plots where the rates of active, passive and total uptake processes are plotted against the initial media concentrations (Appendices 42, 43 and 44) for the three donors (HU8116, HU8119 and HU1411) are detailed.

The individual uptake kinetic parameter values for GSK2879552 in donors HU8116, HU8119 and HU1411 were, V_{max} 68.7, 100 154 pmol/min/10^6 cells, respectively, $K_{m,u}$ 1.43, 13.6, 25.4 µM, respectively, $P_{diff,u}$ 0.50, 1.01, 1.21 µL/min/10^6 cells, respectively and Fu_{cell} 0.48, 0.27, 0.26 respectively. The mean (± standard error of the mean) uptake kinetic parameter values for GSK2879552 were, V_{max} 108 ± 25.0 pmol/min/10^6 cells, $K_{m,u}$ 13.5 ± 6.94 µM, $P_{diff,u}$ 0.91 ± 0.21 µL/min/10^6 cells and Fu_{cell} 0.34 ± 0.07. The correlation matrix is detailed in Appendix 45.

The $CL_{active,\ u}$ were also calculated (V_{max} / K_m) in donors HU8116, HU8119 and HU1411 and were 48.2, 7.31 and 6.06 µL/min/10^6 cells, respectively. The mean (± standard error of the mean) value was 20.5 ± 13.9.

4.5. Discussion

4.5.1. Introduction

In this part of the study, the uptake kinetic parameters (V_{max}, $K_{m,u}$, $P_{diff,u}$ and Fu_{cell}) of GSK2879552 have been determined in three cryopreserved adult human hepatocyte cell lines using a mechanistic model described previously by Ménochet et al 2012, in order to help understand the role of the hepatic transporters in the disposition of GSK2879552. In addition, a new modelling software (UptakeFIT) became available during this study and is compared with the Ménochet model.

4.5.2. Donor choice and functionality

The donors used to determine the uptake of GSK2879552 were the same as for rosuvastatin and so the reasons for choosing them are the same as outlined previously in Chapter 5, section 5.2.2.

4.5.3. Mechanistic Modelling Data

The uptake of GSK2879552 was determined in three cryopreserved adult human hepatocytes (HU1411, HU8116 and HU8119) over 60 minutes and six different concentrations. The uptake profiles for each of the three donors showed that steady state kinetics were achieved from 40-60 minutes at media concentrations of GSK2879552 at and above 3.3 µM. This is important, because it is believed that this phase of the uptake process helps describe the P_{diff} and Fu_{cell} parameters and the initial linear phase (0-2 minutes) describes the K_m and V_{max} values [Appendices 67-72].

Although the model fitted all of the data from all of the donors and generated predicted values for the four parameters, the coefficients of variations (CV) suggested that the data were variable. The uptake clearance values (CL_{uptake}) at the lowest and highest media concentrations were similar and this would suggest that there is no involvement by a saturable process. Without an active uptake process, there are too many parameters in the model, which has lead to values with high variability. The variability is such that it is difficult to have confidence in the numbers generated. This has been a very useful and key learning about the utility of the model and its limitations. It may have been more appropriate to have conducted a smaller study to determine whether there was evidence for active uptake. A study to determine the uptake of GSK2879552 at one concentration (low e.g. 0.3 µM so as

not to saturate any active uptake) over a time course (60 minutes) with and without incubation with a cocktail of inhibitors. However, the non-clinical *in vivo* and clinical *in vitro* data suggested that GSK2879552 would be a prime candidate to be a substrate for a transporter. Rat data would suggest that bioavailability was complete and that renal clearance accounted for 30% of the elimination. The inference is that 70% of the dose is eliminated *via* biliary secretion, probably as unchanged parent drug, because metabolism was not observed in human hepatocytes. The question remains as to where this 70% of the drug actually goes. Ideally, an absorption, distribution, metabolism and excretion study, using radio-labelled compound with individual rats housed in meta-bowls over a time period (24-48 hours) and collecting tissues and excreta over time and analysing the carcass would show where drug-related compound accumulated. Bile-duct cannulated rats would also show whether GSK2879552 is excreted in the bile. The icing on the cake would be to analyse the samples using radio-label HPLC to determine whether parent is eliminated unchanged or whether there are metabolites produced.

4.5.4. UptakeFIT Mechanistic Modelling Data

The UptakeFIT model supplied by Capkr is based heavily upon the mechanistic model described by Ménochet. The model has been compared and contrasted in Chapter 3, sections 3.4.3 and 3.4.4. The model has generated values for the parameters, but as with the Matlab coded model there is variability in the CVs generated for the parameters in all of the donors, which does not give confidence in the values.

A comparison of the estimates of the four parameters between the Matlab model and the UptakeFIT model shows that by and large the two models predict similar values. However, the estimates are not always as close as with rosuvastatin discussed earlier Chapter 3. This maybe simply due to the data itself, the model is over-parametised and is trying to fit active uptake parameters using data that does not show active uptake. The other difference is in the way the initial intracellular concentration (T=0) is determined. With the Matlab coded model the value is interpolated back through the linear time points (i.e. 0-2 minutes) using Excel. In the UptakeFIT model the initial intracellular concentration value is determined using an empirical equation (Equation 4.1.) derived from the regression of cell initial concentrations to media initial concentrations using data from three different sets of uptake experiments with rosuvastatin generated at Capkr.

Equation 4.1.

$$Cell_{init} = \frac{C_{media} * 1000}{0.197 * C_{media} + 9.282} * 100$$

$Cell_{init}$ represents the cell initial concentration conditions (nM) and C_{media} represents the initial concentration in the media (μM). The question of a blanket approach was raised in the previous chapter. With GSK2879552, using an equation based upon rosuvastatin uptake kinetics determined experimentally by Capkr previously may not be appropriate for different molecules. For example, the binding of rosuvastatin and GSK2879552 in the media were very different, with values of 0.797 and 0.226, respectively, which may explain some of differences observed. As discussed previously, it also highlights the problems of using a locked-in software. The UptakeFIT model also details a correlation matrix and it is quite clear from Appendix 85 that all of the parameters are heavily correlated in all of the donors.

4.6. Conclusions

- No active saturable uptake was observed with GSK2879552 in cryopreserved plated human hepatocytes
- Both models calculated the uptake kinetic parameters, however the error associated with each value made the data unreliable. This has shown the limitations of the model.

Table 4.1. Summary of the uptake kinetic parameters of GSK2879552 in plated cryopreserved adult human hepatocytes from three donors, HU8116, HU8119 and HU1411 using a mechanistic two-compartment model developed by Menochet et al (2012a) and the UptakeFIT model. Each of the four individual parameters is the mean ± standard deviation (coefficient of variation %) derived from the simultaneous fitting of all of the incubations. Also detailed are the mean and standard error of the mean (SEM) for each of these parameters for the three donors.

Mechanistic Model Developed by Menochet et al 2012a					
Donor	V_{max} (pmol/min/10^6 cells)	$K_{m,u}$ (µM)	$CL_{active,u}$ (µL/min/10^6 cells)	$P_{diff,u}$ (µL/min/10^6 cells)	Fu_{cell}
HU8116	0.31 ± 0.28 (90)	0.54 ± 0.80 (148)	0.56	0.85 ± 0.67 (8.4)	0.19 ± 0.02 (7.8)
HU8119	169 ± 406 (240)	23.0 ± 37.0 (161)	2.41	0.50 ± 6.24 (1223)	0.56 ± 6.89 (1204)
HU1411	25.6 ± 16.9 (66)	6.43 ± 3.52 (54)	7.34	4.05 ± 0.66 (16)	0.08 ± 0.01 (16)
Mean ± SEM	65.1 ± 53.6	10.0 ± 6.86	3.97 ± 1.96	1.80 ± 1.15	0.29 ± 0.15
UptakeFIT Model					
Donor					
HU8116	68.7 ± 29.0 (42.3)	1.43 ± 0.73 (51)	48.2	0.50 ± 1.60 (318)	0.48 ± 1.52 (316)
HU8119	100 ± 129 (129)	13.6 ± 12.9 (12.9)	7.31	1.01 ± 2.89 (285)	0.27 ± 0.76 (284)
HU1411	154 ± 229 (149)	25.4 ± 24.9 (98)	6.06	1.21 ± 3.21 (266)	0.26 ± 0.69 (265)
Mean ± SEM	108 ± 25.0	13.5 ± 6.94	20.5 ± 13.9	0.91 ± 0.21	0.34 ± 0.07

Table 4.2. Summary of the uptake clearance (CL_{uptake}) of GSK2879552 in plated cryopreserved adult human hepatocytes. The CL_{uptake} for each individual was calculated by taking the mean over the linear range (0-2 minutes) at all of the concentrations used (0.1, 0.3, 1, 3, 10, 30 and 100 µM). Further the mean (± standard error of the mean) was calculated from the three donors.

Concentration (µM)	CL_{uptake} (µL/min/10^6 Cells)			
	HU8116	HU8119	HU1411	Mean ± SEM
0.3	2.39 ± 0.25	1.57 ± 0.32	2.70 ± 0.20	2.22 ± 0.59
1	2.50 ± 0.24	1.29 ± 0.30	2.52 ± 0.07	2.10 ± 0.71
3	2.47 ± 0.22	1.28 ± 0.16	2.46 ± 0.21	2.07 ± 0.69
10	2.44 ± 0.20	1.40 ± 0.20	2.07 ± 0.10	1.97 ± 0.53
30	2.27 ± 0.21	1.28 ± 0.13	2.47 ± 0.21	2.01 ± 0.64
100	2.70 ± 0.38	1.51 ± 0.39	1.94 ± 0.17	2.05 ± 0.60

CHAPTER 5: FINAL CONCLUSIONS

The main aim of this study was to determine the uptake kinetic parameters of rosuvastatin in cryopreserved adult human hepatocytes using a new mechanistic model, which allowed the simultaneous fitting of all of the intracellular concentrations of rosuvastatin at all of the time points and media concentrations. The advantages of this approach are that to calculate P_{diff} it is not necessary to cool the cells to 4ºC or use a cocktail of inhibitors. In addition, the fraction unbound (Fu_{cell}) in the cell is also derived. This parameter is becoming very important to understand the potential of a drug to elicit a response from a target, whether to explain a lack of efficacy or cause a drug-drug interaction (DDI). In addition, the department at GSK has acquired a new technique to understand the disposition of new chemical entities and generate important parameters that may then be useful in further modelling studies.

Another aim of the study was to determine the inhibitory effect of cyclosporin A (CsA) and its main metabolite cyclosporin AM1 (AM1) on the uptake of rosuvastatin in the human hepatocytes. Clinical DDI have been reported between CsA and rosuvastatin and these data may allow the extrapolation of *in vitro* to *in vivo* kinetics and provide an understanding of the interplay between different disposition mechanisms, with particular regard to the potential to predict DDI. Another area of interest was also investigated, the apparent time-dependent inhibition of uptake transporters by CsA. In this study there was no apparent difference between co- and pre-incubation for either CsA or AM1, which may be due to the substrate choice and/or the cell type.

In this study, human cryopreserved hepatocytes were used in the uptake and inhibition studies with rosuvastatin. In the uptake experiments, variability was observed in the parameters calculated using both models between the three adult donors. Variability has been observed with human hepatocytes previously, in terms of probe substrate uptake and also in terms of the expression of uptake transporters, such as OATPs [Shitara 2003a; Shitara 2004; Prasad et al 2014]. When designing an uptake study using human hepatocytes this potential for variability will need to be considered. With more simple in vitro assays, such as expressed cell lines which are used more frequently in early discovery DMPK, continuity between different batches is required, as comparisons in the parameters generated are often made between different compounds. However, rather than being a possible limitation in the

experimental design, the variability observed in the hepatocytes from different donors may actually be welcome to help predict/understand the variability observed within the population, whether the differences are in PK profiles or DDI.

Finally, the uptake parameters were determined using GSK2879552 in the same cryopreserved human hepatocytes. Although non-clinical and *in vitro* human data suggested that GSK2879552 would be a prime candidate to be a substrate of an uptake transporter, it would appear that is not. This has been a key and important learning with regards understanding the model(s) and their limitations.

5.1. Future studies

- Continue to determine the pre-and co-incubation increase in potency with cyclosporin A (and cyclosporin AM1). Use estradiol glucuronide as the probe substrate with hepatocytes and rosuvastatin with the OATP1B1 over-expressed cell lines. This would show whether the phenomena is substrate or cell assay related. Depending upon the outcome consider other inhibitors and substrates.
- Use the uptake parameters and the inhibition parameters to populate in silico models. The inhibition data for CsA and AM1 were of interest to SimCYP™ (personal communication).
- Test the uptake mechanistic models with alternative and more challenging substrates i.e. a substrate with moderate/good permeability that is also a transporter substrate.
- Evaluate the role of sodium taurocholate co-transporting polypeptide (NTCP) in the uptake of rosuvastatin in human hepatocytes. In this study there did not appear to a role using a sodium free media. However, residual sodium in hepatocytes may confuse the interpretation.
- Consider the new hepatocyte models that are available, in particular the 3D and flow through systems, to evaluate rosuvastatin uptake kinetics.

APPENDICES

Appendix 1. Radio-chromatogram integration for the purity check of [^{3}H]-rosuvastatin.

Name (H-3)	Retention (mins)	Start (mins)	End (mins)	Height (cps)	Area (Counts)	%ROI (%)	%Total (%)
Bkg 1	2.32	1.60	9.53	2.0			
Rosuvastatin	15.48	15.25	15.85	630.0	6813.6	76.04	69.91
Region 1	17.85	17.65	18.08	124.0	1505.1	16.80	15.44
Region 2	19.28	19.15	19.50	53.0	642.3	7.17	6.59
Bkg 2	26.80	23.60	30.62	2.0			
3 Peaks					8961.1	100.00	91.95
Total Area					9745.6		100.00
Background					1355.5		0.73
Unallocated Area					713.2		7.32

Appendix 2. Radio-HPLC conditions for the determination of the radio-chemical purity of [^{3}H]-β-Estradiol-17-β-D-glucuronide.

Chromatography System	Agilent 1100 Series G1312A	
Autosampler	Agilent 1100 Series G1367A	
UV Detector	Agilent 1100 Series G1314A	
Radio Detector	β-Ram by LabLogic (Model 3)	
Column	Zorbax ODS 5µm (250 x 4.6mm) Agilent Technologies	
Solvent A	1% (w/v) tetraethyl ammonium acetate tetrahydrate (TEAA) in de-ionized water pH 4	
Solvent B	Methanol	
Elution Conditions	Time (minutes)	% B
	0	35
	5	35
	25	70
	30	70
	35	35
	40	35
Temperature	25°C	
UV Absorbance (nm)	210	
Eluate Flow Rate (mL/min)	1.0	
Scintillant Flow Rate (mL/min)	3.0	
Scintillant	FlowLogic Maxcount	

Appendix 3. Representative radio-chromatogram for the purity check of [^{3}H]-β-Estradiol-17-β-D-glucuronide.

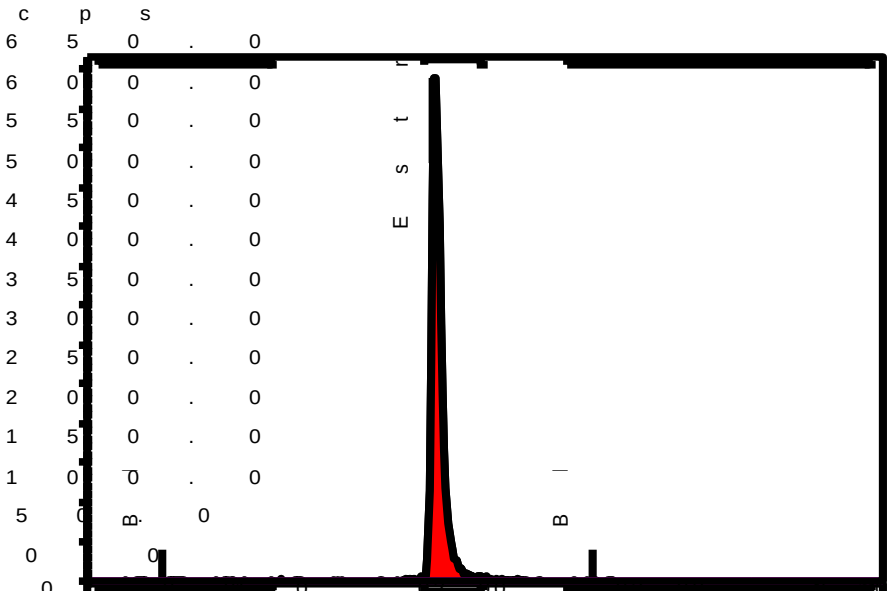

Name (H-3)	Retention (mins)	Start (mins)	End (mins)	Height (cps)	Area (Counts)	%ROI (%)	%Total (%)
Bkg 1	3.78	0.58	9.25	3.0			
Estradiol Glucuronide	17.42	17.00	19.87	641.0	19604.3	100.00	98.75
Bkg 2	25.38	24.10	39.37	2.0			
1 Peak					19604.3	100.00	98.75
Total Area					19851.9		100.00
Background							1.65
Unallocated Area					-80.5		-0.41

Appendix 4. Preparation and dilutions of the analyte (rosuvastatin) working solutions.

Working Solution	Final Concentration (μg/mL)	Volume of Spiking Solution	Volume of DMF (μL)
A1/B1	10	A/B 100 μL	900
A2/B2	1	A1/B1 100 μL	900
A3/B3	0.1	A2/B2 100 μL	900

Appendix 5. Preparation of the rosuvastatin calibration standards.

Standard Concentration in Matrix (ng/mL)	Volume of Spiking Solution (μL)				Volume of Matrix (μL)
	A3 0.1 μg/mL	A2 1 μg/mL	A1 10 μg/mL	A 100 μg/mL	
1	5				495
2	10				490
4	20				480
20		10			490
100			5		495
500			25		475
800				4	496
1000				5	495

Appendix 6. Preparation of the rosuvastatin quality control/validation standards.

QC Concentration in Matrix (ng/mL)	Volume of Spiking Solution (μL)			Volume of Matrix (μL)
	B3 0.1 μg/mL	B1 10 μg/mL	B 100 μg/mL	
3	15			485
200		10		490
800			4	496

Appendix 7. Preparation and dilutions of the internal standard [$^{2}H_{7}$ $^{15}N_{2}$]-rosuvastatin.

Working Solution	Final Concentration (ng/mL)	Volume of Spiking Solution (μL)	Total Volume Acetonitrile/Methanol/Formic acid 95/5/0.1 v/v/v (mL)
C1	500	250 μL of solution C	1000

Appendix 8. HPLC conditions to analyse rosuvastatin

Autosampler	Waters Aquity System
Injector Wash Solvent 1	40/30/30 Acetonitrile / IPA / 0.1% Formic acid
Injector Wash Solvent 2	40/30/30 Acetonitrile / IPA / 0.1% Formic acid
Typical Injection Volume	10 μL
Chromatography System	Waters Aquity System
Flow Rate	0.80 mL/min
Analytical Column	50 x 3mm i.d. Synergi Fusion 4 μm
Column Temperature	45°C
Run Time	1.5 minutes
Mobile Phase A	Water containing 0.1% (v/v) formic acid
Mobile Phase B	Acetonitrile
Isocratic Composition A:B	48:52 (v/v)

Appendix 9. MS/MS conditions to analyse rosuvastatin

Mass Spectrometer	Applied Biosystems/MDS Sciex API-4000
Split Ratio	none
Ionisation Interface and Temperature	TurboIonSpray® at 650°C
Pause Time	5 msec
Gas 1 Setting (Air)	40 psi
Gas 2 Setting (Air)	60 psi
Curtain Gas Setting (Nitrogen)	25
Collision Gas Setting (Nitrogen)	7
DP Value	50
CE Value	48

Appendix 10. Solvents used for LC/MS

Reagent	Function	Preparation
ACN:Water:IPA containing formic acid (0.1%), 4:3:3	Solvent Wash 1	Formic acid (1 mL) in ACN (400 mL), water (300 mL) and IPA (300 mL)
ACN:Water:IPA containing formic acid (0.1%), 4:3:3	Solvent Wash 2	Formic acid (1 mL) in ACN (400 mL), water (300 mL) and IPA (300 mL)
Water containing formic acid (0.1%, v/v)	Mobile Phase A	Formic acid (1 mL) in water (made up to 1000 mL)
ACN	Mobile Phase B	As Supplied

ACN = Acetonitrile and IPA = Isopropanol

Appendix 11. The kinetic profiles of [^{3}H]-β-Estradiol-17-β-D-glucuronide uptake in plated paediatric human hepatocytes at 6 concentrations (0.3–100 μM) over a 30 minute incubation. Lines represent the predicted uptake profile based upon a mechanistic two-compartmental model describing the changes in drug concentrations in both the cells and the incubation media over time. Data points are duplicate measurements.

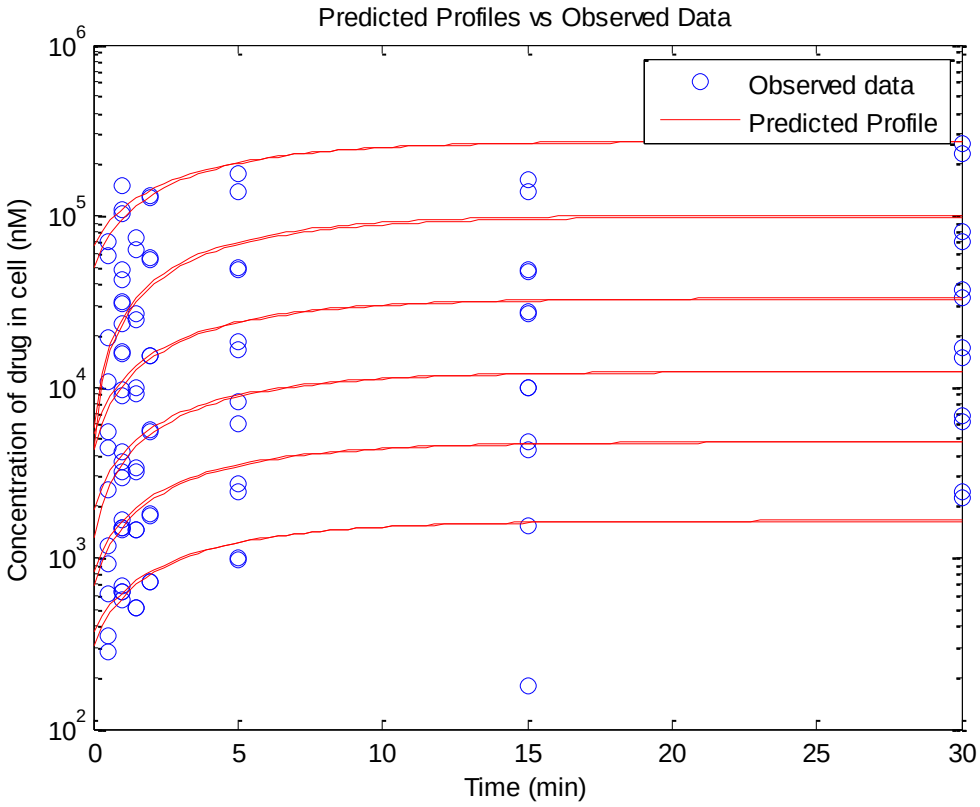

Appendix 12. The kinetic profiles of rosuvastatin uptake in plated paediatric human hepatocytes at 6 concentrations (0.3–100 μM) over a 45 minute incubation. Lines represent the predicted uptake profile based on a mechanistic two-compartmental model describing the changes in drug concentrations in both the cells and the incubation media over time. Data points are duplicate measurements.

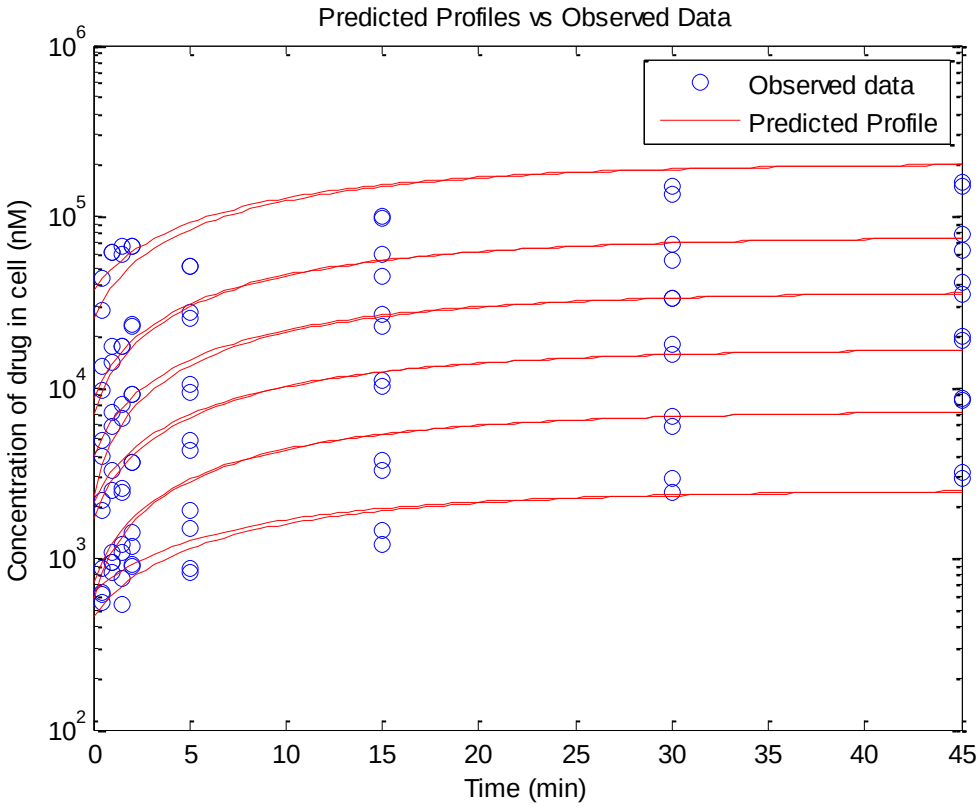

Appendix 13. The kinetic profiles of rosuvastatin uptake in plated paediatric human hepatocytes at 6 concentrations (0.3–100 μM) over a 45 minute incubation in a sodium free media. Lines represent the predicted uptake profile based on a mechanistic two-compartmental model describing the changes in drug concentrations in both the cells and the incubation media over time (equations 1 and 2). Data points are duplicate measurements.

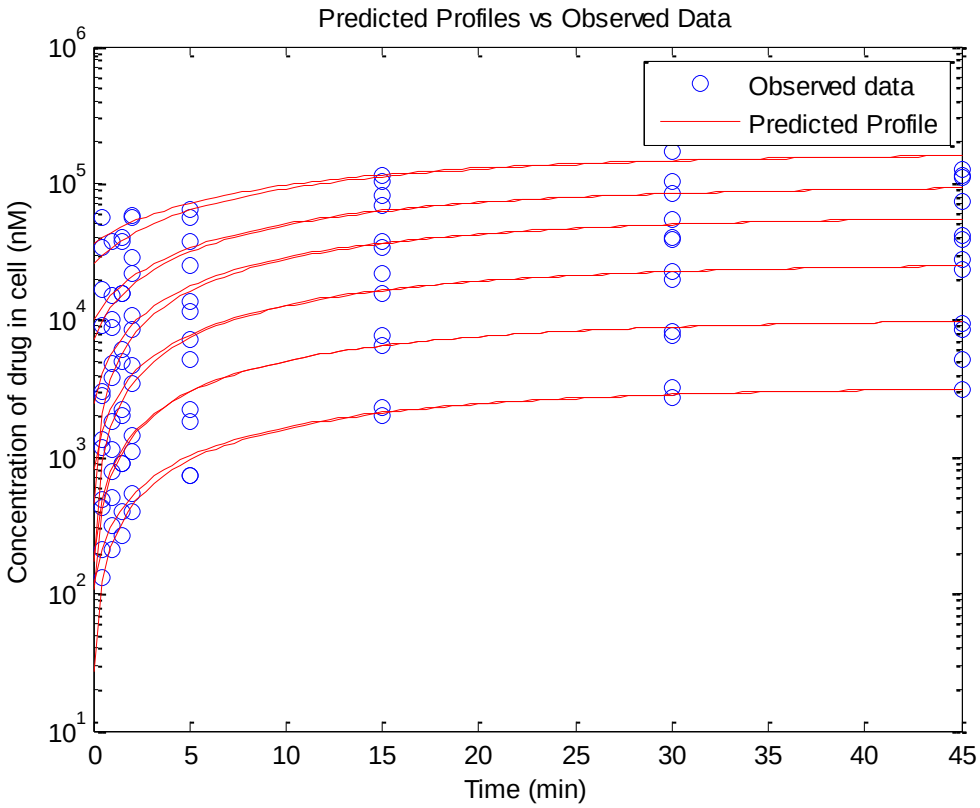

Appendix 14. Inhibition of estradiol glucuronide uptake determined at a concentration of 0.1 µM over 5 minutes in plated paediatric human hepatocytes by cyclosporin A over 10 concentrations (0.003-6 µM). Mean data (n=4 per inhibitor concentration) are depicted.

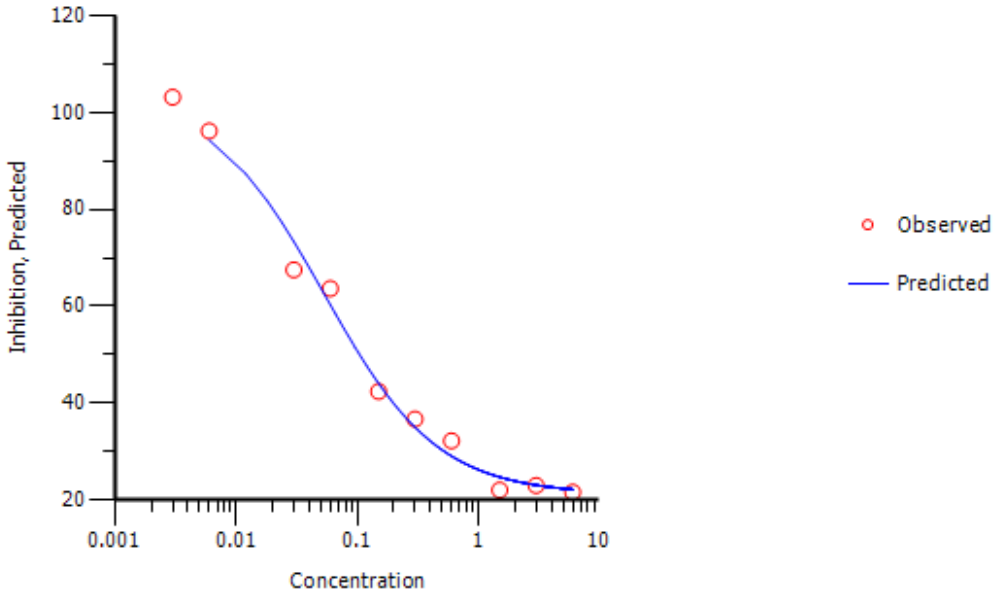

Appendix 15. Inhibition of rosuvastatin uptake determined at a concentration 1 µM over 5 minutes in plated paediatric human hepatocytes by cyclosporin A over 10 concentrations (0.003-12 µM). Mean data (n=4 per inhibitor concentration) are depicted.

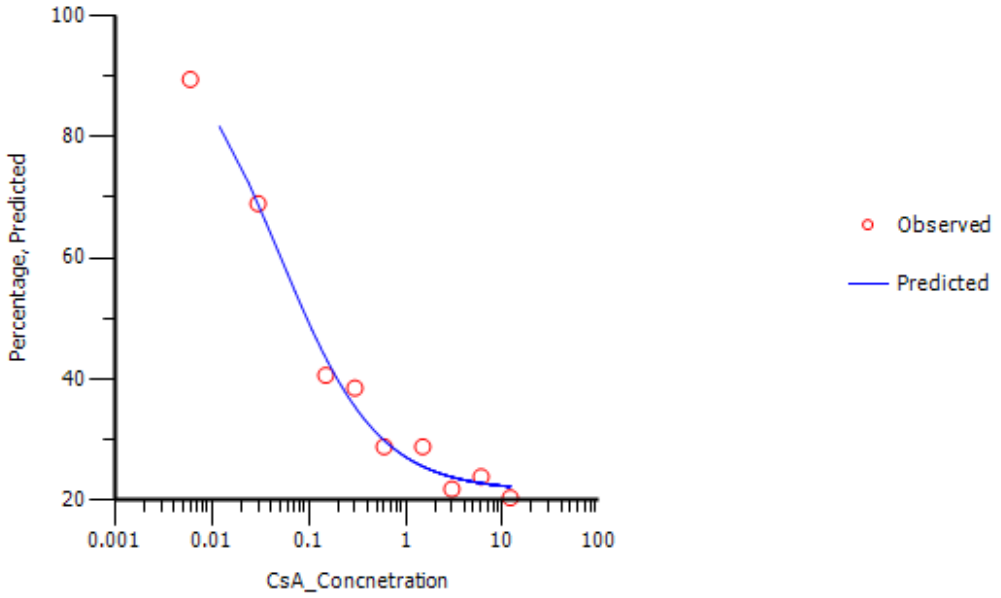

Appendix 16. Inhibition of rosuvastatin uptake determined at a concentration of 1 µM over 5 minutes in plated paediatric human hepatocytes by rifampicin with 10 concentrations (0.025-50 µM). Mean data (n=4 per inhibitor concentration) are depicted.

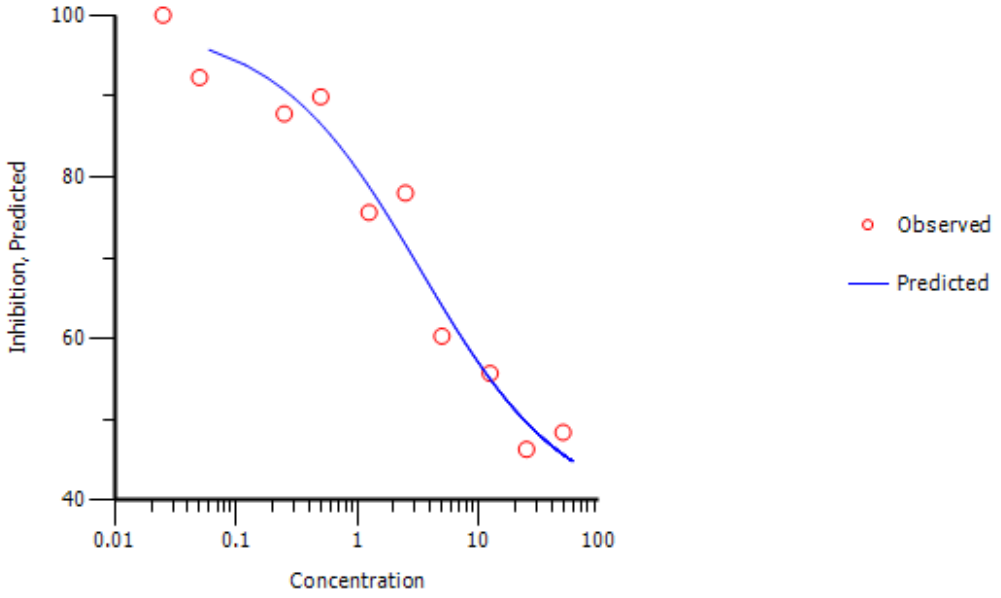

Appendix 17. The graphic user interface (GUI) of the UptakeFIT modelling software.

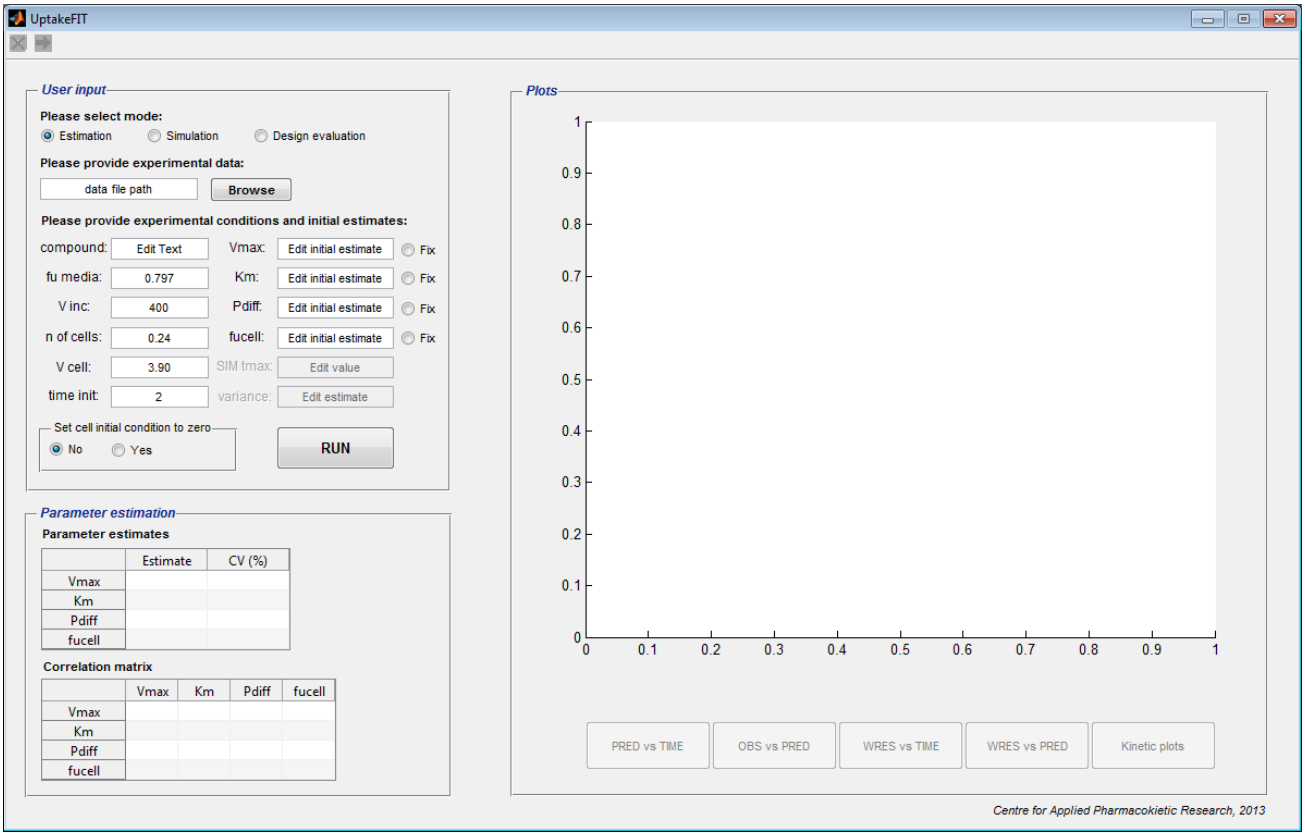

Appendix 18. The kinetic profiles of rosuvastatin uptake in plated adult human hepatocytes from donor HU8116 at 6 concentrations (0.3–100 μM) over a 60 minute incubation. Lines represent the predicted uptake profile based upon a mechanistic two-compartmental model describing the changes in drug concentrations in both the cells and the incubation media over time. Data points are triplicate measurements.

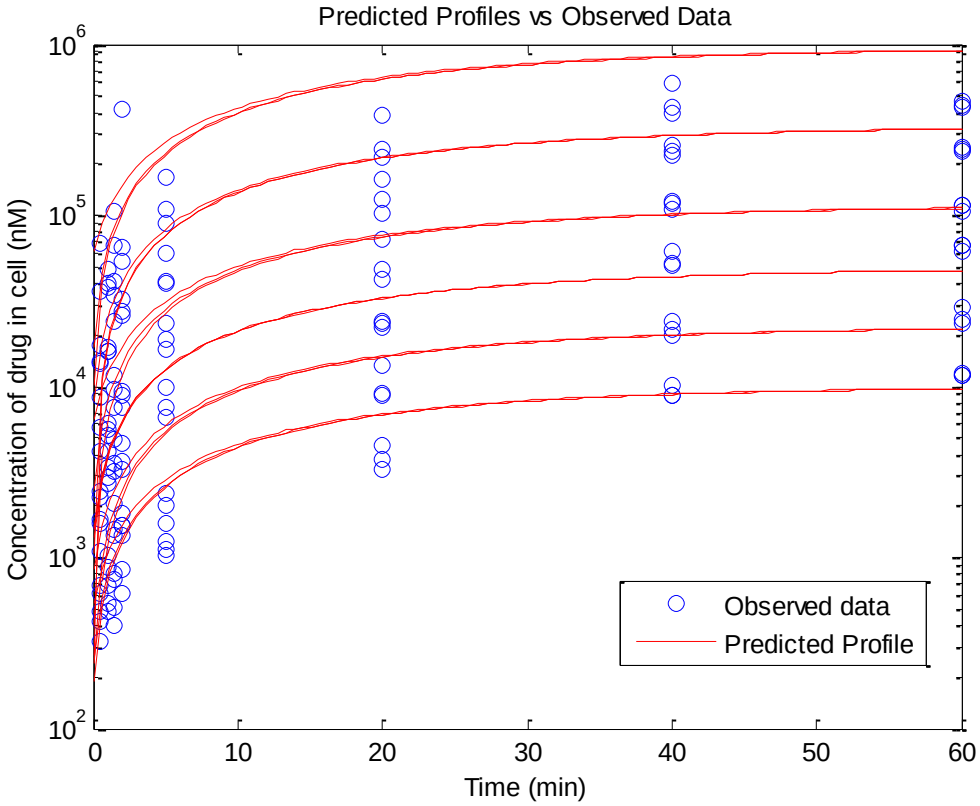

Appendix 19. The kinetic profiles of rosuvastatin uptake in plated adult human hepatocytes from donor HU8119 at 6 concentrations (0.3–100 µM) over a 60 minute incubation. Lines represent the predicted uptake profile based upon a mechanistic two-compartmental model describing the changes in drug concentrations in both the cells and the incubation media over time. Data points are triplicate measurements.

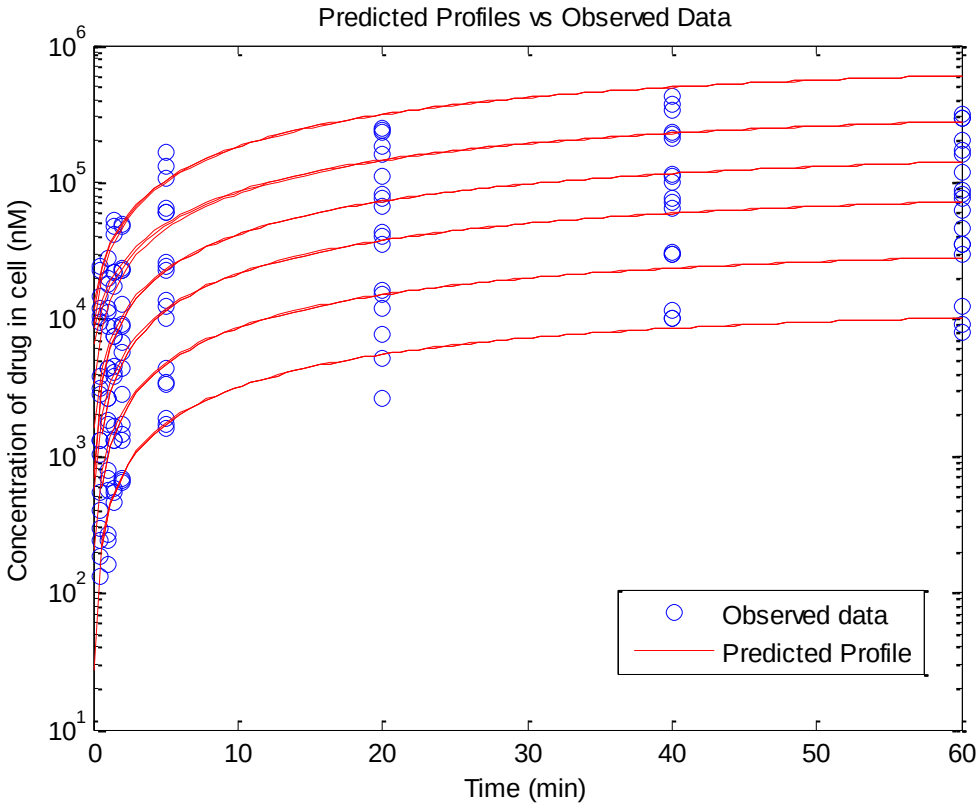

Appendix 20. The kinetic profiles of rosuvastatin uptake in plated adult human hepatocytes from donor HU1411 at 6 concentrations (0.3–100 μM) over a 60 minute incubation. Lines represent the predicted uptake profile based upon a mechanistic two-compartmental model describing the changes in drug concentrations in both the cells and the incubation media over time. Data points are triplicate measurements.

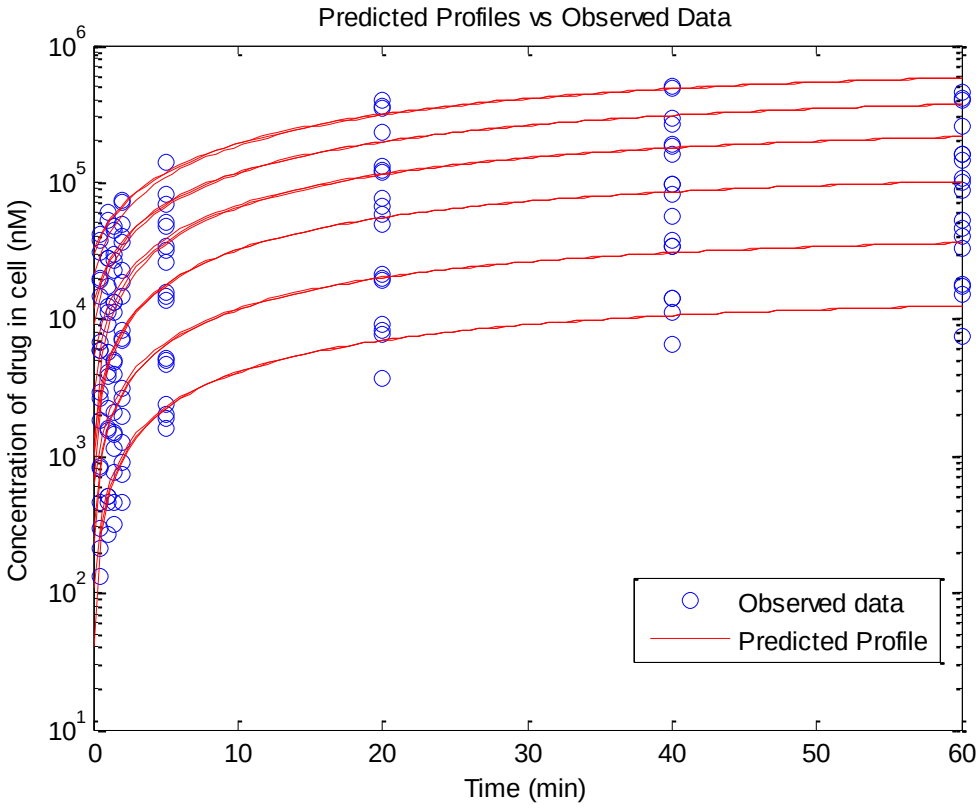

Appendix 21. The predicted versus observed data from donor HU8116. The line of unity (solid) and the upper (2-fold) and lower (2-fold, dotted) are depicted.

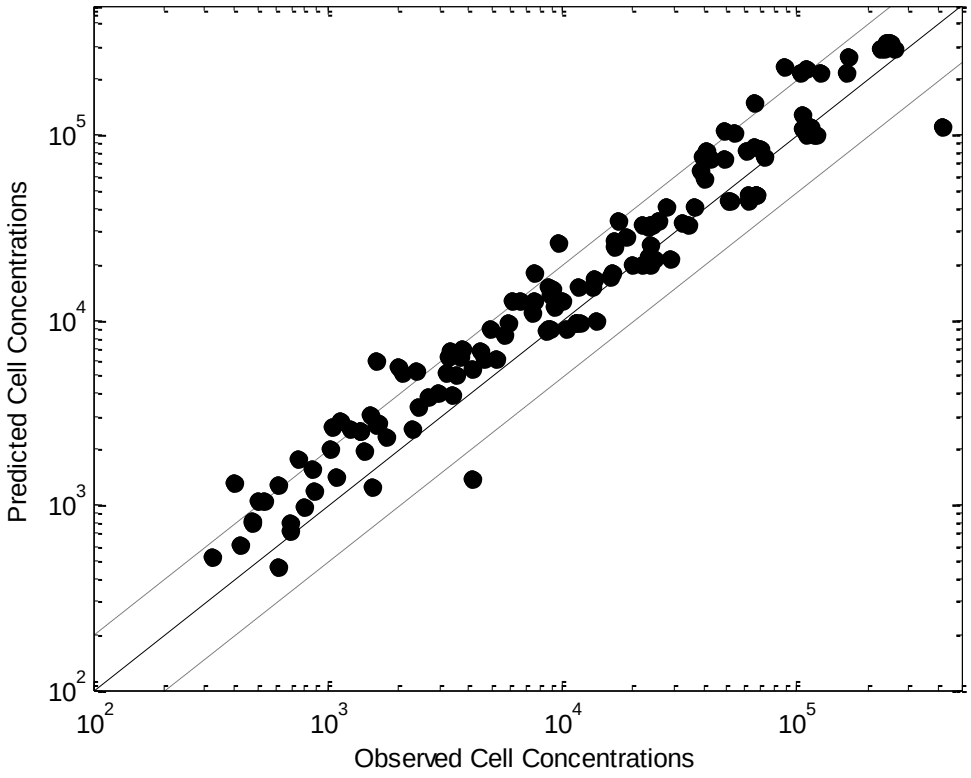

Appendix 22. The predicted versus observed data from donor HU8119. The line of unity (solid) and the upper (2-fold) and lower (5%) 2-fold, dotted) are depicted.

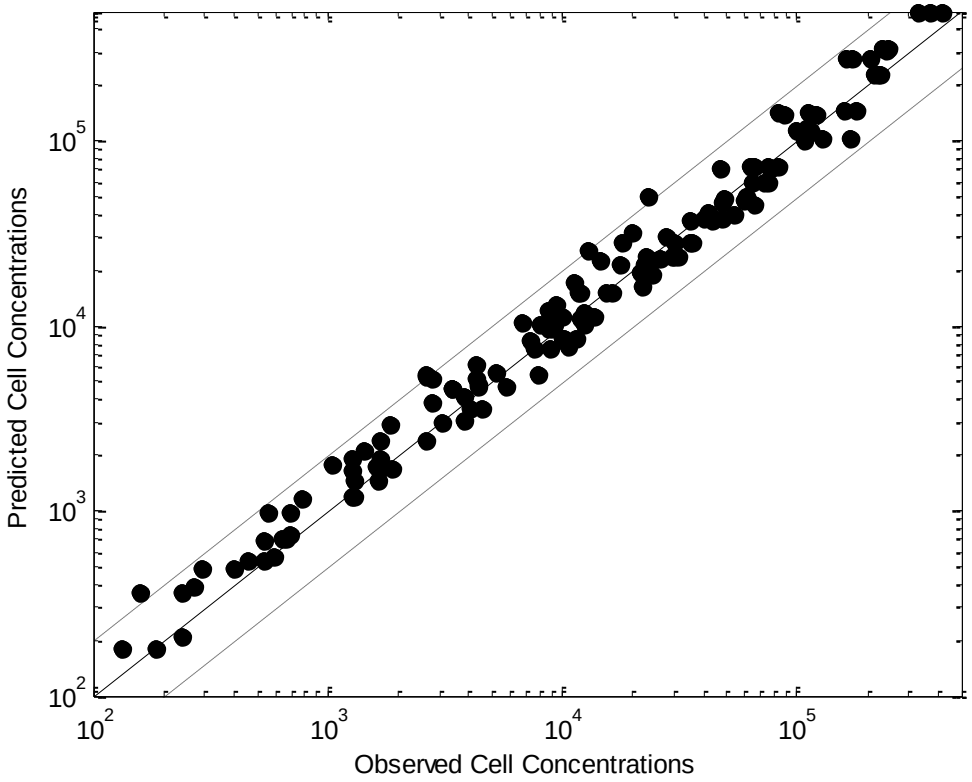

Appendix 23. The predicted versus observed data from donor HU1411. The line of unity (solid) and the upper (2-fold) and lower (2-fold, dotted) are depicted.

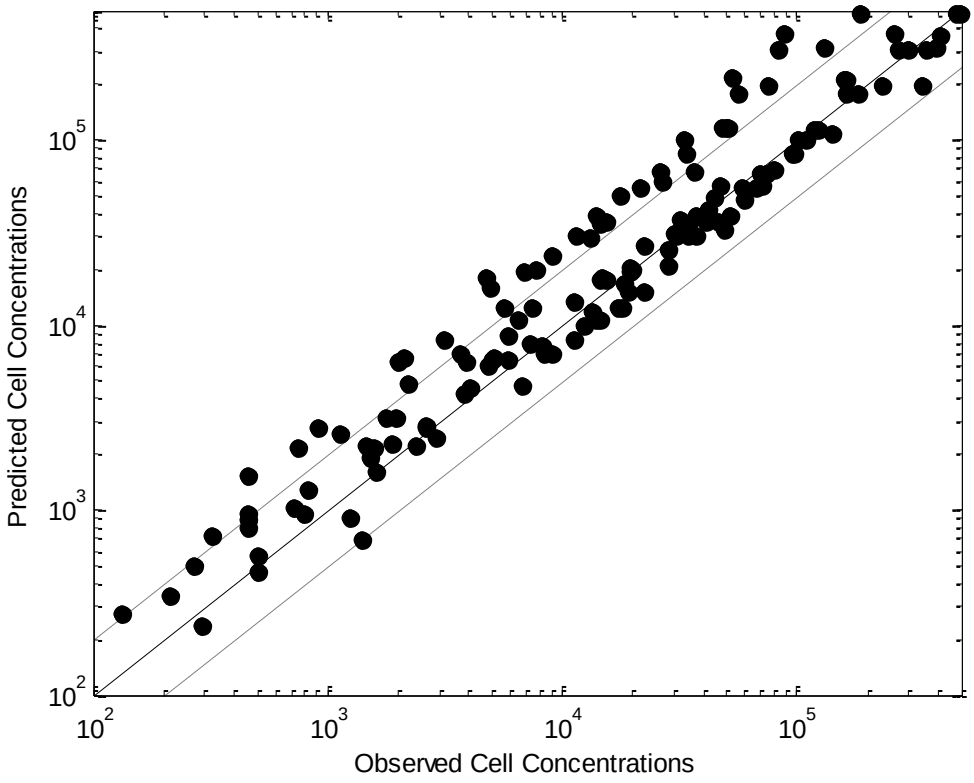

Appendix 24. Profiles of rosuvastatin intracellular concentrations in cryopreserved human hepatocytes (donors HU8116, HU8119 and HU1411) following incubation in a media containing rosuvastatin at a concentration of 0.33 µM at selected time points up to 60 minutes.

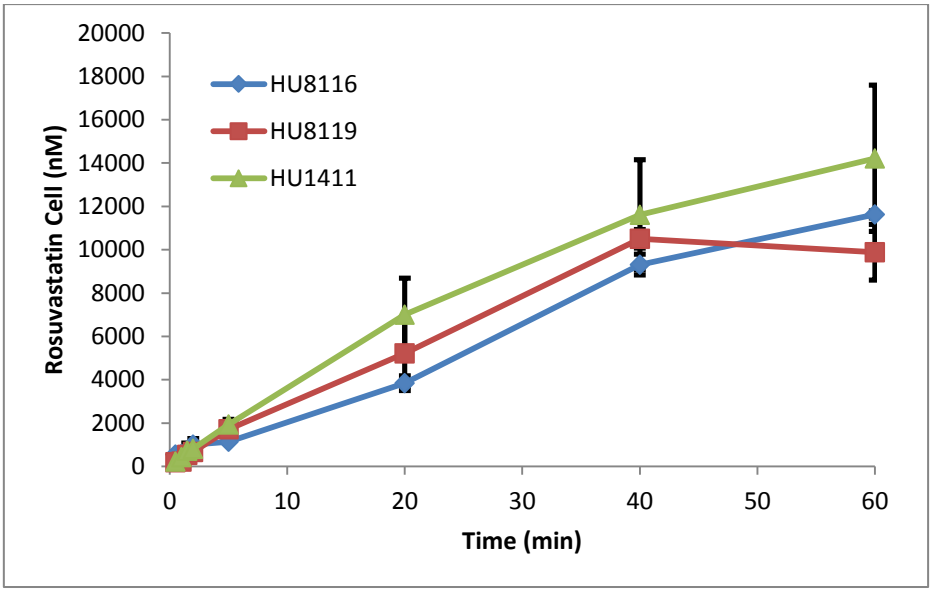

Appendix 25. Profiles of rosuvastatin intracellular concentrations in cryopreserved human hepatocytes (donors HU8116, HU8119 and HU1411) following incubation in a media containing rosuvastatin at a concentration of 1.0 µM at selected time points up to 60 minutes.

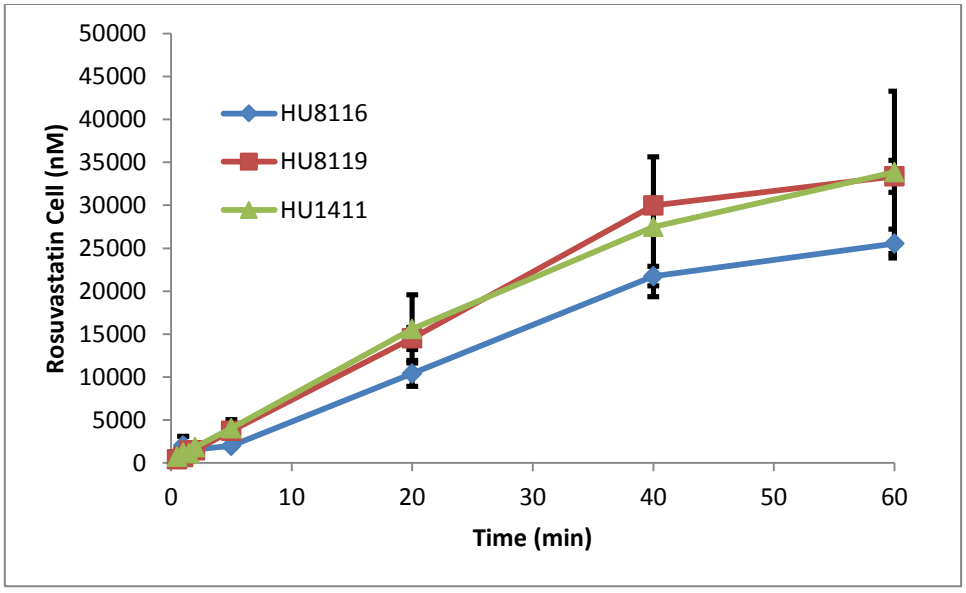

Appendix 26. Profiles of rosuvastatin intracellular concentrations in cryopreserved human hepatocytes (donors HU8116, HU8119 and HU1411) following incubation in a media containing rosuvastatin at a concentration of 3.3 µM at selected time points up to 60 minutes.

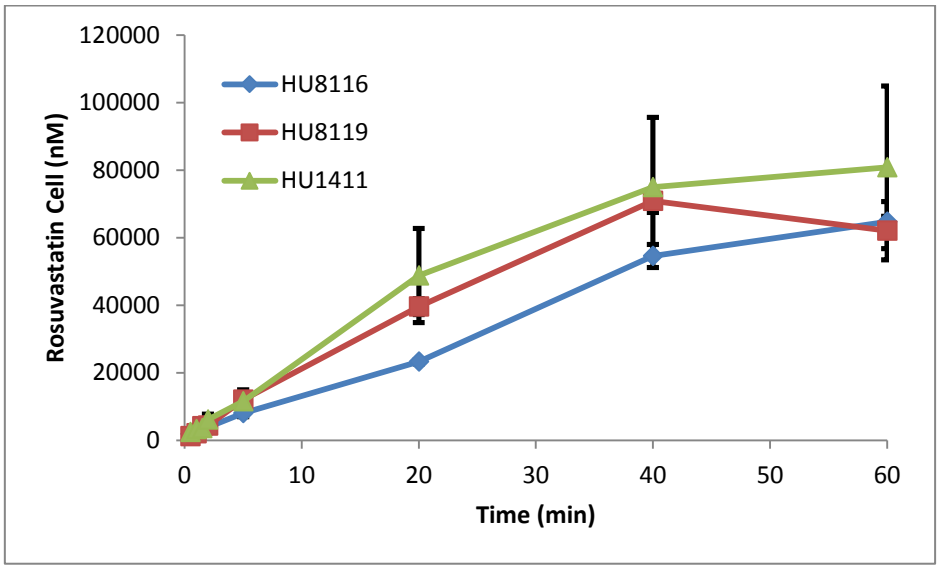

Appendix 27. Profiles of rosuvastatin intracellular concentrations in cryopreserved human hepatocytes (donors HU8116, HU8119 and HU1411) following incubation in a media containing rosuvastatin at a concentration of 10 µM at selected time points up to 60 minutes.

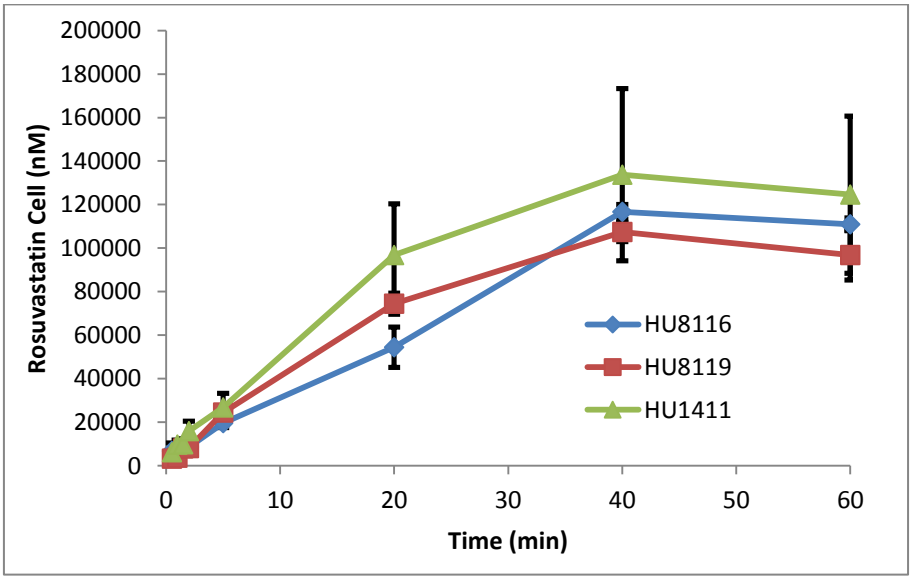

Appendix 28. Profiles of rosuvastatin intracellular concentrations in cryopreserved human hepatocytes (donors HU8116, HU8119 and HU1411) following incubation in a media containing rosuvastatin at a concentration of 30 µM at selected time points up to 60 minutes.

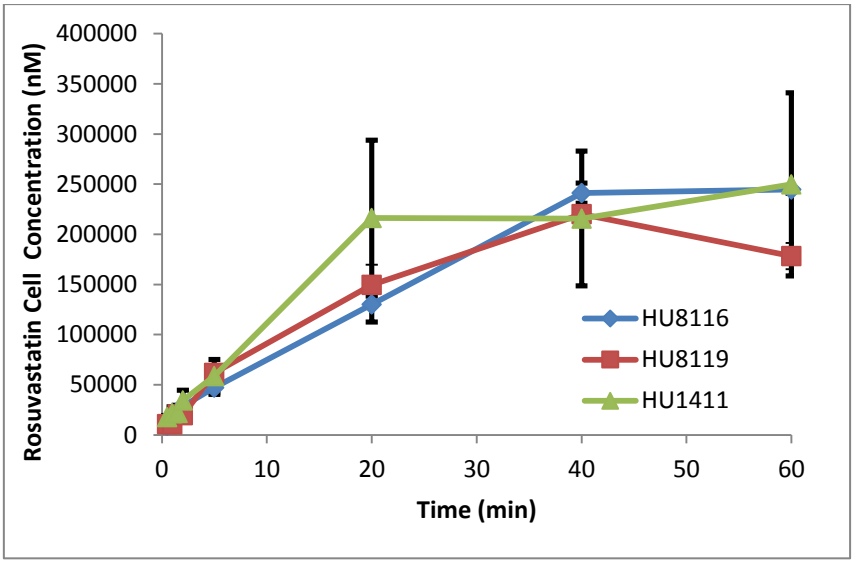

Appendix 29. Profiles of rosuvastatin intracellular concentrations in cryopreserved human hepatocytes (donors HU8116, HU8119 and HU1411) following incubation in a media containing rosuvastatin at a concentration of 100 µM at selected time points up to 60 minutes.

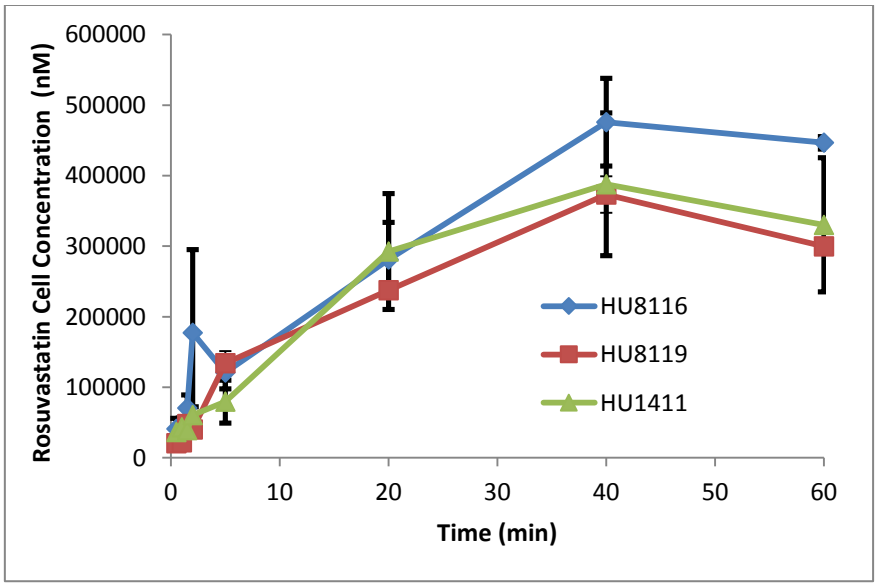

Appendix 30. Plot of the predicted cell concentration – time profiles (solid lines) with the observed cell concentrations (solid dots) for the uptake of rosuvastatin in adult human hepatocytes (donor HU8116) at 6 concentrations (0.3–100 µM) over a 60 minute incubation from the uptake FIT model. Data points are triplicate measurements.

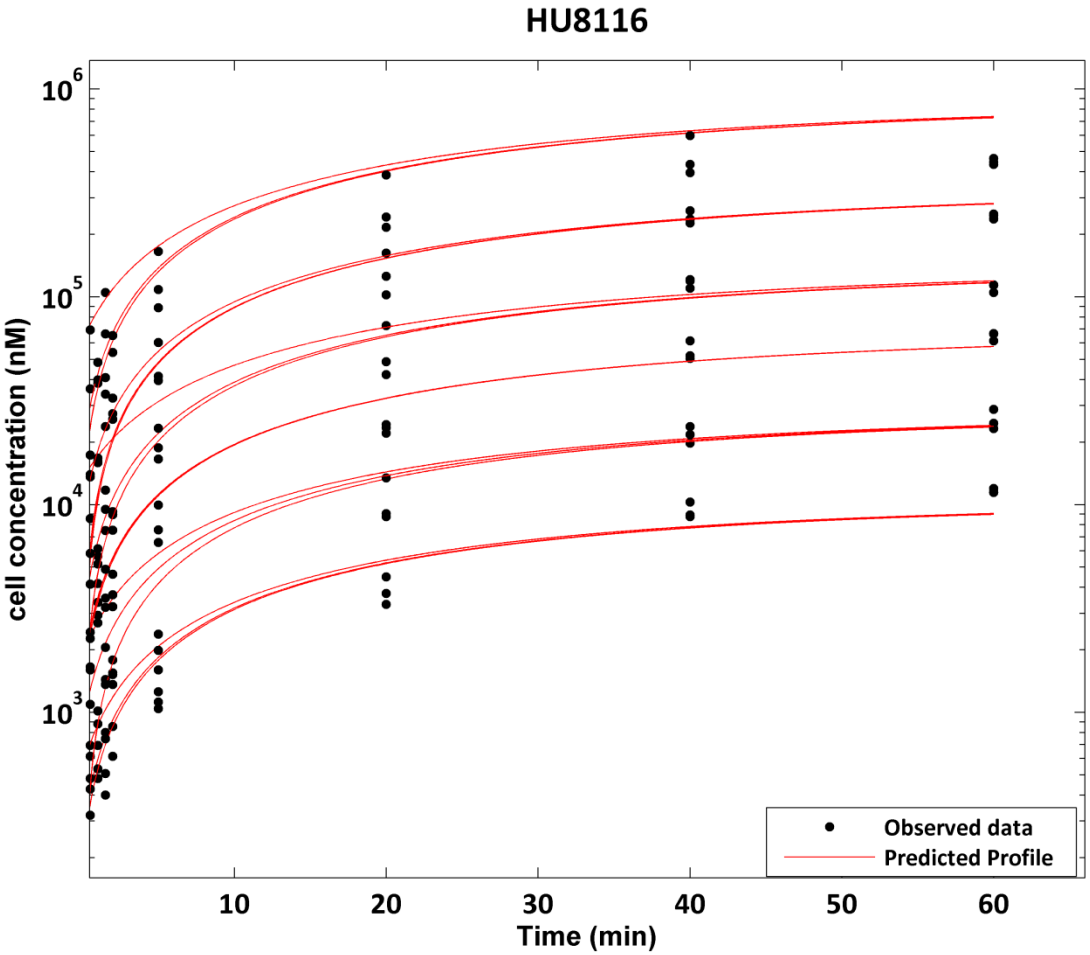

Appendix 31. Plot of the predicted cell concentration – time profiles (solid lines) with the observed cell concentrations (solid dots) for the uptake of rosuvastatin in adult human hepatocytes (donor HU8119) at 6 concentrations (0.3–100 μM) over a 60 minute incubation from the uptake FIT model. Data points are triplicate measurements.

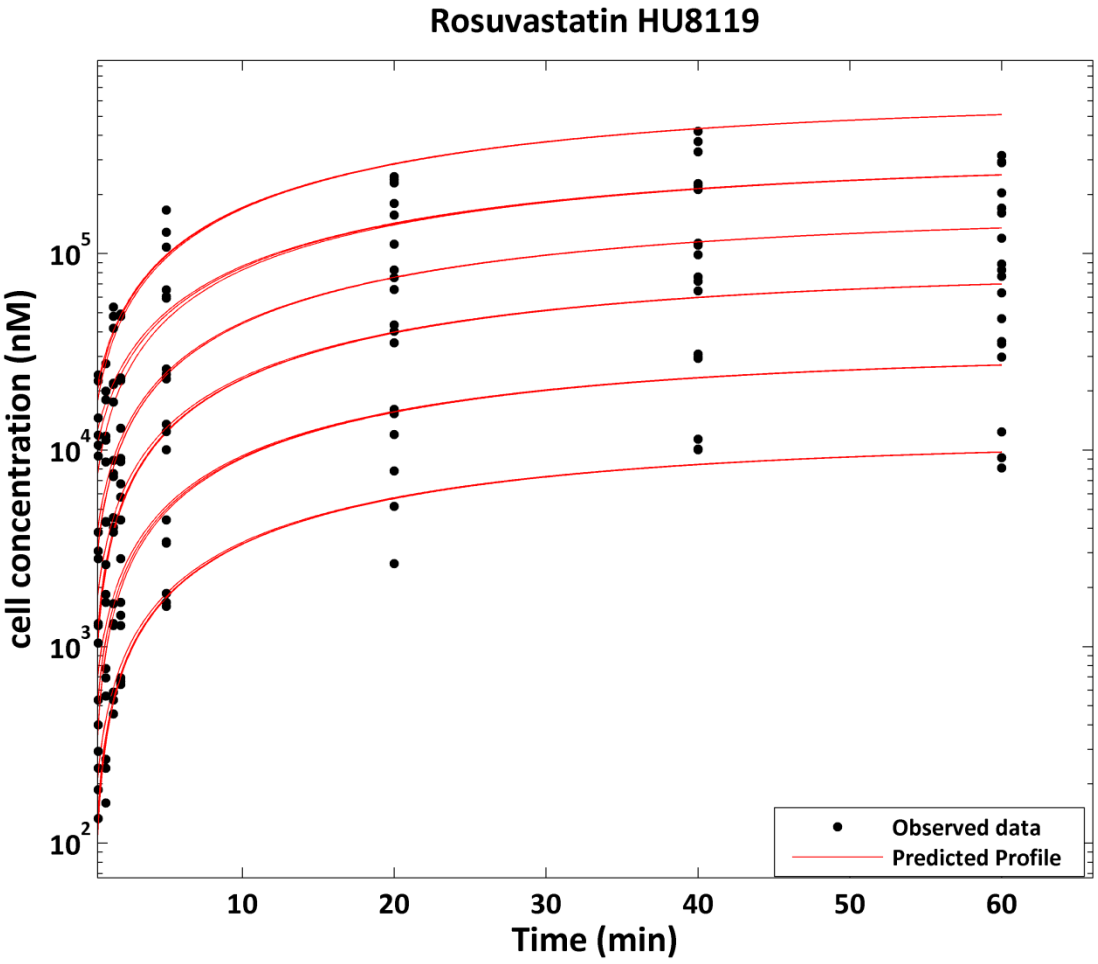

Appendix 32. Plot of the predicted cell concentration – time profiles (solid lines) with the observed cell concentrations (solid dots) for the uptake of rosuvastatin in adult human hepatocytes (donor HU1411) at 6 concentrations (0.3–100 µM) over a 60 minute incubation from the uptake FIT model. Data points are triplicate measurements.

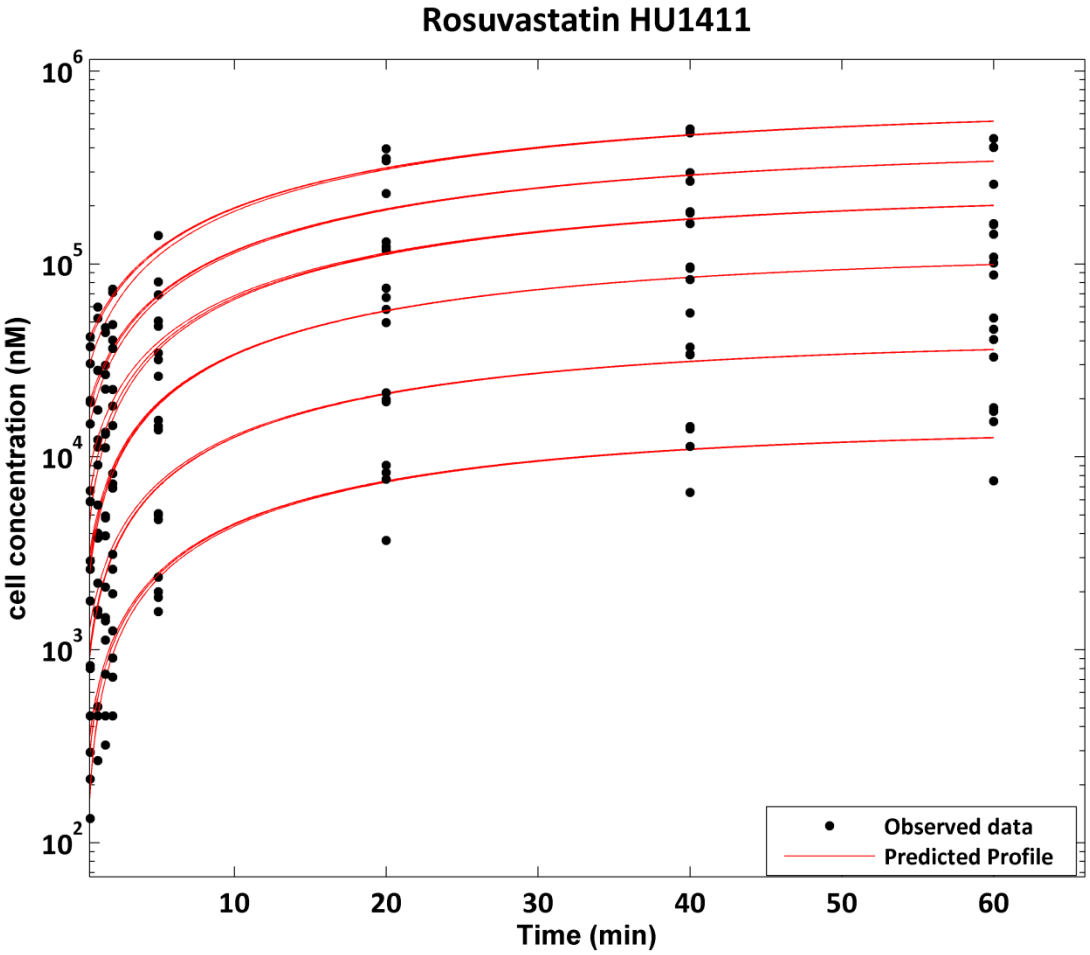

Appendix 33. Plot of the observed versus predicted cell concentrations for the uptake of rosuvastatin in adult human hepatocytes (donor HU8116) at 6 concentrations (0.3–100 μM) over a 60 minute incubation from the uptake FIT model. Data points are triplicate measurements.

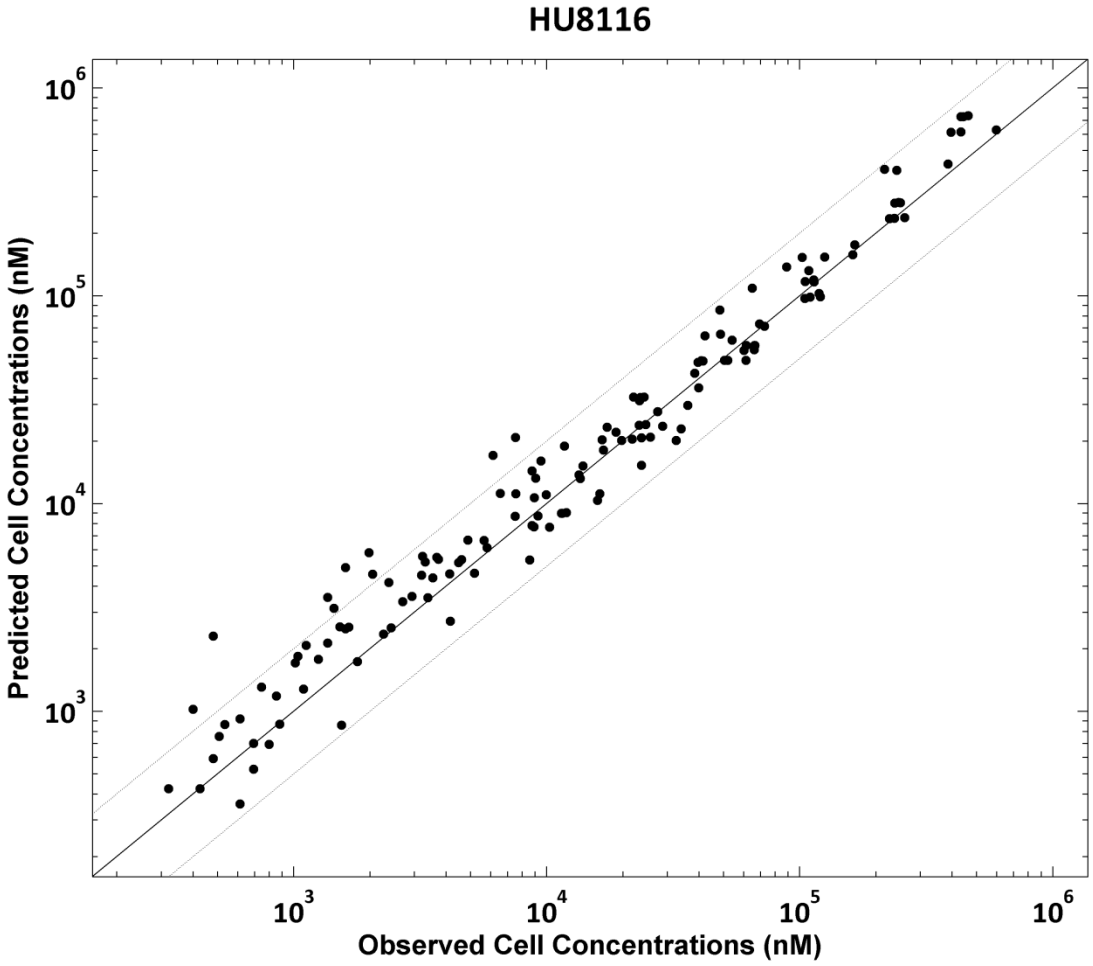

Appendix 34. Plot of the observed versus predicted cell concentrations for the uptake of rosuvastatin in adult human hepatocytes (donor HU8119) at 6 concentrations (0.3–100 μM) over a 60 minute incubation from the uptake FIT model. Data points are triplicate measurements.

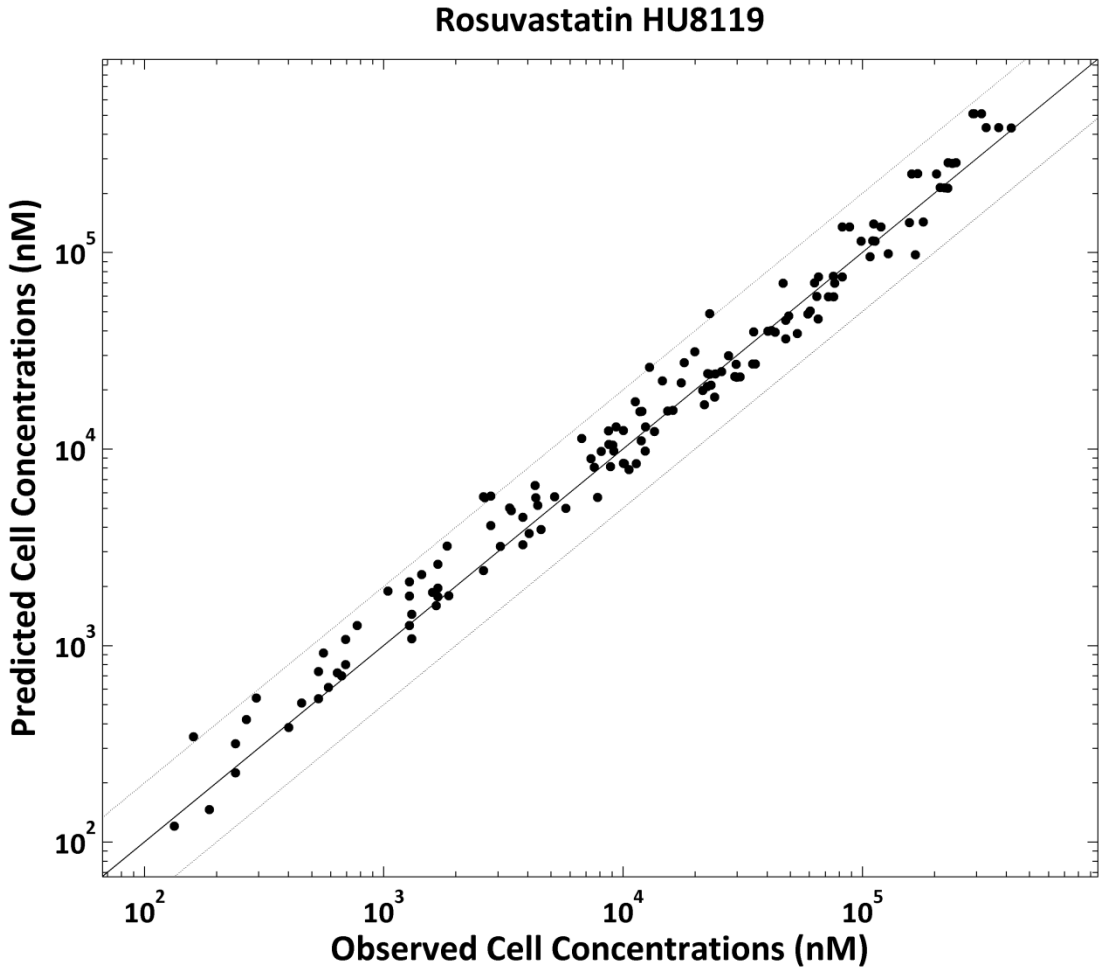

Appendix 35. Plot of the observed versus predicted cell concentrations for the uptake of rosuvastatin in adult human hepatocytes (donor HU1411) at 6 concentrations (0.3–100 μM) over a 60 minute incubation from the uptake FIT model. Data points are triplicate measurements.

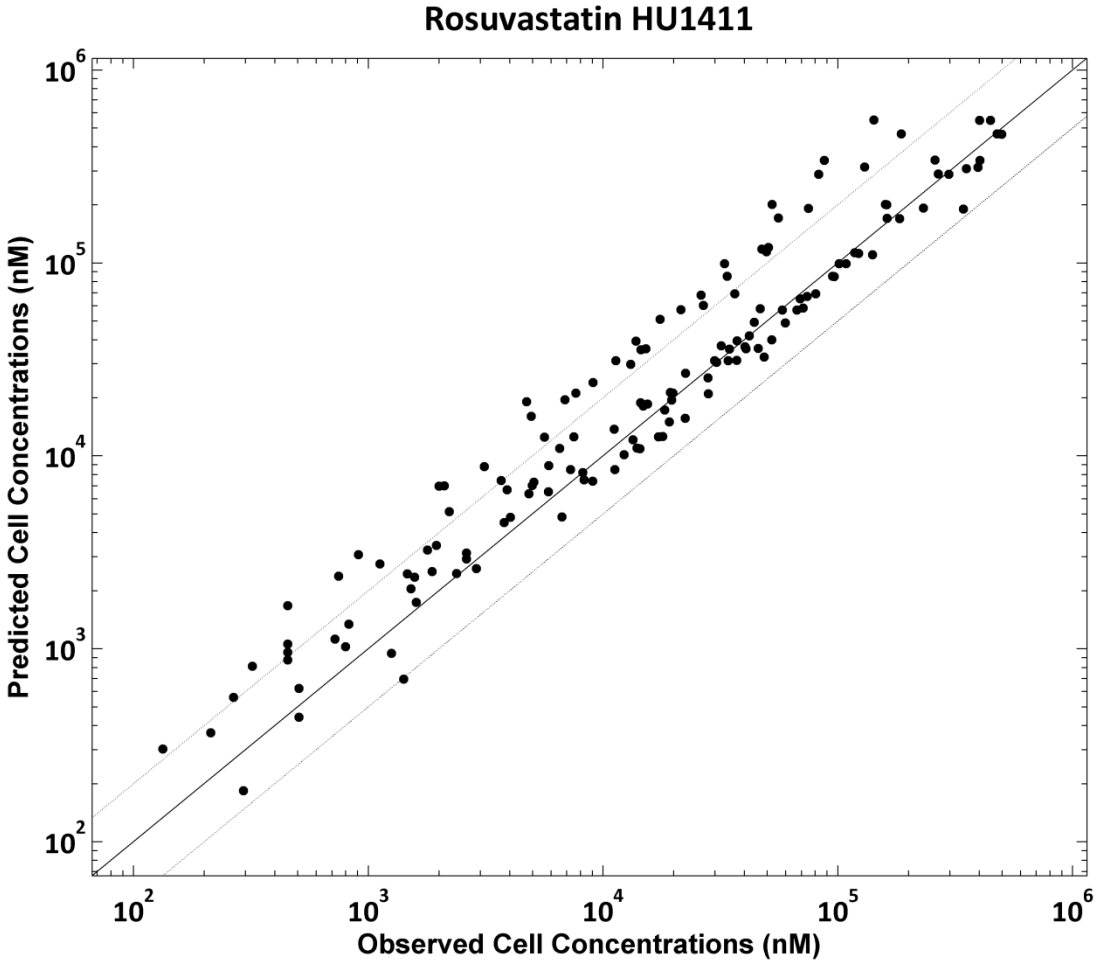

Appendix 36. Plot of the weighted residuals versus predicted cell concentrations for the uptake of rosuvastatin in human hepatocytes (donor HU8116) at 6 concentrations (0.3–100 μM) over a 60 minute incubation from the uptake FIT model.

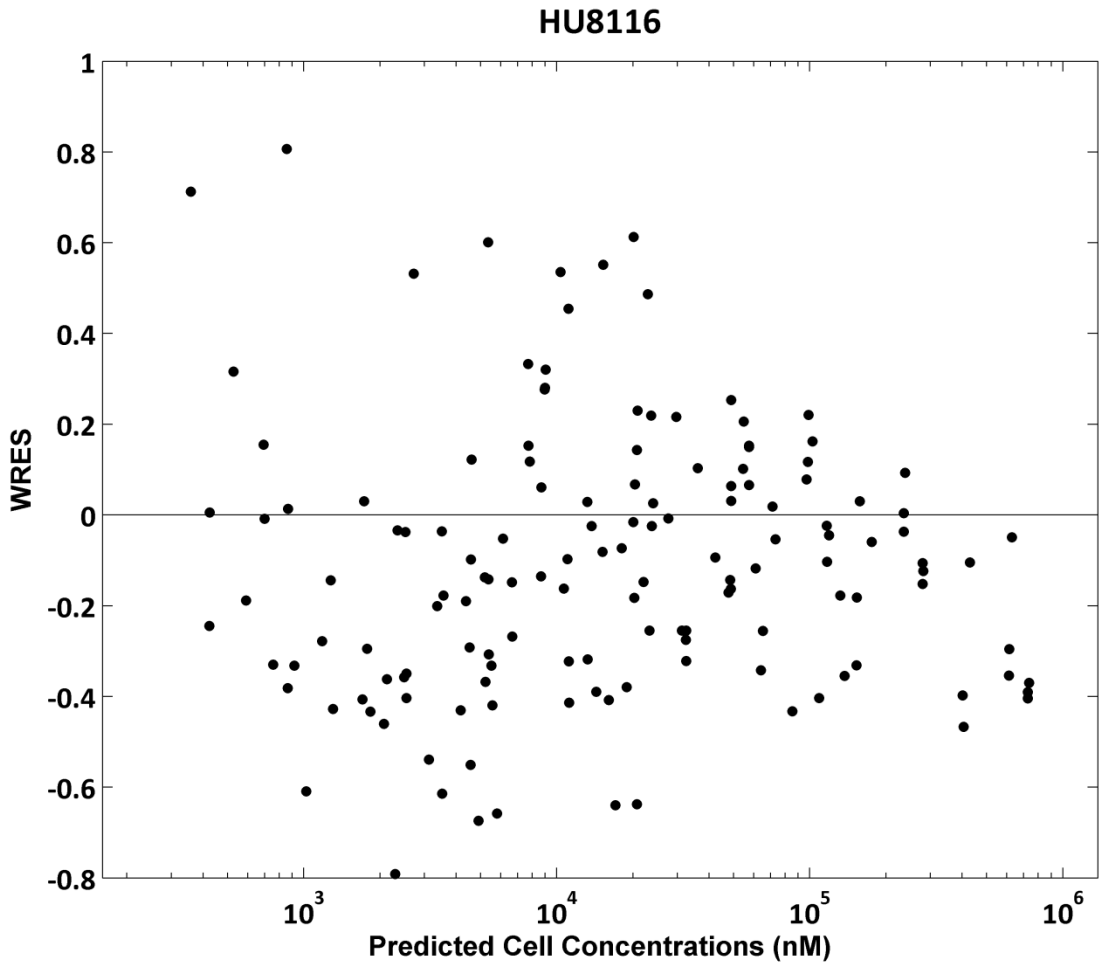

Appendix 37. Plot of the weighted residuals versus predicted cell concentrations for the uptake of rosuvastatin in human hepatocytes (donor HU8119) at 6 concentrations (0.3–100 μM) over a 60 minute incubation from the uptake FIT model.

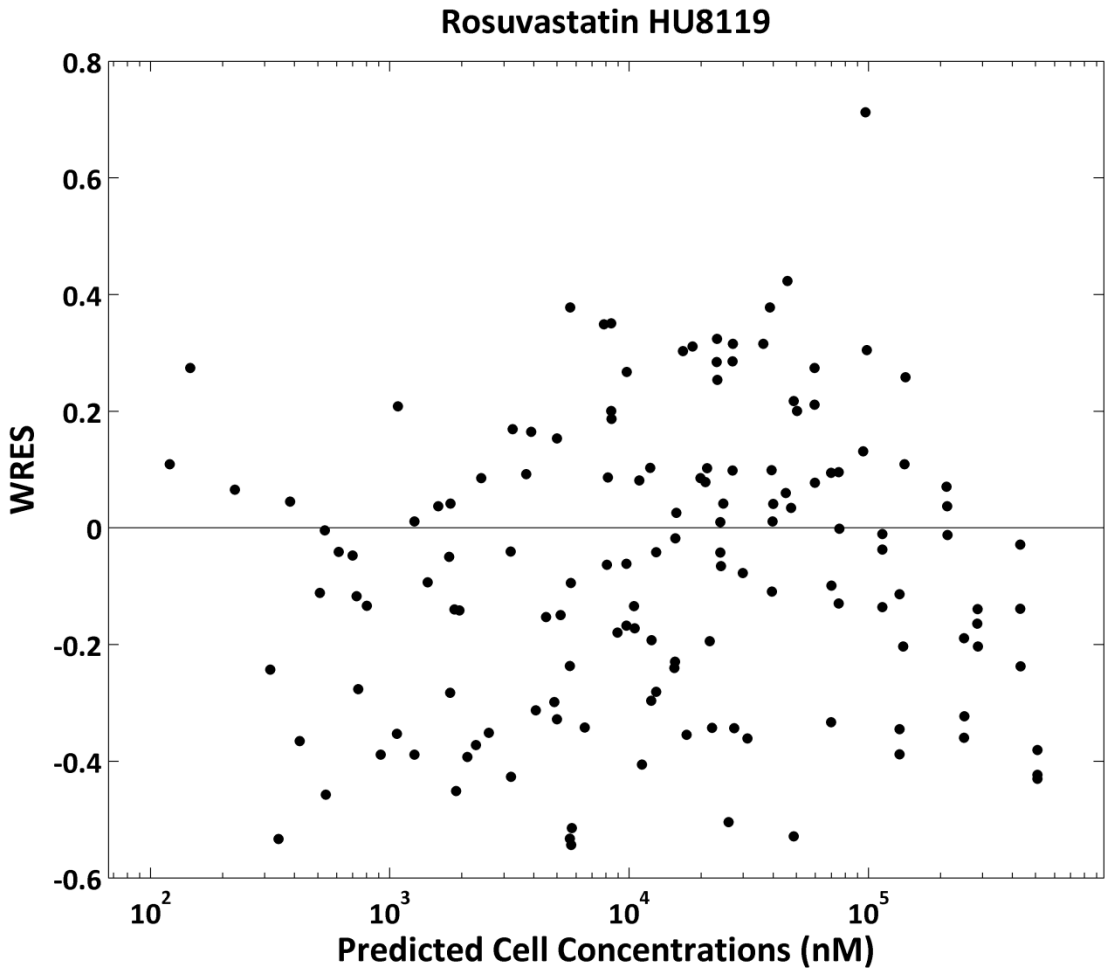

Appendix 38. Plot of the weighted residuals versus predicted cell concentrations for the uptake of rosuvastatin in human hepatocytes (donor HU1411) at 6 concentrations (0.3–100 μM) over a 60 minute incubation from the uptake FIT model.

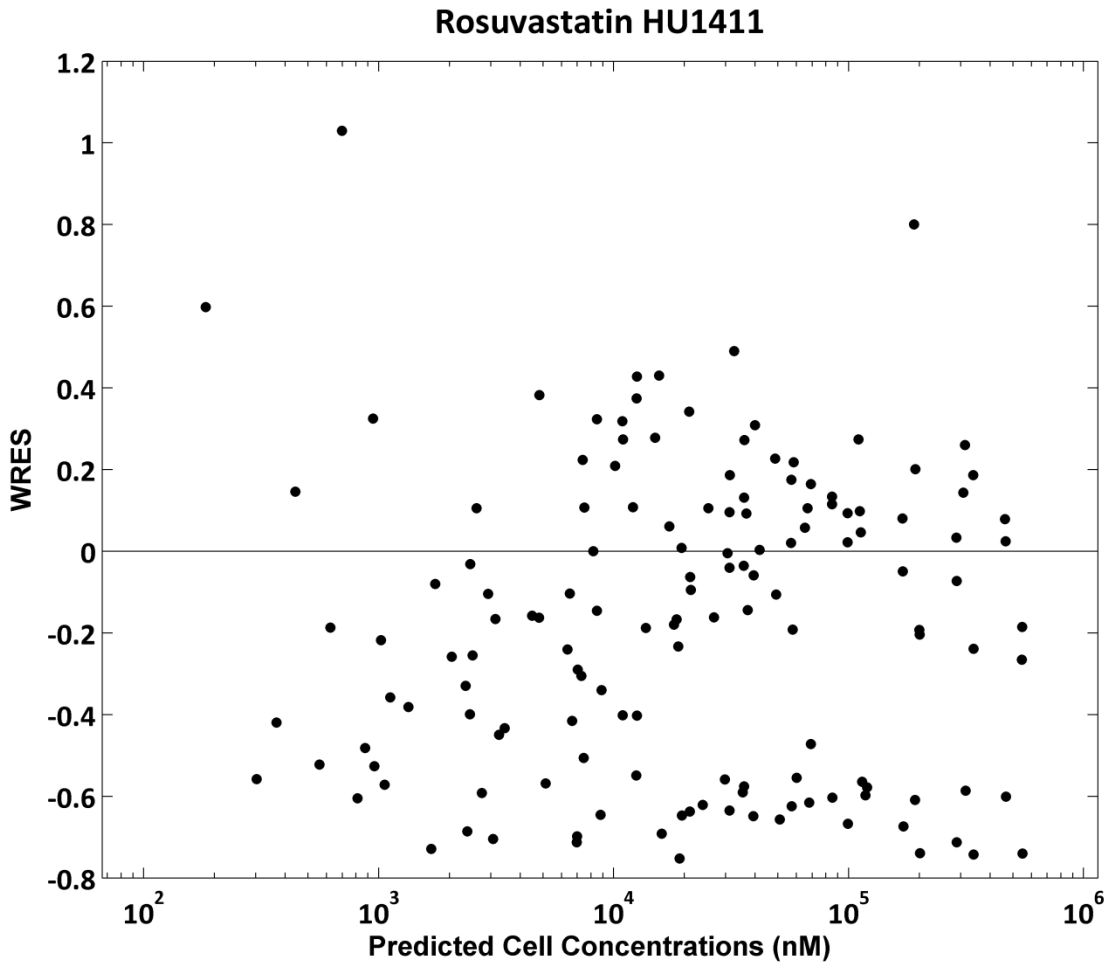

Appendix 39. Plot of the weighted residuals versus time for the uptake of rosuvastatin in human hepatocytes (donor HU8116) at 6 concentrations (0.3–100 µM) over a 60 minute incubation from the uptake FIT model.

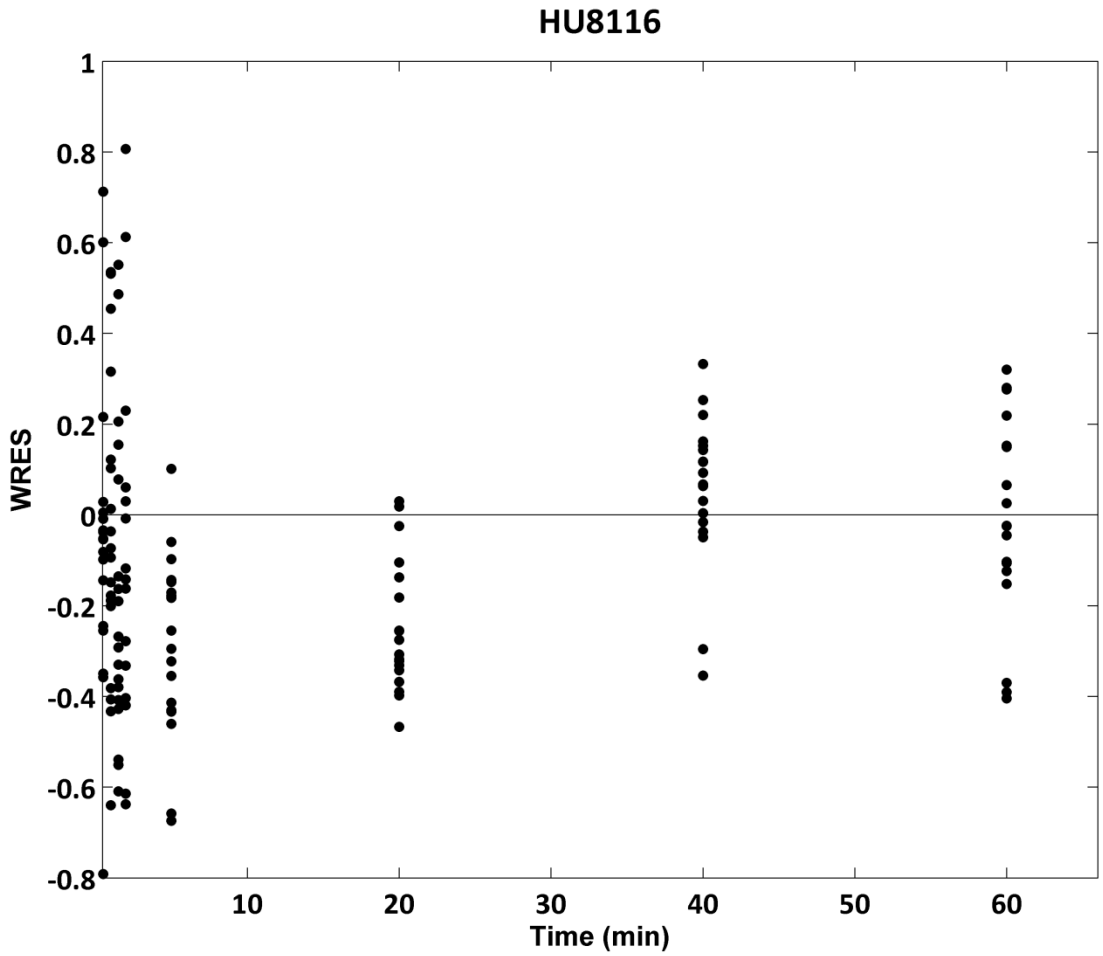

Appendix 40. Plot of the weighted residuals versus time for the uptake of rosuvastatin in human hepatocytes (donor HU8119) at 6 concentrations (0.3–100 µM) over a 60 minute incubation from the uptake FIT model.

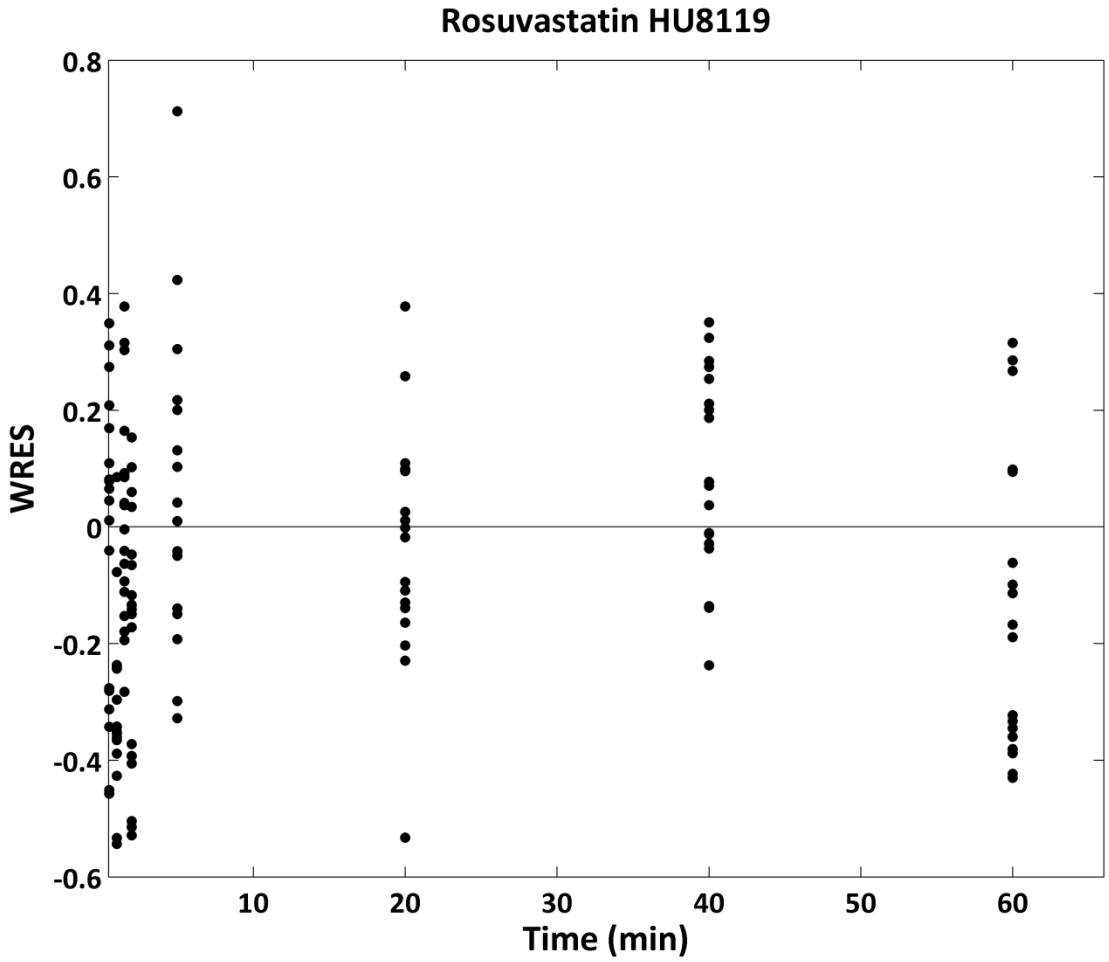

Appendix 41. Plot of the weighted residuals versus time for the uptake of rosuvastatin in human hepatocytes (donor HU1411) at 6 concentrations (0.3–100 µM) over a 60 minute incubation from the uptake FIT model.

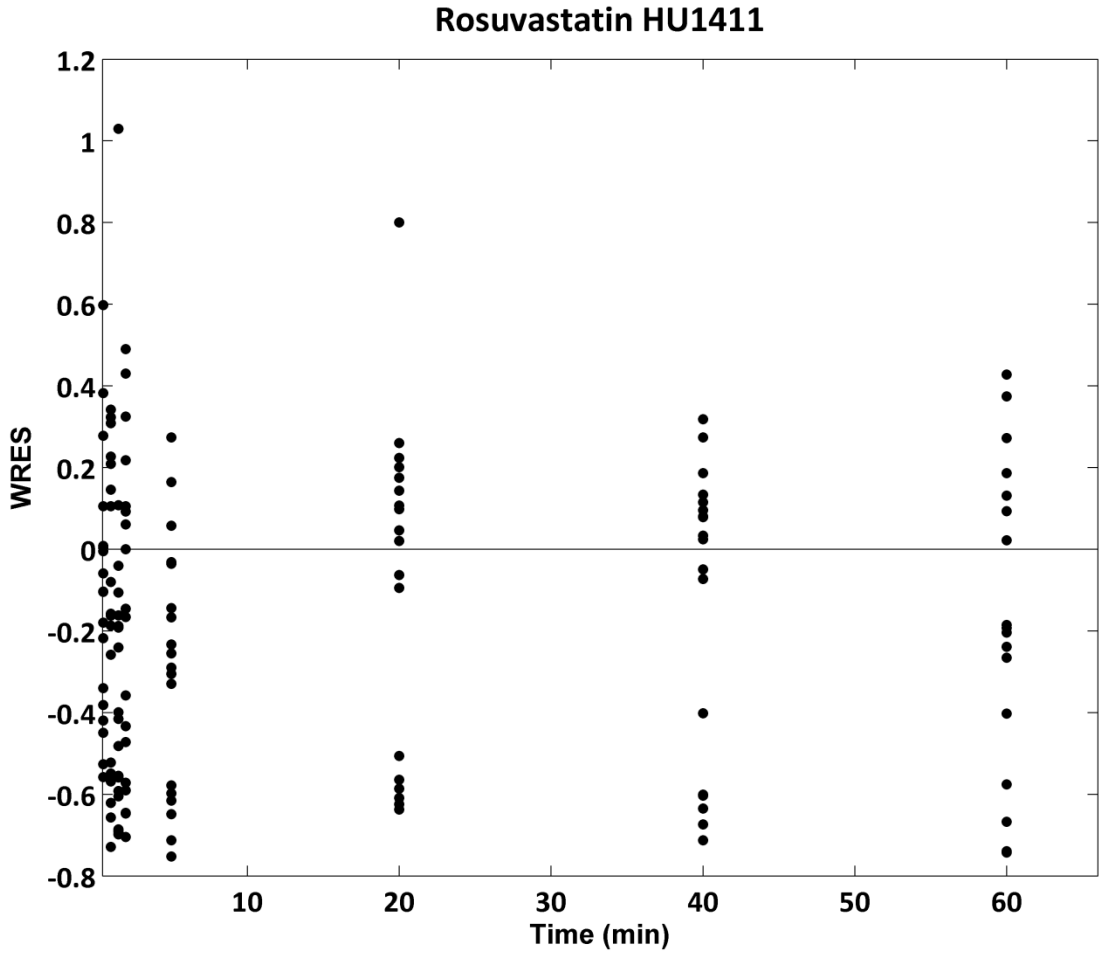

Appendix 42. Summary of the correlation matrix produced by the UptakeFIT model of the uptake of rosuvastatin by three adult human cryopreserved hepatocytes (HU8116, HU8119 and HU1411) and a paediatric human cryopreserved hepatocyte (HU4048).

HU1411	Vmax	Km	Pdiff	fucell
Vmax	1	0.952	-0.7776	0.8536
Km		1	-0.7376	0.7566
Pdiff			1	-0.9159
fucell				1
HU8116	Vmax	Km	Pdiff	fucell
Vmax	1	0.9396	-0.6373	0.5886
Km		1	-0.6033	0.4039
Pdiff			1	-0.3378
fucell				1
HU8119	Vmax	Km	Pdiff	fucell
Vmax	1	0.9532	-0.7044	0.752
Km		1	-0.6495	0.624
Pdiff			1	-0.7088
fucell				1
HU4048	Vmax	Km	Pdiff	fucell
Vmax	1	0.9223	-0.5744	0.7746
Km		1	-0.6337	0.5888
Pdiff			1	-0.6021
fucell				1

Appendix 43. Inhibition of rosuvastatin uptake determined at a concentration 1 µM over 3 minutes in plated adult human hepatocytes (donor 8116) by cyclosporin A over 10 concentrations (0.003-6 µM) both with and without pre-incubation. Mean data (n=3 per inhibitor concentration) are depicted.

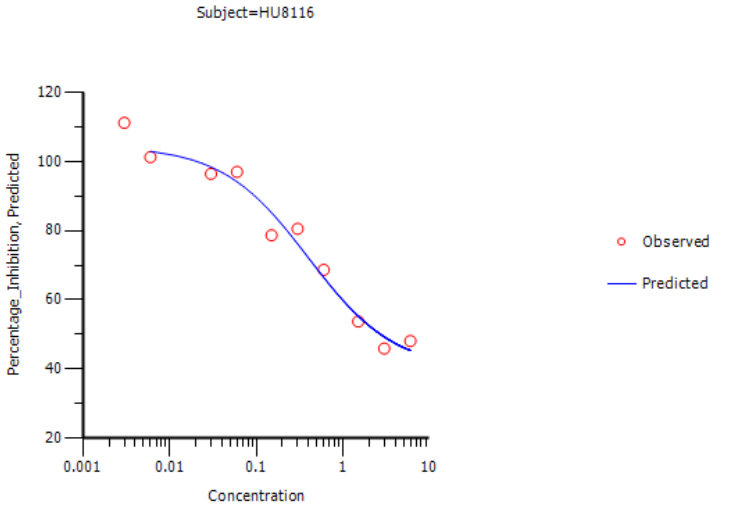

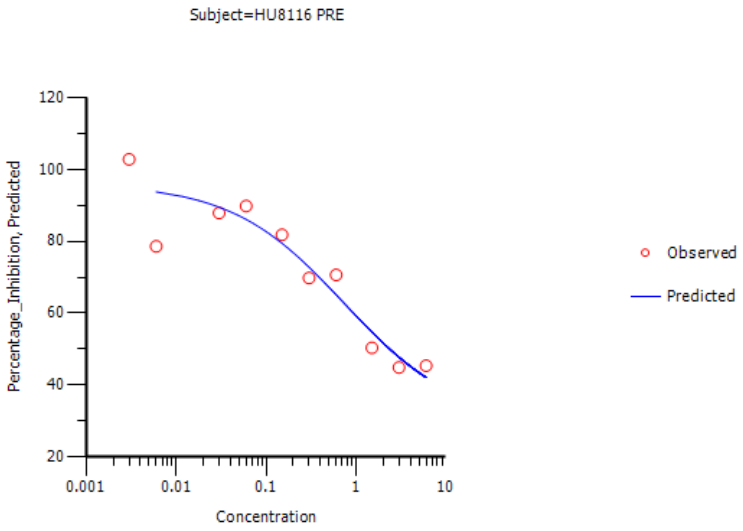

Appendix 44. Inhibition of rosuvastatin uptake determined at a concentration 1 µM over 3 minutes in plated adult human hepatocytes (donor 8119) by cyclosporin A over 10 concentrations (0.003-6 µM) both with and without pre-incubation. Mean data (n=3 per inhibitor concentration) are depicted.

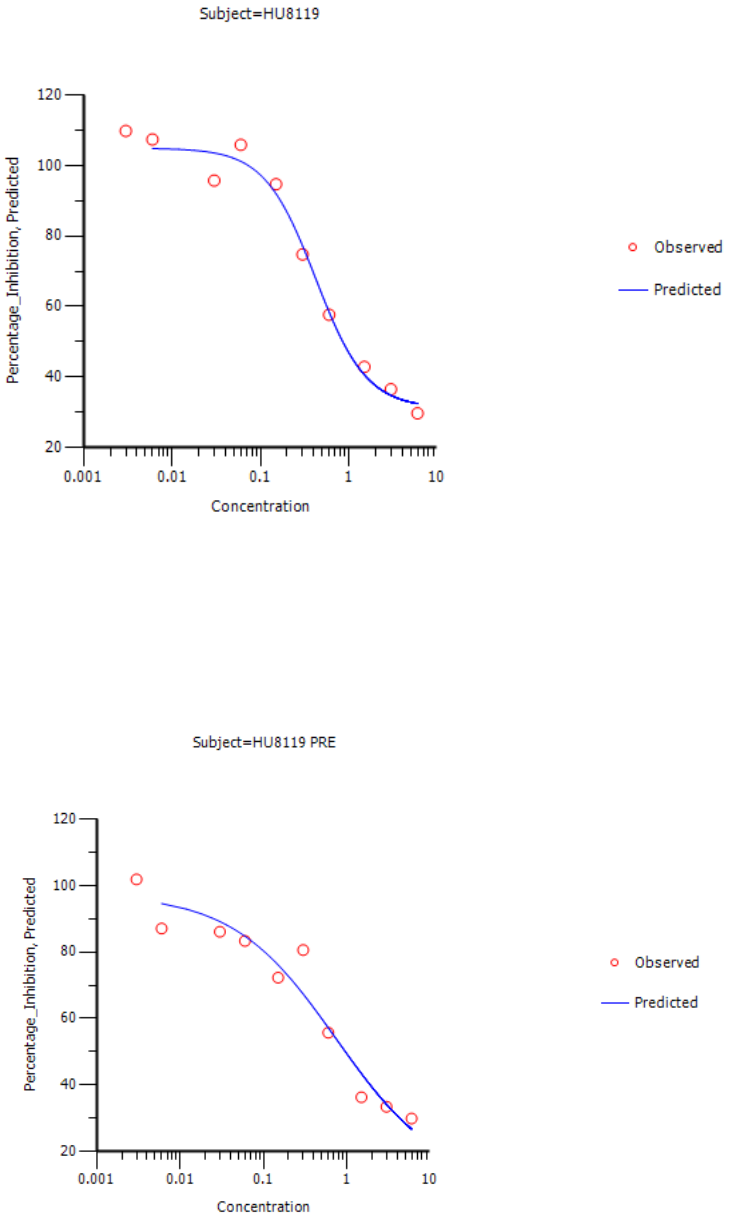

Appendix 45. Inhibition of rosuvastatin uptake determined at a concentration 1 µM over 3 minutes in plated adult human hepatocytes (donor 1411) by cyclosporin A over 10 concentrations (0.003-6 µM) both with and without pre-incubation. Mean data (n=3 per inhibitor concentration) are depicted.

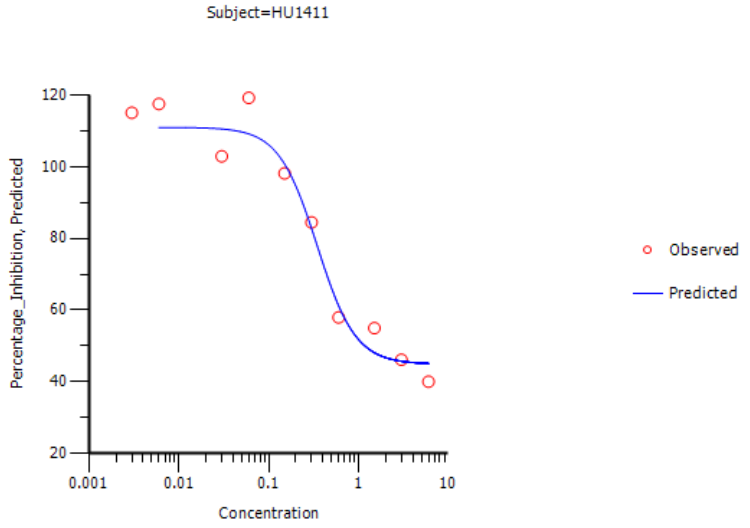

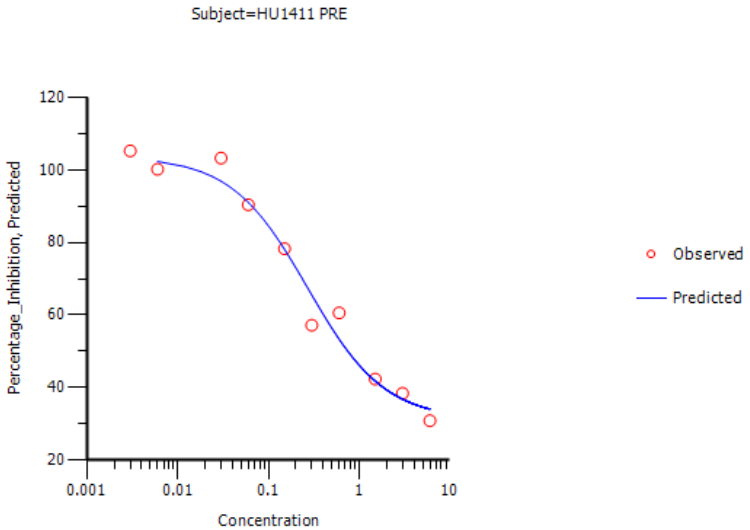

Appendix 46. Inhibition of rosuvastatin uptake determined at a concentration 1 µM over 3 minutes in plated adult human hepatocytes (donor 8116) by cyclosporin AM1 over 10 concentrations (0.003-6 µM) both with and without pre-incubation. Mean data (n=3 per inhibitor concentration) are depicted.

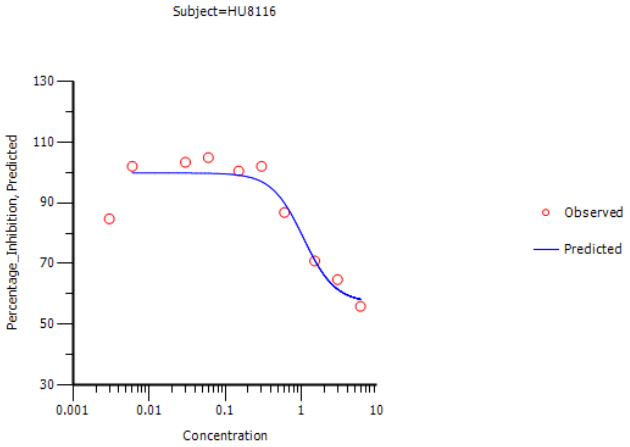

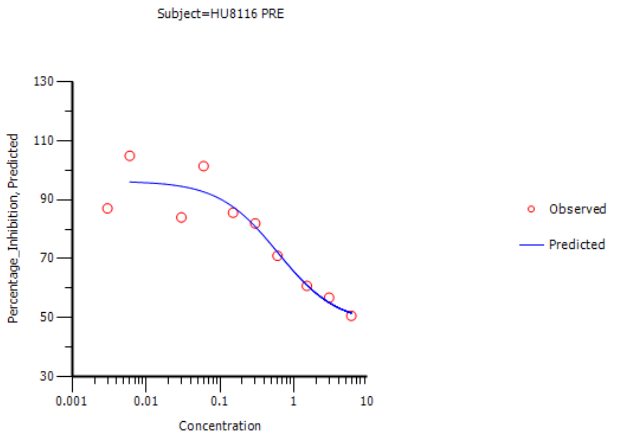

Appendix 47. Inhibition of rosuvastatin uptake determined at a concentration 1 µM over 3 minutes in plated adult human hepatocytes (donor 8119) by cyclosporin AM1 over 10 concentrations (0.003-6 µM) both with and without pre-incubation. Mean data (n=3 per inhibitor concentration) are depicted.

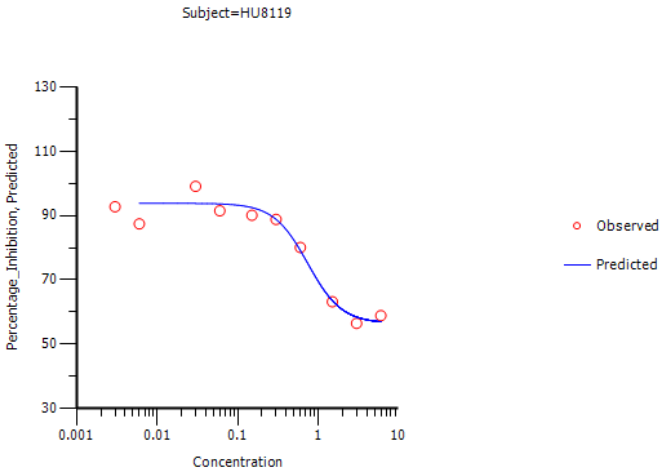

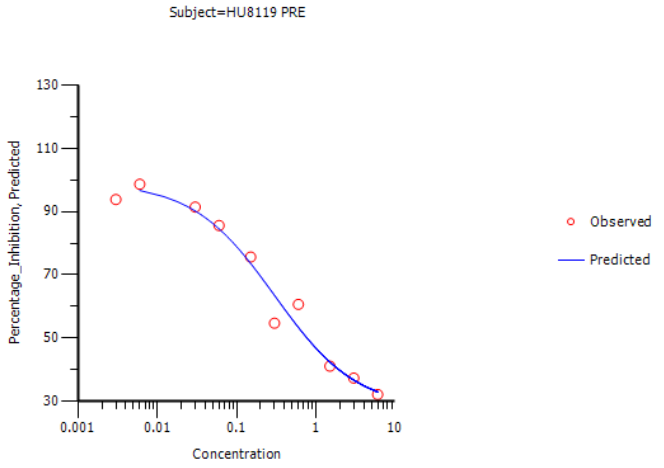

Appendix 48. Inhibition of rosuvastatin uptake determined at a concentration 1 µM over 3 minutes in plated adult human hepatocytes (donor 1411) by cyclosporin AM1 over 10 concentrations (0.003-6 µM) both with and without pre-incubation. Mean data (n=3 per inhibitor concentration) are depicted.

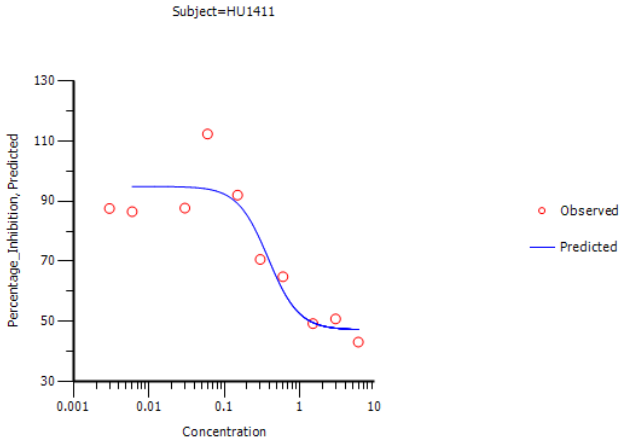

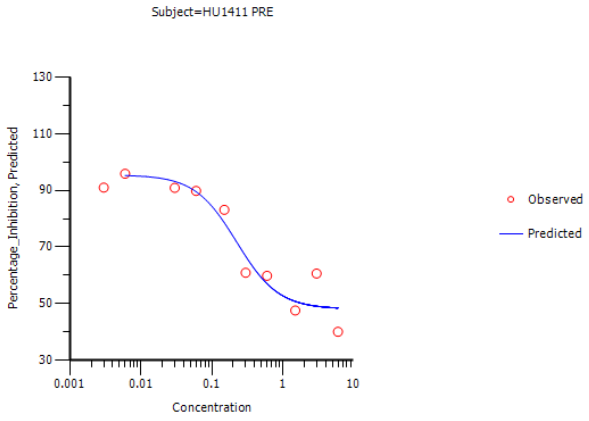

Appendix 49. Correlation matrix of the parameters derived by the inhibition model 108 in Phoenix WinNonLin to determine the inhibition of rosuvastatin by cyclosporin A with and without pre-incubation in the three adult human donors.

Subject	Parameter	E_{max}	IC_{50}	E_0	Gamma
HU1411	E_{max}	1			
	IC_{50}	0.24	1		
	E_0	0.63	-0.29	1	
	Gamma	-0.60	-0.17	-0.37	1
HU1411 PRE	E_{max}	1			
	IC_{50}	0.49	1		
	E_0	0.66	-0.18	1	
	Gamma	-0.83	-0.40	-0.55	1
HU8116	E_{max}	1			
	IC_{50}	0.73	1		
	E_0	0.63	0.03	1	
	Gamma	-0.89	-0.63	-0.60	1
HU8116 PRE	E_{max}	1			
	IC_{50}	0.92	1		
	E_0	0.60	0.28	1	
	Gamma	-0.93	-0.82	-0.65	1
HU8119	E_{max}	1			
	IC_{50}	0.45	1		
	E_0	0.61	-0.20	1	
	Gamma	-0.75	-0.37	-0.44	1
HU8119 PRE	E_{max}	1			
	IC_{50}	0.92	1		
	E_0	0.60	0.28	1	
	Gamma	-0.93	-0.82	-0.65	1

Appendix 50. Correlation matrix of the parameters derived by the inhibition model 108 in Phoenix WinNonLin to determine the inhibition of rosuvastatin by cyclosporin AM1 with and without pre-incubation in the three adult human donors.

Subject	Parameter	E_{max}	IC_{50}	E_0	Gamma
HU1411	E_{max}	1			
	IC_{50}	0.28	1		
	E_0	0.59	-0.26	1	
	Gamma	-0.57	-0.19	-0.33	1
HU1411 PRE	E_{max}	1			
	IC_{50}	0.56	1		
	E_0	0.60	-0.16	1	
	Gamma	-0.81	-0.45	-0.48	1
HU8116	E_{max}	1			
	IC_{50}	0.74	1		
	E_0	0.56	-0.01	1	
	Gamma	-0.86	-0.63	-0.51	1
HU8116 PRE	E_{max}	1			
	IC_{50}	0.98	1		
	E_0	0.47	0.32	1	
	Gamma	-0.94	-0.91	-0.58	1
HU8119	E_{max}	1			
	IC_{50}	0.50	1		
	E_0	0.56	-0.18	1	
	Gamma	-0.73	-0.39	-0.40	1
HU8119 PRE	E_{max}	1			
	IC_{50}	0.95	1		
	E_0	0.50	0.27	1	
	Gamma	-0.93	-0.86	-0.58	1

Appendix 51. Preparation and dilutions of the analyte (GSK2879552) working solutions.

Working Solution	Final Concentration (µg/mL)	Volume of spiking solution	Volume of DMF (µL)
A1/B1	10	100 µL A/B	900
A2/B2	1	100 µL A1/B1	900
A3/B3	0.1	100 µL A2/B2	900
A4/B4	0.01	100 µL A3/B3	900

Appendix 52. Preparation of the GSK2879552 calibration standards.

Standard concentration in matrix (ng/mL)	Volume of spiking solution (µL)					Volume of matrix (µL)
	A4 (0.01 µg/mL)	A3 (0.1 µg/mL)	A2 (1 µg/mL)	A1 (10 µg/mL)	A (100 µg/mL)	
0.1	5					495
0.2	10					490
0.4	20					480
1		5				495
2		10				490
4		20				480
20			10			490
100				5		495
500				25		475
800					4	496

Appendix 53. Preparation of the GSK2879552 quality control/validation standards.

Standard concentration in matrix (ng/mL)	Volume of spiking solution (µL)					Volume of matrix(µL)
	B4 (0.01 µg/mL)	B3 (0.1 µg/mL)	B2 (1 µg/mL)	B1 (10 µg/mL)	B (100 µg/mL)	
0.3	15					485
3		15				485
100				5		495
400				20		480
700					3.5	

Appendix 54. Preparation and dilutions of the internal standard [$^2H_3$]-GSK2879552.

Working Solution	Final Concentration (ng/mL)	Volume of spiking solution	Volume of acetonitrile/methanol/formic acid (95/5/0.1) (µL)
C1	500	250 µL C	1000

Appendix 55. HPLC conditions to analyse GSK2879552

Autosampler	ACQUITY UPLC
Injector Wash Solvent 1(strong)	40/30/30 Acetonitrile / IPA / 0.1% Formic acid
Injector Wash Solvent 2 (weak)	0.1% Formic acid (aq.)
Typical Injection Volume	5 µL
Flow Rate	0.75 mL/min
Flow Rate	50 x 2.1mm, i.d. 1.8 µm, HSST3, Waters
Column Temperature	60°C
Column Divert	Not used
Run Time	2.5 min
Mobile Phase A	10 mM Ammonium Formate (pH 3)
Mobile Phase B	Acetonitrile

Gradient Profile:

Time (min)	% A	% B
0.0	90	10
0.1	90	10
1.0	40	60
1.01	10	90
2.0	10	90
2.01	90	10
2.5	90	10

Analyte	Precursor ion (m/z)	Product ion (m/z)	Dwell time (msec)	Polarity	Typical RT (min)
GSK2879552	365	232	75	Positive	0.5
[$^2H_3$]-GSK2879552	368	232	75	Positive	0.5

Appendix 56. MS/MS conditions to analyse GSK2879552

Mass Spectrometer	Applied Biosystems/MDS Sciex API-4000
Split Ratio	none
Ionisation Interface and Temperature	TurboIonSpray® at 650°C
Pause Time	5 msec
Gas 1 Setting (Air)	40 psi
Gas 2 Setting (Air)	60 psi
Curtain Gas Setting (Nitrogen)	25
Collision Gas Setting (Nitrogen)	7
DP Value	50
CE Value	48

Appendix 57. Solvents used for LC/MS

Reagent	Function
ACN:Water:IPA containing formic acid (0.1%), 4:3:3	Solvent Wash 1
ACN:Water:IPA containing formic acid (0.1%), 4:3:3	Solvent Wash 2
Ammonium formate (10 mM) aqueous (pH 3.0)	Mobile Phase A
ACN	Mobile Phase B

ACN = Acetonitrile and IPA = Isopropanol

Appendix 58. The kinetic profiles of GSK2879552 uptake in plated adult human hepatocytes from donor HU8116 at 6 concentrations (0.3–100 μM) over a 60 minute incubation. Lines represent the predicted uptake profile based upon a mechanistic two-compartmental model describing the changes in drug concentrations in both the cells and the incubation media over time. Data points are duplicate measurements.

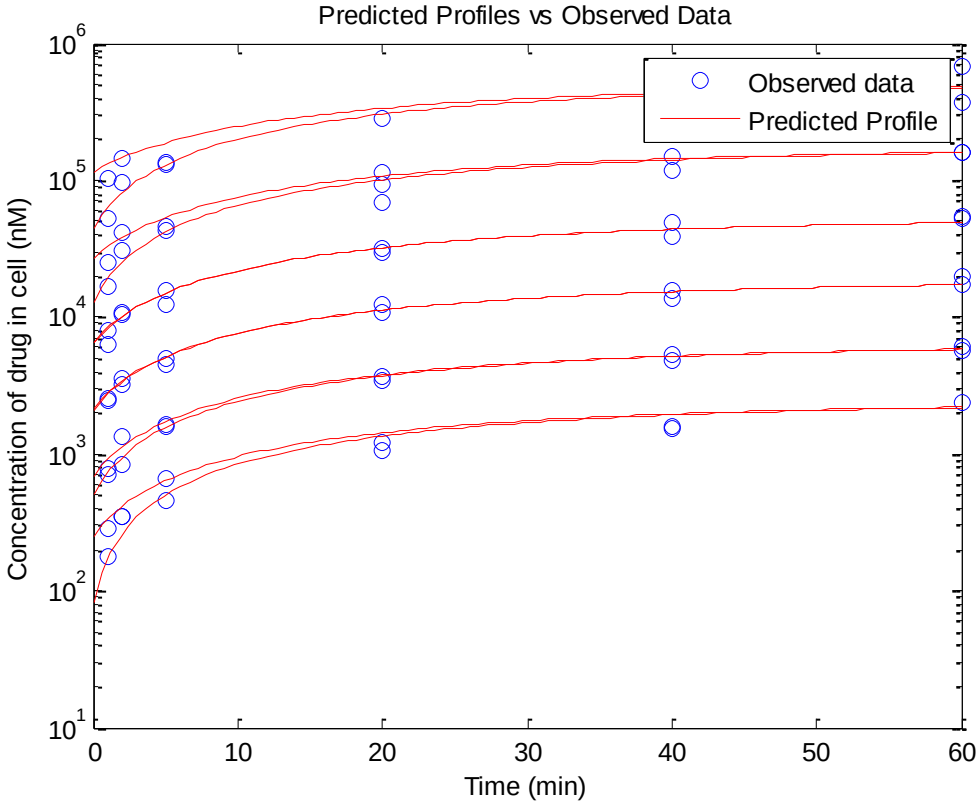

Appendix 59. The kinetic profiles of GSK2879552 uptake in plated adult human hepatocytes from donor HU8119 at 6 concentrations (0.3–100 μM) over a 60 minute incubation. Lines represent the predicted uptake profile based upon a mechanistic two-compartmental model describing the changes in drug concentrations in both the cells and the incubation media over time. Data points are duplicate measurements.

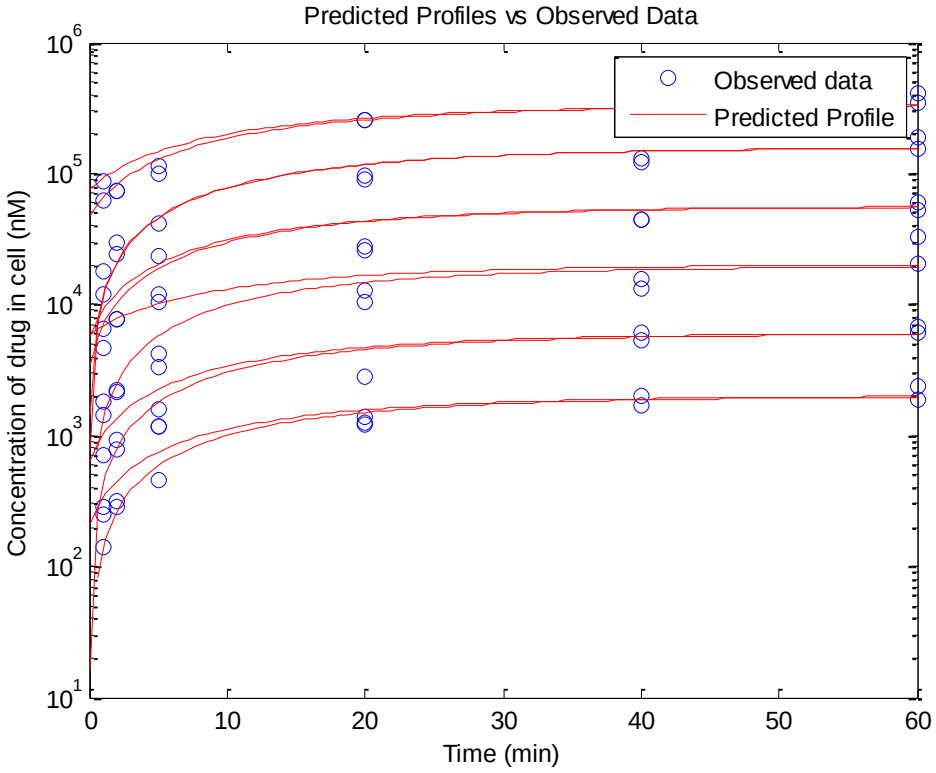

Appendix 60. The kinetic profiles of GSK2879552 uptake in plated adult human hepatocytes from donor HU1411 at 6 concentrations (0.3–100 μM) over a 60 minute incubation. Lines represent the predicted uptake profile based upon a mechanistic two-compartmental model describing the changes in drug concentrations in both the cells and the incubation media over time. Data points are duplicate measurements.

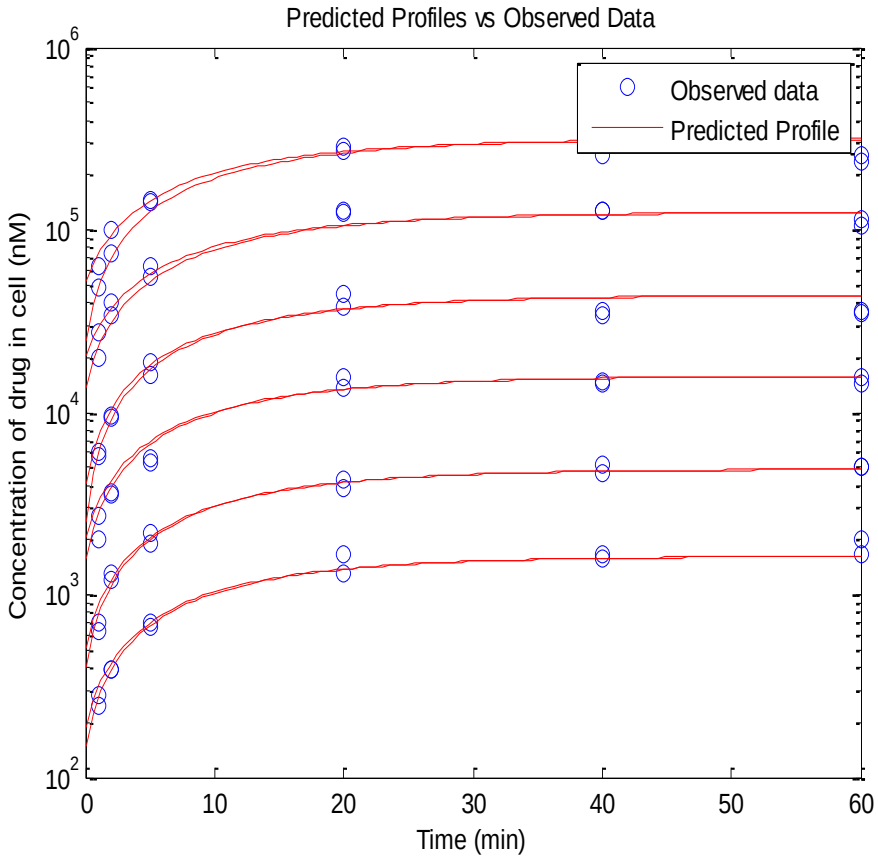

Appendix 61. The predicted versus observed data from donor HU8116. The line of unity (solid) and the upper (2-fold) and lower (2-fold, dotted) are depicted.

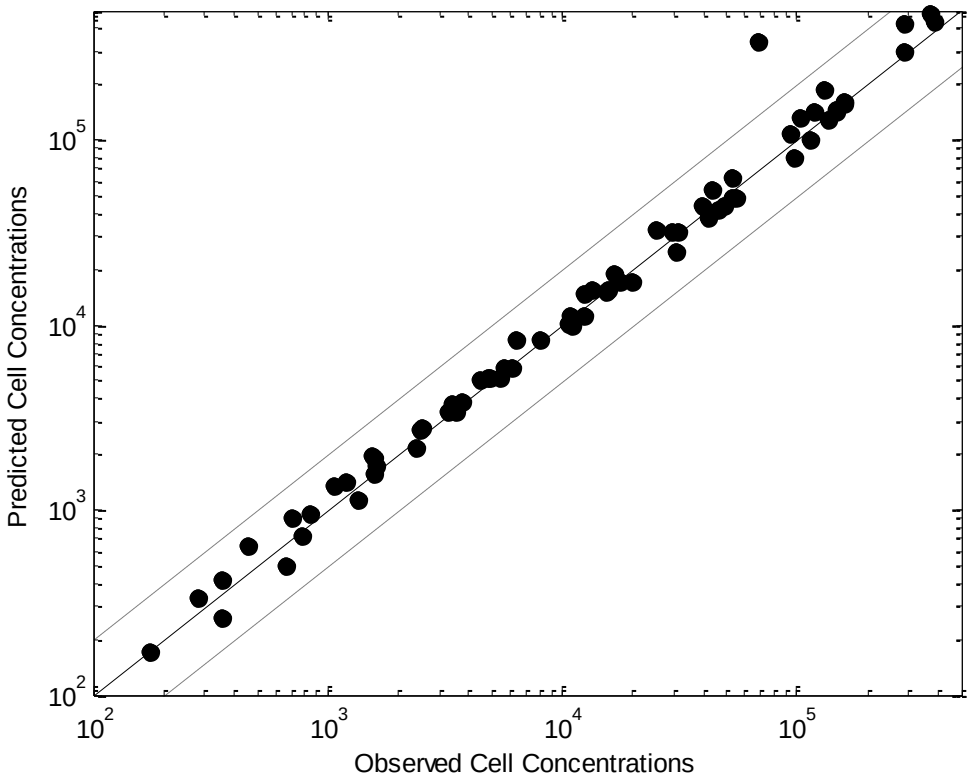

Appendix 62. The predicted versus observed data from donor HU8119. The line of unity (solid) and the upper (2-fold) and lower (5%) 2-fold, dotted) are depicted.

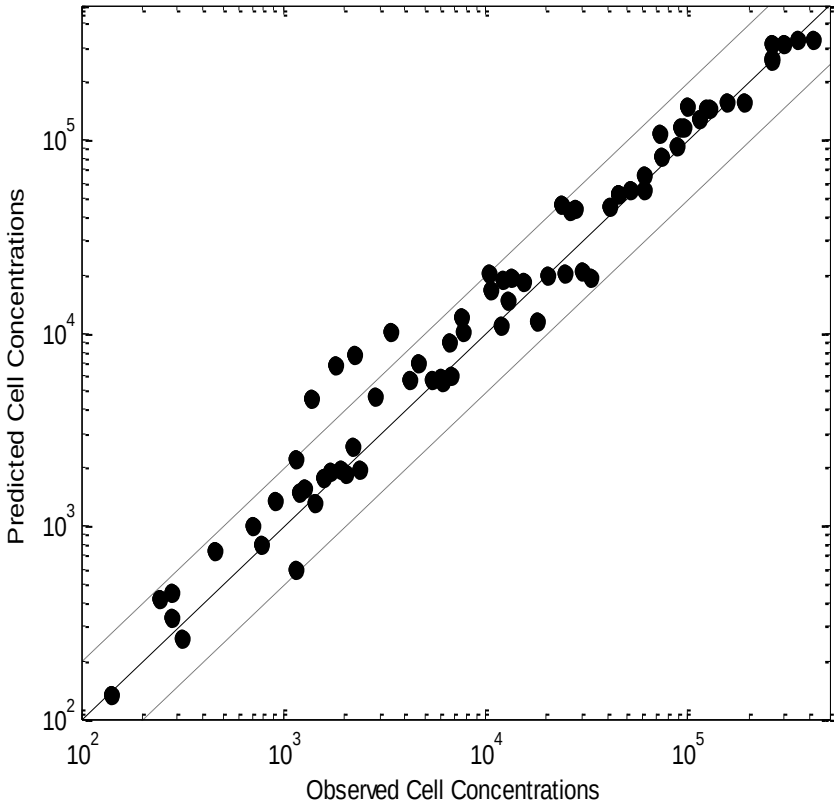

Appendix 63. The predicted versus observed data from donor HU1411. The line of unity (solid) and the upper (2-fold) and lower (2-fold, dotted) are depicted.

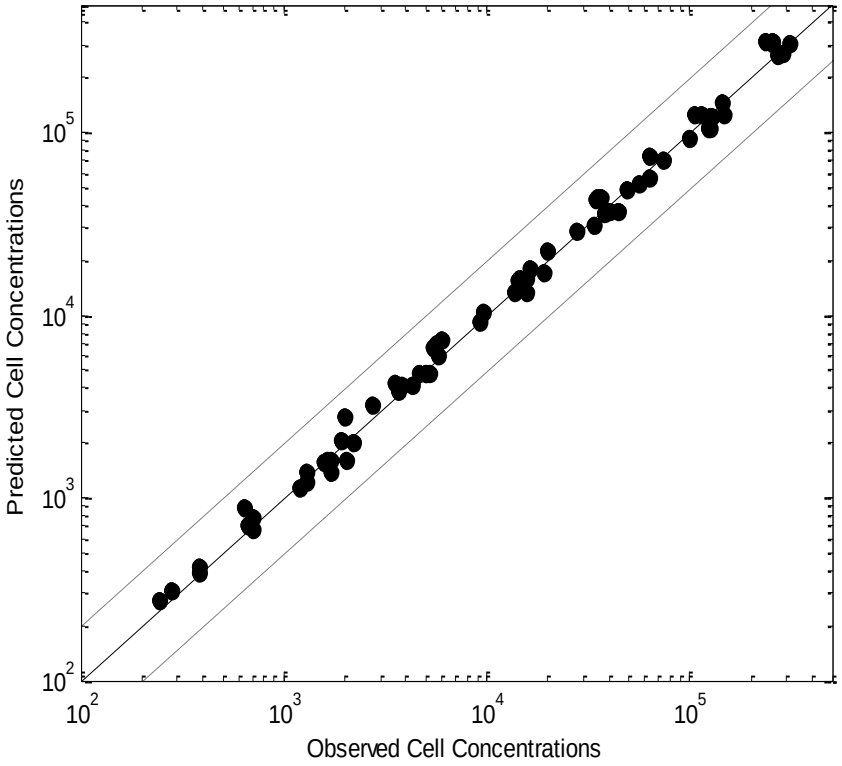

Appendix 64. Profiles of GSK2879552 intracellular concentrations in cryopreserved human hepatocytes (donors HU8116, HU8119 and HU1411) following incubation in a media containing GSK2879552 at a concentration of 0.33 µM at selected time points up to 60 minutes.

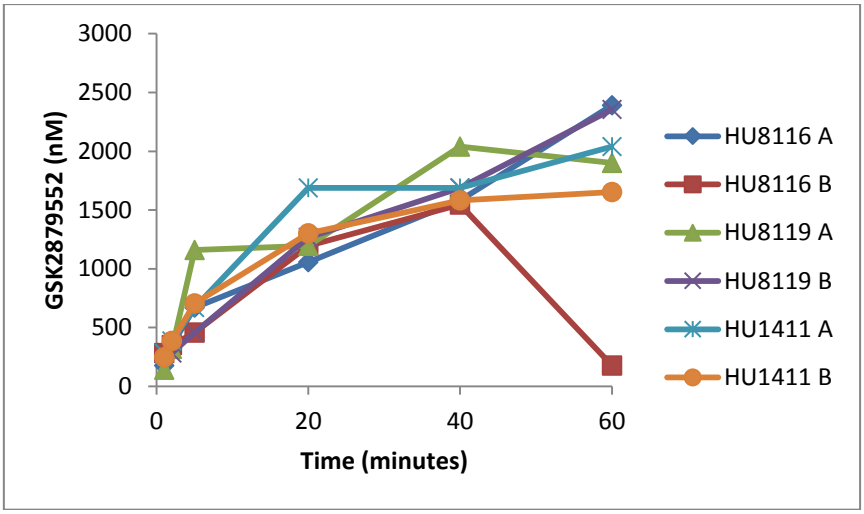

Appendix 65. Profiles of GSK2879552 intracellular concentrations in cryopreserved human hepatocytes (donors HU8116, HU8119 and HU1411) following incubation in a media containing GSK2879552 at a concentration of 1.0 µM at selected time points up to 60 minutes.

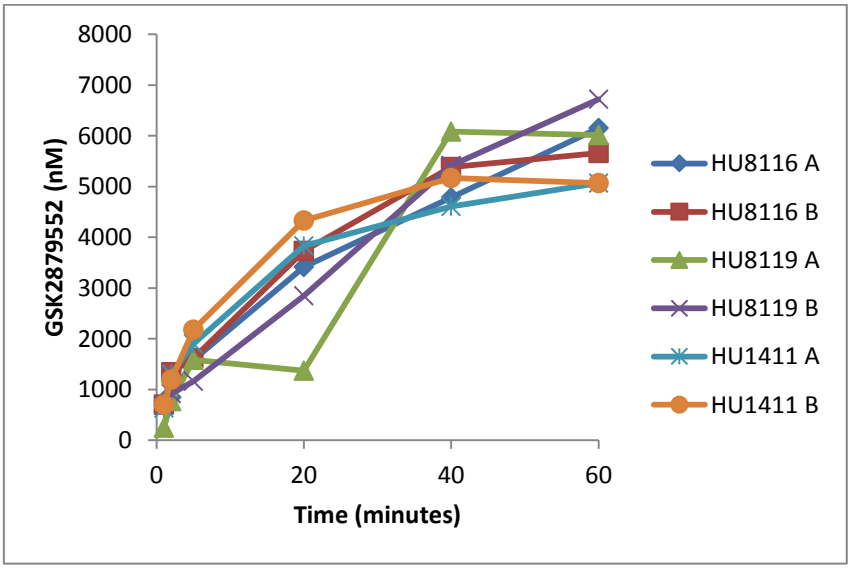

Appendix 66. Profiles of GSK2879552 intracellular concentrations in cryopreserved human hepatocytes (donors HU8116, HU8119 and HU1411) following incubation in a media containing GSK2879552 at a concentration of 3.3 µM at selected time points up to 60 minutes.

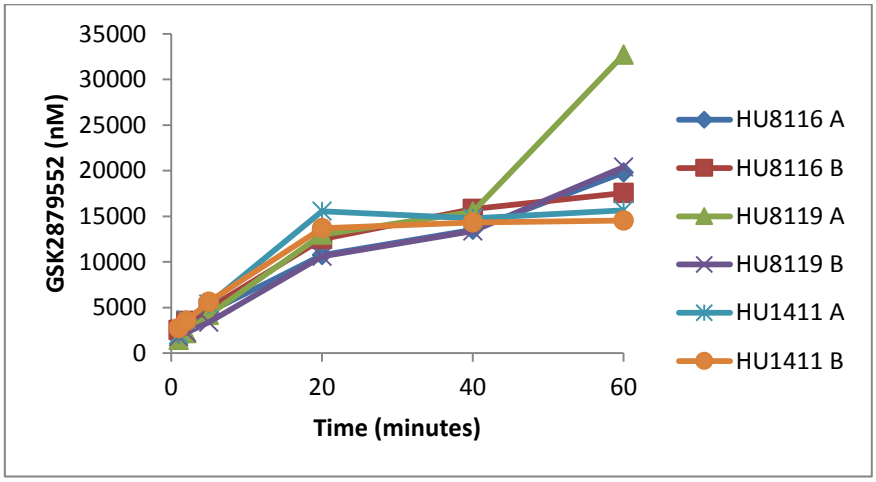

Appendix 67. Profiles of GSK2879552 intracellular concentrations in cryopreserved human hepatocytes (donors HU8116, HU8119 and HU1411) following incubation in a media containing GSK2879552 at a concentration of 10 µM at selected time points up to 60 minutes.

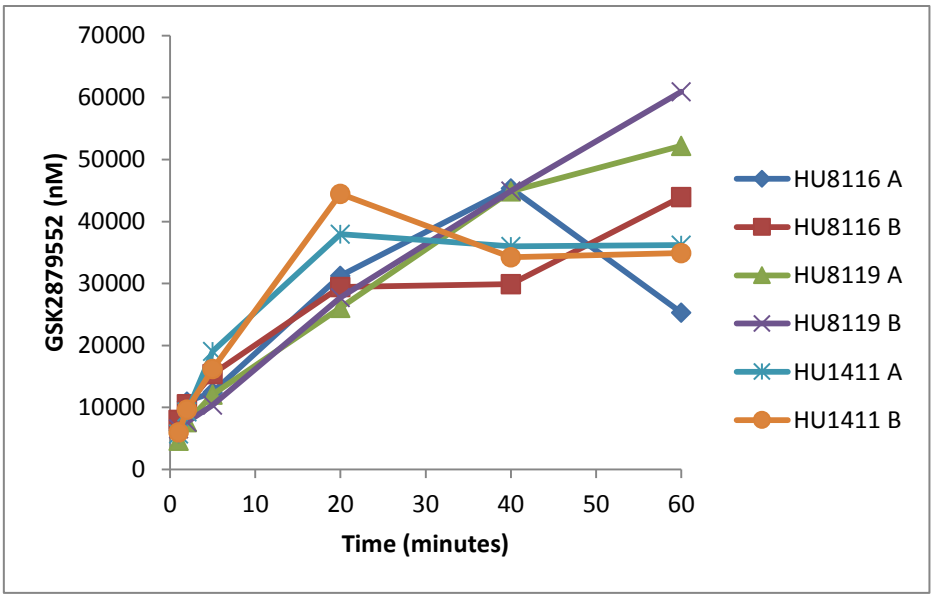

Appendix 68. Profiles of GSK2879552 intracellular concentrations in cryopreserved human hepatocytes (donors HU8116, HU8119 and HU1411) following incubation in a media containing GSK2879552 at a concentration of 30 µM at selected time points up to 60 minutes.

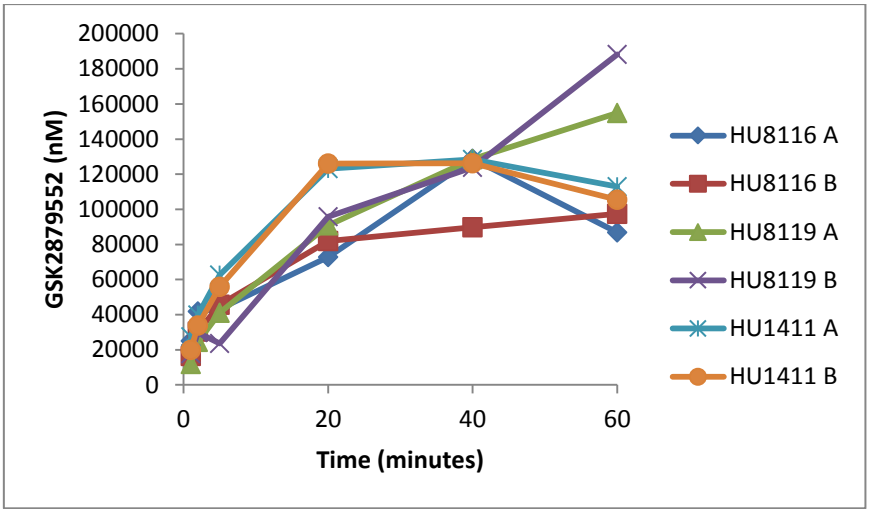

Appendix 69. Profiles of GSK2879552 intracellular concentrations in cryopreserved human hepatocytes (donors HU8116, HU8119 and HU1411) following incubation in a media containing GSK2879552 at a concentration of 100 µM at selected time points up to 60 minutes.

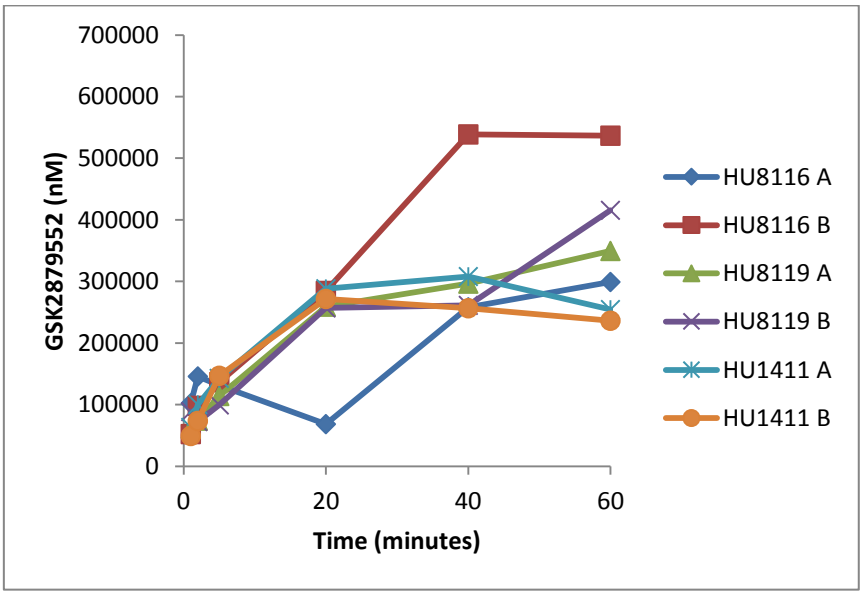

Appendix 70. Plot of the predicted cell concentration – time profiles (solid lines) with the observed cell concentrations (solid dots) for the uptake of GSK2879552 in adult human hepatocytes (donor HU8116) at 6 concentrations (0.3–100 µM) over a 60 minute incubation from the uptake FIT model. Data points are duplicate measurements.

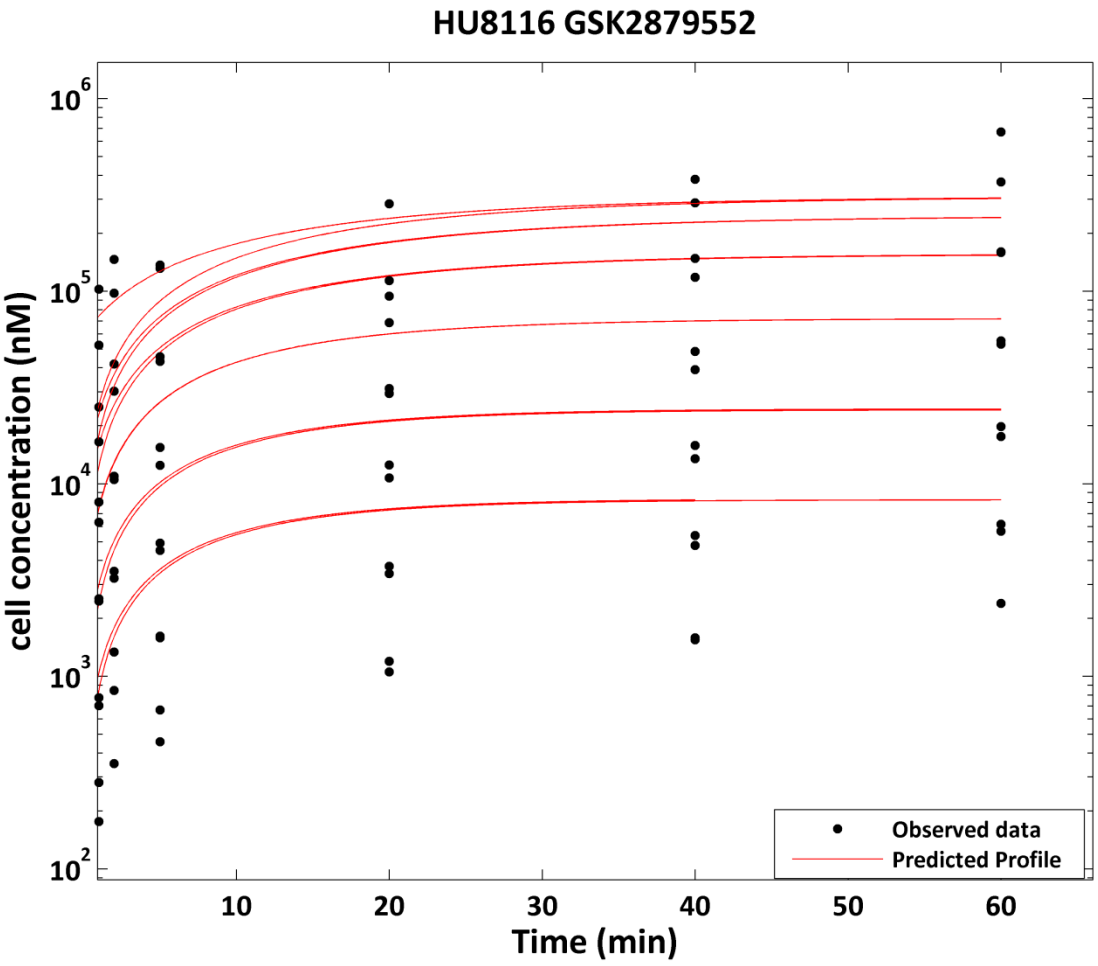

Appendix 71. Plot of the predicted cell concentration – time profiles (solid lines) with the observed cell concentrations (solid dots) for the uptake of GSK2879552 in adult human hepatocytes (donor HU8119) at 6 concentrations (0.3–100 µM) over a 60 minute incubation from the uptake FIT model. Data points are duplicate measurements.

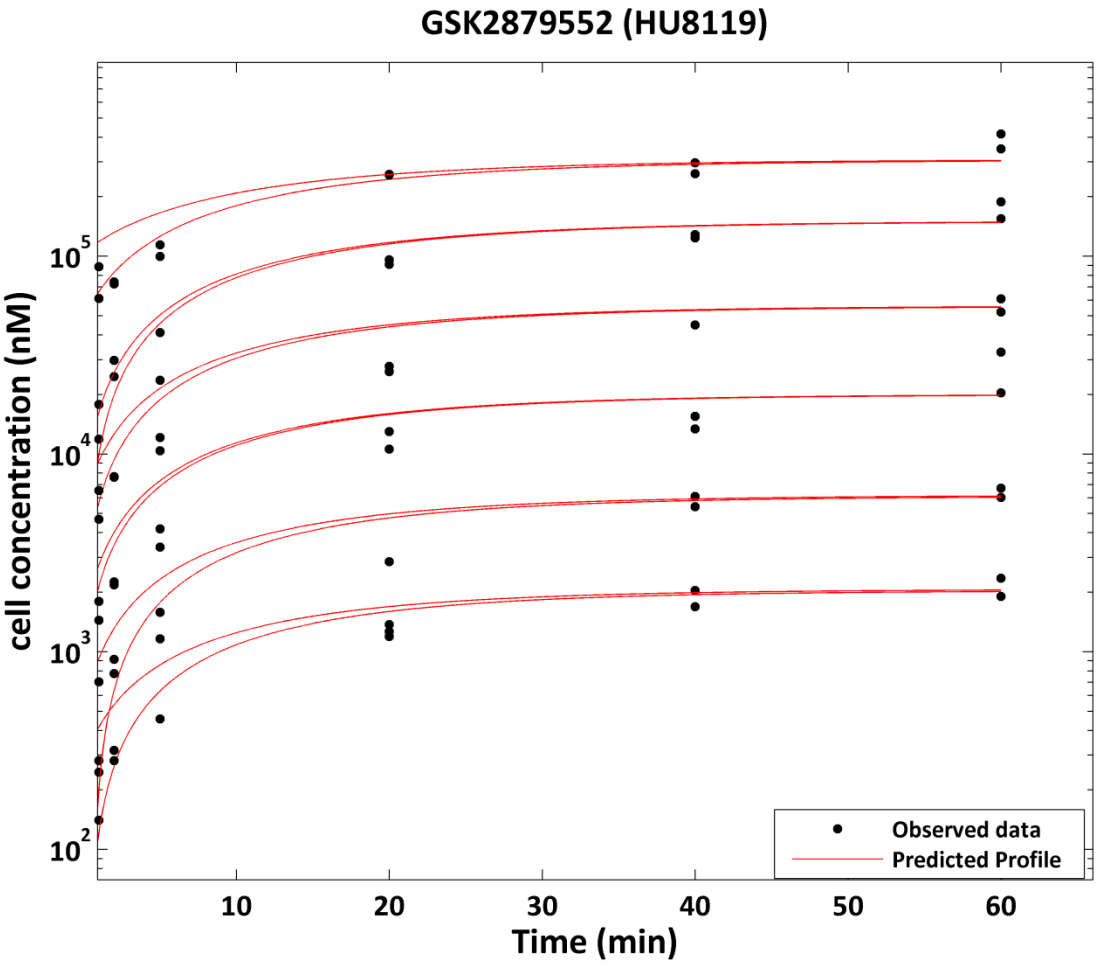

Appendix 72. Plot of the predicted cell concentration – time profiles (solid lines) with the observed cell concentrations (solid dots) for the uptake of GSK2879552 in adult human hepatocytes (donor HU1411) at 6 concentrations (0.3–100 µM) over a 60 minute incubation from the uptake FIT model. Data points are duplicate measurements.

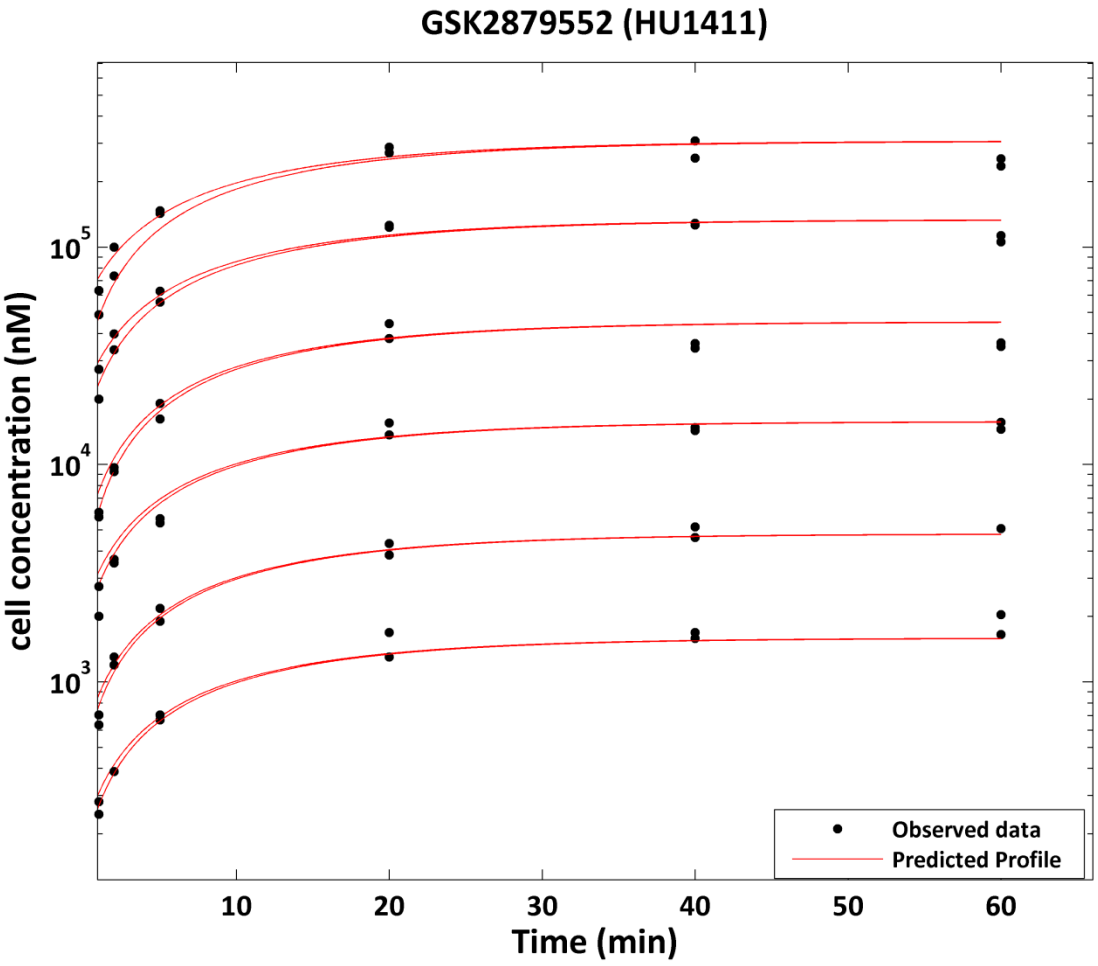

Appendix 73. Plot of the observed versus predicted cell concentrations for the uptake of GSK2879552 in adult human hepatocytes (donor HU8116) at 6 concentrations (0.3–100 μM) over a 60 minute incubation from the uptake FIT model. Data points are duplicate measurements.

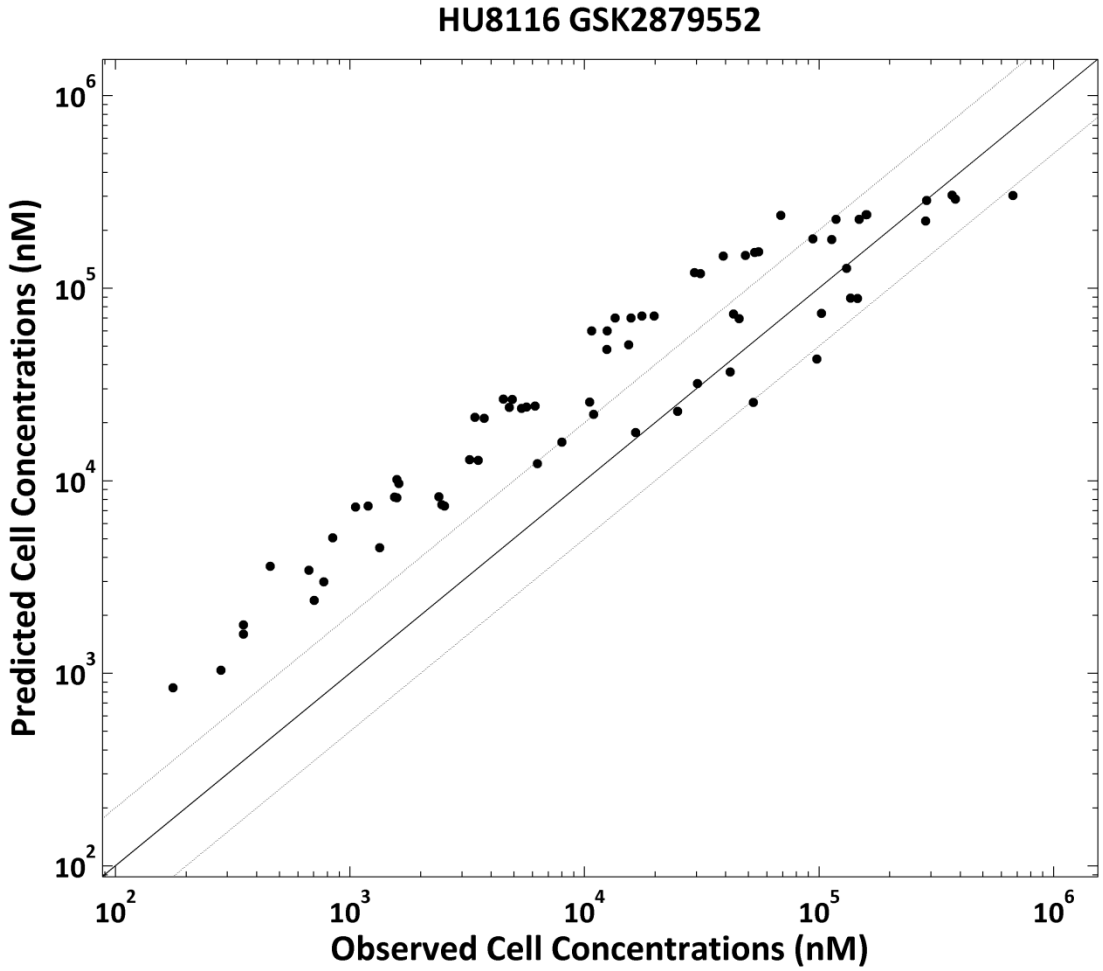

Appendix 74. Plot of the observed versus predicted cell concentrations for the uptake of GSK2879552 in adult human hepatocytes (donor HU8119) at 6 concentrations (0.3–100 μM) over a 60 minute incubation from the uptake FIT model. Data points are duplicate measurements.

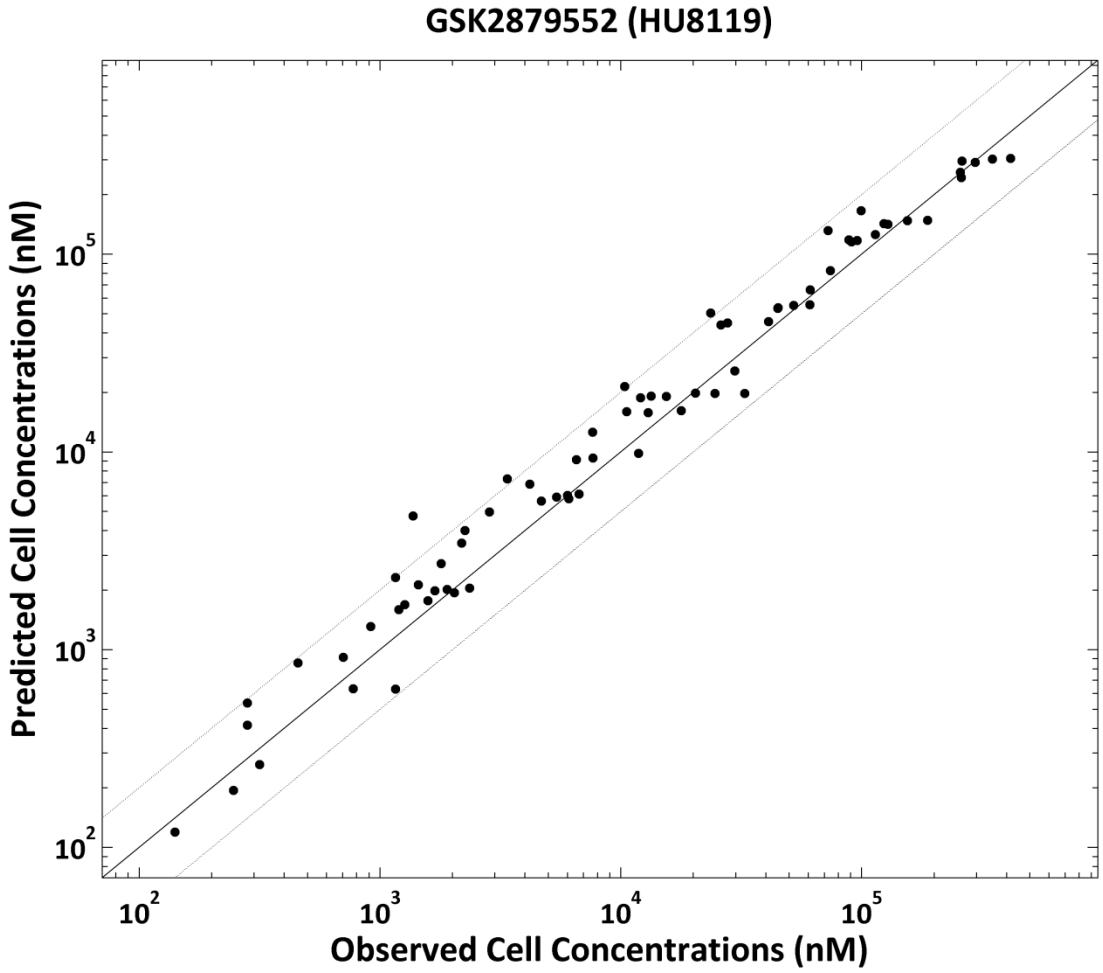

Appendix 75. Plot of the observed versus predicted cell concentrations for the uptake of GSK2879552 in adult human hepatocytes (donor HU1411) at 6 concentrations (0.3–100 μM) over a 60 minute incubation from the uptake FIT model. Data points are duplicate measurements.

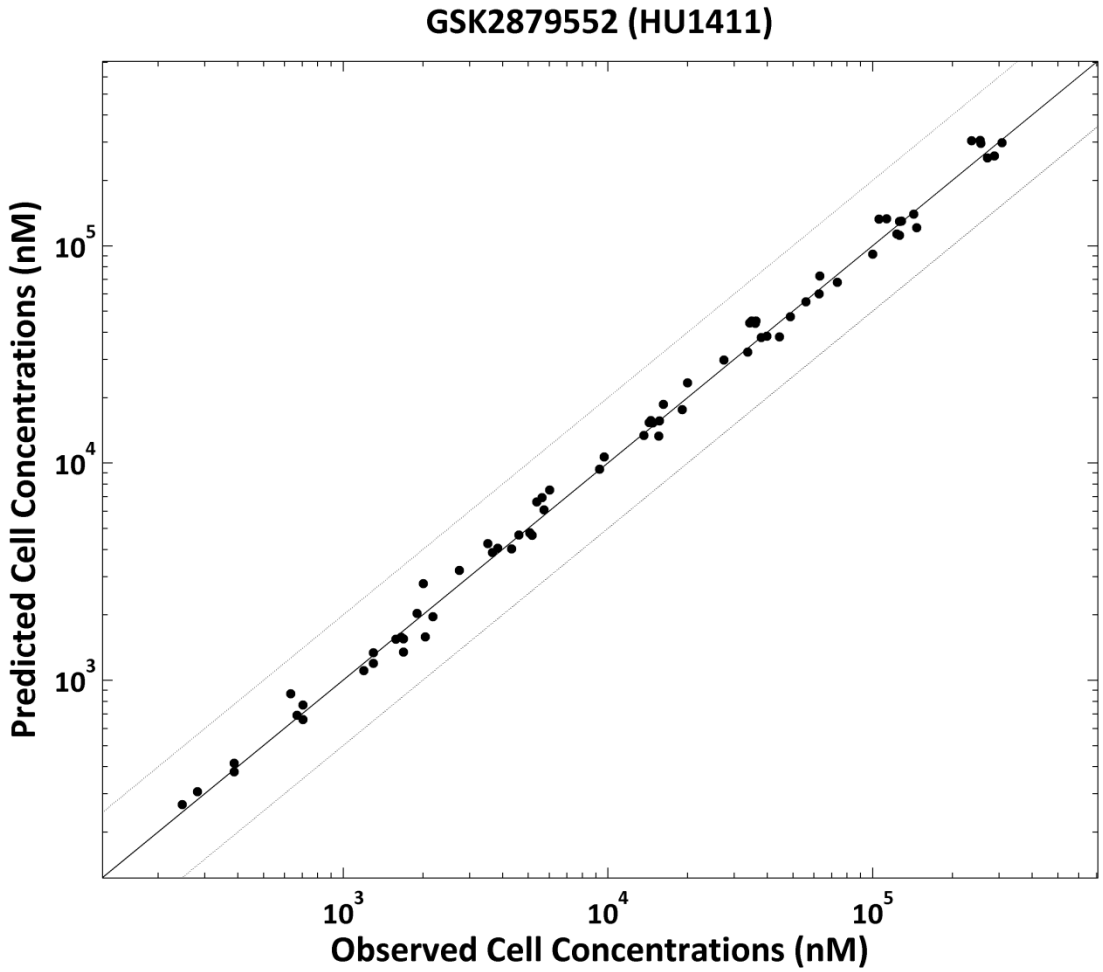

Appendix 76. Plot of the weighted residuals versus predicted cell concentrations for the uptake of GSK2879552 in human hepatocytes (donor HU8116) at 6 concentrations (0.3–100 μM) over a 60 minute incubation from the uptake FIT model.

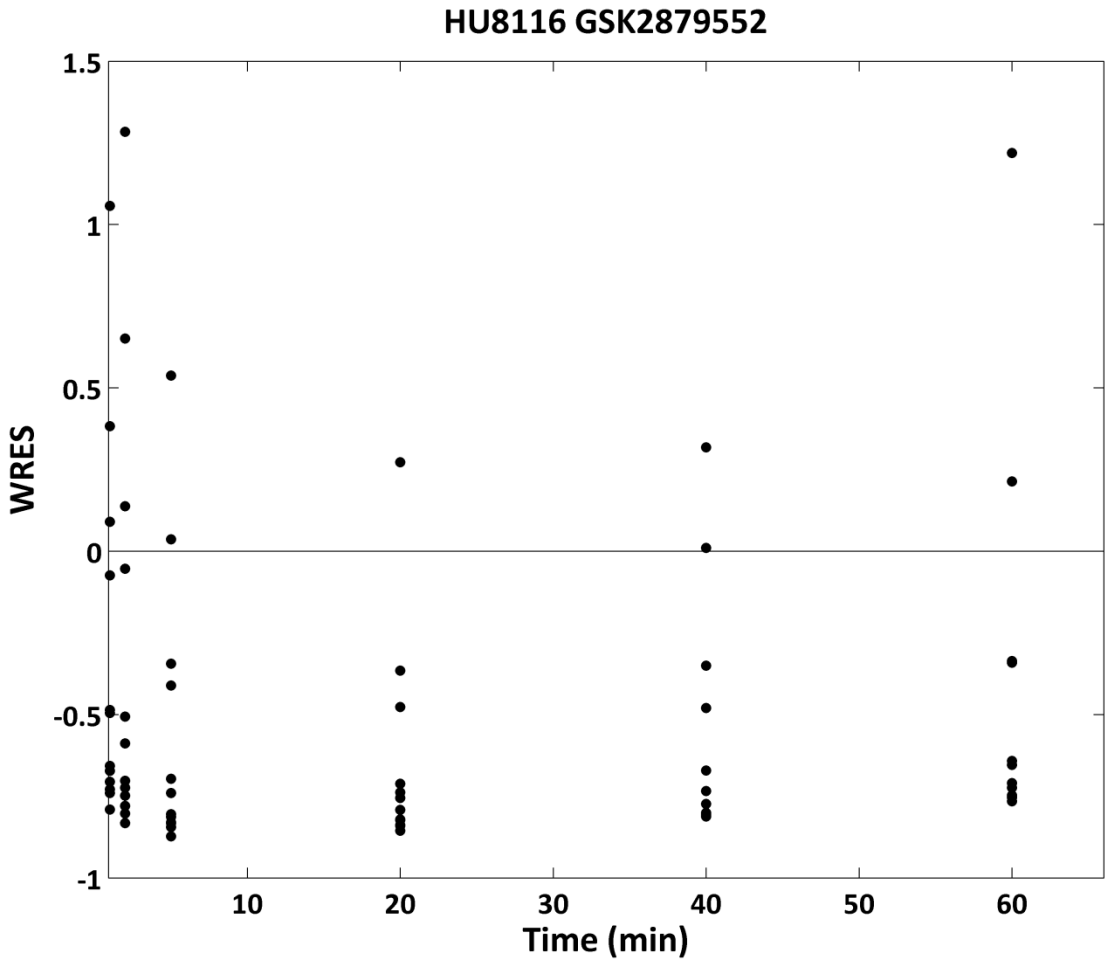

Appendix 77. Plot of the weighted residuals versus predicted cell concentrations for the uptake of GSK2879552 in human hepatocytes (donor HU8119) at 6 concentrations (0.3–100 μM) over a 60 minute incubation from the uptake FIT model.

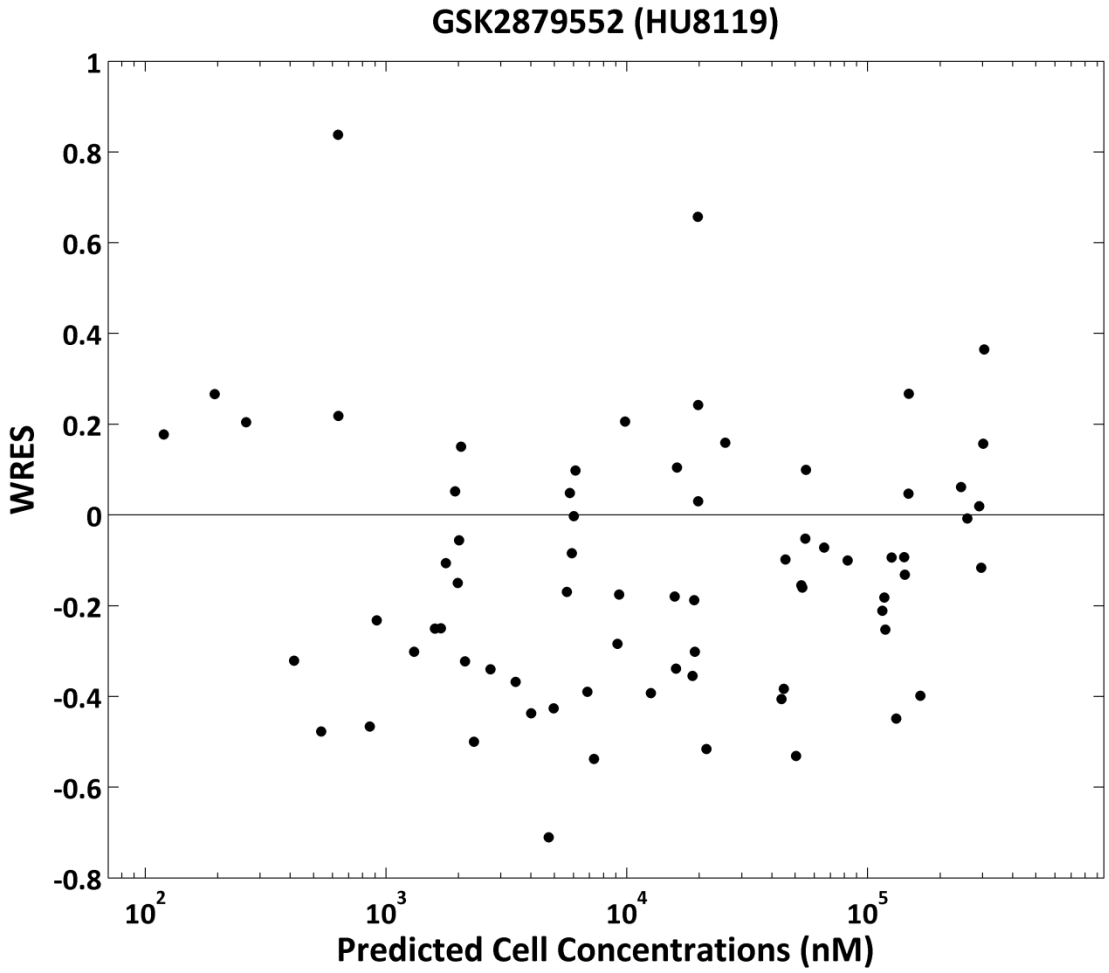

Appendix 78. Plot of the weighted residuals versus predicted cell concentrations for the uptake of GSK2879552 in human hepatocytes (donor HU1411) at 6 concentrations (0.3–100 μM) over a 60 minute incubation from the uptake FIT model.

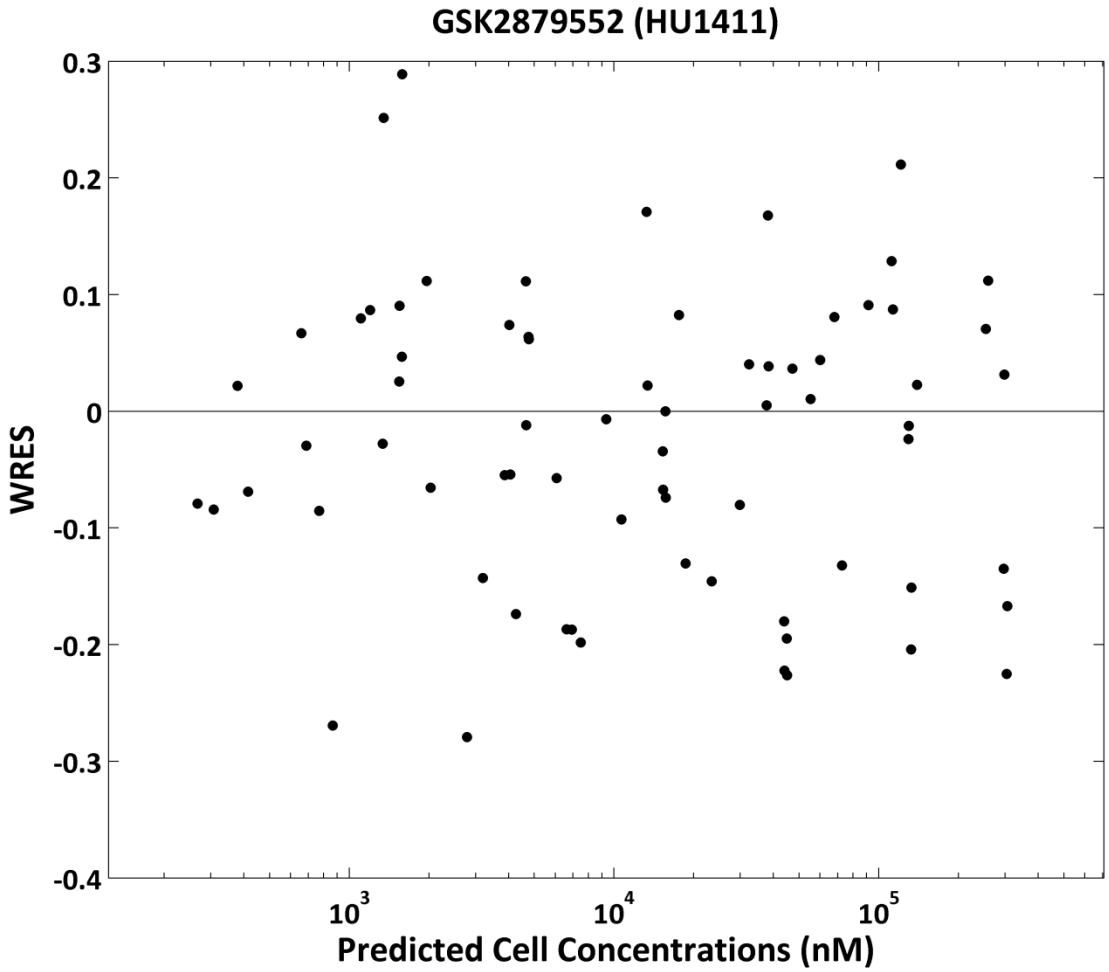

Appendix 79. Plot of the weighted residuals versus time for the uptake of GSK2879552 in human hepatocytes (donor HU8116) at 6 concentrations (0.3–100 µM) over a 60 minute incubation from the uptake FIT model.

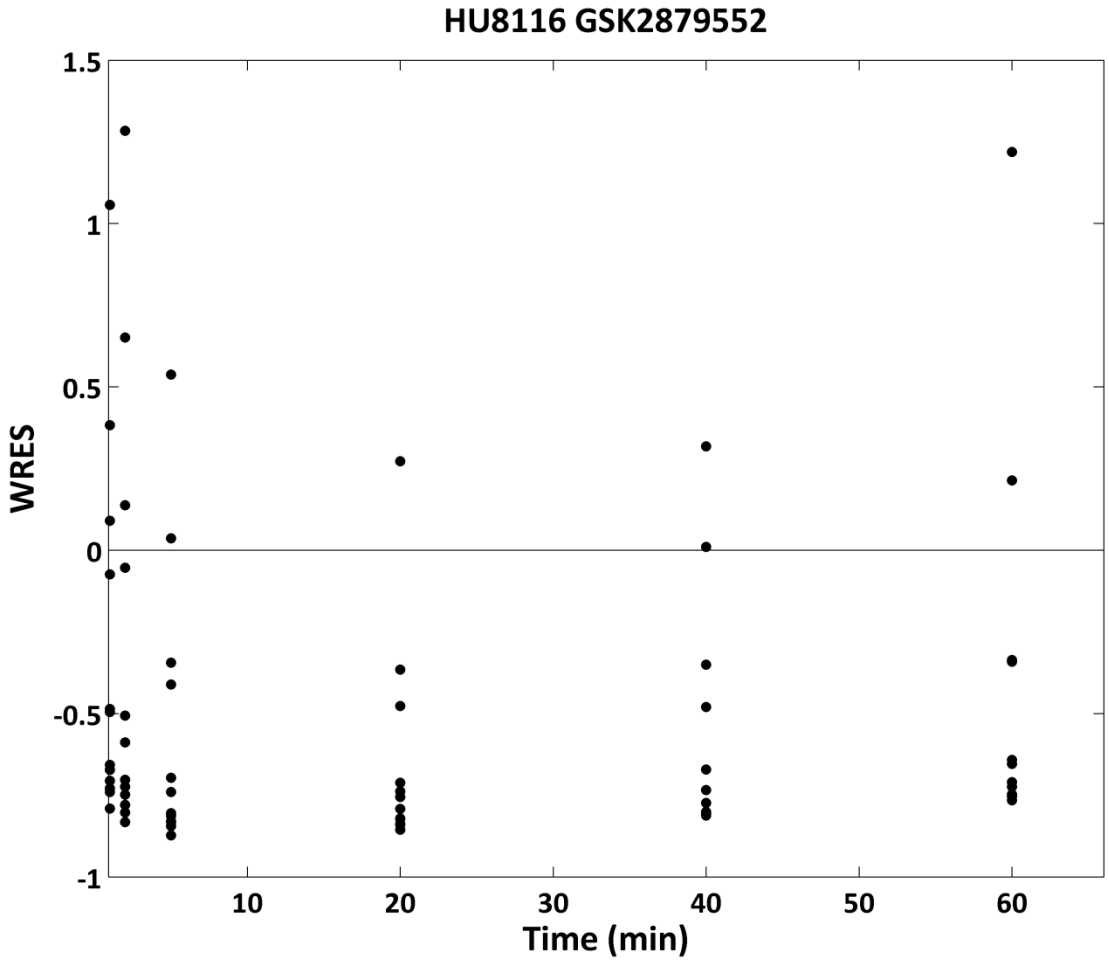

Appendix 80. Plot of the weighted residuals versus time for the uptake of GSK2879552 in human hepatocytes (donor HU8119) at 6 concentrations (0.3–100 µM) over a 60 minute incubation from the uptake FIT model.

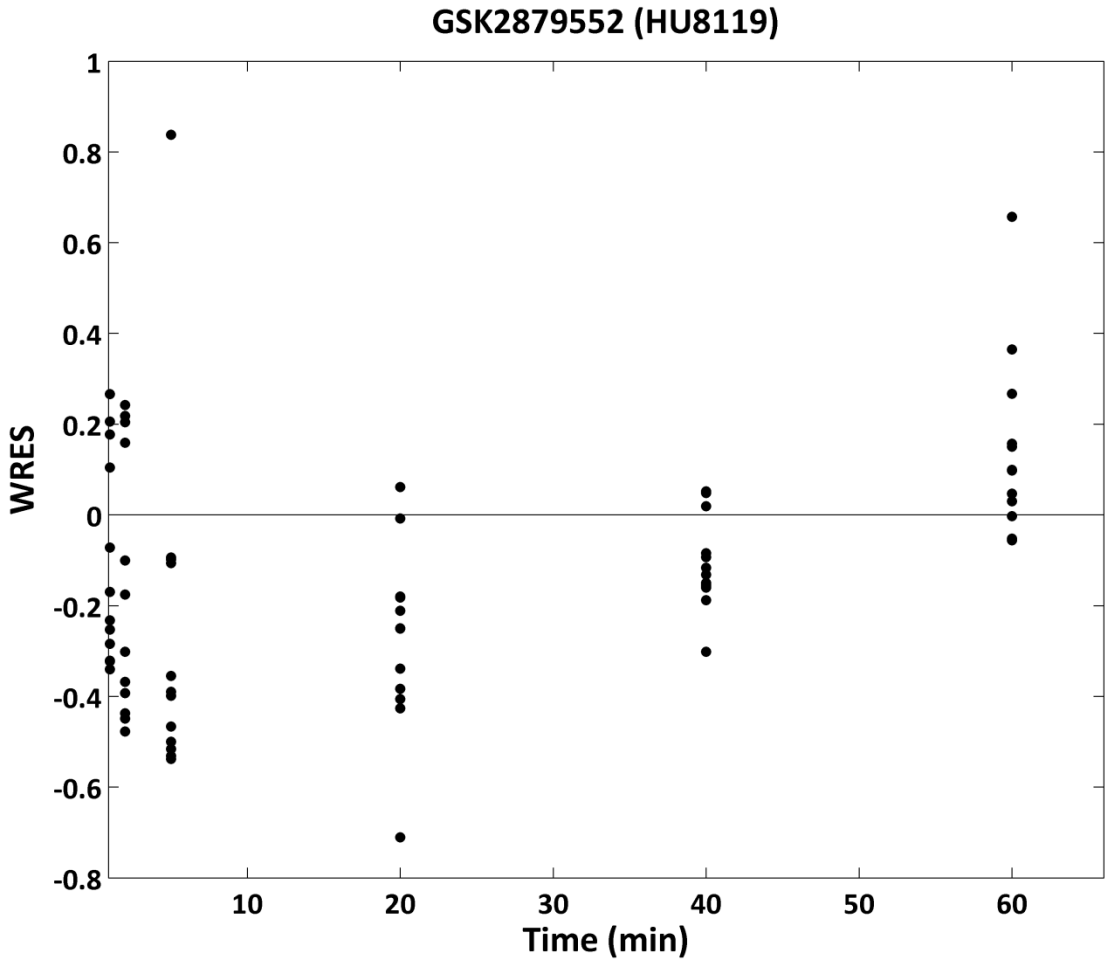

Appendix 81. Plot of the weighted residuals versus time for the uptake of GSK2879552 in human hepatocytes (donor HU1411) at 6 concentrations (0.3–100 µM) over a 60 minute incubation from the uptake FIT model.

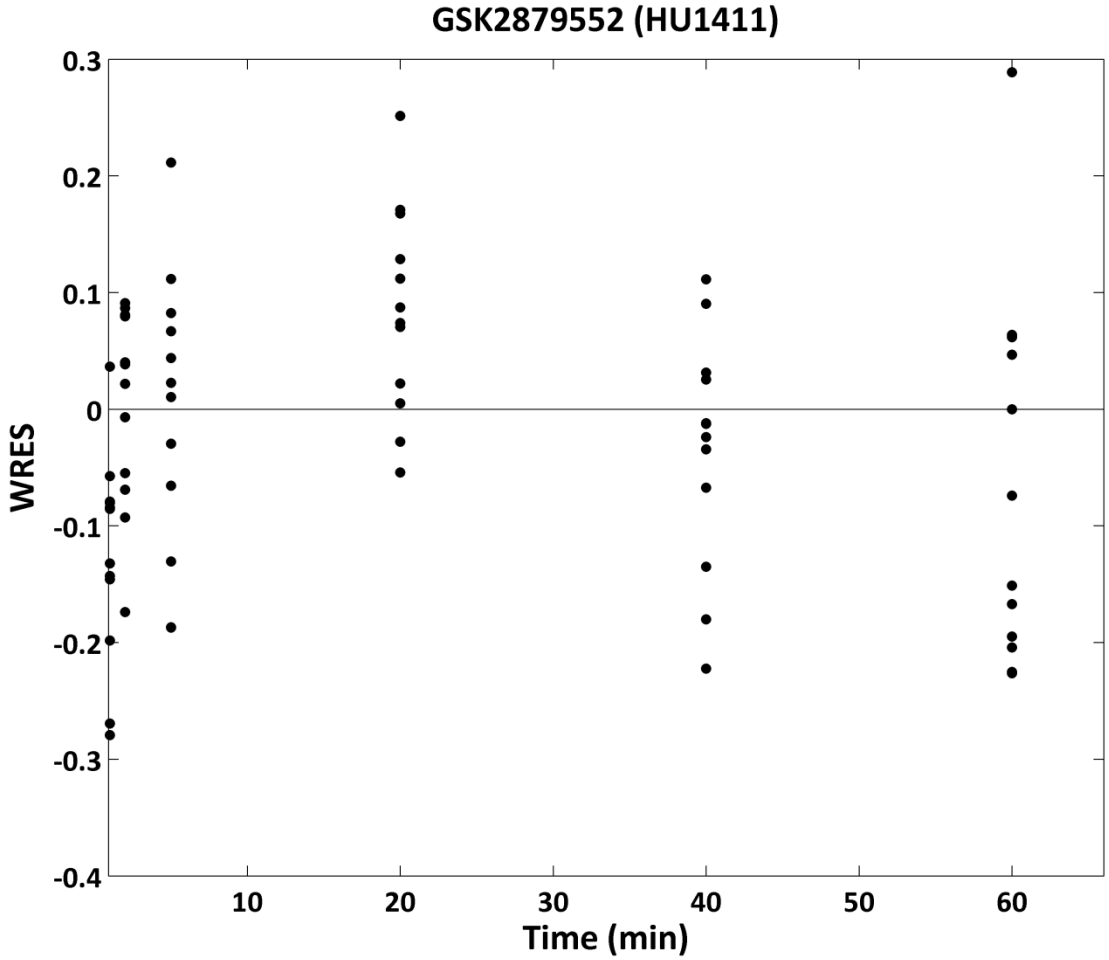

Appendix 82. Summary of the correlation matrix produced by the UptakeFIT model of the uptake of GSK2879552 by three adult human cryopreserved hepatocytes (HU8116, HU8119 and HU1411).

HU1411	Vmax	Km	Pdiff	fucell
Vmax	1	0.9975	-0.995	0.9957
Km		1	-0.9878	0.988
Pdiff			1	-0.9997
fucell				1
HU8116	Vmax	Km	Pdiff	fucell
Vmax	1	0.9104	-0.7967	0.8291
Km		1	-0.7684	0.7782
Pdiff			1	-0.9958
fucell				1
HU8119	Vmax	Km	Pdiff	fucell
Vmax	1	0.9938	-0.9799	0.983
Km		1	-0.959	0.9616
Pdiff			1	-0.9992
fucell				1

Bibliography

Abe K, Bridges AS, Yue W, and Brouwer KL (2008). In vitro biliary clearance of angiotensin II receptor blockers and 3-hydroxy-3-methylglutaryl-coenzyme A reductase inhibitors in sandwich-cultured rat hepatocytes: comparison with in vivo biliary clearance. J. Pharmacol. Exp. Ther., Vol. **326**:983-990.

Abe K, Bridges AS, and Brouwer KL (2009). Use of sandwich-cultured human hepatocytes to predict biliary clearance of angiotensin II receptor blockers and HMG-CoA reductase inhibitors. Drug Metab. Dispos., Vol. **37**:447-452.

Akao H, Polisecki E, Kajinamib K, Trompet S, Robertsone M, Forde I, Jukemad W, de Craend A,Westendorpd R, Shepherd J, Packard C, Buckley B, Schaefer E (2012). Genetic variation at the SLCO1B1 gene locus and low density lipoprotein cholesterol lowering response to pravastatin in the elderly. Atherosclerosis, Vol. **220**:413– 417.

Akhlaghi F and Trull AK (2002). Distribution of Cyclosporin A in Organ Transplant Recipients. Clin Pharm, Vol. **41** (9):615-637.

Amundsen R, Christensen H, Zabihyan B, and Åsberg A (2010) Cyclosporin A, but not tacrolimus, shows relevant inhibition of organic anion-transporting protein 1B1-mediated transport of atorvastatin. Drug Metab. Dispos., Vol. **38**:1499–1504.

Annaert P, Ye ZW, Stieger B and Augustijns P (2010). Interaction of HIV protease inhibitors with OATP1B1, 1B3, and 2B1. Xenobiotica, Vol. **40** (3):163–176.

Aoyama T, Omori T, Watabe S, Shioya A, Ueno T, Fukuda N and Matsumoto Y (2010). Pharmacokinetic/Pharmacodynamic Modeling and Simulation of Rosuvastatin Using an Extension of the Indirect Response Model by Incorporating a Circadian Rhythm. Biol. Pharm. Bull., Vol. **33** (6):1082—1087.

Aquilante C, Kiser JJ, Anderson PL, Christians U, Kosmiski LA, Daily EB, Hoffman KL, Hopley CW, Predhomme JA, Schniedewind B, and Sidhom MS (2011). Influence of SLCO1B1 Polymorphisms on the Drug-Drug Interaction Between Darunavir/Ritonavir and Pravastatin. J. Clin. Pharm., DOI: 10.1177/0091270011427907.

Arnadottir M, Eriksson L-O, Thysell H and Karkas JD (1993). Plasma concentration profiles of simvastatin 3-hydroxy-3-methyl-glutaryl-coenzyme A reductase inhibitory activity in kidney transplant recipients with and without cyclosporin. Nephron, Vol. **65** (3):410-413.

Åsberg A, Hartmann A, Fjeldsa E, Bergan S, and Holdaas H (2001). Bilateral pharmacokinetic interaction between cyclosporine A and atorvastatin in renal transplant recipients. American Journal of Transplantology, Vol. **1** (4):382-386.

Åsberg A 2003. Interaction Between CsA and Lipid Lowering Drugs. Drugs, Vol. **63** (4):367-378.

Ayrton A and Morgan P (2001). Role of transport proteins in drug absorption, distribution and excretion. Xenobiotica, Vol. **31** (8/9):469-497.

Ayrton A and Morgan P (2008). Role of transport proteins in drug discovery and development: a pharmaceutical perspective. Xenobiotica, Vol. **38** (7/8):676–708.

Bailey DG (2010). Fruit juice inhibition of uptake transport: a new type of food–drug interaction. Brit. J. Clin. Pharmaco., Vol. **70** (5):645-655.

Baker M and Parton T (2007) Kinetic determinants of hepatic clearance: plasma protein binding and hepatic uptake. Xenobiotica, Vol. **37**:1110-1134.

Bednarczyk D (2010) Fluorescence-based assays for the assessment of drug interaction with the human transporters OATP1B1 and OATP1B3. Anal. Biochem., Vol. **405:**50–58.

Berry MN and Friend DS (1969). High yield preparation of isolated rat liver parenchymal cells. J. Cell Biol., Vol. **43**:506-520.

Berry MN and Philips JW (2000). The isolated hepatocyte preparation: 30 years on. Biochemical Society Transactions, Vol. **28**, part 2.

Bi YA, Kazolias D, and Duignan DB (2006). Use of Cryopreserved Human Hepatocytes in Sandwich Culture to Measure Hepatobiliary Transport. Drug Metab. Dispos., Vol. **34**:1658–1665.

Bi Y, Kimoto E, Sevidal S, Jones HM, Barton HA, Kempshall S, Whalen KM, Zhang H, Ji C, Fenner KS, El-Kattan AF and Lai Y (2012). In Vitro Evaluation of Hepatic Transporter-Mediated Clinical Drug-Drug Interactions: Hepatocyte Model Optimization and Retrospective Investigation. Drug Metab. Dispos., Vol. **40** (6):1085–1092.

Bi YA, Qiu X, Rotter CJ, Kimoto E, Piotrowski M, Varma MV, Ei-Kattan AF, and Lai Y (2013). Quantitative assessment of the contribution of sodium-dependent taurocholate co-transporting polypeptide (NTCP) to the hepatic uptake of rosuvastatin, pitavastatin and fluvastatin. Biopharm Drug Dispos. Aug 30. doi: 10.1002/bdd.1861.

Bloomer J, Derimanov G, Dumont E, Ellens H and Matheny C (2013). Optimizing the in vitro and clinical assessment of drug interaction risk by understanding co-medications in patient populations. Expert Opin, DOI 10.1517/17425255.2013.781582.

Bow DA, Perry JL, Miller DS, Pritchard JB, and Brouwer KL (2008). Localization of P-gp (Abcb1) and Mrp2 (Abcc2) in freshly isolated rat hepatocytes. Drug Metab. Dispos., Vol. **36**:198-202.

Brown CD, Windass AS, Bleasby K, and Lauffart B (2001) Rosuvastatin is a high affinity substrate of hepatic organic anion transporter OATP-C (Abstract). Atherosclerosis Supplement 2:90.

Brown HS, Griffin M, and Houston JB (2007). Evaluation of Cryopreserved Human Hepatocytes as an Alternative in Vitro System to Microsomes for the Prediction of Metabolic Clearance. Drug Metab. Dispos., Vol. **35**:293–301.

Brown H, Wilby AJ, Alder J and Houston JB (2010). Comparative Use of Isolated Hepatocytes and Hepatic Microsomes for Cytochrome P450 Inhibition Studies: Transporter-Enzyme Interplay. Drug Metab. Dispos., Vol. **38** (12):2139–2144.

Busti AJ, Bain AM, Hall RG, 2nd, Bedimo RG, Leff RD, Meek C, and Mehvar R (2008). Effects of Atazanavir/Ritonavir or Fosamprenavir/Ritonavir on the Pharmacokinetics of Rosuvastatin. J. Cardiovasc. Pharmacol., Vol. **51**:605–610.

Campana C, Iacona I,. Regazzi MB, Gavazzi A, Perani G, Raddato V, Montemartini C and Vigano M (1995). Efficacy and pharmacokinetics of simvastatin in heart transplant recipients. Annual Pharmacotherapy, Vol. **29** (3):235-239.

Campbell SD, de Moraisa SM and Xub JJ (2004). Inhibition of human organic anion transporting polypeptide OATP 1B1 as a mechanism of drug-induced hyperbilirubinemia. Chemico-Biological Interactions, Vol. **150**, page179–187.

Chen J and Raymond K (2006). Roles of rifampicin in drug-drug interactions: underlying molecular mechanisms involving the nuclear pregnane X receptor. Annals of Clinical Microbiology and Antimicrobials, Volume 5:3.

Crouse JR (2008). An evaluation of rosuvastatin: Pharmacokinetics, efficacy and tolerability. Expert Opin. Drug Metab. Toxicol., Vol **4**:287-304.

Cui Y, König J, Leier I, Buchholz U and Keppler D (2000). Hepatic uptake of bilirubin and its conjugates by the human organic anion transporter SLC21A6. J Biol Chem. Vol. **30**:9626-9630.

Davies B and Morris T (1993). Physiological Parameters in Laboratory Animals and Humans. Pharm. Res., Vol. **10** (7):1093-1095.

De Bruyn T, Ye ZW, Peeters A, Sahi J, Baes M, Augustijns PF, and Annaert PP (2011). Determination of OATP-, NTCP- and OCT-mediated substrate uptake activities in individual and pooled batches of cryopreserved human hepatocytes. Eur. J. Pharm. Sci., Vol. **43**:297-307.

De Bruyn T, Van Westen G, Jzerman AP, Stieger B, de Witte P, Augustijns PF and Annaert PP (2013). Structure–based identification of OATP1B1/3 inhibitors. Mol. Pharmacol., published on April 9, doi:10.1124/mol.112.084152.

Deng JW, Song IS, Shin HJ, Yeo CW, Cho DY, Shon JH et al. (2008). The effect of SLCO1B1*15 on the disposition of pravastatin and pitavastatin is substrate dependent: the contribution of transporting activity changes by SLCO1B1*15. Pharmacogenetic Genomics, Vol **18:**424–433.

Deng S, Chen XP, Cao D, Yin T, Dai ZY, Luo J, Tang L and Li YJ (2009). Effects of a Concomitant Single Oral Dose of Rifampicin on the Pharmacokinetics of Pravastatin in a Two-Phase, Randomized, Single-Blind, Placebo-Controlled, Crossover Study in Healthy Chinese Male Subjects. Clinical Therapeutics, Vol. **31** (6):1256-1263.

Dresser GK, Kim RB and Bailey DG (2005). Effect of Grapefruit Juice Volumes on the Reduction of Fexofenadine Bioavailability: Possible Role of Organic Anion Trasnporting Polypeptides. Clin. Pharmacol. Ther., Vol. **77** (3):170-177.

Dunn CJ, Wagstaff AJ, Perry CM, Plosker GL and Goa KL (2001). An Updated Review of the Pharmacokinetic Properties, Clinical Efficacy and Tolerability of a Microemulsion-Based Formulation (Neoral®) in Organ Transplantation. Drugs, Vol. **61** (13):1957-2016

Eron J Jr, Yeni P, Gathe J Jr, Estrada V, DeJesus E, Staszewski S, Lackey P, Katlama C, Young B, Yau L, Sutherland-Phillips D, Wannamaker P, Vavro C, Patel L, Yeo J, and Shaefer M (2006). The KLEAN study of fosamprenavir-ritonavir versus lopinavir-ritonavir, each in combination with abacavir-lamivudine, for initial treatment of HIV infection over 48 weeks: a randomised non-inferiority trial. The Lancet, Vol. **368** (9534):476 – 482.

Fahr A 1993. Cyclosporin Clinical Pharmacokinetics. Clinical Pharmacokinetics, Vol. **24** (6):472-495.

Faulds, D, Goa, KL and Benfield P (1993). Cyclosporin. Drugs, Vol. **45** (6):953-1040.

Fehrenbach T, Cui Y, Faulstich H, and Keppler D (2003) Characterization of the transport of the bicyclic peptide phalloidin by human hepatic transport proteins. Naunyn Schmiedebergs Arch Pharmacol, Vol. **368**:415–420.

Fenner KS, Jones HM, Ullah M, Kempshall S, Dickins M, Lai Y, Morgan P, and Barton HA (2012). The evolution of the OATP hepatic uptake transport protein family in DMPK sciences: from obscure liver transporters to key determinants of hepatobiliary clearance. Xenobiotica, Vol. **42**:94-106.

Frezard F and Garnier-Suillerot A (1998) Permeability of lipid bilayer to anthracycline derivatives. Role of the bilayer composition and of the temperature. Biochim. Biophys. Acta., Vol. **1389**:13-22.

Fukuda H, Ohashi R, Tsuda-Tsukimoto M, and Tamai I (2008). Effect of Plasma Protein Binding on in Vitro-in Vivo Correlation of Biliary Excretion of Drugs Evaluated by Sandwich-Cultured Rat Hepatocytes. Drug. Metab. Dispos., Vol. **36** (7):1275-1282.

García MJ, Reinoso RF, Sánchez AN Prous JR (2003). Clinical Pharmacokinetics of Statins. Methods Findings Experimental Clinical Pharmacology, Vol. **25**(6):457-481.

Gardiner P and Paine SW (2011). The Impact of Hepatic Uptake on the Pharmacokinetics of Organic Anions. Drug. Metab. Dispos., Vol **39**:1930-1938.

Gertz M, Cartwright C, Hobbs MJ, Kenworthy K, Houston JB and Galetin A (2012). Cyclosporine inhibition of hepatic and intestinal CYP3A4, uptake and efflux transporters: Application of PBPK modelling in the assessment of drug-drug interaction potential. Pharm. Res., Vol. **30**:761–780.

Giacomini KM et al for The International Transporter Consortium 2010. Membrane transporters in drug development. Nature Reviews Drug Discovery, Vol. **3**:215-236.

Guguen-Guillouzo C and Guillouzo A (2010). In Methods in Molecular Biology 640. DOI 10.1007/978-1-60761-688-7_1. Editor P Maurel.

Gui C, Miao Y, Thompson L, Wahlgren B, Mock M, Stieger B, Hagenbuch B (2008). Effect of pregnane X receptor ligands on transport mediated by human OATP1B1 and OATP1B3. Eur. J. Pharmacol. Vol. **14**:57-65.

Gui C, Wahlgren B, Lushington GH, Hagenbuch B (2009). Identification, Ki determination and CoMFA analysis of nuclear receptor ligands as competitive inhibitors of OATP1B1-mediated estradiol-17beta-glucuronide transport. Pharmacol Res. Vol. **60**:50-56.

Guillouzo A, Rialland L, Fautrel F and Guyomard C (1999). Survival and function of isolated hepatocytes after cryopreservation. Chemico-Biological Interactions, Vol. **121**:7-16.

Guillouzo A, Corlu A, Aninat C, Glaise D, Morel F, Guguen-Guillouzo C (2007). The human hepatoma HepaRG cells: A highly differentiated model for studies of liver metabolism and toxicity of xenobiotics. Chemico-Biological Interactions, Vol. **168**:66–73.

Gullestad L, Nordal K.P, Berg K.J, Cheng H, Schwartz M.S and Simonsen S (1999). Interaction between lovastatin and cyclosporine after heart and kidney transplantation. Transplant Proceedings, Vol. **31** (5):2163-5

Hagenbuch B and Meier PJ (2004). Organic anion transporting polypeptides of the OATP/ SLC21 family: phylogenetic classification as OATP/ SLCO super family, new nomenclature and molecular/functional properties. Pflugers Archives, Vol. **447** (5):653-665.

Hall C, Lueshen E, Mosat A and Linninger A (2012). Interspecies Scaling in Pharmacokinetics: A Novel Whole-Body Physiologically Based Modeling Framework to Discover Drug Biodistribution Mechanisms In Vivo. J. Pharm. Sci., Vol. **101**:1221–1241.

Hallifax D and Houston JB (2006) Uptake and intracellular binding of lipophilic amine drugs by isolated rat hepatocytes and implications for prediction of in vivo metabolic clearance. Drug. Metab. Dispos., Vol. **34**:1829-1836.

Hallifax D, Galetin A and Houston JB (2008). Prediction of metabolic clearance using fresh human hepatocytes: Comparison with cryopreserved hepatocytes and hepatic microsomes for five benzodiazepines. Xenobiotica, Vol. **38** (4):353–367.

He YJ, Zhang W, Chen Y, Guo D, Tu JH, Xu LY, Tan ZR, Chen BL, Li Z, Zhou G, Yu BN, Kirchheiner J, Zhou HH (2009). Rifampicin alters atorvastatin plasma concentration on the basis of SLCO1B1 521TNC polymorphism. Clinica. Chimica. Acta., Vol. **405**:49–52.

Hedman M, Neuvonen PJ, Neuvonen M, Holmberg C, and Antikainen M (2004). Pharmacokinetics and pharmacodynamics of pravastatin in paediatric and adolescent cardiac transplant recipients on a regimen of triple immunosuppression. Clin. Pharmacol. Ther., Vol. **75**:101-109.

Hermann M, Åsberg A, Christensen H, Holdaas H, Hartmann A and Reubsaet JLE (2004). Letters to the Editor. Clin. Pharmacol. Ther., Vol. **76** (4):388-91.

Hino H, Tateno C, Sato H, Yamasaki C, Katayama S, Kohashi T, Aratani A, Asahara T, Dohi K and Yoshizato K 1999. A Long-Term Culture of Human Hepatocytes Which Show a High Growth Potential and Express Their Differentiated Phenotypes. Biochem. Biophys. Res. Commun., Vol. **256**:184–191.

Hinton L, Galetin A and Houston J (2008). Multiple Inhibition Mechanisms and Prediction of Drug-Drug Interactions: Status of Metabolism and Transporter Models as Exemplified by Gemfibrozil-Drug Interactions. Pharm. Res., Vol. **25** (5):1063-1074.

Hirano M, Maeda K, Shitara Y and Sugiyama Y (2004). Contribution of OATP2 (OATP1B1) and OATP8 (OATP1B3) to the Hepatic Uptake of Pitavastatin in Humans. J. Pharmacol. Exp. Ther., Vol. **311:**139–146.

Hirano M, Maeda K, Shitara Y and Sugiyama Y (2006). Drug-Drug Interaction Between Pitavastatin and Various Drugs via OATP1B1. Drug Metab. Dispos., Vol. **34** (7):1229-1236.

Hirouchi M, Kusuhara H, Onuki R, Ogilvie BW, Parkinson A and Sugiyama Y (2009). Construction of Triple-Transfected Cells [Organic Anion-Transporting Polypeptide (OATP) 1B1/Multidrug Resistance-Associated Protein (MRP) 2/MRP3 and OATP1B1/MRP2/MRP4] for Analysis of the Sinusoidal Function of MRP3 and MRP4. Drug Metab. Dispos., Vol. **37**:2103–2111.

Ho RH, Tirona RG, Leake BF, Glaeser H, Lee W, Lemke CJ, Wang Y and Kim RB (2006). Drug and Bile Acid Transporters in Rosuvastatin Hepatic Uptake: Function, Expression, and Pharmacogenetics. Gastroenterology, Vol. **130**:1793–1806.

Hobbs M, Parker C, Birch H, and Kenworthy K (2011). Understanding the Interplay of Drug Transporters Involved in the Disposition of Rosuvastatin in the Isolated Perfused Rat Liver using a Physiologically-Based Pharmacokinetic Model. Xenobiotica, Vol. **42** (4):327–338.

Hochman JH, Pudvah N, Qiu J,Yamazaki M, Tang C, Lin JH and Prueksaritanont T (2004). Interactions of Human P-glycoprotein with Simvastatin, Simvastatin Acid and Atorvastatin. Pharm. Res., Vol. **21** (9 September):1686-1691.

Hoffmaster KA, Turncliff RZ, LeCluyse EL, Kim RB, Meier PJ, and Brouwer KL (2004). P-glycoprotein expression, localization, and function in sandwich-cultured primary rat and human hepatocytes: relevance to the hepatobiliary disposition of a model opioid peptide. Pharm. Res., Vol. **21**:1294-1302.

Hollenberg PF (2002). Characteristics and Common Properties Of Inhibitors, Inducers and Activators Of CYP Enzymes. Drug Met Reviews, Vol.**34** (1&2):17–35.

Houston J and Galetin A (2008). Methods for predicting in vivo pharmacokinetics using data from in vitro assays. Current Drug Metabolism, Vol. **9**:940-951.

Howard RB, Christensen AK, Gibbs FA, Pesch LA (1967). The enzymatic preparation of isolated intact parenchymal cells from rat liver. J. Cell Biol., Vol. **35**:675–684.

Hsiao P, Sasongko L, Link JM, Mankoff DA, Muzi M, Collier AC and Unadkat JD (2006). Verapamil P-glycoprotein Transport across the Rat Blood-Brain Barrier: Cyclosporine, a Concentration Inhibition Analysis, and Comparison with Human Data. The J. Pharmacol. Exp. Ther.,Vol. **317** (2):704-710.

Huang L, Wang Y and Scott Grimm S (2006). ATP-Dependent Transport of Rosuvastatin in Membrane Vesicles Expressing Breast Cancer Resistance Protein. Drug Metab. Dispos., Vol. **34** (5):738-742.

Ieiri I, Higuchi S and Sugiyama Y (2009). Genetic polymorphisms of uptake (OATP1B1, 1B3) and efflux (MRP2, BCRP) transporters: implications for inter-individual differences in

the pharmacokinetics and pharmacodynamics of statins and other clinically relevant drugs. Expert Opin. Drug Metab. Toxicol., Vol. **5** (7):703-729.

Iusuf D, van Esch A, Hobbs MJ, Taylor M, Kenworthy K, van de Steeg E, Wagenaar E and Schinkel A (2013). Organic anion transporting polypeptides 1a/1b control systemic exposure of rosuvastatin in mice, without affecting its liver exposure. Mol. Pharmacol., Vol. **83**:919–929.

Iusuf D, Sparidans RW, van Esch A, Hobbs MJ, Kenworthy K, van de Steeg E, Wagenaar E, Beijnen JH and Schinkel A (2012). Organic anion-transporting polypeptides 1a/1b control the hepatic uptake of pravastatin in mice. Molecular Pharmaceutics (accepted July 2012) Ishikawa et al 2004. The Genetic Polymorphism of Drug Transporters: Functional Analysis Approaches. Pharmacogenomics, Vol. **5** (1):67-99.

Jennen D, Magkoufopoulou C, Ketelslegers HB, van Herwijnen M, Kleinjans J, van Delft J (2010). Comparison of HepG2 and HepaRG by Whole-Genome Gene Expression Analysis for the Purpose of Chemical Hazard Identification. Toxicol. Sci., Vol. **115** (1):66–79.

Jones HM, Barton HA, Lai Y, Bi YA, Kimoto E, Kempshall S, Tate SC, El-Kattan A, Houston B, Galetin A, and Fenner KS (2012). Mechanistic Pharmacokinetic Modeling for the Prediction of Transporter-Mediated Disposition in Humans from Sandwich Culture Human Hepatocyte Data. Drug. Metab. Dispos., Vol. **40** (5):1007–1017.

Kalliokoski A and Niemi M (2009). Impact of OATP transporters on pharmacokinetics. Br. J. Pharmaco., Vol. **158:**693–705.

Kameyama Y, Yamashita K, Kobayashi K, Hosokawa M, and Chiba K (2005). Functional characterization of SLCO1B1 (OATP-C) variants, SLCO1B1*5, SLCO1B1*15 and SLCO1B1*15+C1007G, by using transient expression systems of HeLa and HEK293 cells. Pharmacogenet Genomics, Vol. **15**:513–522.

Karlgren M, Ahlin G, Bergström CA, Svensson R, Palm J and Artursson P (2012a). In Vitro and In Silico Strategies to Identify OATP1B1 Inhibitors and Predict Clinical Drug–Drug Interactions. Pharm. Res., Vol. **29:**411–426.

Karlgren M, Vildhede A, Norinder U, Wisniewski JR, Kimoto E, Lai Y, Haglund U and Artursson P (2012b). Classification of Inhibitors of Hepatic Organic Anion Transporting Polypeptides (OATPs): Influence of Protein Expression on Drug−Drug Interactions. J. Med. Chem. Vol. **55**:4740−4763.

Keskitalo JE, Kurkinen1 KJ, Neuvonen PJ and Niemi M (2008). ABCB1 haplotypes differentially affect the pharmacokinetics of the acid and lactone forms of simvastatin and atorvastatin. Clin. Pharmacol. Ther., Vol. **84** (4):457-461.

Keskitalo JE, Zolk O, Fromm MF, Kurkinen KJ, Neuvonen PJ and Niemi M (2009a). ABCG2 polymorphism markedly affects the pharmacokinetics of atorvastatin and rosuvastatin. Clin. Pharmacol. Ther., Vol. **86** (2):197-203.

Keskitalo JE, Pasanen MK, Neuvonen PJ and Niemi M (2009b). No significant effect of ABCB1 haplotypes on the pharmacokinetics of fluvastatin, pravastatin, lovastatin, and rosuvastatin. Br. J. Clin. Pharmacol., Vol. **68** (2):207-213.

Keskitalo JE, Kurkinen KJ, Neuvonen M, Backman JT, Neuvonen PJ & Niemi M (2009c). Different effects of the ABCG2 c.421C>A SNP on the pharmacokinetics of fluvastatin, pravastatin and simvastatin. Pharmacogenomics, Vol. **10**:1617-1624.

Kimoto E, Walsky R, Zhang H, Bi YA, Whalen KM, Yang YS, Linder C, Xiao Y, Iseki K, Fenner KS, El-Kattan AF, and Lai Y (2012). Differential modulation of cytochrome P450 activity and the effect of 1-aminobenzotriazole on hepatic transport in sandwich-cultured human hepatocytes. Drug Metab. Dispos., Vol. **40**:407-411.

Kiser JJ, Gerber JG, Predhomme JA, Wolfe P, Flynn DM and Hoody DW (2008). Drug/Drug Interaction Between Lopinavir/Ritonavir and Rosuvastatin in Healthy Volunteers. Journal Acquired Immune Deficiency Syndrome Vol. **47** (5):570-578.

Kitamura S, Maeda K, Wang Y, and Sugiyama Y (2008) Involvement of multiple transporters in the hepatobiliary transport of rosuvastatin. Drug Metab. Dispos., Vol. **36:**2014–2023.

Kotani N, Maeda K, Watanabe T, Hiramatsu M, Gong LK, Bi YA, Takezawa T, Husuhara H, and Sugiyama Y (2011). Culture-period-dependent changes in the uptake of transporter substrates in sandwich-cultured rat and human hepatocytes. Drug Metab. Dispos., Vol. **39**:1503-1510.

Kukongviriyapan V and Stacey NH (1988). Inhibition of Taurocholate Transport by Cyclosporin A in Cultured Rat Hepatocytes. The J. Pharm. Exp. Ther. Vol. **247**, No. 2:685-689.

Lau Y, Okochi H, Huang Y and Benet LZ (2006). Multiple Transporters Affect the Disposition of Atorvastatin and Its Two Active Hydroxy Metabolites: Application of in Vitro and ex Situ Systems. J. Pharmacol. Exp. Ther., Vol. **316**:762–771.

Lau YY, Huang Y, Frassetto L, and Benet LZ (2007) Effect of OATP1B transporter inhibition on the pharmacokinetics of atorvastatin in healthy volunteers. Clin. Pharmacol. Ther., Vol. **81**:194–204.

LeCluyse EL (2001). Human hepatocyte culture systems for the in vitro evaluation of cytochrome P450 expression and regulation. Eur. J. Pharm. Sci., Vol. **13**:343–368.

Lennernas H 2003. Clinical Pharmacokinetics of Atorvastatin. Clin. Pharmacokinet., Vol. **42**:1141-1160.

Leonhardt M, Keiser M, Oswald S, Ku¨hn J, Jia J, Grube M, Kroemer HK, Siegmund W, and Weitschies W (2010) Hepatic uptake of the magnetic resonance imaging contrast agent Gd-EOB-DTPA: role of human organic anion transporters. Drug Metab. Disp., Vol. **38**:1024–1028.

Li A et al (2010). Improved Extrapolation of Hepatobiliary Clearance from in Vitro Sandwich Cultured Rat Hepatocytes through Absolute Quantification of Hepatobiliary Transporters. Mol. Pharmaceutics., Vol. **7**:630-641.

Li N, Singh P, Mandrell KM, and Lai Y (1999). Cryopreserved human hepatocytes: characterization of drug-metabolizing enzyme activities and applications in higher throughput screening assays for hepatotoxicity, metabolic stability, and drug–drug interaction potential. Chemico-Biological Interactions, Vol. **121**:17–35.

Li P, Wang GJ, Robertson TA and Roberts MS (2009). Liver Transporters in Hepatic Drug Disposition: An Update. Current Drug Metabolism, Vol. **10**:482-498.

Liao M, Raczynski AR, Chen M, Chuang BC, Zhu Q, Shipman R, Morrison J, Lee D, Lee FW, Balani SK and Xia CQ (2010). Inhibition of Hepatic Organic Anion-Transporting Polypeptide by RNA Interference in Sandwich-Cultured Human Hepatocytes: An In Vitro Model to Assess Transporter-Mediated Drug-Drug Interactions. Drug Metab. Dispos., Vol. **38**:1612-1622.

Lu C, Liao M, Cohen L and Xia CQ (2010). Emerging In Vitro Tools to Evaluate Cytochrome P450 and Transporter-Mediated Drug-Drug Interactions. Current Drug Discovery Technologies, Vol. **7**:199-222.

McGinnity DF, Soars MG, Urbanowicz RA, and Riley RJ (2004). Evaluation of Fresh and Cryopreserved Hepatocytes as In Vitro Drug Metabolism Tools for the Prediction of Metabolic Clearance. Drug Metab. Dispos., Vol. **32**:1247–1253.

Madan A, Dehaan R, Mudra D, Carroll K, Lecluyse E and Parkinson A (1999). Effect of cryopreservation on cytochrome P450 enzyme induction in cultured rat hepatocytes. Drug Metab. Dispos., Vol. **27**:327-335.

Maeda K and Sugiyama Y 2010. The Use of Hepatocytes to Investigate Drug Uptake Transporters. Methods Molecular Biology, Vol. **640**:327-53.

Martin PD, Warwick MJ, Dane AL, Brindley C, and Short T (2003). Absolute Oral Bioavailability of Rosuvastatin in Healthy White Adult Male Volunteers. Clin. Ther., Vol. **25** (10):2553- 2563.

Matsushima S, Maeda K, Ishiguro N, Igarashi T, and Sugiyama Y (2008) Investigation

of the inhibitory effects of various drugs on the hepatic uptake of fexofenadine in humans. Drug Metab. Dispos., Vol. **36**:663-669.

Mehvar R and Chimalakonda AP (2004). Hepatic disposition of cyclosporine A in isolated perfused rat livers. J. Pharm Pharmaceut Sci, Vol. **7** (1):47-54.

Ménochet K, Kenworthy KE, Houston B, and Galetin A (2012a) Use of Mechanistic Modeling to Assess Interindividual Variability and Interspecies Differences in Active Uptake in Human and Rat Hepatocytes. Drug Metab. Dispos., Vol. **40** (9):1744-1756.

Ménochet K, Kenworthy KE, Houston B, and Galetin A (2012b) Simultaneous Assessment of Uptake and Metabolism in Rat Hepatocytes: A Comprehensive Mechanistic Model. J. Pharmacol. Exp. Ther., Vol. **341**:2-15.

Mitry R, Hughes RD and Dhawan A 2002. Progress in human hepatocytes: isolation, culture & cryopreservation seminars. Cell. Dev. Biol., Vol. **13**:463–467.

Moldeous P and Jernstrom B (1983). Interaction of glutathione with reactive intermediates. In: Functions of Glutathione; Biochemical, Physiological, Toxicological and Clinical Aspects, pp99-108. Raven Press, New York.

Mudra D (2001). Preparation of Hepatocytes. Curr. Prot. Tox., 14.2.1-14.2.13

Nakakariya M, Ono M, Amano N, Moriwaki T, Maeda K, and Sugiyama Y (2012). In vivo biliary clearance should be predicted by intrinsic biliary clearance in sandwich-cultured hepatocytes. Drug Metab. Dispos., Vol. **40**:602-609.

Neuvonen PJ, Niemi M and Backman JT (2006). Drug interactions with lipid lowering drugs. Mechanisms and Clinical Relevance. Clin. Pharmacol. Ther., Vol. **80** (6):565-581.

Neuvonen PJ (2010). Drug interactions with HMG-CoA reductase inhibitors (statins): The importance of CYP enzymes, transporters and pharmacogenetics. Curr. Opin. Investig. D., Vol. **11** (3):323-332.

Niemi M, Pasanen MK and Neuvonen PJ (2006). SLCO1B1 polymorphism and sex affect the pharmacokinetics of pravastatin but not fluvastatin. Clin. Pharmacol. Ther., Vol. **80**:356-366.

Niemi M, Pasanen MK and Neuvonen PJ (2011). Organic Anion Transporting Polypeptide 1B1: a Genetically Polymorphic Transporter of Major Importance for Hepatic Drug Uptake. Pharmacol. Rev., Vol.. **63**:157–181.

Noe´ J , Portmann R, Brun ME and Funk C (2007). Substrate-Dependent Drug-Drug Interactions between Gemfibrozil, Fluvastatin and Other Organic Anion-Transporting Peptide (OATP) Substrates on OATP1B1, OATP2B1 and OATP1B3. Drug Metab. Dispos., Vol. **35**:1308–1314.

Nezasa K, Takao A, Kimura K, Takaichi M, Inazawa K and Koike M (2002a). Pharmacokinetics and disposition of rosuvastatin, a new 3-hydroxy-3-methylglutaryl coenzyme A reductase inhibitor, in rat. Xenobiotica, 325: 715-727.

Nezasa K, Higaki K, Takeuchi M, Nakano M and Koike M (2003). Uptake of rosuvastatin by isolated rat hepatocytes: comparison with pravastatin. Xenobiotica, 33: 379–388.

Nezasa K, Higaki K, Matsumura T, Inazawa K, Hasegawa H, Nakano M and Koike M (2002b). Liver-Specific Distribution of Rosuvastatin in Rats: Comparison with Pravastatin and Simvastatin. Drug Metab Disp 30: 1158–1163.

Olbricht C, Wanner C, Eisenhauer T, Kliem V, Doll R, Boddaert M, O'Grady P, Krekler M, Mangold B and Christians U (1997). Accumulation of lovastatin, but not pravastatin, in the blood of cyclosporine-treated kidney graft patients after multiple doses. Clin. Pharmacol. Ther., Vol. **62**: 311–321.

Pahlda R, Lambert J, Ansko P, Winstanely P, Davies PDO and Kiivet R-A (1999). Comparative bioavailability of three different formulations of rifampicin. J. Clin. Pharmacol Ther. Vol. **24**:219-225.

Paine SW, Parker AJ, Gardiner P, Webborn PJ, and Riley RJ (2008). Prediction of the pharmacokinetics of atorvastatin, cerivastatin, and indomethacin using kinetic models applied to isolated rat hepatocytes. Drug Metab. Dispos., Vol. **36**:1365-1374.

Pang KS and Rowland M (1977). Hepatic clearance of drugs. I. Theoretical considerations of a "well-stirred" model and a "parallel tube" model. Influence of hepatic blood flow, plasma and blood cell binding, and the hepatocellular enzymatic activity on hepatic drug clearance. J Pharmacokinet Biopharm, Vol. **5**:625-653.

Park JW, Siekmeier R and Merz M (2002). Pharmacokinetics of pravastatin in heart-transplant patients taking cyclosporin A. Int. J. Clin. Pharmacol Ther., Vol. **10**:439-450.

Parker AJ and Houston JB (2008) Rate-limiting steps in hepatic drug clearance: comparison of hepatocellular uptake and metabolism with microsomal metabolism of saquinavir, nelfinavir, and ritonavir. Drug Metab. Dispos., Vol. **36**:1375-1384.

Pasanen, M., Neuvonen, M, Neuvonen, PJ and & Niemi, M (2006). SLCO1B1 polymorphism markedly affects the pharmacokinetics of simvastatin acid. Pharmacogenet Genom, Vol. **16**:873–879.

Pasanen MK, Fredrikson H, Neuvonen PJ and Niemi M (2007). Different Effects of SLCO1B1 Polymorphism on the pharmacokinetics of Atorvastatin and Rosuvastatin. Clin. Pharmacol. Ther., Vol. **82**:726-733.

Petzinger E and Fuckel D (1992) Evidence for a saturable, energy-dependent and carrier mediated uptake of oral antidiabetics into rat hepatocytes. Euro. J. Pharmacol, Vol. **213**:381–391.

Pham PA, la Porte CJL, Lee LS, van Heeswijk R, Sabo JP, Elgadi MM, Piliero PJ, Barditch-Crovo P, Fuchs E, Flexner C, and Cameron DW (2009). Differential Effects of Tipranavir plus Ritonavir on Atorvastatin or Rosuvastatin Pharmacokinetics in Healthy Volunteers. Antimicrob Agents Ch, Vol. **53** (10):4385–4392.

Poirier A, Lave T, Portmann R, Brun ME, Senner F, Kansy M, Grimm HP and Funk C (2008). Design, Data Analysis, and Simulation of in Vitro Drug Transport Kinetic Experiments Using a Mechanistic in Vitro Model. Drug Metab. Dispos., Vol. **36** (12):2434–2444.

Poirier A, Cascais AC, Funk C, and Lave T (2009). Mechanistic Modeling of Hepatic Transport from Cells to Whole Body: Application to Napsagatran and Fexofenadine. Mol Pharmaceut Vol. **6**:1716–1733.

Polli JW, Olson KL, Chism JP, St. John-Williams L, Yeager RL, Woodard SM, Otto V, Castellino S and Demby VE (2009). An unexpected synergist role of P-glycoprotein and breast cancer resistance protein on the central nervous system penetration of the tyrosine kinase inhibitor lapatinib (N-{3-chloro-4-[(3-fluorobenzyl)oxy]phenyl}-6-[5-({[2-(methylsulfonyl)ethyl]amino}methyl)-2-furyl]-4-quinazolinamine; GW572016). Drug Metab. Dispos., Vol. **37**:439-442.

Poulin P and Theil FP 2000. A priori prediction of tissue:plasma partition coefficients of drugs to facilitate the use of physiologically-based pharmacokinetics models in drug discovery. J. Pharm. Sci., Vol. **89**:16-35.

Prasad B, Evers R, Gupta A, Hop C, Salphati L, Shukla S, Ambudkar S and. Unadkat JD (2104). Interindividual Variability in Hepatic Organic Anion-Transporting Polypeptides and P-Glycoprotein (ABCB1) Protein Expression: Quantification by Liquid Chromatography Tandem Mass Spectroscopy and Influence of Genotype, Age, and Sex. Drug Metab. Dispos. Vol. **42**, 78–88.

Prueksaritanont T, Koike M, Hoener BA and Benet LZ (1992). Transport and Metabolism of Cyclosporine in Isolated Rat Hepatocytes. Biochem Pharmacol, Vol. **43**, No. 9:1997-2006.

Puviani AC, Ottolenghi C, Tassinari B, Pazzi Pand Morsiani E 1998. An update on high-yield hepatocyte isolation methods and on the potential clinical use of isolated liver cells. Comparative Biochemistry and Physiology Part A, Vol. 121, page:99–109.

Regazzi MB, Iacona I, Campana C, Gavazzi A, Vigano M and Perani G (1994). Clinical efficacy and pharmacokinetics of HMG-CoA reductase inhibitors in heart transplant patients treated with cyclosporin A. Transplant Proceedings, Vol. 26 (5), page: 2644-5.

Riley RJ, Grime K and Weaver R (2007). Time-dependent CYP inhibition. Expert Opin. Drug Metab. Toxicol. Vol. **3**(1):51-66.

Rodgers T, Leahy D and Rowland M (2005). Physiologically Based Pharmacokinetic Modeling 1: Predicting the Tissue Distribution of Moderate-to-Strong Bases. J. Pharm. Sci., Vol. **94**:1259-1276.

Rodgers T and Rowland M (2006). Physiologically Based Pharmacokinetic Modeling 2: Predicting the Tissue Distribution of Acids, very weak bases, neutrals and zwitterions. J. Pharm. Sci., Vol. **95**:1238-1257.

Sasaki M, Suzuki H, Ito K, Abe T and Sugiyama Y (2002). Transcellular Transport of Organic Anions Across a Double-transfected Madin-Darby Canine Kidney II Cell Monolayer Expressing Both Human Organic Anion-transporting Polypeptide (OATP2/SLC21A6) and Multidrug Resistance-associated Protein 2 (MRP2/ABCC2). J. Biol. Chem., Vol. **277**:6497–6503.

Satoh H, Yamashita F, Tsujimoto M, Murakami H, Koyabu N, Ohtani H and Sawada Y (2005). Citrus Juices Inhibit the Function of Human Organic Anion-Transporting Polypeptide OATP-B. Drug Metab. Dispos., Vol. **33**:518–523.

Schaefer O, Ohtsuki S, Kawakami H, Inoue T, Liehner S, Saito A, Sakamoto A, Ishiguro N, Matsumaru T, Terasaki T, and Ebner T (2012). Absolute quantification and differential expression of drug transporters, cytochrome P450 enzymes, and UDP-glucuronosyltransferases in cultured primary human hepatocytes. Drug Metab. Dispos., Vol. **40**:93-103.

Schneck DW, Birmingham BK, Zalikowski JA, Mitchell PD, Wang Y, Martin PD, Lasseter KC, Brown CD, Windass AS and Raza A (2004). The effect of gemfibrozil on the pharmacokinetics of rosuvastatin. Clin. Pharmacol. Ther., Vol. **75**:455-463.

Seglen PO 1976. Preparation of isolated rat liver cells. Method Cell. Biol., Vol. **13**:29–83.

Seithel A, Eberl S, Singer K, Auge D, Heinkele G, Wolf NB, Dorje F, Fromm MF and König J (2007). The Influence of Macrolide Antibiotics on the Uptake of Organic Anions and Drugs mediated by OATP1B1 and OATP1B3. Drug Metab. Dispos. Vol. **35**:779-86.

Shedlofsky SI, Sinclair PR, Sinclair JF and Bonkovsky HL (1984). Increased glutathione in cultured hepatocytes associated with induction of cytochrome P-450. Lack of effect of glutathione depletion on induction of cytochrome P-450 and delta-aminolevulinate synthase. Biochem Pharmacol. Vo 1;**33**(9):1487-91.

Shitara Y, Li A, Kato Y, Lu C, Ito K, Ito T and Sugiyama Y (2003a). Function of Uptake Transporters for Taurocholate and Estradiol 17β-D-Glucuronide in Cryopreserved human hepatocytes. Drug Metab. Pharmaco., Vol. **18**:33-41.

Shitara Y, Itoh T, Sato H, Li AP and Sugiyama Y (2003b) Inhibition of Transporter-Mediated Hepatic Uptake as a Mechanism for Drug-Drug Interaction between Cerivastatin and Cyclosporin A. J. Pharmacol. Exp. Ther., Vol. **304**:610–616.

Shitara Y, Hirano M, Sato H, and Sugiyama Y (2004) Gemfibrozil and its glucuronide inhibit the organic anion transporting polypeptide 2 (OATP2/OATP1B1: SLC21A6)-mediated hepatic uptake and CYP2C8-mediated metabolism of cerivastatin: analysis of the mechanism of the clinically relevant drug-drug interaction between cerivastatin and gemfibrozil. J. Pharmacol. Exp.Ther., Vol. **311**:228–236.

Shitara Y and Sugiyama Y (2006). Pharmacokinetic and pharmacodynamic alterations of 3-hydroxy-3-methylglutaryl coenzyme A (HMG-CoA) reductase inhibitors: Drug–drug interactions and interindividual differences in transporter and metabolic enzyme functions. Pharmacol. Therapeut., Vol. **112**:71–105.

Simonson SG, Raza A, Martin PD, Mitchell PD, Jarcho JA, Brown CDA, Windass AS and Schneck DW (2004). Rosuvastatin pharmacokinetics in heart transplant recipients

administered an antirejection regimen including Cyclosporin. Clin. Pharmacol.Ther. Vol. **76**:167-77.

Smith NF, Figg WD and Sparreboom A (2005). Role of the liver-specific transporters OATP1B1 and OATP1B3 in governing drug elimination. Expert Opin Drug Met. Tox., Vol. **1**(3):429-445.

Soars MG, McGinnity DF, Grime K, and Riley RJ (2007). The pivotal role of hepatocytes in drug discovery. Chemico-Biological Interactions, Vol. **168**:2–15.

Stevenson DJ, Morgan C, McLellan LI and Grant MH (2007) Reduced glutathione levels and expression of the enzymes of glutathione synthesis in cryopreserved hepatocyte monolayer cultures. Toxicology in Vitro, Vol. **21**:527-532.

Terry C and Hughes R (2009). An Optimised Method for Cryopreservation of Human Hepatocytes. Hepatocyte Transplantation, Vol. **481**, Chapter 3.

Tirona RG, Leake BF, Wolkoff AW, and Kim RB (2003) Human organic anion transporting polypeptide-C (SLC21A6) is a major determinant of rifampin mediated pregnane X receptor activation. J. Pharmacol. Exp. Ther., Vol. **304**:223–228.

Tirona R and Kim R. (2007). Organic anion-transporting polypeptides. In Drug Transporters 75-105, John Wiley Press.

Tomlinson B, Hu1 M, Lee VWY, Lui SSH, Chu TTW, Poon EWM, Ko1 GTC, Baum L, Tam LS and Li EK (2010). ABCG2 Polymorphism is Associated with the Low-Density Lipoprotein Cholesterol Response to Rosuvastatin. Nature, Vol. **87** (5):558-562.

Treiber A, Schneiter R, Delahaye S, and Clozel M (2004). Inhibition of organic anion transporting polypeptide-mediated hepatic uptake is the major determinant in the pharmacokinetic interaction between bosentan and cyclosporin A in the rat. J. Pharmacol. Exp. Ther., Vol. **308**:1121-1129.

Treiber A, Schneiter R, Hausler S and Stieger B (2007). Bosentan Is a Substrate of Human OATP1B1 and OATP1B3: Inhibition of Hepatic Uptake as the Common Mechanism of Its Interactions with Cyclosporin A, Rifampicin, and Sildenafil. Drug Metab. Dispos., Vol. **35** (8):1400–1407.

Ulvestad M, Bjorquist P, Molden E, Asberg A, and Andersson TB (2011). OATP1B1/1B3 activity in plated primary human hepatocytes over time in culture. Biochem. Pharm., Vol. **82**:1219–1226.

Ulvestad Maria (2007). Comparison of Three In Vitro Models Expressing the Membrane Drug Transporter OATP1B1. Master thesis http://hdl.handle.net/10852/12201.

Van De Steeg E, Van Der Kruijssen CMM, Wagenaar E, Burggraaff JEC, Mesman E, Kenworthy KE, and Schinkel AH (2009). Methotrexate Pharmacokinetics in Transgenic Mice with Liver-Specific Expression of Human Organic Anion-Transporting Polypeptide 1B1 (SLCO1B1). Drug Metab. Dispos., Vol. **37** (2):277-281.

Van Waterschoot RAB and Schinkel AH (2011). A critical analysis of the interplay between cytochrome P450 3A and P-glycoprotein: Recent insights from knockout and transgenic mice. Pharmacological Reviews 63:A-U.

Vavricka SR, Van Montfoort J, Ha HR, Meier PJ and Fattinger K (2002). Interactions of rifamycin SV and rifampicin with organic anion uptake systems of human liver. Hepatology, Vol. **36**:164–172.

Watanabe T, Kusuhara H, Maeda K, Shitara Y and Sugiyama Y (2009). Physiologically Based Pharmacokinetic Modeling to Predict Transporter-Mediated Clearance and Distribution of Pravastatin in Humans. J. Pharmacol. Exp. Ther., Vol. **328** (2): 652–662.

Xia CQ, Liu N, Miwa GT and Xia LSG (2007). Interactions of CsA with Breast Cancer Resistance Protein. Drug Metab. Dispos., Vol. **35** (4): 576–582.

Yabe Y, Galetin A and Houston JB (2011). Kinetic Characterization of Rat Hepatic Uptake of 16 Actively Transported Drugs. Drug Metab. Dispos., Vol. **39**:1808–1814.

Yamashiro W, Maeda K, Hirouchi M, Adachi Y, Hu Z and Sugiyama Y (2006). Involvement of Transporters in the Hepatic Uptake and Biliary Excretion of Valsartan, a Selective Antagonist of the Angiotensin II AT1-Receptor, in Humans. Drug Metab. Dispos., Vol. **37** (7):1247-1254.

Yamazaki M, Li B, Louie SW, Pudvah NT, Stocco R, Wong W, Abramovitz M, Demartis A, Laufer R, Hochman JH, Prueksaritanont T, Lin JH (2005). Effects of fibrates on human organic anion-transporting polypeptide 1B1-, multidrug resistance protein 2- and P-glycoprotein-mediated transport. Xenobiotica, Vol. **35**:737-753.

Yang H and Elmquist WF (1996). The binding of cyclosporin A to human plasma: an in vitro microdialysis study. Pharm Res. Vol. **13**(4):622-627.

Zhao P, Zhang L, Grillo JA, Liu Q, Bullock JM, Moon YJ, Song P, Brar SS, Madabushi R, Wu TC, Booth BP, Rahman NA, Reynolds KS, Gil Berglund E, Lesko LJ and Huang S-M (2011). Applications of Physiologically Based Pharmacokinetic (PBPK) Modeling and Simulation During Regulatory Review. Clin. Pharmacol Ther., Vol. **89** (2):259–267.

Zhang P, Tian X, Chandra P, and Brouwer KL (2005). Role of glycosylation in trafficking of Mrp2 in sandwich-cultured rat hepatocytes. Mol. Pharmacol., Vol. **67**:1334-1341.

Zhang W, Deng S, Chen X, Zhou G, Xie H-T, He F-Y, Cao D, Li Y-J, and Zhou H-H (2008). Pharmacokinetics of Rosuvastatin When Coadministered with Rifampicin in Healthy Males: A Randomized, Single-Blind, Placebo-Controlled, Crossover Study. Clin. Ther., Vol. **30** (7):1283-1289.

Zhang ZY and Wong NY (2005). Enzyme Kinetics for Clinically Relevant CYP Inhibition. Curr. Drug Metab., Vol. **6**:241-247.